Optical Design for Stationary Solar Concentrators

Nilsson, Johan

2007

Optical Design for Stationary Solar Concentrators

Johan Nilsson

Division of Energy and Building Design
Department of Architecture and Built Environment
Lund University
Faculty of Engineering LTH, 2007
Report EBD-T--07/7

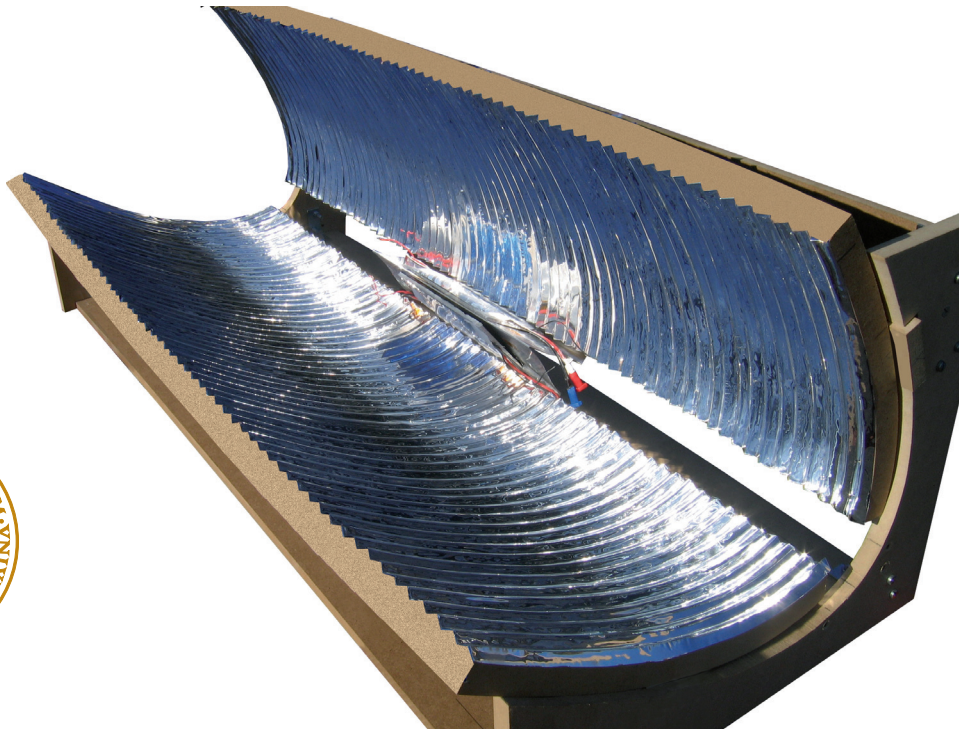

Lund University

Lund University, with eight faculties and a number of research centres and specialized institutes, is the largest establishment for research and higher education in Scandinavia. The main part of the University is situated in the small city of Lund which has about 103 700 inhabitants. A number of departments for research and education are, however, located in Malmö. Lund University was founded in 1666 and has today a total staff of 5 500 employees and 40 000 students attending 140 degree programmes and 1 600 subject courses offered by 66 departments.

Division of Energy and Building Design

Reducing environmental effects of construction and facility management is a central aim of society. Minimising the energy use is an important aspect of this aim. The recently established division of Energy and Building Design belongs to the department of Architecture and Built Environment at the Lund University, Faculty of Engineering LTH in Sweden. The division has a focus on research in the fields of energy use, passive and active solar design, daylight utilisation and shading of buildings. Effects and requirements of occupants on thermal and visual comfort are an essential part of this work. Energy and Building Design also develops guidelines and methods for the planning process.

Optical Design for Stationary Solar Concentrators

Johan Nilsson

Doctoral Dissertation

Keywords

Solar concentrators, parabolic reflectors, structured reflectors, photovoltaic cells, photovoltaic-thermal systems, optical efficiency, non-imaging optics, optical properties, non uniform irradiance distribution, building integrated photovoltaics, ray tracing, solar cell modelling

The English language corrected by L. J. Gruber BSc(Eng) MICE MIStructE.
Layout: Hans Follin, LTH, Lund.
Cover photo: Johan Nilsson and Erik Forsberg

Printed by KFS AB, Lund 2007

Report No EBD-T--07/7
Optical Design for Stationary Solar Concentrators.
Department of Architecture and Built Environment, Division of Energy and Building Design,
Lund University, Lund

ISSN 1651-8136
ISBN 978-91-85147-22-9

Lund University, Lund Institute of Technology
Department of Architecture and Built Environment
Division of Energy and Building Design
P.O. Box 118
SE-221 00 LUND
Sweden

Telephone: +46 46 - 222 73 52
Telefax: +46 46 - 222 47 19
E-mail: ebd@ebd.lth.se
Home page: www.ebd.lth.se

to my father

Abstract

Solar electricity is one of the most promising technologies for our future electricity supply. By using concentrators, it is possible to reduce the cost of generating photovoltaic electricity. This thesis discusses how to design stationary low concentrating systems for photovoltaic or PV/Thermal applications.

The first chapters briefly explain the optics of solar energy concentrators. The theoretical maximum concentration ratios of two dimensional and three dimensional systems were derived using the concept of étendue conservation and a review of current concentrators was presented.

In order to improve existing concentrators, it is important to identify the most significant losses. This was done by characterization of an asymmetrically truncated CPC fitted with standard solar cells. The non uniform irradiance distribution on the cells was identified as the single most important reason for electrical losses.

To address the problems of non uniform irradiance distribution, a structured reflector was introduced in the characterized system. The structured reflector created a more homogeneous light distribution on the cells, but because of larger optical losses, it was difficult to show any improved performance. It was expected that the more uniform distribution would improve the annual output, but to what extent was difficult to estimate.

A new simulation based method for evaluation of photovoltaic concentrators was therefore developed. It consisted of three steps, optical simulations of the concentrator, electrical simulations to evaluate how the light distribution affected the output, and finally annual simulations to get an estimate of the annual electrical output.

Using the new method, two new concentrators were developed. One of the systems was intended for roof integration, and the other for wall integration. Both systems were fitted with structured reflectors. The concentration ratio of both systems was increased compared to their references in order to utilize the optimum potential of the structured reflectors. It was shown that the roof concentrator would yield 191 kWh per m^2 solar cells. This was 20% higher than the reference system. The wall concentrator

was estimated to generate 213 kWh per m^2 solar cells, which was 10% higher than the reference wall concentrator.

Measurements on the newly developed roof concentrator showed that the more uniform irradiance distribution and increased concentration ratio increased the electrical output in the meridian plane. However, because of low manufacturing precision it was difficult to demonstrate this for all angles of incidence.

The last chapter of the thesis discusses the advantages and disadvantages of possible changes to stationary photovoltaic concentrators. The chapter ends by defining a set of rules on how to design stationary concentrators with standard cells for maximum annual electrical output.

Contents

Nomenclature

Latin

A,a	aperture area	[m^2]
b_0	incidence angle modifier coefficienct	[-]
C	concentration ratio	[-]
C_g	geometrical concentration ratio	[-]
C_{max}	maximum concentration ratio	[-]
f	focal point	[-]
FF	fill factor	[-]
f_L	incidence angle modifier for glazing	[-]
f_l	focal length	[m]
$G_{incident}$	incident irradiation	[W]
$G_{collected}$	incident irradiation	[W]
h	distance between source aperture and solar cell	[m]
I	current	[A]
I_0	dark current	[A]
I_{1000}	short-circuit current at an incident irradiance of 1000W/m^2	[A]
I_L	light generated current	[A]
I_{SC}	short-circuit current	[A]
I_{SC}^{conc}	short-circuit current of concentrator module	[A]
$I_{SC}^{reference}$	short-circuit current of reference module	[A]
K	incidence angle modifier according to McIntire	[-]
K_L	longitudinal incidence angle modifier according to McIntire	[-]
K_T	transversal incidence angle modifier according to McIntire	[-]
k_x	x directional component	[-]
k_y	y directional component	[-]
k_y	z directional component	[-]
L	length of CPC	[m]
n	index of refraction	[-]
n_x	ideality factor of diode x	[-]
P_{max}	maximum power delivered by the cell	[W]
R	resistance	[Ω]
R_B	base resistance	[Ω]
R_C	contact resistance	[Ω]

R_E	emitter resistance	[Ω]
R_F	finger resistance	[Ω]
R_L	load resistance	[Ω]
R_{SH}	shunt resistance	[Ω]
R_S	series resistance	[Ω]
R_T	transverse optical efficiency of concentrator	[-]
V	voltage	[V]
V_{OC}	open-circuit voltage	[V]

Greek

α	solar altitude	[°]
β	aperture normal tilt relative to a horizontal surface	[°]
γ	solar azimuth angle	[°]
η_0	optical efficiency at normal incidence	[-]
$\eta_{diffuse}$	system efficiency for diffuse irradiation	[-]
η_{direct}	system efficiency for direct irradiation	[-]
$\eta_{electric}$	electrical efficiency at standard test conditions	[-]
η_{opt}	optical efficiency for direct irradiation	[-]
$\eta_{opt,diff}$	optical efficiency for diffuse irradiation	[-]
θ	angle of incidence	[°]
θ_i	angle of incidence	[°]
θ_L	longitudinal angle of incidence	[°]
θ_{max}	maximum angle of incidence accepted by the system	[°]
θr	reflected angle	[°]
θ_T	transverse projected angle of incidence	[°]
θ_t	transmitted angle	[°]
ρ_B	base resistivity	[Ωcm^2]
ρ_C	contact resistivity	[Ωcm^2]
ρ_E	emitter sheet resistivity	[Ω/□]
ρ_F	finger resistivity	[Ω/cm]
τ	mirror tilt angle of V-trough	[°]
Φ	angle between the optical axis and the reflector in a CPC	[°]
ϕ	rotation angle around the z-axis	[°]

List of papers

I. Nilsson J., Håkansson H., Karlsson B. (2007) *Electrical and thermal characterization of a PV-CPC hybrid*. Solar Energy, Vol. 81 (7), pp. 917-928

II. Nilsson J., Håkansson H., Karlsson B. (2006) *Measurements of the effects of non-uniform irradiance distribution on standard PV cells*. Proceedings of the 21st European Photovoltaic Solar Energy Conference and Exhibition, Dresden, Germany

III. Nilsson J., Brogren M., Helgesson A., Karlsson B., Roos A. (2006) *Biaxial model for the incidence angle dependence of the optical efficiency of photovoltaic systems with asymmetric reflectors*. Solar Energy, Vol. 80 (9), pp. 1199-1212

IV. Nilsson J., Leutz R., Karlsson B. (2007) *Micro-structured reflector surfaces for a stationary asymmetric parabolic solar concentrator.* Solar Energy Materials and Solar Cells, Vol. 91 (6), pp. 525-533

V. Nilsson J. (2007) *A new simulation based evaluation method for photovoltaic concentrators.* Submitted to Solar Energy Materials and Solar Cells in September 2007

VI. Nilsson J., Karlsson B. (2007) *Design of stationary photovoltaic concentrators for homogenized irradiance distribution.* Submitted to Applied Optics in September 2007

VII. Fieber A., Nilsson J., Karlsson B. (2004) *PV performance of a multifunctional PV/T hybrid solar window.* Proceedings of the 19th European Photovoltaic Solar Energy Conference and Exhibition, Paris, France

VIII. Rosencrantz T., Nilsson J., Karlsson B. (2005) *A new model and method for determination of the incidence angle dependent g-value of windows and sunshades*. Proceedings of North Sun 2005, Vilnius, Lithuania

Acknowledgements

The largest part of this work was financed by FORMAS, The Swedish Research Council for Environment, Agricultural Sciences and Spatial Planning. The last part was financed by STEM, the Swedish Energy Agency.

I wish to thank my supervisors Prof. Björn Karlsson and Dr. Håkan Håkansson for their support. Björn for always being positive, having valuable comments on my work and for always keeping me on my toes. Håkan for helping me with measurements and for being an inventor who always has new ideas on how to solve the problem.

Dr. Ralf Leutz and Prof. Harald Ries of Philipps University of Marburg, Germany, are acknowledged for teaching me the fundamentals of optics and optical simulations, and for welcoming me to Marburg.

I would also like to acknowledge my colleagues Bengt Hellström and Bengt Perers for valuable discussions which have helped me many times.

I have appreciated the cooperation with Helena Gajbert, Tobias Rosencrantz, Andreas Fieber, Maria Brogren and Anna Helgesson in co-authoring the articles.

Everyone at the division of Energy and Building Design is acknowledged for being part of a warm and friendly working environment.

Finally, I wish to thank my family for their fantastic support at all times.

1 Introduction

1.1 Background

It is no longer necessary to explain why we need to use renewable energy resources for the future energy supply. One of the renewable technologies that has received great attention in recent years is photovoltaics. By the end of 2005, 1.4 GW of PV power was installed in Germany and 1.4 GW in Japan (IEA-PVPS 2006). By the end of that year, globally installed PV power was 3.7 GW, which tells us that these two countries alone represent 77% of the globally installed PV power. The reason for the relatively high installed PV power in these two countries is that large subsidies are available. The feed-in tariff in Germany, which in May 2007 was € 0.49/kWh (IEA-PVPS 2007), has been very successful and the installed power in Germany increased by 80% in 2005. For this reason, the model has been transferred to other European countries in slightly modified form. Spain is one of the countries where it has been introduced, and large installations are now being commissioned due to the new subsidies.

In countries without subsidies, however, the market for PV is almost non existent. The average installation price for grid-connected PV systems in 2005 was US$ 6.6/Wp which explains the low interest in countries without subsidies.

It may be asked whether it reasonable not to subsidize PV since it is a renewable energy technology, and most other energy technologies have received considerable subsidies in the past. However, if PV is to be competitive in a market without subsidies, the cost has to go down considerably. Building integration of PV is attractive as a means of lowering the cost of PV installations. If the modules are integrated into the built environment, this has a large potential to reduce the cost of the module mounting, both in terms of space and components. Wall or roof integration are examples of such integration that will decrease the system cost. Another benefit from building integration is that energy production will be located at the point of use. There is in most cases a large difference between the cost of electricity generation and the price of the electricity at the consumer side which is largely due to taxes and fees that are outside the control of the utilities. To be able to compete with conventional electricity production,

the cost of 1 kWh of photovoltaic electricity probably has to be around € 0.02 if it is to be an interesting option for the utilities. On the other hand, if the consumer can produce the PV electricity as a means of reducing the amount of bought electricity, the cost is allowed to be at least 5 times higher while still being a good investment.

A promising technology for reducing the cost of the PV installation is to concentrate the light with mirrors or lenses in order to increase the irradiance on the cells. The rationale for this technology is that the cost of the mirrors is considerably lower than the cost of the cells, and by replacing cell area with reflector area; the total system cost will be lower.

Concentrators for photovoltaics are often divided into three groups; high, medium, and low concentration systems. High concentration systems is the term commonly used for systems with concentration ratios greater than 100. In order to achieve such high concentrations it is necessary for the systems to track the sun in two dimensions. The high flux that is generated by the concentrators makes it possible to generate electricity by other means than photovoltaics. One possibility is to use the resulting high temperatures to produce thermal power. The electricity will then be generated by steam turbines or sterling cycles. It is also possible to produce heat for industrial processes that require high grade thermal energy. If the concentrator is used to concentrate the irradiation onto a photovoltaic cell, the cell can be extremely small due to the small spot size. If the cell is small, the price of the materials used will be low due to the low material consumption and it is possible to use advanced cell concepts that otherwise would be too expensive. Parabolic dishes or lenses are used to obtain high levels of concentration for photovoltaics. Concentrating lens systems for high concentration photovoltaics are discussed by Miñano, González, and Benítez (1995) and by Leutz et. al. (1999). Parabolic dishes are discussed by Feuermann and Gordon (2001). Central receivers with heliostat fields reflecting the light towards the receiver used to obtain solar thermal power are described by Vant-Hull and Hildebrandt (1976) and Schramek and Mills (2003).

Medium concentration systems concentrate light 10-100 times. Such systems require one-axis tracking. The concentrators are translationally symmetric, i.e. trough shaped. It can be shown that the concentration of translationally symmetric concentrators is independent of the light incident parallel to the axis of symmetry, and this removes the constraint of two-axis tracking. The existing systems are based on parabolic reflectors (Coventry 2005 and Sala et. al. 1996) or Fresnel lenses (Piszczor et. al. 1993). The PV cells have to be designed for concentrator applications due to the high intensities (Luque, Sala, and Arboiro 1998) and thus high currents, and the systems require cooling of the cells. The heat is collected by heat exchangers in some systems, or dissipated passively in others.

Low concentration systems concentrate light 1 to 10 times. These systems can be stationary or one-axis tracking. If they are stationary it is possible to integrate the systems rationally into buildings without moving parts or complex mounting. Another benefit from the low concentration ratio is that in principle it should be possible to use standard PV cells made for non-concentrating applications. This will reduce the cost significantly. Cooling still has to be applied in most cases to maintain cell efficiency, but as for the other concentrator categories, the heat generated by the cooling can be utilized if the system is well designed. Most systems are based on two dimensional Compound Parabolic Concentrators (CPCs) in some form (Mills 1978, Karlsson and Wilson 1999, and Mallick et. al. 2004), but other geometries are also considered (Fraidenraich 1998 and Luque 1989).

High and medium concentration systems are suitable for large scale power generation due to their higher complexity. The cost reduction can here be achieved by scaling up the system size. Low concentration systems are well suited for small scale energy production at the point of use and since they are stationary they are also an interesting application for building integration.

1.2 Objectives

The aim of this thesis has been to improve the efficiency of stationary low concentrating systems with standard PV cells. Most concentrating systems rely on concentrator cells in order to be efficient. These cells are expensive compared to standard cells, and are made in smaller volumes. If standard cells can be used, the total system cost will be reduced considerably. The investigated concentrators were parabolic reflector troughs with low cost reflector materials such as aluminium or steel.

The first objective was to characterize the state of the art low concentration systems that are available today and to quantify the losses in order to gain a better understanding of the loss mechanisms. Previous studies have shown that one of the major sources of losses in the system is the high local irradiance created by the parabolic reflectors (Brogren, Nostell, and Karlsson 2001). The highly non uniform irradiance distribution on the cells reduces the electrical output considerably. The losses are due partly to the elevated local temperatures and partly to the high local currents in the cells at the point of high irradiance. The problems of high global cell temperatures can be reduced by using water cooled hybrid absorbers. When the cell is cooled, it is possible to reduce the average cell temperature, but it is difficult to reduce the local temperature at the points of high irradi-

ance. The high local irradiance was therefore one of the main problems addressed in this thesis due to the large resistive losses in the cells at high currents, and to the elevated local temperatures.

Another objective was to formulate accurate models for the efficiency of the concentrators to assist the development of new concentrators. This was addressed by measurements on full size prototypes, and by modelling of the optical and electrical characteristics of the system.

Once the design tools were found, the most important goal of the thesis was to develop new stationary concentrators that can demonstrate improved annual electrical output.

1.3 Outline

Chapter 2 gives an introduction to the theory of light concentration and the limits of concentration. Important concepts used in the literature such as étendue, conservation of phase space and skew rays are explained. The theoretical limits of two and three dimensional concentrators are derived using these concepts.

Design principles for concentrators are discussed in Chapter 3. The edge-ray principle is explained and used to derive ideal two-dimensional concentrators. The chapter describes existing two- and three-dimensional symmetrical concentrators such as the V-trough and the CPC. It also describes asymmetrical concentrators as well as truncated non imaging parabolic concentrators.

Modelling and performance limitations of solar cells are the topic of Chapter 4. One dimensional and two dimensional models of the solar cell are discussed. The effects of increasing temperature and irradiance, and non-uniform irradiance distribution, are also discussed. These effects are an important part of the thesis as they are the main sources of electrical losses in low concentrating systems.

Chapter 5 describes ray tracing, the optical simulation method used throughout the thesis to characterize the optical properties of the concentrators. A commercial ray tracing package was used to perform the simulations, and the benefits of using a commercial package instead of a problem specific program written by the author are discussed.

A two dimensional solar cell model of the electrical output is described in Chapter 6. The model is based on an existing model and has been modified to take non uniform irradiance distribution into account. The characteristics of the model are described, and the usage is explained. Verification of the model is also discussed.

The different measurements that were made during the work on this thesis are described in Chapter 7. The method used to measure current-voltage characteristics, including short-circuit current, is explained. Another important measurement, the irradiance distribution over the cells in the concentrator, is also described. A method for measuring the effects of non uniform irradiance distribution on the cells was developed as part of the work for this thesis, and the method is described in this chapter.

Chapter 8 summarizes the findings of Article I, characterization of the MaReCo hybrid with two different reflector materials. The two prototypes are compared from the aspects of short-circuit current, fill factor, current-voltage characteristics and irradiance distribution. The absorber angle and placement of PV cells are discussed. The chapter also presents annual output simulations of heat and electricity for the two prototypes.

The effects of non uniform irradiance distribution on standard PV cells are discussed in Chapter 9. The influence of the profile of the light distribution is analysed. Parabolic mirrors produce a line of high irradiance, and the way the position of this line influences the electrical output of the cell is also discussed.

A model for estimating the output of heat and electricity using measurements of the optical efficiency is presented in Chapter 10. The model is used to estimate the output of a wall integrated asymmetric CPC and the estimates are compared to actual measurements of the electrical output. The reason why stationary concentrators show good performance at northern latitudes such as in Sweden is discussed at the end of the chapter.

Article IV is summarized in Chapter 11. It presents simulations on micro-structured reflectors in a MaReCo concentrator. The structured reflectors have a homogenizing effect on the irradiance distribution on the absorber, as well as increasing the concentration ratio. The chapter discusses the expected changes to the annual output using the new reflectors and presents ideas on how to improve current concentrator designs.

In order to evaluate how changes in the optical system influence the electrical output instantaneously as well as annually, a new model for evaluating solar concentrators is developed in Chapter 12. It is completely based on simulations and yields an estimate of the annual electrical output.

Using the evaluation method developed in the previous chapter, two new concentrators for standard PV cells are developed in Chapter 13 based on the findings from Chapter 11. One stationary concentrator for roof integration and one for wall integration is developed.

Measurements on the roof concentrator developed in Chapter 13 are presented in Chapter 14. The light distribution and current-voltage characteristics were measured in order to show how the structured reflector influences the electrical output.

In Chapter 15, conclusions on how to build a stationary concentrator are presented. Different ideas on how to improve the output are analysed and compared to each other.

Chapter 16 describes the author's contribution to articles VII and VIII, as well as other related work.

2 The optics of concentrating systems

2.1 Concentration ratio

The geometric concentration ratio of a concentrating system is defined as the ratio between the entry aperture and the exit aperture, or

$$C = \frac{A_1}{A_2} \qquad \text{Equation 2.1}$$

where A_1 is the area of the entry aperture and A_2 is the area of the exit aperture.

Concentrators can be divided into two groups, two dimensional concentrators (2D) and three dimensional concentrators (3D). Three dimensional concentrators such as e.g. the 3D Compound Parabolic Concentrator change all three direction vectors of the incoming rays, i.e. the direction cosines, and will typically concentrate the incoming irradiation to a spot. Two dimensional concentrators are symmetric around one axis, only two of the direction cosines are affected by the concentrator. The light in an axisymmetric concentrator is concentrated to a line.

According to the laws of thermodynamics it is not possible to concentrate light infinitely, there is a theoretical upper limit for the concentration ratio. These limits for a two and a three dimensional concentrator will be derived in the following sections.

I will use the concept of étendue, and the conservation of this quantity, to derive the maximum concentration ratio. The étendue of an optical system is a measure of the power transmitted along the beam, or the flux transfer. For paraxial rays, it is defined according to Equation 2.2, where a is the aperture area, n is the index of refraction of the medium that the beam is passing through, and θ_{max} is the maximum angular extent of a beam that will still strike the exit aperture. Figure 2.1 shows the parameters of Equation 2.2.

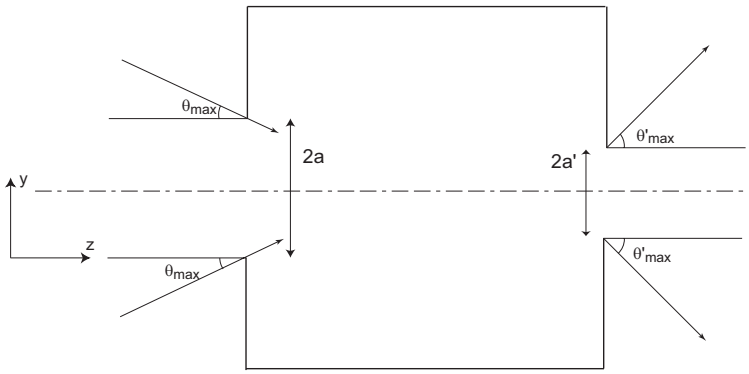

Figure 2.1 *Two dimensional concentrator modelled as a black box. The maximum angle of acceptance is* θ_{max}.

$$étendue = n^2 a^2 \theta_{max}^2 \qquad \text{Equation 2.2}$$

The étendue of an ideal, lossless, optical system is conserved at any point throughout the system (Winston et. al. 2005), i.e. the étendue of the entry aperture is equal to the étendue of the exit aperture. This will be used in the derivation of the maximum concentration ratio. Conservation of étendue means that the flux transmitted through the system is constant; if, for example, the entry beam is larger, the system will accept a smaller angular interval of the beam.

A ray of light in optics is defined by three position coordinates somewhere along the path of the ray and by three direction coordinates (direction cosines) at this point. The phase space of an optical system consists of all possible rays that can exist in the system, i.e. all combinations of the six coordinates that describe possible rays in the system. The volume in phase space filled up by a light source is the physical extent of the source in three dimensions and the angular extent of the source. The magnitude of this six dimensional volume can never be increased in any optical system, but the shape of the volume can be arbitrary. This statement is equal to Equation 2.2, if e.g. the width of the beam of light is decreased, the angular extent, the three direction coordinates, will increase.

Changes in the phase space volume of the beam entering the system have to be compensated by equal changes at the exit aperture, which for a system with rays at finite angles with the optical axis results in Equation 2.3, where dk_x and dk_y are the direction cosines of the incident rays.

$$n^2 dxdydk_x dk_y = n'^2 dx' dy' dk_x' dk_y' \qquad \text{Equation 2.3}$$

The coordinate system at the exit aperture can be chosen arbitrarily without affecting the conservation (Winston et. al. 2005).

The maximum concentration ratio will now be derived for the two dimensional case where the incident ray is unchanged in the x-direction. Figure 2.1 models a two dimensional concentrator as a black box. It has an entry aperture of $2a$ and an exit aperture of $2a'$.

The system is axisymmetric in the x-direction, and accepts light in the interval $-\theta_{max}$ to θ_{max}. The light exits the system with exit angles in the interval $-\theta'_{max}$ to θ'_{max}.

k_y will then be equal to:

$$k_y = \sin(\theta)$$

and dk_y is equal to:

$$dk_y = \cos(\theta)d\theta$$

The conserved quantity is then defined as:

$$n\cos(\theta)dyd\theta = n'\cos(\theta')dy'\,d\theta'$$

integrating this expression results in:

$$\int_0^{2a}\int_{-\theta_{max}}^{\theta_{max}} n\cos(\theta)dyd\theta = \int_0^{2a'}\int_{-\theta'_{max}}^{\theta'_{max}} n'\cos(\theta')dy'\,d\theta'$$

or, after integration:

$$4an\sin(\theta_{max}) = 4a'n'\sin(\theta'_{max})$$

The concentration ratio is defined as the ratio between the entry aperture and the exit aperture, and we obtain:

$$C = \frac{a}{a'} = \frac{n'\sin(\theta'_{max})}{n\sin(\theta_{max})}$$

This expression has its maximum when the exit angle is equal to 90°, and the maximum concentration ratio for a two dimensional concentrator is therefore:

$$C_{\max} = \frac{n'}{n \sin(\theta_{\max})}$$ Equation 2.4

Consider the same black box model for a three dimensional system, with an entry aperture of A_1 and en exit aperture of A_2. The maximum angle of incidence is a cone with an angle of θ_{max}.

The direction cosines are in this case:

$$k_x = \sin(\theta)\sin(\varphi)$$
$$k_y = \sin(\theta)\cos(\varphi)$$

where φ is the rotation angle around the z-axis in the xy-plane, and

$$dk_y dk_x = \cos(\theta)\sin(\theta)d\theta d\varphi$$

The conserved quantity for the three dimensional case is:

$$n^2 \cos(\theta)\sin(\theta)dxdyd\theta d\varphi = n'^2 \cos(\theta')\sin(\theta')dx'\,dy'\,d\theta'\,d\varphi'$$

Integrating this expression, we get:

$$n^2 A_1 \int_0^{2\pi} \int_0^{\theta_{\max}} \cos(\theta)\sin(\theta)d\theta d\varphi = 2\pi n^2 A_1 \frac{\sin^2(\theta_{\max})}{2} = \pi n'^2 A_2 \sin^2(\theta'_{\max})$$

The concentration ratio, as stated by Equation 2.1, will be:

$$C = \frac{A_1}{A_2} = \frac{n'^2 \sin^2(\theta'_{\max})}{n^2 \sin^2(\theta_{\max})}$$

Again, maximum concentration ratio is obtained when the exit angle is 90°, and the maximum concentration ratio of a three dimensional system is:

$$C_{\max} = \left(\frac{n'}{n \sin(\theta_{\max})} \right)^2$$ Equation 2.5

To obtain this maximum concentration is of course difficult in practice, it assumes no losses anywhere in the system, neither due to manufacturing imperfections or to non-ideal materials used in the system. But the derivation of the theoretical maximum concentration ratio shows two important points in designing concentrator systems. First of all, the smaller

the angular interval of acceptance, the higher the concentration ratio. Secondly, it is important to have rays exiting at all angles up to 90° to get a high concentration ratio.

Another way to increase the concentration ratio is to use a dielectric medium with an index of refraction > 1 inside the concentrator. Due to the laws of refraction, the beam will be refracted to a smaller angle of incidence when the medium has a higher index of refraction than the surroundings. This makes it possible to accept light at a larger angular interval, an effect that can be utilized to decrease the acceptance angle of the system while still accepting the original angular interval. Figure 2.2 shows a concentrator filled with a dielectric material with index of refraction n', which could e.g. be low iron glass with n'=1.523 which in that case would increase the concentration ratio by 52% (Zacharopoulos et. al. 2000).

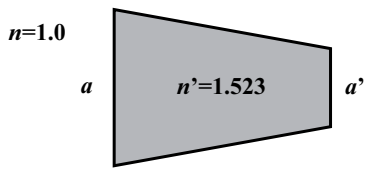

Figure 2.2 *Concentrator filled with low-iron glass for increasing the concentration ratio. Low iron glass has an index of refraction n' of 1.523.*

There are several definitions of concentration ratio. The theoretical maximum concentration ratio is the ideal concentration ratio of a system. The geometrical concentration ratio is the ratio between the entry aperture size and the exit aperture size. The ratio between the flux at the entry aperture and the flux at the exit aperture is called the optical concentration ratio. Unless stated differently, the term concentration ratio will refer to the geometrical concentration ratio throughout this thesis.

2.2 Skew rays

A skew ray is a ray that is not within any of the meridian planes of the system. The meridian planes are the three planes containing two axes in Figure 2.3.

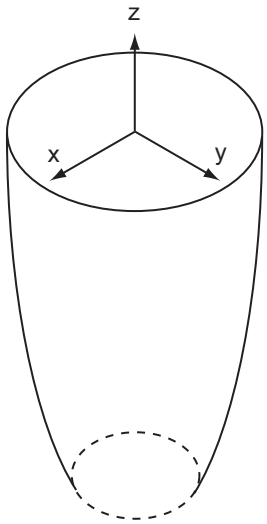

Figure 2.3 *The three meridian planes of a three dimensional concentrator are the planes containing two of the coordinate axes i.e. the xy-plane, the xz-plane, and the yz-plane.*

For a two dimensional system, e.g. one defined by the plane of the x and the z axes and axisymmetric in the y direction, a skew ray would be any ray with a non-zero y directional cosine, k_y. For such a system, the k_y component will not influence where the ray will strike the exit aperture in the x direction. The optical performance of an axisymmetric two dimensional system is thus not affected by skew rays. For three dimensional concentrators there will always be rays out of the meridian planes as long as the incident light has a non-zero x or y-component. This means that parallel rays that will strike the reflector at the same z-coordinate in Figure 2.3 will be reflected in different directions due to the fact that the surface normals will be different. For the two dimensional case, parallel rays that strike one of the reflectors at the same z-coordinate will have identical directional cosines after the reflection. This shows the importance of taking skew rays into consideration when analysing three dimensional concentrators.

3 Design of concentrators for Solar Energy applications

3.1 Design - The edge-ray principle and the string method

I will first describe an important principle used in the design of ideal concentrators, the edge-ray principle. It can be shown that if all rays along the edge of the aperture, incident at the extreme angle of acceptance, are transported to the rim of the exit aperture, this is sufficient for transferring all the incident rays within the interval of acceptance to the exit aperture (Winston et. al. 2005). This is equivalent to saying that the phase space boundary of the beam is transported to the exit aperture. If this is achieved, we have constructed an ideal concentrator.

The first problem discussed will be the two dimensional problem illustrated in Figure 3.1. Transporting the boundary of the phase space volume from *a* to *a'* is in this case identical to transporting all the light within an angle of $\pm\theta_{max}$ from aperture *a* to aperture *a'* since θ_{max} represents the boundary in directional space and the extent of the aperture represents the boundary in position space.

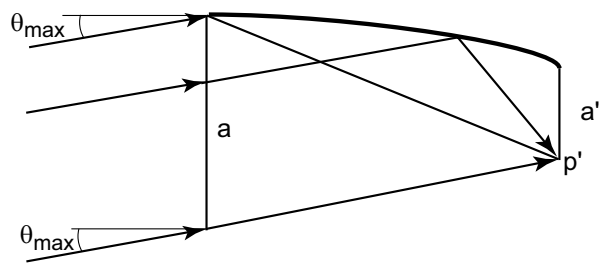

Figure 3.1 *Concentrator with flat absorber All rays at the extreme angle θ_{max} emerge through the rim point p' of the exit aperture.*

The basis of the method is Fermat's principle which states that the optical path length between the object and the image in an image forming system is the same for all rays. If strings are used instead of rays, we get the edge-ray principle. The method will be explained by developing one ideal two dimensional concentrator for a flat absorber and one ideal two dimensional concentrator for a cylindrical absorber.

Figure 3.2 shows the solution to the problem using the string method for a flat absorber. A rod is placed at the entry aperture, and it is tilted θ_{max} from the horizontal, where θ_{max} is the maximum angle at which the system will accept rays. A string is tied to a ring that is put around the rod at one end, and fastened to the absorber at point *d*.

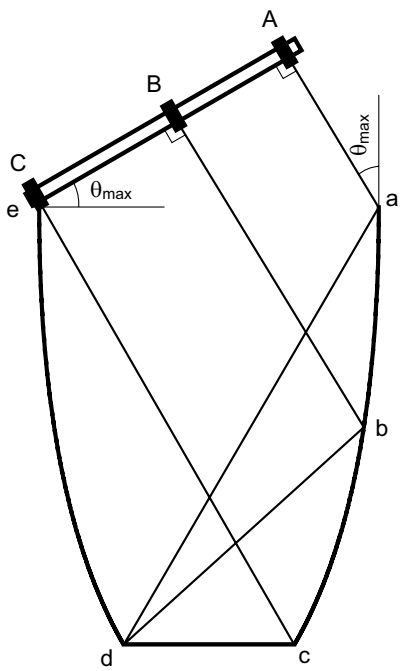

Figure 3.2 *String method for creating an ideal concentrator for a flat absorber. The ring at the end of the string is free to move along the rod from A to C.*

When the ring is placed at the end of the string at point *A*, the length of the string should be such that the string *Aad* is taut. The length of the string is now fixed and will keep this length throughout the whole design process. A pencil is now placed at *a*, which will be the first point of the reflector. The ring is then moved from *A* to *C* and the pencil is simulta-

neously moved from *a* to *c* in the figure while keeping the string taunt and the angle between the rod and the string at 90°. The pencil will now generate the shape of the reflector.

When the ring reaches point *C*, the pencil will be at point *c*. When this method is applied to the flat absorber as shown here, the generated concentrator shape is a parabola with the optical axis along *cC*. The optical term for this concentrator is CPC, Compound Parabolic Concentrator. It is discussed in more detail in Section 3.3.

Applying Fermat's principle of equal optical path lengths of the edge rays yields:

$$Cc + cd = ad + ea\sin(\theta_{\max})$$

Looking at the figure, we see that *Cc*=*ad* and we get:

$$cd = ea\sin(\theta_{\max})$$

The concentration ratio is defined as the entry aperture divided by the exit aperture:

$$C = \frac{ea}{cd} = \frac{ea}{ea\sin(\theta_{\max})} = \frac{1}{\sin(\theta_{\max})}$$

This proves that the new concentrator is indeed ideal.

Figure 3.3 shows an example with a cylindrical absorber such as e.g. a vacuum tube for heat collection. The edge-ray principle generalized for non planar absorbers states that all rays incident at θ_{max} should be reflected once and strike the absorber tangentially to its surface. All rays with a smaller angle of incidence will then reach the cylinder at an angle smaller than 90° with the surface normal.

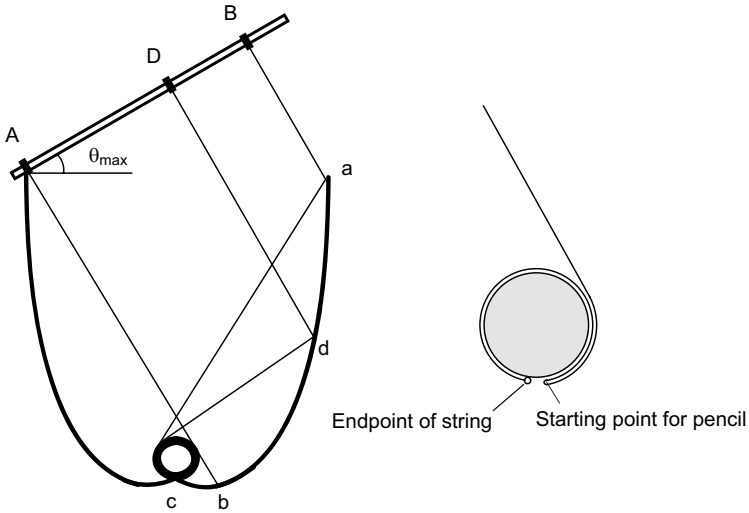

Figure 3.3 *String method for construction of an ideal concentrator for a cylindrical absorber. The reflector is plotted when the ring is moved from A to B.*

The rod is placed in the same way as in the example of the flat absorber, but the string is in this case fastened at point *c*. The loop of the string is placed at point *A*, and it is wound around the absorber as shown to the right in the figure. The length is adjusted as in the previous example. The pencil is placed at point *c*, and the string is kept stretched as the pencil is moved from *c* to *b*. When the pencil reaches *b*, the loop of the string is moved slowly from *A* to *B*, keeping the pencil in a position to keep the string stretched and at right angles to the rod. The resulting geometry is an involute from *c* to *b*, and the rest of the mirror from *b* to *a* is at each point sloped to reflect the ray incident at θ_{max} onto the tangent of the absorber.

The constructed geometries for both the flat and the circular absorber are ideal and fulfil the theoretical maximum concentration ratio $1/\sin\theta$, since all the light incident at angles less than θ_{max} will be absorbed in a system without optical losses or imperfections.

3.2 The light cone concentrator and the V-trough

One of the first three dimensional concentrator systems used for the collection of light was the light cone (Williamson 1952). Figure 3.4 shows a cross section of a cone concentrator.

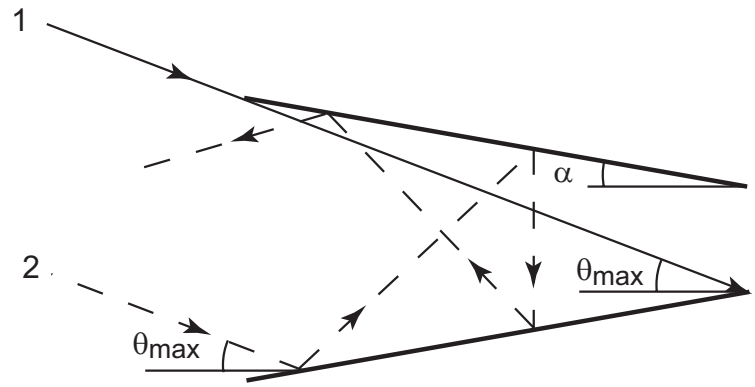

Figure 3.4 *Cross section of a light cone concentrator. Some of the rays incident at angle θ_{max} are turned back instead of striking the exit aperture.*

The design is straightforward, it is formed by mirrors mounted at an angle α and rotated around the axis of symmetry. This makes the manufacture of the concentrator simple. The length of the concentrator should be such as to make ray 1 in Figure 3.4, incident at the desired extreme angle θ_{max}, strike the edge of the exit aperture. Given a certain exit aperture, this results in an expression for the length of the concentrator. As can be seen in the figure, some of the rays incident at the same angle, such as ray 2, are reflected out of the system. For skew rays, rays out of the symmetry planes, the fraction of rays reflected back out is even larger.

The two dimensional version of the cone concentrator is the V-trough (Hollands 1971). It consists of planar mirrors mounted as in the cross section shown in Figure 3.4. Due to the axial symmetry of the V-trough, skew rays are not a problem, but the problem illustrated in Figure 3.4 still exists.

The cone concentrator and V-trough are clearly not ideal as some light is discarded, but if the shape of the reflectors could be changed for the system to accept ray 2 and skew rays, they would approach ideal concentration. This leads to the development of the compound parabolic concentrator that will be discussed in the next section.

3.3 Two dimensional compound parabolic concentrators

When the edge-ray principle is applied to the flat absorber case as was done in Section 3.1, the result is the two dimensional CPC shown in Figure 3.2. This concentrator achieves the maximum theoretical concentration ratio.

A parabolic mirror will reflect all light incident along its optical axis to the focal point. As Figure 3.5 illustrates, light which falls in at a positive angle of incidence will be reflected below the focus, as ray 2 in the figure. Light from negative angles, such as ray 1, will be reflected above the focus.

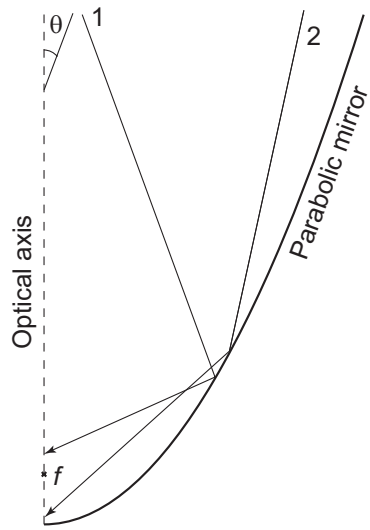

Figure 3.5 *Parabolic mirror with its optical axis drawn as a dashed line. The focal point is indicated by f. The angle of incidence θ is positive clockwise.*

The concentrator is constructed by tilting the parabola in order to make the optical axis parallel to the angle of incidence of the extreme rays. If, for example, the CPC is supposed to accept rays at 20°, the parabola is tilted 20°. This is shown in Figure 3.6.

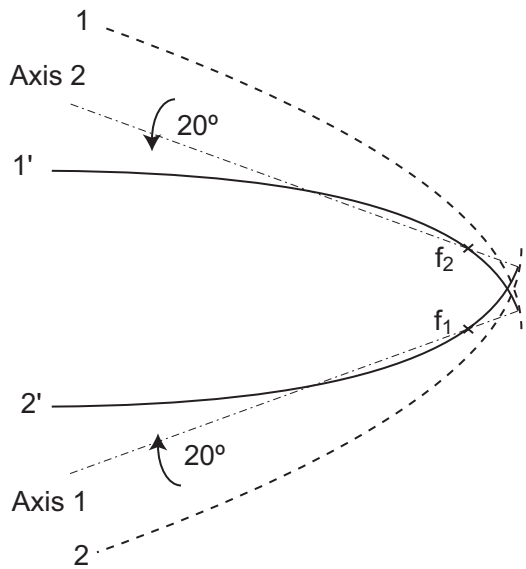

Figure 3.6 *Construction of a CPC with an acceptance angle of 20°. The original parabolas are rotated 20° from 1 to 1' and from 2 to 2'.*

The CPC in Figure 3.6 has an acceptance angle of 20°. Parabolas 1 and 1' have their focus at f_1 and parabolas 2 and 2' have their focus at f_2. The absorber will cover the area between f_1 and f_2. The original parabolas are drawn with dashed lines. The parabolas are identical, but mirrored and displaced a distance of 2*a'* from each other. 2*a'* is then the absorber width. The optical axis of both original parabolas is horizontal in the figure. To construct the CPC, the parabolas are rotated to the angle of acceptance, in this case 20°, around their respective focal points. This is how parabolas 1' and 2' are obtained. The resulting optical axes are drawn in the figure. The parabolas are cut off at the focal point of each parabola. Light at incidence angles larger than the angle of acceptance will be reflected from one of the mirrors to the other mirror and out of the system. Light incident at smaller angles will strike the absorber at a point between the focal point and the mirror.

A mathematical description of the CPC in polar coordinates is given in Equation 3.1 (Winston et. al. 2005). The parameters in the equations are shown in Figure 3.7.

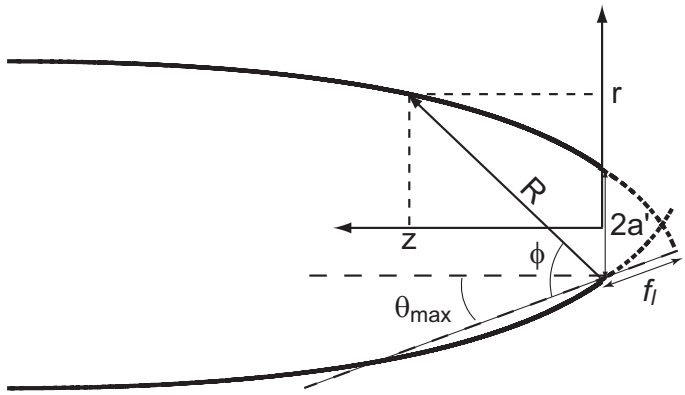

Figure 3.7 *Construction of a two dimensional CPC. The focal length of the upper parabola is indicated by f_l. The dashed parts of the parabolas are cut off to form the CPC.*

$$R = \frac{2f_l}{1-\cos(\phi)}$$

$$r = R\sin(\phi-\theta_{max}) - a' = \frac{2f_l \sin(\phi-\theta_{max})}{1-\cos\phi} - a'$$

$$z = R\cos(\phi-\theta_{max}) = \frac{2f_l \cos(\phi-\theta_{max})}{1-\cos\phi} \qquad \text{Equation 3.1}$$

$$f_l = a'(1-\cos(90+\theta_{max}) = a'(1+\sin\theta_{max})$$

$$2a' = \frac{2f}{1-\cos(90+\theta_{max})}$$

f_l is the focal length of the parabolas.

The full length of the CPC from entry aperture to absorber is determined by the acceptance angle $\theta_{max.}$ A ray incident along this angle of incidence should be reflected to the edge of the absorber which yields Equation 3.2 that expresses the length of the system, L, as a function of the absorber width and the acceptance angle.

$$L = \frac{a'(1+\sin\theta_{max})\cos(\theta_{max})}{\sin^2(\theta_{max})} \qquad \text{Equation 3.2}$$

The two dimensional CPC is an ideal concentrator with a concentration ratio of $1/\sin\theta_{max}$. It is ideal since all light incident at angles less than the angle of acceptance will arrive at the absorber, and it satisfies Equation 2.4.

Due to the translational symmetry of the trough system, the direction component of the rays parallel to the translational axis of symmetry does not influence where the ray will strike the absorber in the r-direction. This is determined by the two components in the plane of the paper in Figure 3.7.

As can be seen in Figure 3.6 and Figure 3.7, the CPC is deep in comparison with the width of the absorber. This is both impractical and costly when the concentrator is manufactured. Increasing the concentration ratio is equal to reducing the angle of acceptance, and this will result in a considerably deeper trough. Truncating the trough will not have a large impact on the entry aperture, if e.g. the leftmost third of the length of the trough of Figure 3.6 were truncated it would only reduce the aperture area by 3%. Studies on truncation have been made by e.g. Winston and Hinterberger (1975), Carvalho et. al. (1985), and Rabl (1976).

Since the maximum concentration ratio is $n/\sin\theta_{max}$ it is possible to increase the concentration ratio by filling the trough with a dielectric with an index of refraction greater than unity. It can be shown that the criterion for total internal reflection between the dielectric and the outside air in all possible reflections in a CPC is that the index of refraction is greater than $\sqrt{2}$ (Winston et. al. 2005). If such a material is used for the CPC, it is possible to construct a lossless concentrator without reflectors which will lead to a very high flux throughput.

3.4 Wedge type CPCs

Figure 3.8 shows a CPC of wedge type. The parabolic mirrors have identical parameters and share the same focal point.

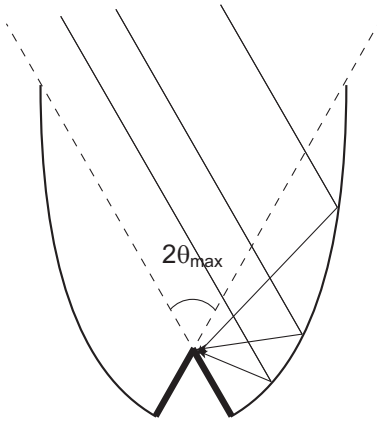

Figure 3.8 *CPC of wedge type. Both mirrors have the same focal point on the top of the absorbers.*

The absorber is mounted from the focal point to the reflector along the optical axis of the parabola. When the light is incident along the optical axis, at an angle of incidence of θ_{max} with the normal of the aperture as shown in the figure, all the light is concentrated to the focal point. When the angle of incidence is less than θ_{max}, the light is focused at the absorber below the focal point. This two dimensional concentrator is ideal, the concentration ratio is $1/\sin(\theta_{max})$.

3.5 Three dimensional compound parabolic concentrators

The three dimensional CPC is constructed by rotating the two dimensional CPC around the z axis of Figure 3.7. All the rays incident in the meridian plane with an angle of incidence less than θ_{max} will be collected at the exit aperture, just as was the case for the two dimensional CPC. But the three dimensional CPC is not an ideal concentrator since some of the skew rays outside the meridian plane, but inside the angle of acceptance, are reflected back out of the concentrator instead of being collected at the exit aperture.

The three dimensional CPC can be described mathematically in polar coordinates with z as described by Equation 3.1 but with r replaced by x and y according to Equation 3.3.

$$x = \frac{2f \sin\psi \sin(\phi - \theta_{max})}{1 - \cos\phi} - a' \sin\psi$$
$$y = \frac{2f \cos\psi \sin(\phi - \theta_{max})}{1 - \cos\phi} - a' \cos\psi$$

Equation 3.3

ψ in Equation 3.3 is the azimuth angle introduced to account for the rotation of the two dimensional system.

Since the three dimensional CPC is not ideal, it is interesting to find ways to improve the performance of the concentrator. One option is to fill it with a dielectric material with an index of refraction greater than 1 as was discussed in the previous section about two dimensional CPCs. However, the volume of a three dimensional CPC is large, and the cost of manufacturing the concentrator increases significantly when it is filled with a dielectric material.

One solution to this problem is to make a small CPC and introduce it at the exit aperture of a concentrator filled with air and use the CPC as a secondary concentrator. This will increase the concentration ratio of all non-ideal concentrators, or increase the interval of acceptance of any concentrator. The small size of the secondary CPC, due to the fact that the size of the entry aperture of this CPC is the same as the exit aperture of the first concentrator, solves the problem of high manufacturing cost for the full size CPC. In theory, this two stage system makes it possible to approach the theoretical limit of $n^2/\sin^2(\theta_{max})$.

The three dimensional CPC is mostly used in solar tracking applications where a very high irradiance level at the exit aperture is desired e.g. as secondary concentrator heliostat fields (Schmitz et. al. 2005).

3.6 Asymmetrical CPCs

The annual irradiation at different angles outside the atmosphere is symmetrical over the year with peaks at the summer and winter solstices. The angles of incidence of the peaks differ depending on the latitude, and at northern latitudes the solar altitude of the winter peak is close to the horizon. This, in combination with a large cloud cover, considerably reduces the winter peak which makes the yearly irradiation asymmetrical with just one peak in the summer (Rönnelid and Karlsson 1997). This can be seen from Figure 3.9 that shows the annual direct irradiation projected onto the meridian plane for two sites, Lund, Sweden, lat. 55.72° and Sydney, Australia, lat. -33.92°.

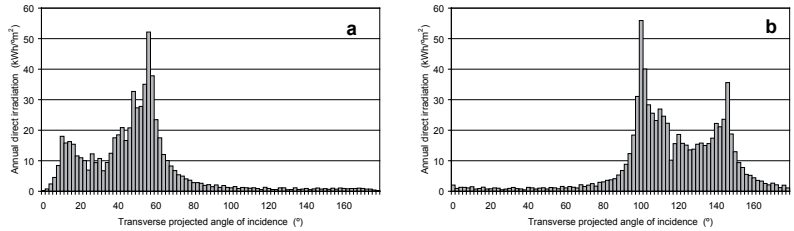

Figure 3.9 *Annual direct irradiation distribution in Lund (a) and in Sydney (b) on a surface facing south. The winter peak in Lund is suppressed. Both peaks are visible in Sydney.*

The fact that there is only one main peak at northern latitudes such as Lund makes it possible to use stationary concentrators that will collect most of the annual irradiation without tracking the sun.

Figure 3.10 shows an example of an asymmetrical CPC that accepts all light incident between 10° and 60° from the horizontal.

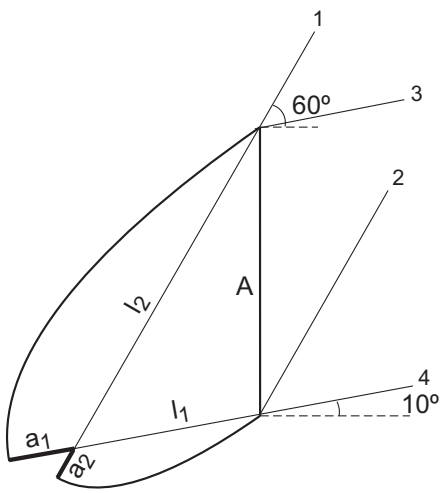

Figure 3.10 *Asymmetrical CPC with acceptance angles 10° and 60°.*

The concentration ratio of an asymmetrical CPC is different from that of the symmetrical CPC since the interval of acceptance is asymmetrical around the normal to the aperture. The concentration ratio of an ideal

asymmetrical CPC is defined by Equation 3.4. Note that the angle is positive for both the upper and lower limits in Figure 3.10.

$$C_{\max} = \frac{2}{\sin(\theta_1) - \sin(\theta_2)} \qquad \text{Equation 3.4}$$

It can be derived using Fermat's principle which states that the path lengths of ray 1 and ray 2 in Figure 3.10 have to be equal, and the same applies to the path lengths of ray 3 and ray 4. For ray 1 and ray 2 this leads to:

$$l_2 + a_2 = l_1 - a_1 + A\sin 60$$

For ray 3 and ray 4 the equation is:

$$l_2 - a_2 = l_1 + a_1 + A\sin 10$$

Subtracting the two equations yields:

$$2a_2 = A\sin(60) - A\sin(10) - 2a_1$$

$$2(a_1 + a_2) = A(\sin 60 - \sin 10)$$

$$C = \frac{A}{a_1 + a_2} \Rightarrow C = \frac{2}{\sin 60 - \sin 10} = 2.89$$

The maximum flux concentration of an asymmetrical CPC is $2/\tan(\theta_{max}/2)$ (Mills and Giutronich 1978) where θ_{max} is the interval of acceptance. The interval of acceptance in the example of Figure 3.10 is equal to 60°-10°=50° and the maximum flux concentration is thus 2/(tan(50/2))=4.29. This occurs at the extreme angles of incidence 10° and 60°. The maximum limit can only be obtained if the absorber is placed along the optical axis of the parabola; in all other cases it will be lower.

3.7 Asymmetrically truncated CPCs

Figure 3.11 shows an example of a stationary, asymmetrically truncated wedge-CPC, the MaReCo (MaximumReflectorCollector) which is designed to be placed on a horizontal surface. It is symmetrical in the sense that both parabolic mirrors have the same focal distance and focal point, indicated by *f* in the figure. However, it is truncated asymmetrically to

collect as much irradiation as possible per reflector area at Swedish latitudes (Rönnelid and Karlsson 2003). Another change from the classic wedge-CPC is that one of the absorbers has been removed and the remaining one has been designed to accept irradiation on both sides. The irradiation will reach the absorber on both sides due to the circular section inserted between the endpoints of the two parabolas, indicated by *B* and *C* in the figure. The circular section will always reflect all incoming irradiation onto the absorber.

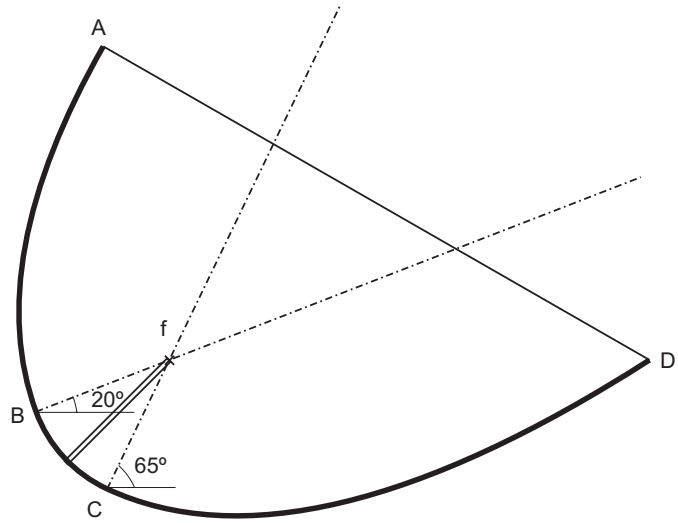

Figure 3.11 *Stand-alone MaReCo, a stationary asymmetrically truncated wedge-CPC. Both parabolas have a common focal point in f. The acceptance interval is between 20° and 65°.*

Since the yearly irradiation is incident in an asymmetric angular interval, where most of the light arrives in the summer at high solar altitudes, the front reflector is larger than the back reflector to collect as much annual irradiation as possible. A system such as this is ideal; it collects all light incident between solar altitudes of 20° and 65° i.e. the tilts of the back and front reflector. Depending on the angles at which the irradiation maxima occur, and the way the irradiation is distributed during the year at different latitudes, the length and the tilt of the reflectors will change and create other asymmetrical forms for other latitudes.

As the concentrator is ideal before truncation, the concentration ratio should be $1/\sin(\theta_{max})=1/\sin((65-20)/2)=2.61$ but due to the truncation, the geometrical concentration ratio is 2.5.

One interesting option is to remove one of the reflectors. If the back reflector is removed it is possible to make a concentrator that works well for high solar altitudes. If the front reflector is removed, it is possible to integrate the concentrator into a façade without using too much space. As less irradiation is incident on a vertical surface than on a horizontal surface, the back reflector collects less light but this could in many cases be compensated for by the fact that it is easy to integrate into a building. Figure 3.12 shows an asymmetric concentrator where the front reflector has been removed and the absorber has been turned slightly.

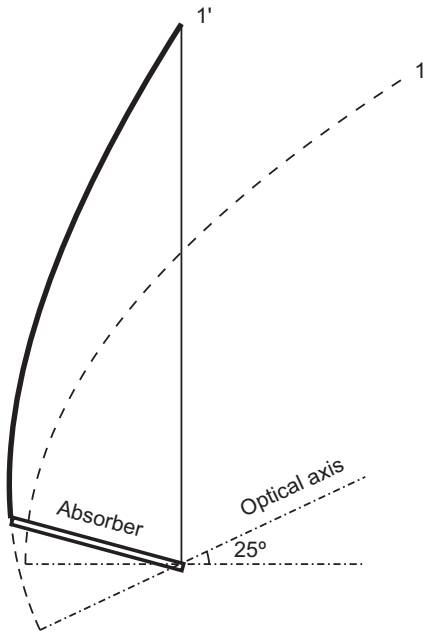

Figure 3.12 *Back reflector concentrator for wall integration. The parabola is tilted 25°, which is the lower acceptance limit of the concentrator.*

As can be seen in the figure, the parabola has been rotated 25° which means that the system accepts irradiation at solar altitudes above 25°. This example is easy to fit into a wall element due to its small width compared with its height.

4 Modelling of solar cells

4.1 Basic models

In order to simulate the electrical characteristics of solar cells, different circuit models are used depending on the level of detail in the simulations, and on the characteristics that need to be studied. One of the most simplified circuit models of the solar cell is shown in Figure 4.1. It consists of a light dependent current generator, I_L, and a diode, D, connected in parallel with the generator.

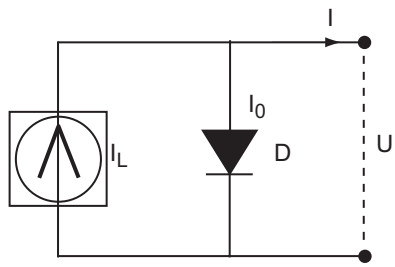

Figure 4.1 One diode model of a solar cell.

The current, I, is:

$$I = I_L - I_0\left(e^{\left(\frac{qU}{kT}\right)} - 1\right) \qquad \text{Equation 4.1}$$

T is the cell temperature and the parameters of the equation are defined in Figure 4.1.

When light is incident on a photovoltaic cell, the charge carriers are transported to the contacts by the electrical field in the depletion region of the cell. When a voltage is applied across the cell, e.g. when a load is connected to the cell, the field is reduced. This increases the recombination rate in the cell, and the current decreases since fewer charge carriers

are transported to the contacts. In the circuit model shown in Figure 4.1 an increased voltage U over the cell causes more current to go through the diode instead of through the load which decreases I.

This simple circuit model is enough to describe the cell output characteristics for most applications. When slightly more detailed modelling of the cell is needed; the two diode circuit model is used. This is shown in Figure 4.2.

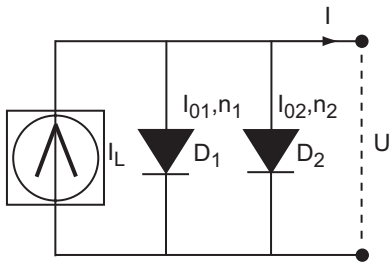

Figure 4.2 Two diode model of solar cell.

In the two diode circuit model, the recombination that limits the current I is modelled with two diodes instead of one. D_1 represents the recombination in the neutral region of the cell and the ideality factor, n_1, is set to 1. D_2 models the recombination in the depletion region, where the ideality factor, n_2, equals 2.
To describe the intrinsic resistance of the cell, a slightly larger equivalent circuit model of the cell is used. Figure 4.3 illustrates this circuit for the one diode model.

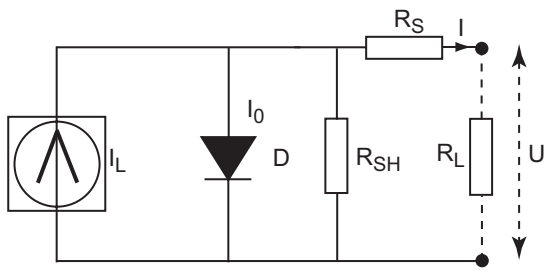

Figure 4.3 Equivalent circuit representing a solar cell.

The current through the load, I, for this circuit is:

$$I = I_L - I_0\left(e^{\frac{q(V+IR_S)}{nkT}} - 1\right) - \frac{V + IR_S}{R_{SH}} \qquad \text{Equation 4.2}$$

where I_L is the light generated current of the cell, R_{SH} the shunt resistance, and R_S the series resistance.

The series resistance R_S represents the bulk resistance of the semiconductor material, the resistance of the metallic contacts and interconnections, and the resistance between the semiconductor and the contacts. The shunt resistance R_{SH} represents the impurities and defects around the PN-junction of the cell. If the series resistance of the cell is high, the voltage across the load R_L decreases and this reduces the output power. If the shunt resistance is low, some of the charge carriers will go around the PN-junction instead of being transported by the field to the cell contacts.

The equivalent circuit model in Figure 4.3 assumes that the resistance is evenly distributed over the whole cell, the temperature distribution is uniform over the cell, and the cell is illuminated uniformly. When these conditions are not present, more complicated models are needed.

4.1.1 Two dimensional modelling of non-uniform characteristics of solar cells

A common approach to a more detailed model of the solar cell is to divide it into smaller elements. The idea is that if the elements are made appropriately small, the cell's electrical characteristics can be modelled in arbitrarily high detail. The number of elements and the dimensions of each element are decided by the problem studied. A suitable element division for modelling the non-uniform characteristics of the solar cell is shown in Figure 4.4.

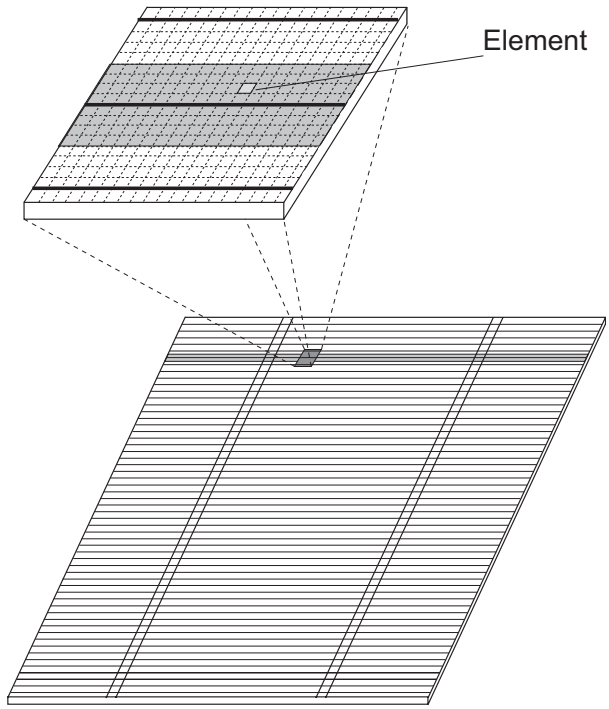

Figure 4.4 *Solar cell divided into small model elements. The expanded top part of the figure shows a model element located in the strip segment marked in grey in the lower part of the figure.*

The cell is first divided into strip segments. Each strip segment contains one finger, and runs along the full width of the cell. The figure shows one strip segment highlighted in grey. Each segment is in itself divided into elements as shown in the figure.

The elements have to be small enough to describe the non-uniform parameter. If e.g. the model is to be used for non-uniform irradiation distributions over the cell, the size of the elements determines the resolution of the light distribution. If it is used to model partial shading from a rectangular object, 2-4 elements within the strip segment might be enough, and if the irradiation distribution comes from a three dimensional concentrator, the number of elements has to be very high in order to describe the irradiation profile on the cell. Each element is modelled by an equivalent circuit which is connected to adjacent elements. Since each element is modelled separately, it has its own set of parameters, e.g. shunt resistance, series resistance etc.

When all elements have been connected, the full model of the solar cell becomes a large electrical circuit. Since the complete circuit for a detailed model of the cell is very large, the circuit analysis is most often solved using a numerical method. The most common software used is SPICE (SPICE 2007). It is a general-purpose circuit simulation program for linear and non-linear analysis of circuits. It is an open-source software which means that it is free to download for anyone. SPICE is published by the Electrical Engineering and Computer Sciences Department of the University of California at Berkeley.

4.2 Performance limitations of solar cells

4.2.1 Effects of increasing temperature

The band gap of the semiconductor material decreases when the temperature increases. When the band gap is decreased, more photons will have enough energy to excite an electron to the conduction band, and a larger part of the light spectrum can be utilized. This will lead to an increasing short-circuit current. A commonly used value for silicon cells is an increase of 0.06%/K.

When the temperature is increased, the recombination rate in the cell increases. This reduces the electrical field in the depletion region, which means that the open-circuit voltage, V_{OC}, is reduced. The decrease is approximately 0.3%/K for silicon cells (Würfel 2005).

The fill factor, *FF*, represents output losses due to parasitic resistances. It is to the first order only a function of the open-circuit voltage and it decreases as V_{OC} decreases with increasing temperature (Green 1998). The fill factor decreases by 0.15%/K for a standard silicon cell.

The efficiency η_{cell} is proportional to $I_{SC} \cdot V_{OC} \cdot FF$ and this results in a decrease in the efficiency by 0.4%/K. It is therefore of great importance to keep the cells as cold as possible, especially in concentrator systems where the temperatures can be high if cooling is not taken into account when the system is designed.

4.2.2 Effects of increased irradiation

The short-circuit current increases linearly and the open-circuit voltage increases logarithmically with increasing intensity. I_{SC} is a linear function of the light generated current I_L which is proportional to the photon flux incident on the cell. V_{OC} is proportional to $\ln(I_L)$. In principle, this shows

that increased irradiance increases the efficiency of solar cells. However, the internal losses in the cell are proportional to the square of the current, RI^2, and the output power of the cell is proportional to VI, i.e. Iln(I)- RI^2. Figure 4.5 shows the relationship between cell efficiency and homogeneous light intensity of a standard monocrystalline silicon solar cell.

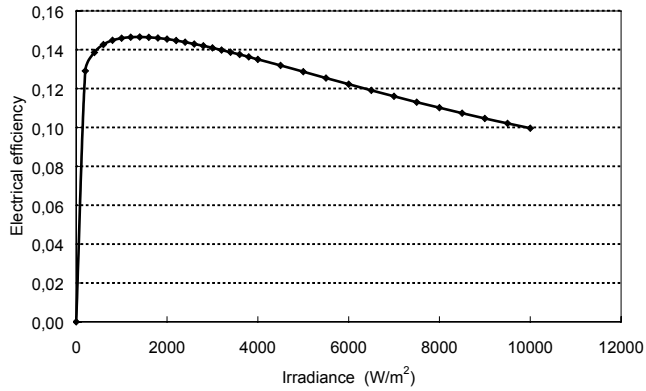

Figure 4.5 Cell efficiency as a function of the incident irradiance.

As can be seen in the figure, the efficiency increases with increasing irradiance at low irradiance levels since the resistive losses are small here. At an irradiance level of 1400 W/m^2 the increase in resistive losses is equal to the efficiency increase due to the light generated current. That is the optimum irradiance for this particular solar cell. As the irradiance continues to increase, the resistive losses increase more than the delivered power and the efficiency drops. For this particular cell, the efficiency drops by 32% when the irradiance rises from 1400 W/m^2 to 10 000 W/m^2.

The optimum irradiance level will increase if the series resistance of the cell is reduced. This is achieved in concentrator cells by decreasing the spacing between the conducting fingers, using a low resistance substrate for the cell, and introducing a back surface field (highly doped back substrate). This will lower the bulk and contact resistances. Using techniques like these makes it possible to manufacture cells optimized for several hundred suns. For more moderate irradiance levels, it is often enough to increase the number of fingers to improve the electrical output.

4.2.3 Effects of non uniform irradiance

The light distribution on the cells in a concentrator is often non uniform. This is true for example for the most commonly used type of stationary concentrators, the compound parabolic trough concentrator. The light incident on such a system is concentrated to a narrow line of high irradiance which can often be 25-30 times the solar beam. At such high light intensities, the problems discussed in the previous section are accentuated. This leads to large resistive losses in cells under non uniform irradiance.

In order to show how the width of the line of high irradiance affects the cell efficiency, simulations with different line widths were performed using a two dimensional solar cell model. The average concentration ratio was 3.5X at all line widths, and the light distribution within the line was rectangular. The irradiance outside the line was constant at 800 W/m^2. The reason for an average concentration ratio of 3.5X is that this is a typical geometrical concentration ratio of stationary low concentration systems.

Figure 4.6 shows the relation between the width of the line of high irradiance and the simulated electrical efficiency. The electrical efficiency was normalized to 1 in order to show the effects more clearly.

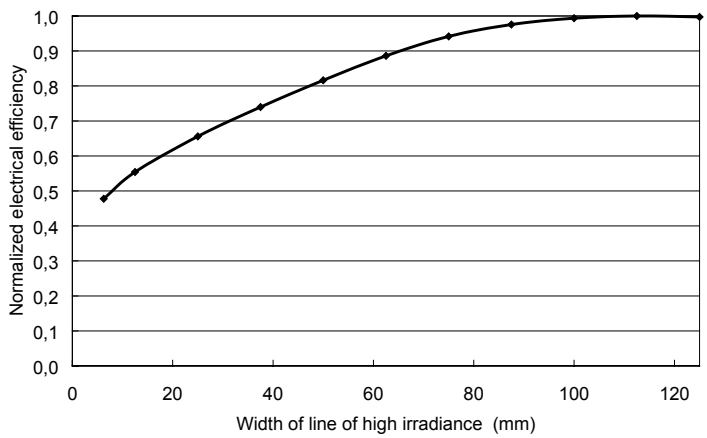

Figure 4.6 *Normalized electrical efficiency of a standard monocrystalline silicon cell as a function of the width of the line of high irradiance at 3.5X average concentration ratio. The electrical efficiency was obtained through simulations.*

As can be seen in the figure, the cell efficiency is reduced by approximately 40% compared to uniform irradiance when the line width is 20 mm. Since this is a common line width of the current generation of concentrators, it shows that the non uniform irradiance distribution has a significant effect on the solar cell output.

5 Monte Carlo ray tracing

The concept used when optical systems are analysed and designed is called geometrical optics. It studies the path of a ray of light as it traverses the optical system.

A ray of light travels through the system and the path of the ray is defined by the origin of the ray and the reflections and refractions along the path to the exit aperture. Irradiation incident on the system follows the path of the ray which makes the concept useful for understanding the characteristics of the optical system.

When it strikes a surface, the ray can be reflected, absorbed, or transmitted. The law of reflection states that the angle between the surface normal and the incoming ray is equal to the angle between the surface normal and the exiting ray. For refraction, the expression is different since it involves the relative speed of light in the new material. Figure 5.1 shows the relation between the ray incident on the surface and the ray leaving the surface for both reflection and refraction.

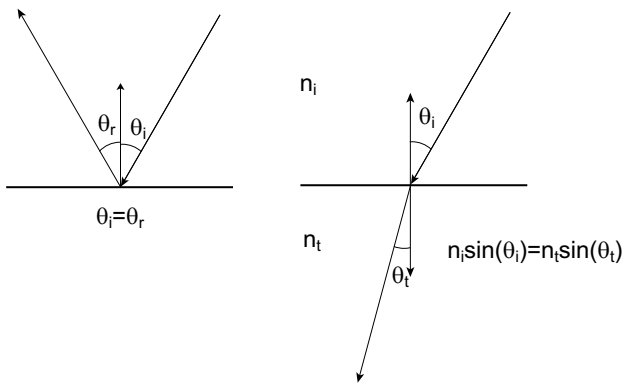

Figure 5.1 *The laws of reflection and refraction. The rays are refracted towards the normal if $n_t > n_i$.*

Monte Carlo ray tracing is the process of using the principles of geometrical optics as a statistical method to get a complete and statistically viable analysis of an optical system. The method will be briefly described in the following.

In three dimensional ray tracing it is necessary to formulate the equations of geometrical optics in vector form, which has been done in Equation 5.1. The geometrical proof can be seen in Figure 5.2.

$$\boldsymbol{r}_t = \boldsymbol{r}_i - 2(\boldsymbol{n} \cdot \boldsymbol{r}_i)\boldsymbol{n} \qquad \text{Equation 5.1}$$

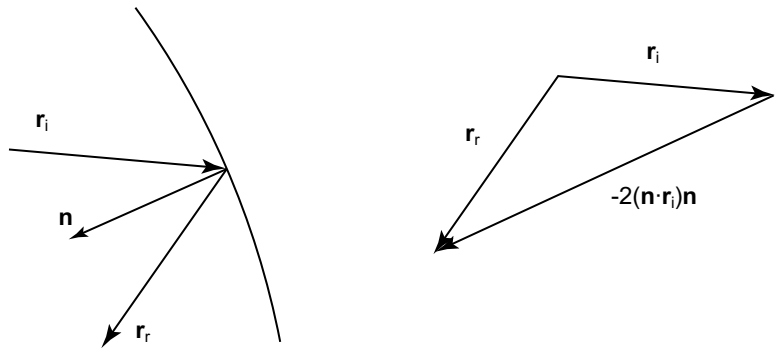

Figure 5.2 Vector formulation of the law of reflection.

In the process of tracing one ray, the starting point is randomized within a certain start area or volume, which is called the *source* of the rays. Depending on the properties of the source, the direction of the ray can be either the same for all rays or randomized in a pattern defined by the source. It could for example be a Gaussian source or a completely diffuse source. The next step is to find the first intersection between the ray and the optical system. It is calculated knowing the origin and the direction of the ray, as well as the geometry of the traced object. At the point of intersection, the surface normal is determined in order to calculate the direction of the ray after interaction with the system. The ray can be reflected, refracted, and/or absorbed. When the new direction of the ray/rays has been calculated, the next intersection is calculated. This process continues until either the ray is lost from the system, completely absorbed, or intersects with the *target* that detects the ray.

The resolution of the detector is an important parameter in the simulation as it is closely connected to the number of rays that has to be traced to obtain a certain statistical accuracy.

The number of rays that needs to hit the detector is calculated according to Equation 5.2:

$$NumberOfRays = \frac{NumberOfPixels}{Accuracy^2} \qquad \text{Equation 5.2}$$

If e.g. the detector has 10 pixels and the desired accuracy at the detector is 1% then the number of rays hitting the detector has to be $10/0.01^2$=100 000 rays.

The ray tracing simulations presented in this thesis have been performed using ZEMAX (ZEMAX 2005), a commercial ray tracing package. The two main benefits in using a commercial software compared with a problem specific Matlab program are that it is easier to simulate different kinds of systems with different characteristics and that the commercial package is well tested and documented. A well tested software can be trusted to give good results as long as the inputs are verified. To go through this process of verification for a new Matlab program is very time consuming. A commercial ray tracing package is generic in the sense that most of the parameters can be changed easily. As it is not made for a specific system or geometry, most geometries can be evaluated. It also has numerous libraries of sources, ways to display output data etc.

6 Modelling of the effects of non uniform irradiance distribution on solar cells

6.1 Electrical model

Non uniform irradiance distribution has been identified as the largest source of losses for parabolic concentrating systems with standard PV cells. Standard cells are optimized for uniform one sun irradiance. If the distribution is uniform, the cells should perform well for irradiance up to three or four suns which was discussed in Section 4.2.2. The low price of these cells compared to concentrator cells makes them ideal for low concentration systems. Owing to their ability to collect irradiation from a large spectrum of incidence angles, parabolic low concentrating systems are a common choice for low concentration systems. However, the parabolic reflector produces a very non uniform irradiance distribution on the cells, and this is the main reason for the high losses.

In order to study the effects of non uniform light distribution on solar cells, a numerical electrical model of the solar cell was used. The model was originally developed by Foss (Foss et. al. 2006) and was modified to take into account a non uniform irradiance distribution. It is a two dimensional electrical model such as described in Section 4.1.1. The division of the cell into elements is shown in Figure 6.1.

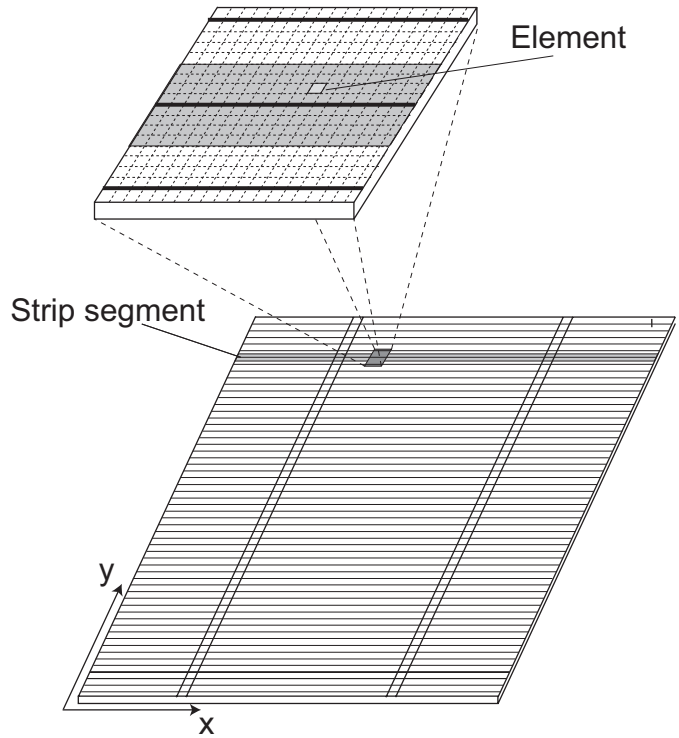

Figure 6.1 *The solar cell divided into strip segments and elements. Also shown is the coordinate system used to explain the model.*

The cell was first divided into strip segments. Each strip segment contained one finger. Since the light distribution in the translationally symmetric stationary concentrators is uniform in the y-direction, it was only necessary to simulate one strip section and multiply by the number of sections to model the full cell.

Each strip segment was separated into elements, which all consisted of an equivalent circuit model as is shown in Figure 6.2.

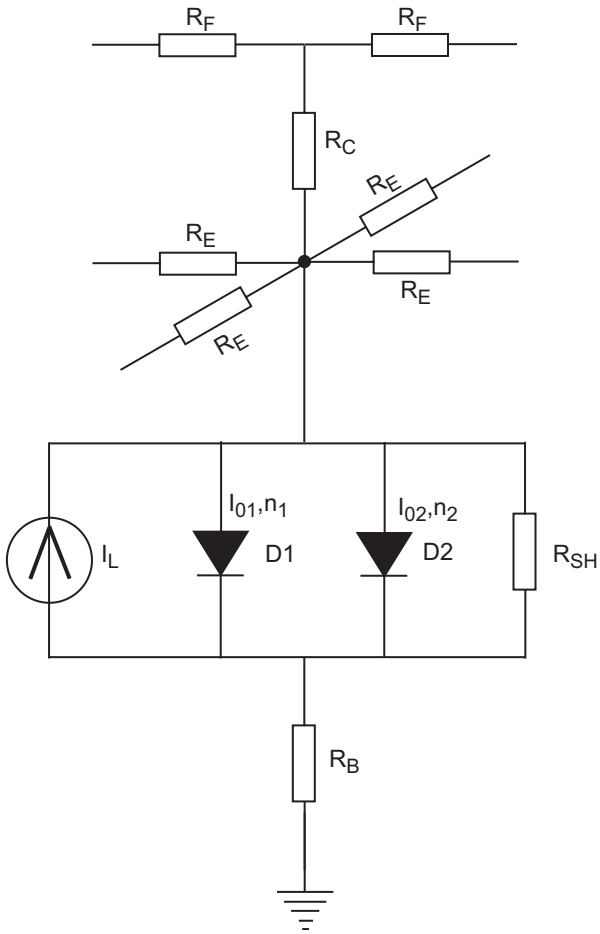

Figure 6.2 Circuit model of one element.

Each element consisted of a two diode model of the cell which was connected to the back of the cell and to adjacent elements. The non uniform light distribution on the cell was modelled by a light dependent current source. Since each element received different amounts of irradiation, the current I_L was different for each element. The diode *D1* modelled the recombination in the neutral region of the cell and diode *D2* modelled the recombination in the depletion region. The diode circuit was connected to the back of the cell with a resistor R_B which modelled the bulk resistivity. Depending on the position of the element, it was connected to two to four neighbouring elements through resistors R_E. If the element was adjacent to one of the bus bars, it was connected to the bus bar instead of

an adjacent element. Due to the relatively low resistance of the bus bar, its resistance was neglected. Elements adjacent to fingers were connected to the finger through a resistance R_C and each element section of the fingers was modelled by a resistance R_F.

The shunt resistance, R_{SH}, the short circuit current, and the saturation currents, I_{01}, and I_{02}, were obtained from a model fit of current-voltage measurements on the specific cell using IVFit (Burgers et. al 1996). The current-voltage characteristics were measured at reference conditions, i.e. an irradiance of 1000 W/m^2 at 20°C, and the software identified the model parameters based on this measured data.

The diode ideality factors, n_1 and n_2, were chosen as 1 and 2 in order for the diodes to model the recombination in the neutral region (*D1*) and recombination in the depletion region (*D2*). The emitter sheet resistivity, ρ_E, and the resistivity of the base resistor, ρ_B, were taken from a publication on a previous study of silicon cell modelling (Foss et. al. 2006). The contact resistivity, ρ_C, was taken from Schroder and Meier (1984) and the finger resistance, ρ_F, was taken from Franklin and Coventry (2002).

Each strip segment was divided into 60 elements in the x-direction and 10 elements in the y-direction. This resulted in elements of 2 mm x 0.02 mm. The number of elements in the x-direction determines the resolution of the light distribution. This means that the model was able to simulate the light distribution with a resolution of 2 mm. This was shown to be enough for the optics used in the stationary concentrator systems. The number of elements in the y-direction models the current transport to the fingers. A high number of elements in this direction highlights the difference between current being generated at the midway between the two fingers and current generated very close to a finger.

The method was used to simulate the effects of non uniform irradiance distribution on a standard monocrystalline solar cell. Using the measured characteristics for the cell at reference conditions, an irradiance of 1000 W/m^2 at 20°C, IVFit was used to obtain the cell parameters. The parameters used in the simulations are shown in Table 6.1.

Table 6.1 Model parameters used in modelling a monocrystalline silicon cell

Parameter	Value
I_L	37 mA/cm^2
I_{01}	1.79e-9 mA/cm^2
I_{02}	7.14e-5 mA/cm^2
n_1	1.0
n_2	2.0
ρ_F	0.6 Ω/cm
ρ_C	0.01 Ωcm^2
ρ_B	1.5e-4 Ωcm^2
ρ_E	38 Ω/□
R_{SH}	11.7 Ω

6.2 Circuit simulations

To simulate the current-voltage characteristics of the full circuit model, e.g. the model discussed in the previous section consisting of 29 000 elements, requires solving a large system of non-linear equations. One possible way to solve it is to use a general purpose non-linear equation solver. However, the EECS Department of the University of California at Berkeley has developed a tool for large circuit analysis. This tool is available free for download. The tool is called SPICE. It is a general-purpose circuit simulation program for linear and non-linear analysis (SPICE 2007). The input to the tool is a text file that specifies the circuit, the kind of analysis that will be performed, and the conditions under which it will be performed. Since the current generator, I_L, in each element is dependent on the irradiation incident on the element, a program was developed for generating the full SPICE circuit file. Using a set of solar cell parameters located in a file and an irradiance distribution file as inputs it generated the circuit file to be simulated by SPICE.

The most useful relationship to describe the operation of the solar cell is its current-voltage characteristics. This was therefore simulated in SPICE by calculating the current through the load of the circuit for a large number of voltages over the load.

6.3 Model validation

The model was validated for a number of light distributions. Measured light distributions and IV-characteristics were compared with simulated IV-characteristics for the same distributions. Figure 6.3 shows two different light distributions, one at 1000 W/m^2 uniform irradiance , and one highly non-uniform light distribution with a peak irradiance of 35 000 W/m^2.

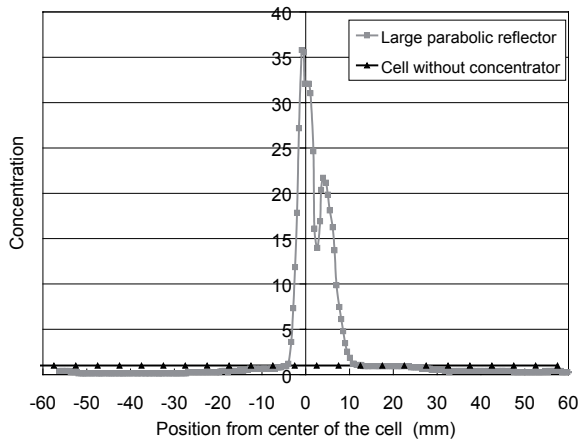

Figure 6.3 Measured light distributions used in the model validation.

The non uniform light distribution was obtained by using a large parabolic reflector to illuminate the cell. A benefit of using a parabolic reflector to create the light distribution was that it creates a distribution that is relevant to solar concentrators. The distribution shown in Figure 6.3 is a typical distribution resulting from a highly specular parabolic reflector.

Using the cell parameters of Table 6.1, and the light distributions of Figure 6.3, the IV-characteristics were simulated. Figure 6.4 shows a comparison between the measured IV-characteristics and the modelled characteristics.

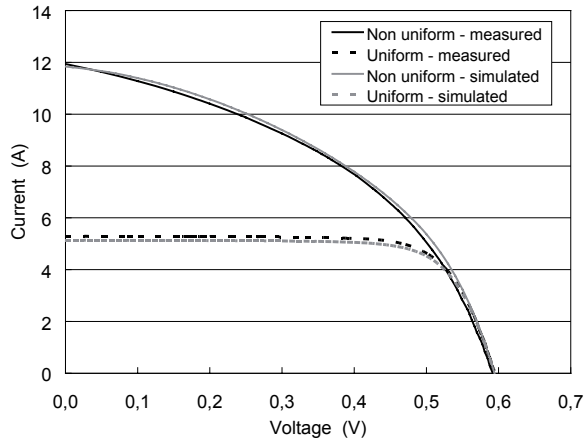

Figure 6.4 *Measured and simulated IV-characteristics for a monocrystalline silicon solar cell under the irradiance conditions of Figure 6.3.*

As can be seen in the figure, the fill factor is significantly reduced for the non uniform light distribution. This is very typical for parabolic concentrators with standard PV cells and it shows that the cells were optimized for uniform one sun irradiance.

As the figure shows, the measured data and simulated data shows good agreement for both the uniform and non uniform irradiance distributions. The fill factor differs by 2.5% for the non uniform distribution, and by 1.0% for the uniform distribution. The short circuit current differs by 1.0% for the non uniform distribution, and by 3% for the uniform distribution. The open circuit voltage is identical within 1% for both irradiance distributions. These figures show that there is good agreement between measured and simulated data.

7 Measurements

7.1 IV characteristics and fill factor

The performance of a photovoltaic cell can be characterised by its current-voltage (IV) characteristic. It describes the relationship between the current extracted from the cell and the voltage across the cell as the resistive load connected to the cell changes. The IV characteristics of PV cells in a concentrator are highly dependent on the concentrator. They are influenced both by the total irradiation on the cells and by the way the light is distributed over the cells. If the concentrator is to be used for photovoltaic applications it is important to measure these characteristics in the concentrator to be able to estimate the efficiency of the complete system.

The characteristics were measured with two different methods. In the first method, an electronic load controlled by a data logger was constructed for the measurements. The electronic load is described in more detail in Appendix A. The data logger sent control signals to the electronic load that was connected to the cells. The load was able to vary the voltage over the cells from 0 to V_{OC} in approximately 100 ms. The current and voltage over the cells were measured simultaneously with a CR-10 data logger from Campbell Scientific. Nine current and voltage pairs were recorded in each measurement. The points were not evenly distributed between 0 and V_{0C}, the majority of the points were taken around the maximum power point. The maximum power point was calculated through a parabolic fit to the three points closest to the maximum power point.

In the second method, the current-voltage characteristics were measured using a box containing 16 resistors. The box was connected to a CR-10 data logger, as in the previous method, and the data logger controlled the resistance of the box. The resistors were each a multiple of each other, each one was 2.04 times larger than the previous resistance. The large number of resistors made it possible to measure over a very large resistance range. Only 8 of the 16 resistors could be utilized at the same time, which limited the range slightly, but since the interval was set depending on the number of solar cells to be measured, this was not a problem in practice. The data logger controlled the box resistance by sending 8 bits to the

box. Depending on the setting of the bits, electric relays combined three resistors to achieve the desired box resistance. Due to the high resolution of the box resistance it was possible to record a large number of current-voltage points for the cells when the current-voltage characteristics were measured. This high resolution was important when measurements were made under conditions when the fill factor was reduced due to unfavourable irradiance conditions.

Figure 7.1 shows an example of an IV-characteristic measured with the electronic load.

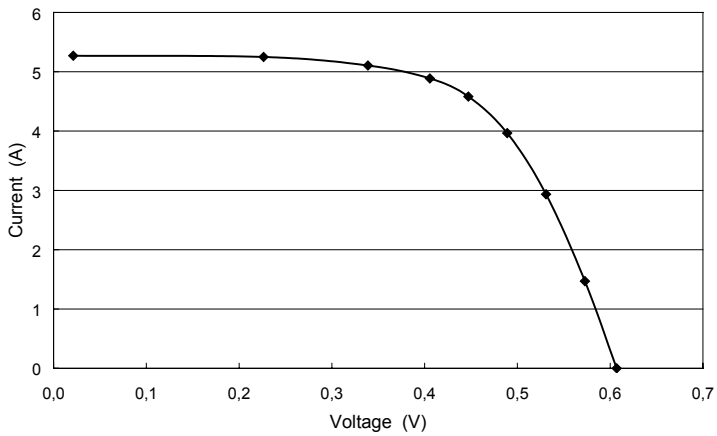

Figure 7.1 IV-characteristic for one cell measured with the electronic load.

Since the short circuit current is proportional to the irradiation, it is important to record the incident irradiance during the measurements. The irradiance was measured using a pyranometer from Kipp & Zonen. The surface of the pyranometer was mounted normal to the sun.

The efficiency of the cells is proportional to the fill factor, which is calculated at the maximum power point. A high fill factor translates into a high efficiency. The fill factor was calculated according to Equation 7.1 where I_{SC} is the short-circuit current, V_{0C} is the open circuit voltage and P_{max} is the power at the maximum power point.

$$FF = \frac{P_{\max}}{I_{SC} \cdot V_{OC}} \qquad \text{Equation 7.1}$$

Figure 7.2 shows typical current voltage characteristics of one cell with a high fill factor and one cell with a low fill factor.

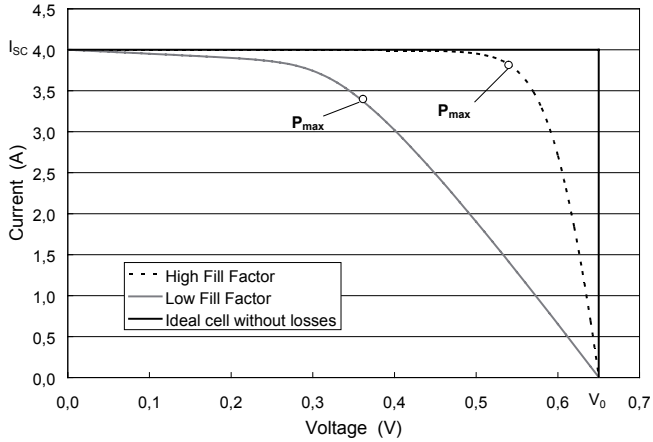

Figure 7.2 *Current-voltage characteristics for two photovoltaic cells. The full line shows an ideal cell without losses. The short-circuit current, open circuit voltage, and the maximum power point are indicated.*

The fill factor for the dashed curve is 0.79 and for the curve labelled Low Fill Factor it is 0.47. The fill factor of the cells in a concentrator is highly dependent on how the light is distributed on the cells; high irradiance levels on small parts of the cell reduce the fill factor considerably. Since the efficiency of the system is proportional to the fill factor, it is important to monitor the fill factor of the PV cells in a parabolic concentrator.

7.2 Optical efficiency

The photovoltaic cells used in the measurements were CIGS thin film cells, polycrystalline silicon cells, and monocrystalline silicon cells.

The short-circuit current of the used photovoltaic cells is independent of the illumination distribution on the cell as long as the strip of light is not very narrow (< 1 mm) (McMahon and von Roedern 1997). Because of the divergence of 0.27° for the solar beam, and the manufacturing precision of the troughs, the concentrated strip of light has a width of approximately 1 cm at maximum concentration. This is sufficient for the short-circuit current to be independent of the irradiance distribution.

The short-circuit current increases with the temperature by approximately 0.06 %/K (Wenham, Green and Watt). In view of other errors in

the measurements, this increase can be neglected for the small temperature increases of the low concentration systems monitored.

Since the short-circuit current of a photovoltaic module in a concentrating system, at a constant temperature, depends only on the irradiation on the module, which is determined solely by the optical efficiency of the concentrator, measurements of the short-circuit current as a function of the angle of incidence can be used to determine the optical efficiency of the concentrator system if it is compared with the short circuit current of a reference module. The reference cells should be identical to the cells used in the concentrator.

The optical efficiency was measured using two different techniques, one that can be used at all times of the year, and one that is used around the spring or autumn equinox. Both methods will be described in the following.

In the first method, the concentrator was placed with the sun in the meridian plane. The transverse projected angle of incidence was varied by rotating the concentrator trough. The concentrator remained in the meridian plane during the entire monitoring since the whole measurement was finished in approximately 5 minutes. The setup is described by Figure 7.3.

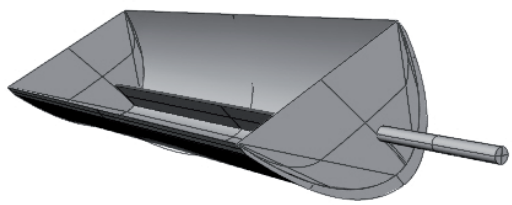

Figure 7.3 *Concentrator trough for measurement of the optical efficiency. The axis attached to the side of the trough is used to record the rotation of the concentrator.*

As can be seen in the figure, an axis was mounted on the gable of the trough at the focal point of the two parabolic mirrors. Between the trough and the axis there was a potentiometer that recorded the rotation of the trough as the axis was fixed at the right end in the figure. The trough was rotated around the axis with the sun in a fixed position in the meridian plane, which made it possible to measure at all transverse angles of incidence. The short circuit current was measured by a data logger that simultaneously recorded the insolation using a pyranometer mounted normal to the sun.

The data logger and the pyranometer were the same as those used in the current-voltage measurements.

A graduated arc was mounted on the side of the trough for manual recording of the transverse angle of incidence. The maximum and minimum angles of incidence were recorded with both the graduated arc and the potentiometer at the beginning of each measurement. These values were used to convert the voltage across the potentiometer into the true angle of incidence in the meridian plane.

Using the measurements of the short-circuit current, the optical efficiency of the system was calculated according to Equation 7.2.

$$\eta_{opt}(\theta_T) = \frac{I_{sc} \cdot 1000}{I_{1000} \cdot C_g \cdot G \cdot \cos(\theta_T - \beta)} \qquad \text{Equation 7.2}$$

I_{1000} is the short circuit current at an irradiance of 1000 W/m^2 on the reference module. C_g is the geometrical concentration of the concentrator system defined as the glazed aperture area divided by the cell area. θ_T is the transverse projected angle of incidence, and G is the total intensity normal to the sun. To get the efficiency relative to the incoming irradiation, the expression was divided by C_g. $G(\cos(\theta_T - \beta))$ is the irradiance on the glazing, where β is the tilt of the aperture normal relative to a horizontal surface. The measurements were performed on very clear days with a low fraction of diffuse irradiance, and the total irradiance was treated as a beam irradiance incident at the angle of incidence of the beam. This method can easily be used any time of the year as long as the trough is small and flexible enough to be rotated.

The second method requires the measurements to be conducted around the equinox. Figure 7.4 shows measurements of the angles of incidence on a south facing surface. One such measurement was performed at Älvkarleby, Sweden (60.5°N, 17.4°E) on September 23, at the autumn equinox. As can be seen from the figure, the transverse projected angle of incidence θ_T was constant at 90-latitude=30° all day. The fact that the transverse projected angle of incidence is constant around the equinox is the basis of this method.

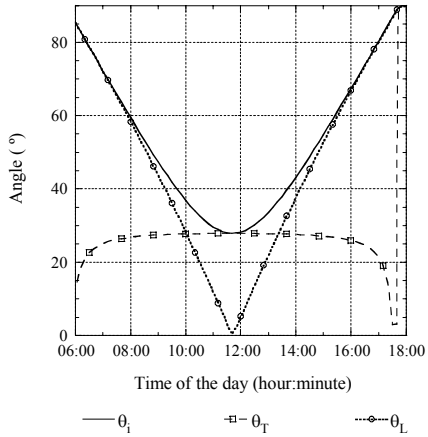

Figure 7.4 *Angles of incidence on a south facing surface during the day on September 23 in Älvkarleby, Sweden.*

At the equinox, the concentrator was rotated 90° around the North-South axis. It was then tilted to the latitude angle around the East-West axis. In this setup, the sun will move in the meridian plane of the concentrator all day, and noon will be equal to a transverse angle of 0°. A reference was mounted parallel to the aperture and the short-circuit currents of the reference and concentrator were measured with a data logger. The optical efficiency was calculated according to Equation 7.3.

$$\eta_{opt}(\theta_T) = \frac{1}{C_g} \frac{I_{SC}^{conc}(\theta_T)}{I_{SC}^{reference}(\theta_T)} \qquad \text{Equation 7.3}$$

To get an optical efficiency between 0 and 1, the measured short-circuit current was divided by the concentration ratio.
This technique requires less labour as it is completely automated; all that is required is that the system is mounted as described above.

7.3 Light distribution on the absorber

The light distribution on the cell is an important parameter for a concentrator since the output of the PV cell or thermal collector is largely

affected by this distribution. High local intensities increase the electrical and thermal losses. The electrical losses can be explained by the fact that the internal resistive losses increase with the square of the current.

The light distribution over the cells in translationally symmetric concentrators is uniform along the axis of symmetry, i.e. it is concentrated to a line along the length of the trough. The cells are placed series connected on this line. It is thus enough to record the distribution in the transverse direction over the cells to make a full measurement of the light distribution as long as there are no large deviations from the translational symmetry. A device, which is shown in Figure 7.5, was constructed for measuring the light distribution.

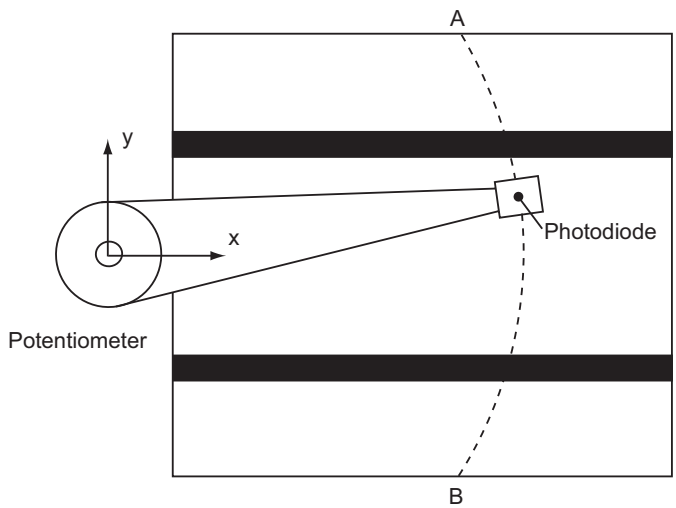

Figure 7.5 *Device for measuring the irradiance distribution over the cells. The lever has a photodiode for measuring the light intensity at one end and is mounted to a potentiometer on the other.*

The device consists of a lever with a photodiode mounted on the tip. It was placed on the cells in the trough, in the plane of the cells. The lever was rotated along the cell surface from *A* to *B* during one distribution measurement. A plate with a small hole was glued over the photodiode to increase the resolution of the detector as the resolution gets higher when the measuring aperture decreases. The centre of rotation for the lever was a potentiometer that recorded the rotation angle of the lever.

The measurement started by measuring the voltage of the potentiometer for point *A* and point *B* to get a conversion factor from potentiometer voltage to angle. The lever was then slowly swept over the surface of the

cell while a data logger recorded the voltage across the potentiometer and the current from the photodiode. The y position for each intensity point was then calculated knowing the length and the angle of the lever. Figure 7.6 shows a typical measured irradiance distribution over the cell.

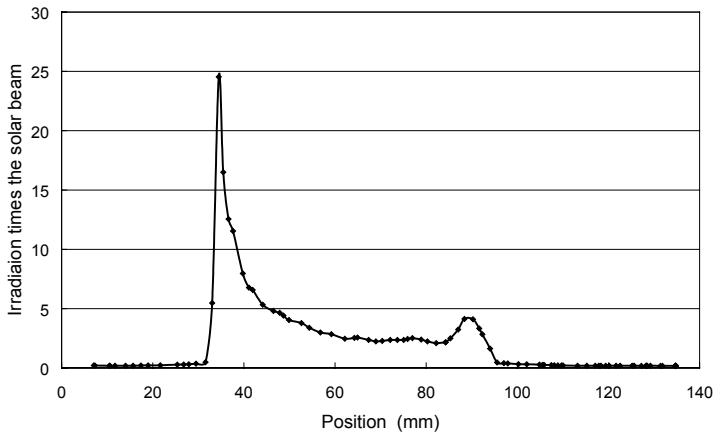

Figure 7.6 *Irradiance distribution over the cell in a MaReCo concentrator. The position on the x-axis is measured from the focal point at the top of the absorber.*

The importance of having a high spatial resolution in the irradiance measurement can clearly be seen in the figure as the irradiance peak is very narrow.

7.4 The effects of non uniform irradiance distribution

The non uniform irradiance distribution resulting from parabolic reflectors was identified as one of the most important reasons for the high losses in parabolic troughs. In order to design systems where this problem is addressed, it was necessary to quantify the losses at different light distributions and irradiance levels.

The electrical output was measured for one cell as a function of three different irradiance distribution variations. In the first set of measurements, the total irradiation on the cell was kept constant while the width of the light distribution was varied. Starting from a very narrow peak of

high irradiance, the peak was made wider and less intense. In the second set of measurements, the irradiance distribution remained constant while the position of the distribution was varied. Starting from one edge of the cell, the distribution was moved over the cell to the other edge. In the third set of measurements, the irradiance level was reduced gradually in a parabolic concentrator in order to enable comparisons with real systems. For each measurement, the current-voltage characteristics and the light distribution were recorded

In order to isolate the effect of non uniform light distribution on PV cells, only one cell was used for each measurement. By using one cell only, effects such as differently illuminated cells, different cell parameters or other problems could be excluded. The cell was mounted on a large aluminium plate which had a cooling fan mounted on the back. This was done in order to eliminate the temperature effects as much as possible.

For the two first sets of measurements, the light source creating the light distribution was a cylindrical halogen lamp that was placed at one of the focal points of an elliptical reflector trough. The cell was placed as close as possible to the second focal point in order to achieve maximum concentration. To limit the exit aperture of the lamp, a reflective screen was placed in the plane of the second focal point. The setup is shown in Figure 7.7.

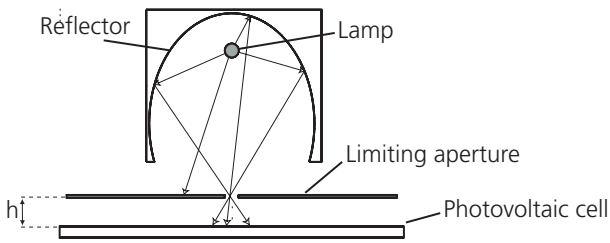

Figure 7.7 *Measurement setup. The light rays illustrate the elliptical mirror and the limiting aperture. h is a measure of the distance between the source aperture and the solar cell.*

For the first set of measurements, the total irradiance remained constant while the width of the light distribution was varied. This was achieved by changing the distance between the solar cell and the aperture shown as h in the figure. The first measurement was taken when the cell was close to the aperture, which created a narrow peak of high irradiance, and the distribution was widened by increasing the distance h. Figure 7.8 shows the resulting light distributions at two distances between the cell and the aperture.

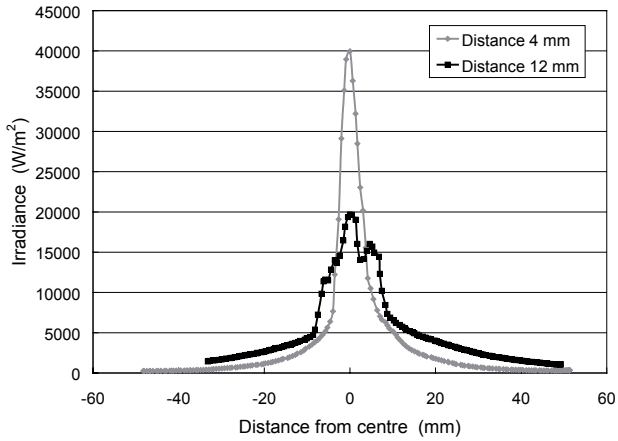

Figure 7.8 *Light distribution on the solar cell when the distance between the source and the aperture was 4 mm and 12 mm.*

As the distance between the light source and the cell was increased, a small fraction of the light directed along the trough axis of symmetry missed the cell. In Figure 7.7, this is the light going into or out of the paper between the aperture and the cell. Using a ray tracing model of the setup, the amount of light lost at different distances between aperture and cell was calculated. It was shown to be a small fraction of the total irradiation, and it was compensated for in the measurements by multiplying the recorded current values by a correction factor.

In the second set of measurements, the light source was placed 4 mm from the cell which resulted in the light distribution that can be seen in Figure 7.8. The cell was then moved, which made the light distribution move from one edge of the cell to the other edge. For all the measurements, the line generated by the lamp was kept parallel to the bus bars.

In the third set of measurements, a large parabolic reflector was used to generate a light distribution that had a very high peak irradiance. This represents the extreme case of highly non uniform irradiance from a reflector. The cell was placed at the focal point, and the light was incident along the optical axis of the reflector. The reflector was then gradually shaded to decrease the peak irradiance. However, due to irregularities in the reflector geometry, the shape of the distribution was also changed. This data can therefore only be used for validation of simulation data or to illustrate the problems of parabolic reflectors.

In all the measured cases, the IV-characteristics were recorded with a resistor box as described in Section 7.1. The irradiance distribution was measured using the technique described in Section 7.3.

8 Electrical and thermal characterization of a concentrating PV/T hybrid

A characterization of the stand-alone MaReCo was performed in order to understand and quantify the characteristics of a concentrating photovoltaic/thermal hybrid (Helgesson, Krohn and Karlsson 2004a).

The system is shown in Figure 8.1.

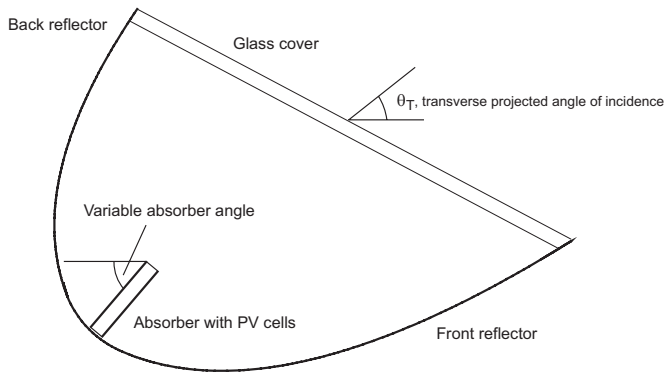

Figure 8.1 *The MaReCo PV-thermal hybrid. Both parabolic reflectors have the same focal point, at the top of the absorber. Photovoltaic cells are laminated on the absorber. The purpose of the glass cover tilted at 30° is to protect the absorber and reflectors. The absorber angle is the angle between the absorber and the horizontal. Also shown is the transverse projected angle of incidence.*

The asymmetrical concentrator is intended to be placed on a horizontal surface. It is designed to collect all direct irradiation between transverse angles of incidence of 20° and 65°. The system is thoroughly described by Adsten, Helgesson, and Karlsson (2005). Two prototypes were evaluated, one with aluminium reflectors and one with aluminium laminated steel

reflectors. The aluminium trough was constructed with a variable absorber angle to make it possible to investigate the influence of the absorber angle on the electrical and thermal output. The aluminium trough had cells facing both the front and back reflector, and the steel trough had cells facing the back reflector. The series connected cells were matched to generate equal current, and since no by-pass diodes were used, it was possible to use the short circuit current as a measure of the incident irradiation. Table 8.1 describes the properties of the two prototypes.

Table 8.1 Properties of the two prototypes. The absorber angle and the description of the reflectors are shown in Figure 8.1.

	Aluminium trough	Steel trough
Cells facing back reflector	2	12
Cells facing front reflector	3	0
Absorber angle	45	20
Trough material	Anodized aluminium	Steel with aluminium coating
Length (m)	1	2

8.1 Reflector materials

MaReCo in its current design is equipped with reflectors made of anodized aluminium but this has some disadvantages. When large troughs are made, the aluminium construction tends to deviate from the profile given by the supporting gables. These deviations, which are seen mostly as dents in the reflector, create undesired reflections. This results in optical losses. It is difficult to produce the aluminium concentrators without these imperfections, and this creates an interest in investigating other materials for the reflector construction. Another problem is the thermal expansion of the aluminium reflectors. When the construction heats up during operation, more dents appear in the reflector.

A newly developed aluminium-polymer-laminated steel reflector was used in one of the troughs to investigate if this could solve the problems with the aluminium reflector. The reflector is manufactured by lamination of an aluminium coated polymer film on a steel sheet. The optical properties and durability of the new material have been investigated by Brogren (2004). The steel base of the reflector makes this material more rigid. The problems due to dents and thermal movement of the reflector were therefore to be solved by using this material. A visual inspection of the two prototypes shows a clear difference in the number of dents be-

tween the two troughs. The optical properties of the steel based reflector are different from those of the aluminium reflector, Figure 8.2 shows the reflectance of the aluminium reflector and the steel based reflector as a function of the wavelength of the incident light. The responsivity of a PV cell as a function of wavelength is also shown in the figure. The responsivity was calculated as the ratio between the current from the illuminated diode and the incident light power.

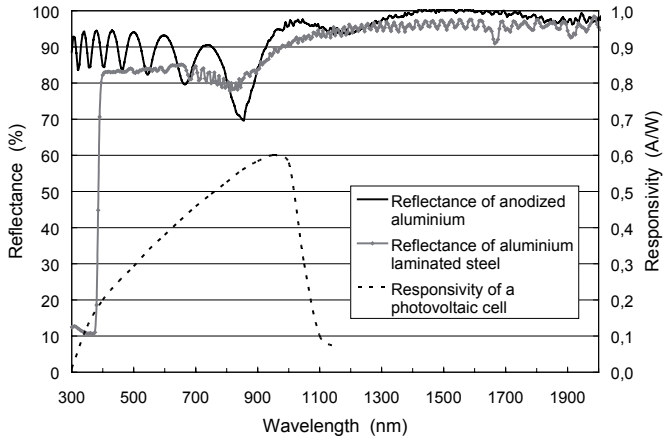

Figure 8.2 *Reflectance as a function of the incident wavelength for the two materials. The responsivity of the silicon cell as a function of the wavelength is also shown to illustrate the relevant wavelength interval.*

The reflectance of the steel based reflector is low below 350 nm due to a plastic coating which absorbs light below this wavelength. This coating is necessary as the thin aluminium film is vacuum coated on the plastic film. It also protects the aluminium surface from oxidation. The total reflectance of the aluminium reflector is higher at most wavelengths, and this influences the total amount of light collected by the concentrators. An optical property that is not visible in Figure 8.2 is that the steel based reflector diffuses the light slightly, whereas the aluminium has an almost specular reflectance.

8.2 Current-Voltage characteristics

The current-voltage (IV) characteristics of the two prototypes were measured according to Section 7.1. It is important to note that the steel based prototype only had cells facing the back reflector, and a comparison between the two materials can only be made for the back reflector.

Figure 8.3 shows the IV characteristics for the reflectors at 35° transverse projected angle. The transverse projected angle of incidence is defined in Figure 8.1. This angle of incidence was chosen to be in the optimum range for the back reflector. The voltage was normalized to show voltage/cell to enable a comparison between the two systems.

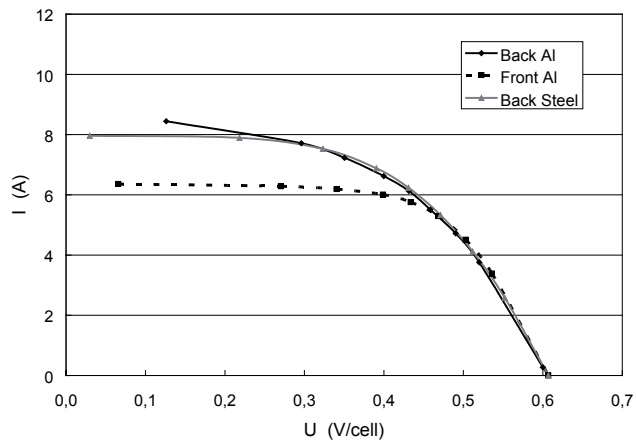

Figure 8.3 IV characteristics at 35° transverse projected angle of incidence.

As can be seen from the figure, the short circuit current of the cells facing the back aluminium reflector is higher than that of the cells in the steel based reflector trough. This is due to the lower total reflectance of the steel based reflector. Due to the partly diffusing reflections of the steel-based reflector, the cells were more uniformly illuminated which gave a higher fill factor for this prototype.

Figure 8.4 shows the IV characteristics at 57° transverse projected angle of incidence. This angle of incidence is within the optimal range for the front reflector.

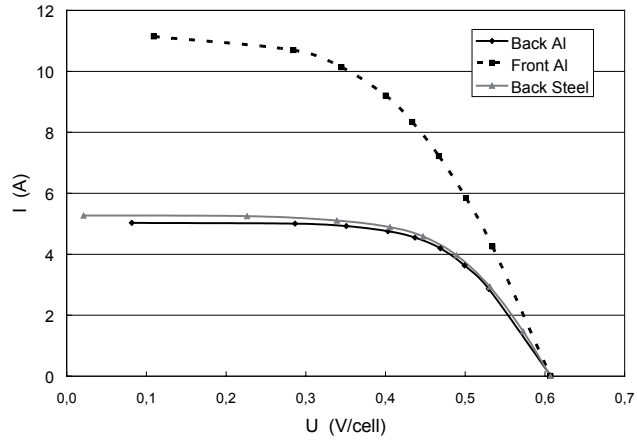

Figure 8.4 IV characteristics at 57° transverse projected angle of incidence.

As expected, the cells facing the front reflector delivered a significantly higher current in this measurement than the cells facing the back reflectors. This is due to the angle of incidence which is beneficial for the front reflector, and to the larger surface area of the front reflector compared with the back reflector.

The maximum power was calculated using a parabolic fit to the IV-curves and the results can be seen in Table 8.2.

Table 8.2 Maximum power calculated from Figure 8.3 and Figure 8.4

Angle of incidence	Back steel reflector	Back Al reflector	Front Al reflector
35°	2.7 W/cell	2.6 W/cell	2.4 W/cell
57°	2.0 W/cell	1.9 W/cell	3.8 W/cell

Interestingly, the maximum power for the steel prototype at both angles of incidence is slightly higher than the power of the aluminium back reflector. This shows that the increased fill factor compensates for the lower short-circuit current.

8.3 Short circuit current

The short circuit current was measured as a function of the transverse angle of incidence according to Section 7.2. Figure 8.5 and Figure 8.6 show the measured short circuit current and fill factor for the cells facing the back reflector.

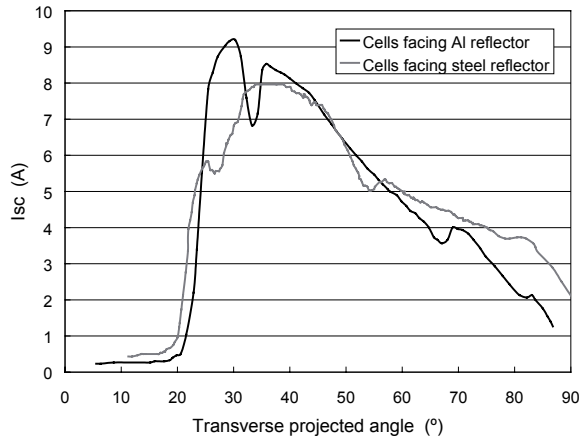

Figure 8.5 *Measured short circuit current for the cells facing the back reflectors.*

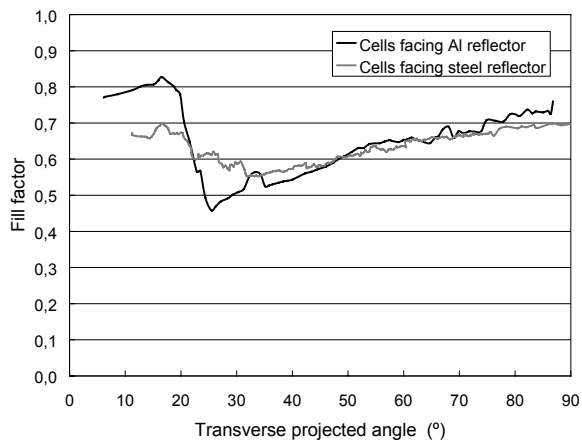

Figure 8.6 *Fill factor for the cells facing the back reflectors.*

The back reflector is designed to collect light in the winter, spring, and autumn and this is validated as the highest currents are measured at low angles of incidence.

As expected, the short circuit current of the cells in the aluminium trough is higher for most angles due to the higher total reflectance. The fact that the short circuit current of the cells facing the steel reflector is higher at large angles of incidence is due to the different absorber angles. This angle affects the distribution of light on the cells and the average number of reflections.

The fill factor is in general higher for the steel reflector system in the range where the short circuit current is high. The strip of light on the cells is slightly wider for the steel reflector trough due to the diffuse reflectance and this increases the fill factor.

The internal losses in the cell are proportional to the square of the current, RI^2, and the output power of the cell is proportional to the current, VI, where the dependence of V on the irradiance can be neglected. As the current increases when the irradiation on the cell increases, the relative losses increase more than the delivered power, and the fill factor decreases. This is discussed in more detail in Section 4.2.2.

Figure 8.7 shows the short circuit current and fill factor of the cells facing the front reflector in the aluminium trough.

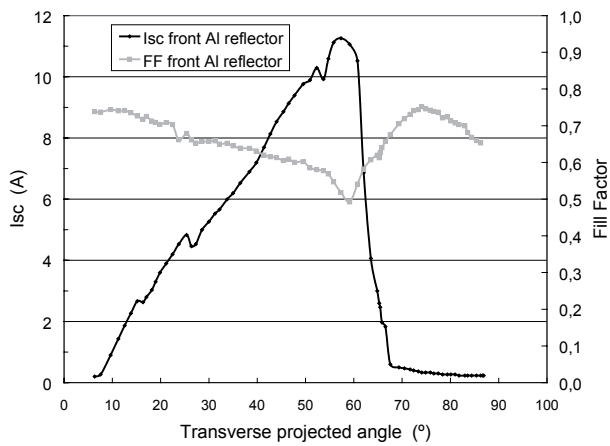

Figure 8.7 *Short circuit current and fill factor of the cells facing the front reflector.*

As in the case of the back reflectors, the fill factor is higher when the short circuit current is lower. The front reflector collects most of the light at

larger transverse angles. It is suitable for collecting the irradiation in the summer.

8.4 Irradiance distribution

As was discussed in the previous section, the output of the cells is affected by the distribution of irradiance on the cells. Figure 8.8 shows the irradiance distribution on the cells facing the back reflector at 33° transverse angle of incidence.

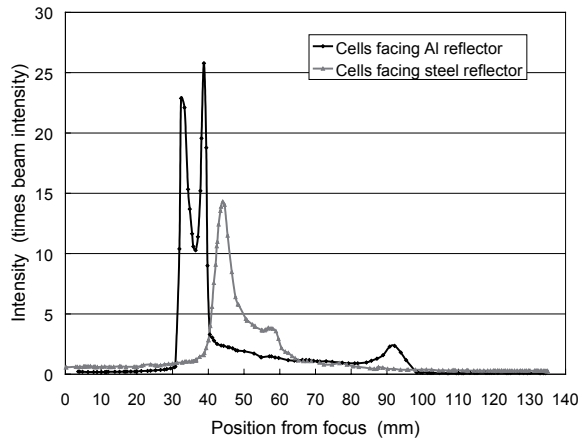

Figure 8.8 *Irradiance on the cells facing the back reflector as a function of the position from the focus. The position is measured from the focal point at the top of the absorber.*

The peak irradiance is higher for the cells in the aluminium trough, 25 times the beam compared with 14 times the beam for the steel trough. The width of the strip of light is approximately 10 mm for the aluminium reflector and 20 mm for the steel reflector. The wider strip of the steel reflector is due to the higher scattering of this reflector.

All the light reaches the cells for both troughs since the intensity is zero at the focal point. If it is not zero at the focal point, it can be an indication that some of the light was redirected past the reflector and out of the trough.

8.5 The influence of the absorber angle on the electrical output

The distribution of light on the cells depends on the absorber angle. The number of reflections at a specific angle of incidence changes as the absorber angle changes. When the absorber is turned towards the horizontal, the back reflector will have a lower average number of reflections, but the front reflector will have more. Simulations show that the annual output will be independent of the absorber angle if the absorber is kept in the same position all year. However, if the absorber can be placed at different angles during the year, turning the absorber towards the back reflector would be favourable for winter, spring and autumn, and turning the absorber towards the front reflector would be favourable during the summer.

8.6 Estimation of the electrical output

The measured short circuit current as a function of the transverse angle of incidence was used to calculate the optical efficiency. It was calculated according to Equation 7.2.

Figure 8.9 shows the calculated optical efficiencies.

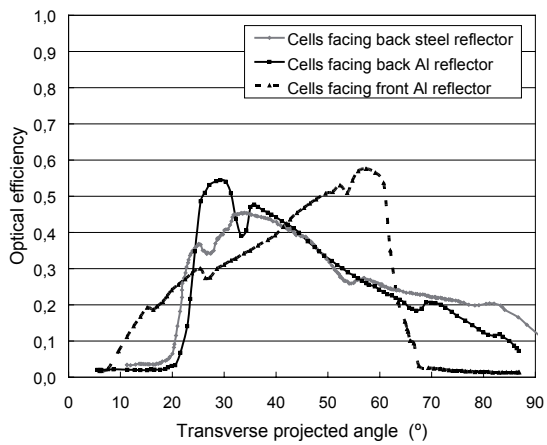

Figure 8.9 *Optical efficiency as a function of the transverse angle of incidence. The back reflectors have a high efficiency at low angles of incidence and the front reflector has a high efficiency at high angles of incidence.*

Using the calculated optical efficiency as a function of the transverse angle of incidence, the annual electrical output was simulated with MINSUN (Chant and Håkansson 1985). MINSUN uses climatic data for a specific site to calculate the annual output for a system with known optical efficiency in the longitudinal and transverse directions. The software is described in more detail in Section 10.4. The transmittance of the cover glazing as a function of the angle of incidence was used to model the optical efficiency in the longitudinal direction. A comparison was made with a standard PV panel that was mounted on the aperture, at 30° tilt from the horizontal, and with a horizontal panel. Table 8.3 shows the result of the simulations

Table 8.3 Annual electrical output as simulated by MINSUN.

Case	Annual output per m^2 cell area	Improvement
Cells facing back Al reflector	168 kWh	22.6%
Cells facing front Al reflector	205 kWh	49.1%
Cells facing back steel reflector	168 kWh	22.6%
Reference at 30° tilt	136 kWh	0%
Horizontal reference	103 kWh	-24.3%

The simulations show that the annual output from the cells facing the back reflectors is the same for both reflector types. An increase of approximately 23 % can be expected compared with the reference. The cells facing the front reflector are expected to deliver 49 % more electricity. This shows that if cells are to be placed on one side of the absorber only, they should be facing the front reflector in order to maximize the electrical output.

8.7 Estimation of the thermal output

MINSUN was also used to calculate the thermal output of the hybrid using the optical efficiency and the known thermal losses of the system. The estimated annual thermal output was 145 kWh/(m^2 glazed area) for a water temperature of 50°C. The low estimated output is probably due to the construction of the prototype absorber, which is shown in Figure 8.10.

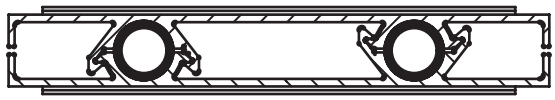

Figure 8.10 *Hybrid PV/thermal absorber (Fieber 2005). The copper pipes inside the absorber transport the heat collecting fluid.*

The absorber is designed for in-situ assembly when the system is erected, but the manufacturing precision is too low. The resulting air gap between the absorber and the pipes creates a large thermal resistance. The low heat conduction to the copper pipes containing the heat collecting fluid increases the absorber temperature, and the increased temperature results in higher thermal losses. The manufacturing precision has to be higher in future prototypes, or a less flexible absorber has to be used to increase the thermal output and reduce the overheating of the photovoltaic cells.

8.8 Placement of the PV cells

MaReCo is designed to maximize the annual collection of irradiation. The front reflector collects most of the irradiation during the summer months, and the back reflector collects more during the rest of the year. If the cells are placed on one side of the absorber, and the other side is used for heat collection only, the electricity generation will be asymmetric over the year. This is an important aspect since the system is intended to be integrated mostly into residential buildings where the use of electricity for household appliances etc. is fairly constant over the year. If the absorber has cells on both sides, this will increase the total annual output considerably, which will be an important factor for the investor that might have limited space for mounting the system.

If space is unlimited, and the most important parameter is to minimize the cost of electricity production, it is probably best to remove the cells from the back side of the absorber since the cells facing the front absorber have the highest annual output. In this case, it would be better to mount two systems with cells facing the front absorber instead of having one system with cells on both sides. However, this will probably not be the case for most applications and the best choice for most situations is therefore to have cells on both sides of the absorber to maximize the annual system performance.

9 Effects of non uniform irradiance distribution on standard PV cells

Due to the high cost of concentrator cells, low concentrating systems with standard cells are a promising alternative for reducing the cost of photovoltaic electricity. However, as was discussed in Section 4.2.2, standard cells perform best at irradiance levels below four to five suns. Moreover, the cells require the irradiance distribution to be uniform in order to perform optimally. This creates a problem since parabolic concentrators, which are the most common choice for low concentrating systems, yield a highly non uniform irradiance distribution on the cells. Even though the geometrical concentration ratio is often 2-3, the peak irradiance can be as high as 25-30 times the solar beam as was discussed in the previous chapter. If the irradiance on the cells could become more uniform, it would improve the electrical output significantly. Since the parabolic two dimensional concentrator is an ideal concentrator, any attempt to redesign this geometry will inevitably lead to optical losses. It is therefore necessary to measure and quantify the effects of non uniform irradiance on the different standard cells in order to get optimization parameters to be used in a new concentrator design where the optical losses due to a redesign have to be compensated for by an improved irradiance distribution.

The effect of changing the width of the irradiance profile at constant total irradiation, and the effect of varying the position of the line of high irradiance on the cell, were therefore measured for two standard cells. The measurements were performed as described in Section 7.4. Two standard cells were investigated, one monocrystalline silicon cell, and one polycrystalline silicon cell. Both were 125 × 125 mm cells. The current-voltage characteristics of both cells at an irradiance of 1000 W/m^2 and 20°C are shown in Figure 9.1.

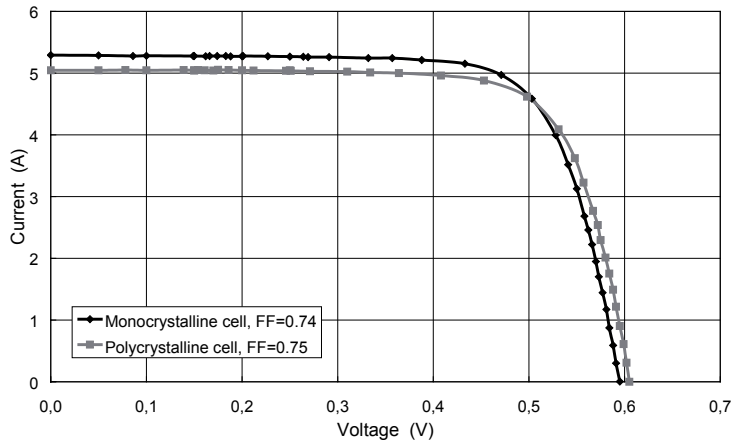

Figure 9.1 *IV-characteristics of the two cells studied under standard conditions.*

As was discussed in Section 7.4, the effects were studied on a single, cooled, cell to remove as many sources of error as possible.

9.1 Electrical output as a function of the width of the irradiance distribution at constant total irradiation

The IV-characteristics and light distribution were measured for 13 light distributions for each cell. The peak irradiance was 40 kW/m^2 in the first measurement and the peak width was 6.6 mm. This is the distribution that can be seen in Fig. 7.8. In the last measurement, the peak irradiance was 6 kW/m^2. At this point, the width was 31 mm. The peak width was calculated as the full width at half maximum (FWHM). Figure 9.2 shows the resulting IV-characteristics for both cells at peak widths of 6.6 mm and 17 mm.

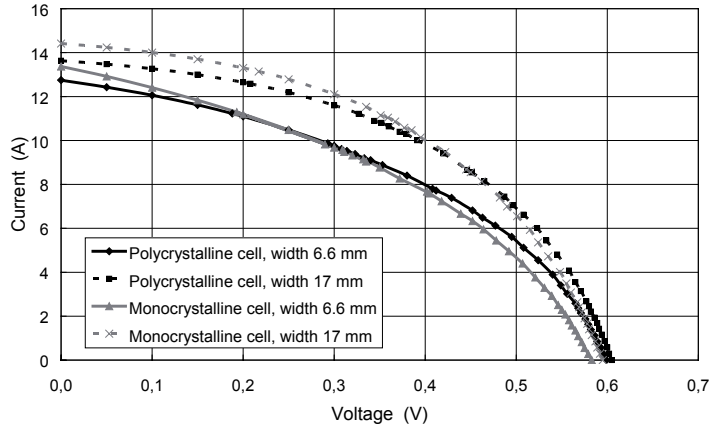

Figure 9.2 *IV-characteristics measured when the peak width was 6.6 mm and 17 mm for the monocrystalline and polycrystalline cells.*

Note that the total irradiation received by the cells is around 3 suns since the short-circuit current is approximately 3 times as high as the reference short-circuit current. This resembles a concentrator with a geometrical concentration ratio between 3 and 4 depending on its optical losses. It was important to make the measurements at elevated irradiance levels such as these since the low concentration systems being studied receive two to four times the standard irradiance during normal operation.

Using the IV-characteristics, the maximum power point at each peak width was calculated. This is shown in Figure 9.3, where the maximum output power as a function of the peak width is shown for both cell types.

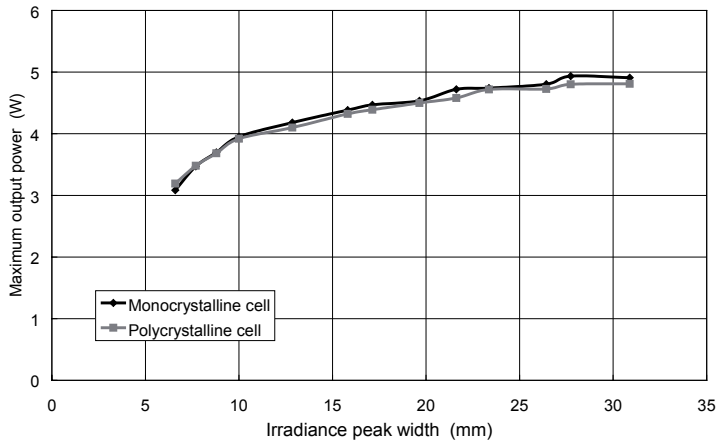

Figure 9.3 *The maximum output power for both cell types as a function of the peak width calculated as FWHM. The maximum power was obtained from IV-measurements.*

Starting from the right in Figure 9.3, an increase in short-circuit current and a decrease in open-circuit voltage were observed when the peak width was decreased. This agrees well with data presented by Franklin and Coventry (2002), and by Lorenzo et. al. (1980). Since the decrease in open-circuit voltage was the largest effect, this resulted in a linear decrease in output power as can be seen in the figure. At small peak widths, widths below 10 mm, the short-circuit current also decreased with decreasing peak width, and this resulted in an exponential decrease in power.

The decrease in open-circuit voltage can be explained by an increased temperature locally at the strip of high irradiance. The cell was cooled from the back side, which kept the global cell temperature close to the ambient temperature, but it was impossible to cool sufficiently the part of the cell that was irradiated with peak irradiance. When the strip was widened and the peak irradiance thereby was lowered, the irradiated area could be cooled more efficiently, and this increased the open-circuit voltage.

Standard cells are designed for uniform irradiance, which is understood from the relatively large finger spacing. The ideal distribution on such a cell is therefore uniform. This is however very difficult to achieve for stationary concentrators, and a trade-off between optical losses and electrical losses has therefore to be considered. As Figure 9.3 shows, the decrease in power as a function of the irradiance peak width is linear at widths above 10-15 mm. If the peak becomes narrower, the electrical losses increase

exponentially. It is therefore recommended that the width is kept above 15-20 mm in order to avoid large electrical losses. The irradiance peak width of existing non imaging parabolic concentrators is often between 10 and 20 mm and since this is on the limit of the exponential power decrease, the systems would certainly benefit if the irradiance profile on the cells could be widened.

9.2 Electrical output as a function of the position of the strip of high irradiance

The light source was moved from edge to edge of the cell while the irradiance distribution width was constant at 6.6 mm. The strip of high irradiance was always kept parallel with the bus bars of the cell. The measurement setup is described in more detail in Section 7.4. Using the IV-characteristics from each position, the fill factor and maximum power were calculated. This is shown in Figure 9.4.

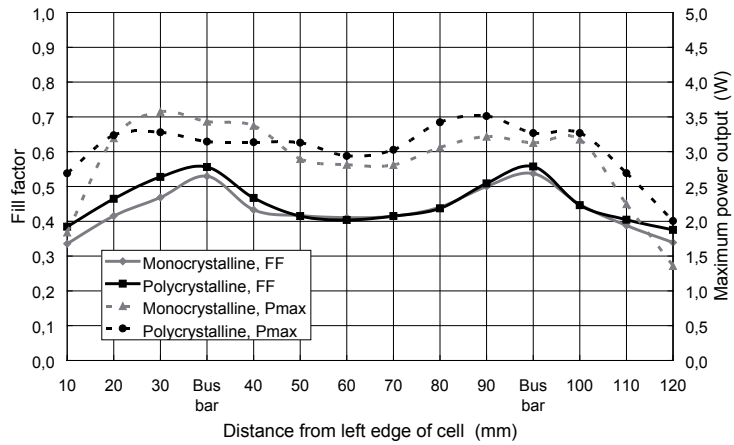

Figure 9.4 *Calculated maximum power output and fill factor as a function of the position of the strip of high irradiance for the monocrystalline and polycrystalline cell.*

It was found that the fill factor increased significantly when the light was focused at the bus bar. This is due to the relatively large series resistance of the standard cell. Obviously, less light reaches the cell for conversion into electricity, and for this reason the maximum power does not occur here.

However, when the light is focused close to the bus bars, the maximum power output reaches its maximum. This is in agreement with the previously presented results from Benítez and Mohedano (1999).

For a stationary concentrator, the strip of high irradiance moves over the cell surface when the sun moves, and it is impossible to direct the light close to the bus bars at all times. If the distance between the strip and the bus bars can be minimized however, the electrical output of the cells can increase by up to 10-15% over the year.

10 Models for estimating the performance of solar energy systems

To be able to size a solar energy installation it is important to estimate its energy output. To predict the output of a system at a specific location requires knowledge of the yearly irradiation at the site, and of the angular dependence of the system efficiency.

Measurement of the optical efficiency at all angles is time consuming and expensive. Models are therefore used to estimate the optical efficiency. These models are based on measurements at certain specific angles, and the model is used to extrapolate these measurements to the full spectrum of incidence angles.

10.1 Planar solar energy systems

The angular dependence of planar solar collectors, glazings, and photovoltaic modules is often estimated using Equation 10.1 (Souka and Safwat 1966 and Duffie and Beckman 1980).

$$K(\theta_i) = 1 - b_0\left(\frac{1}{\cos\theta_i} - 1\right) \qquad \text{Equation 10.1}$$

The equation describes how a certain property of the system decreases as the angle of incidence θ_i increases. b_0 is the incidence angle modifier coefficient which is calculated by fitting measurement data to the model. A commonly used value for glazings and flat plate solar thermal collectors is 0.1-0.2. It is slightly lower for photovoltaic panels.

Figure 10.1 shows a typical angular dependence curve for a planar system calculated from Equation 10.1. In this particular case it is the angular dependence of the transmittance of a glass sheet.

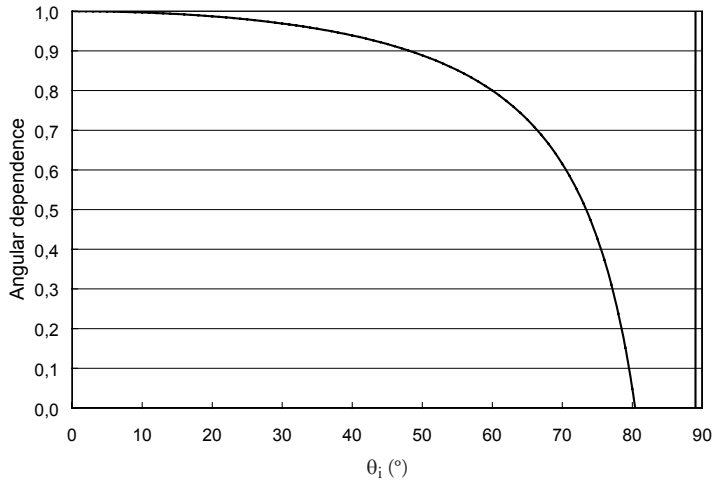

Figure 10.1 *Angular dependence of the transmittance of a glass sheet modelled according to Equation 10.1 (b_0=0.2).*

The model can be widely used to model the system at low and medium angles of incidence. However, at large angles of incidence, the modelled values decrease faster than the physical quantity. This is clear in the figure; the transmittance of a glass sheet is not 0 at 80° angle of incidence. The simplicity of the model has its advantages, and in order to use it for all angles of incidence the dependence at high angles of incidence is often modified slightly. At the start of the rapid decline in efficiency, around 70° in Figure 10.1, the angular dependence is then approximated by a linearly decreasing function ending at 0 % efficiency at 90° angle of incidence.

When complete systems such as e.g. solar collectors or PV panels are modelled, the low model values at high angles of incidence are more accurate since they model shading effects from the frames.

10.2 Biaxial models

Non symmetric systems have to be modelled by a biaxial model that takes into account the difference in angular dependence at different planes of incidence. A commonly used model is shown in Equation 10.2 (McIntire 1982).

$$\eta_{opt} = \eta_0 \cdot K_L(\theta_L,0) \cdot K_T(0,\theta_T) \qquad \text{Equation 10.2}$$

In Equation 10.2, θ_L is the longitudinal angle and θ_T is the transverse projected angle of incidence. The angles are defined in Figure 10.2.

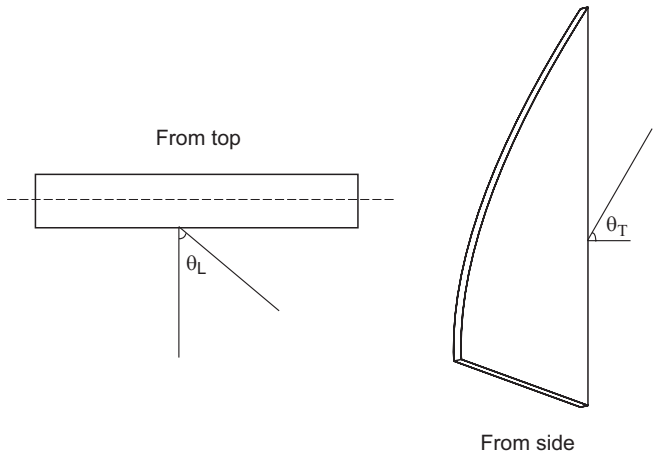

Figure 10.2 *Definition of the longitudinal angle θ_L and the transverse projected angle θ_T.*

This model estimates the optical efficiency η_{opt} by measurements of the angular dependence in the perpendicular longitudinal and transverse directions multiplied by the optical efficiency at normal incidence, η_0.

Measuring at θ_T=0 can be a problem for many asymmetrical concentrators that do not accept light at this angle of incidence; the minimum angle of acceptance is often 15-20° since the annual irradiation below this angle is negligible. This makes the use of the model slightly more complicated

Another, more significant, problem is that this model tends to overestimate the influence of the cover glazing. As the model is a product of two measurements, the influence of the glazing is taken into account twice. The largest error occurs when both the longitudinal and the transverse angles are large.

To solve these problems, a new model that separates the influence of the glazing and the influence of the concentrator is suggested. As was discussed in previous chapters, the optical efficiency of translationally symmetric two dimensional concentrators is determined by its efficiency in the meridian plane. The angle of incidence in this plane is θ_T, and the optical efficiency of a reflector trough will thus be modelled as a function of this

angle. Figure 10.3 shows the measured optical efficiency as a function of the transverse projected angle of incidence for the system shown in Figure 10.2. The optical efficiency was calculated according to Equation 7.3 by dividing the measured short-circuit current of the concentrator module by the short-circuit current of a vertical reference module mounted beside the concentrator.

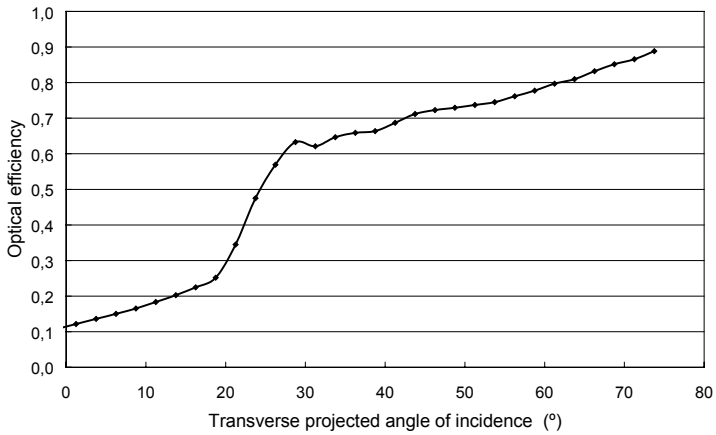

Figure 10.3 *The optical efficiency measured as a function of the transverse projected angle of incidence.*

At equinox, the transverse projected angle of incidence is constant all day for a system facing south. A concentrator for wall integration which was shown in Figure 3.12 was placed facing south for measurements of its optical efficiency. The results of the measurements during two days around equinox are presented in Figure 10.4. The optical efficiency was calculated according to Equation 7.3. The figure shows that the optical efficiency is independent of the longitudinal angle since it is constant all day, when the longitudinal angle changes from -90° to 90°.

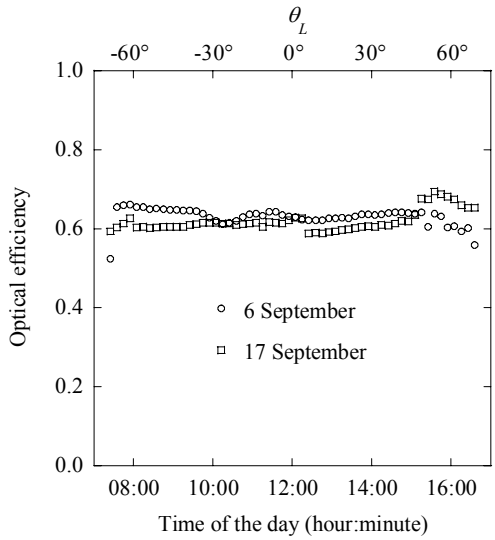

Figure 10.4 *Optical efficiency during two days around equinox. The optical efficiency is constant at changing longitudinal angles.*

The transmittance of a glazing depends on the true angle of incidence on the glazed surface. This leads to Equation 10.3, which defines the proposed biaxial model where R_T models the concentrator, f_L models the glazing, and η_0 normalizes the optical efficiency at normal incidence.

$$\eta_{opt} = \eta_0 \cdot R_T(\theta_T) \cdot f_L(\theta_i) \qquad \text{Equation 10.3}$$

As the transmittance for glass as a function of the angle of incidence is known in most cases, measurements on the concentrator as a function of the transverse angle at zero longitudinal angle are what is required to fully model the system. The model assumes that the glazing can be removed from the system before the measurements are performed. If for some reason this is not possible, R_T can be obtained according to Equation 10.4.

$$R_T = \frac{K(0,\theta_T)}{f_L(\theta_T)} \qquad \text{Equation 10.4}$$

$K(0,\theta_T)$ in Equation 10.4 describes a measurement of the angular dependence in the meridian plane of the concentrator with cover glazing. This

method can for example be useful for outdoor measurement data where the glazing has to be kept on for climate protection.

The longitudinal angular dependence of the absorption of the PV cell in the concentrator is not taken into account in the proposed model. Figure 10.5 shows the absorption as a function of the angle of incidence for a CIGS thin film cell and for a monocrystalline silicon cell (Brogren, Nostell, and Karlsson 2000).

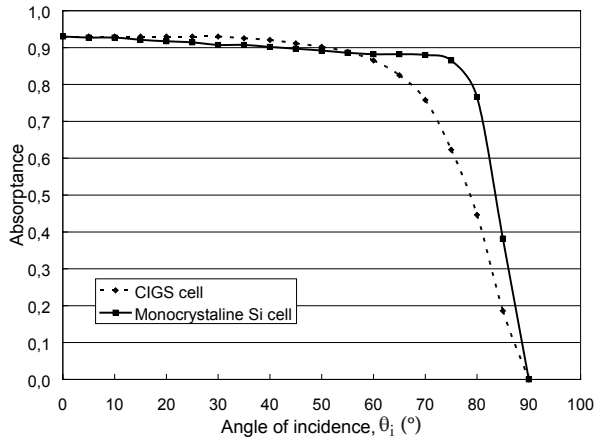

Figure 10.5 *Absorption of a CIGS thin film cell and a monocrystalline silicon cell*

The absorption of both PV cell types is almost constant up to 70°; the absorption will mostly be influenced at large longitudinal angles. Unless the system is mounted facing east or west with maximum irradiation incident at large longitudinal angles, it will not influence the optical efficiency of the system to any relevant extent.

In order to validate the model, measurements of the short circuit current of a concentrating module for wall integration and a reference module mounted on a vertical surface beside the concentrator were performed for two summer months in Älvkarleby, Sweden (60.5°N, 17.4°E). The new model defined by Equation 10.3 was used to estimate the short circuit current of the concentrating module using the current of the reference module. Figure 10.6 shows a comparison between the estimated current and the measured current.

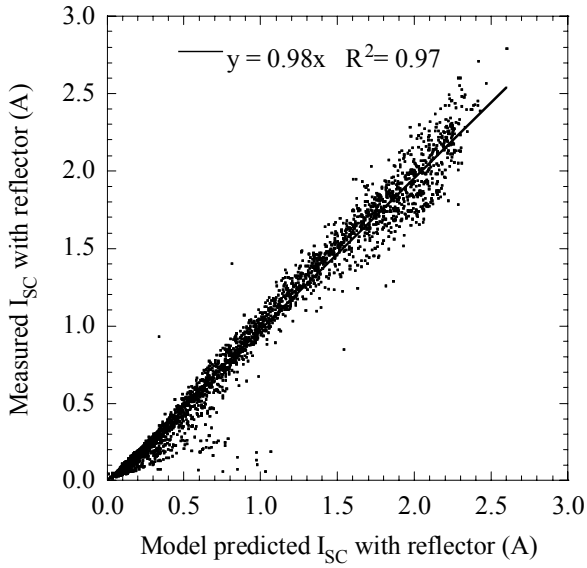

Figure 10.6 *Model predictions versus measured current for a parabolic concentrator for wall integration.*

As can be seen from the figure, the model predicts the short circuit current of the module in the concentrator well for the two summer months.

10.3 Annual direct irradiation

The extraterrestrial irradiation in the north-south vertical plane is symmetric over the year with one peak at the summer solstice and one peak at the winter solstice. These peaks occur at different angles depending on the latitude, the winter peak at 90°-latitude-23.45°, and the summer peak at 90°-latitude+23.45°. At high latitudes such as Sweden, the winter peak is close to the horizon, 6° in Älvkarleby and 11° in Lund. Since the light has to pass trough more atmosphere close to the horizon, the irradiation that arrives in the winter is limited and the peak is suppressed. It is suppressed even further by the large cloud coverage during the winter months, which almost makes the peak disappear. Figure 10.7 shows a diagram of the irradiation incident on a surface tracking the sun in the north-south vertical plane in Lund, Sweden (55.72°N, 13.22°E). It is divided into angular intervals of 2°.

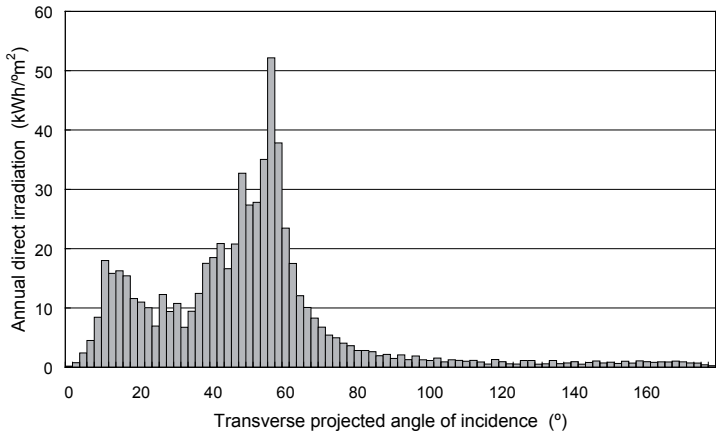

Figure 10.7 *Annual direct irradiation on a one axis solar tracking surface. The transverse projected angle is 0 at the horizon in Lund (55.72°N, 13.22°E).*

The highly asymmetrical irradiation during the year makes stationary asymmetrical concentrators an interesting option since most of the irradiation is concentrated into a small angular interval (Gordon, Lasken, and Ries 1996). If for example a system collects all irradiation between 40° and 65° it will collect 55% of the annual direct irradiation incident on the surface. If the yearly irradiation has two peaks, as is the case for more southern latitudes, it would require the interval of acceptance to be 60°. This would yield a concentration ratio of 1/sin(30°)=2, which is probably too low to justify the increased system complexity of a concentrator compared to a flat module.

10.4 Annual output estimation in Minsun

When a system is to be installed, it is not enough to know the optical efficiency at different angles of incidence. Without taking the annual irradiation on site into consideration, it is impossible to estimate the energy output. This is done in an annual output simulation software. The software that has been used to estimate the annual electrical and thermal output in parts of this thesis is Minsun (Chant and Håkansson 1985). The software was originally developed for solar thermal systems, but can

be used for photovoltaic systems as well. The climate of the site is input as a climate data file which means that it is easy to get output estimates for different sites. The orientation of the system is specified in the input data file, along with the optical efficiency of the system. Using this data, Minsun calculates the solar irradiation incident on the system hour by hour. Having calculated the incident irradiation, the software calculates the hourly system output from system parameters such as incidence angle dependence, loss coefficients, and efficiency coefficients. For a thermal system, output estimates for different collector temperatures are presented monthly in an output data file. The file also shows the total irradiation incident on the system aperture each month. For a photovoltaic system, the output data file shows the incident irradiation and the estimated monthly electricity generation.

11 Structured reflectors

One of the problems facing concentrators for photovoltaic applications is that the performance is lower than expected. In an ideal system, a concentration ratio of three should treble the electrical energy from the modules. However, the performance increase for the current prototype systems is typically 50%-75% of the geometrical concentration ratio. One obvious way to increase the electrical output per cell area is to increase the concentration ratio. If the concentration ratio were increased from 3 to 6, we could at least expect a doubling of the electrical output. However, this would be at the expense of a changed acceptance interval, since the maximum concentration ratio of a stationary, asymmetric concentrator is $2/(\sin\theta_1 - \sin\theta_2)$ where θ_1 and θ_2 are the acceptance angles of the concentrator. If the system is to be used in stationary mode it is not easy to change the acceptance interval since the angular distribution of the irradiation is determined by the latitude and the climate of the site. This sets a limit for the concentration ratio.

Figure 11.1 shows a translationally symmetric concentrator, MaReCo, which was used to evaluate structured reflectors. The figure also shows the local coordinate system that will be used throughout this chapter.

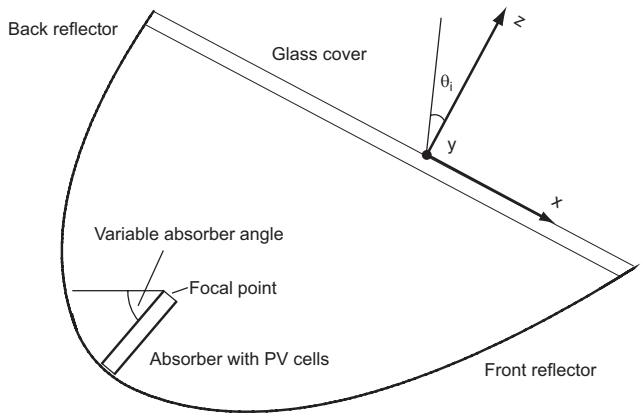

Figure 11.1 *Sketch of a translationally symmetric concentrator, MaReCo. The local coordinate system is shown in the figure.*

A symmetric three dimensional concentrator has a theoretical maximum concentration ratio of $1/\sin^2(\theta_{max})$, as derived in Section 2.1.The difference between two- and three dimensional systems is due to the conservation of the skewness of the two dimensional concentrator (Bortz, Shatz, and Ries 1997). The skewness, which is further discussed in Section 2.2, is the directional component, k_y, of the incident light that is parallel to the axis of symmetry. In Figure 11.1 this axis coincides with the y-axis, which is perpendicular to the paper.

The light at the exit aperture of an ideal three dimensional concentrator fills up the angular phase-space completely. To break the translational symmetry of a two dimensional concentrator such as the MaReCo could be a way to increase the concentration ratio as this would change the skewness of the rays and possibly increase the angular phase-space volume at the exit aperture (Leutz and Ries 2005, and Rönnelid and Karlsson 1998). This can be seen from Equation 2.4 and Equation 2.5 where the increased concentration ratio is due to the non-zero dk_y component, i.e. concentration of the component of the incident light perpendicular to the meridian plane.

The skewness of the rays can in the case of trough concentrators be changed by introducing a structured reflector where the structures are oriented perpendicular to the y-axis of Figure 11.1. Apart from increasing the concentration ratio, a structured reflector might solve the problem that creates the largest electrical losses in the system, the highly non uniform irradiance distribution on the cells. The high local intensity on parts of the cell creates high local currents and temperatures. This creates high resistive losses. Standard cells have a relatively high series resistance, and if standard cells are used in concentrator systems, the high local currents will cause considerable losses that can be observed as a reduced fill factor. The characteristics of the cells are discussed in more detail in Section 4.2.2. A structured reflector widens the narrow strip of light on the cells and this might prove to be an important improvement to the trough design.

11.1 Proposed structures

Figure 11.2 shows three structures that were investigated for increasing the performance of the MaReCo. The structures are small in comparison with the dimensions of the trough, typically in the range of centimetres for a trough of 5m.

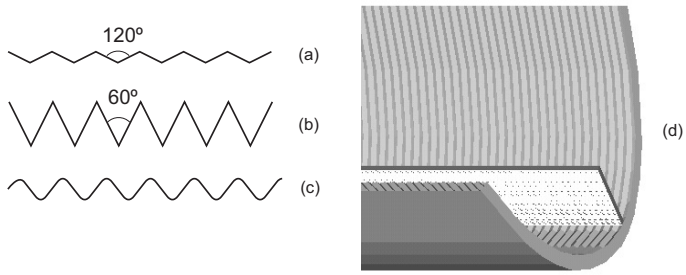

Figure 11.2 *Evaluated structures. Structure (a) is V-shaped with an opening angle of 120°, structure (b) is V-shaped with an opening angle of 60°, and structure (c) is sinusoidal in shape. (d) shows a sketch of a trough fitted with V-shaped reflectors.*

The sun is a light source of almost parallel light, the angular spread is approximately 0.27° (Duffie and Beckman 1980). Using the local coordinate system of Figure 11.1, the incident light can be divided into three directional components; k_x, k_y, and k_z. A translationally symmetric concentrator does not affect the skewness, k_y in the reflections. This means that the angular spread at the absorber is limited to the x-direction. However, maximum concentration ratio is achieved when the exit rays completely fill up the angular phase space at the exit aperture (Bortz, Shatz, and Winston 2001). This means that the rays exit in a hemisphere where all directions are equally probable, and not in a plane. This would be achieved if the k_y components of the light could be mixed in the reflections as is the case for the k_x-components. Structures (a) and (b) of Figure 11.2 will selectively mix the directional components in a controlled pattern due to the planar facets of the microstructure (Leutz and Ries 2003). The sinusoidal structure (c) will mix the directional components more randomly.

Structure (a) and structure (b) are described in Figure 11.3. Figure 11.3a shows the directional components, k_x and k_y, of the incident light projected onto a semicircle.

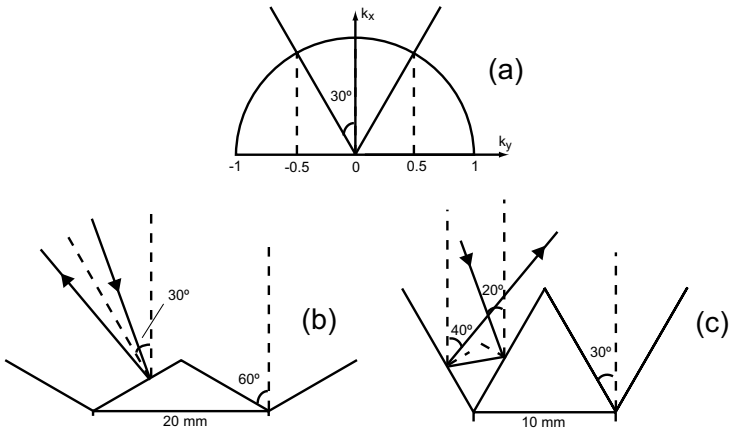

Figure 11.3 *Selective mixing of reflected rays in the two-dimensional phase space. The étendue limited by the angular interval -30<θ<=30 is equal to the étendue comprising the rest of the possible angles. The V-shaped structures reflect all rays of one angular interval into the other, and vice versa, thereby mixing the directional components.*

The étendue limited by the angular interval -30<θ<30 is equal to the étendue comprising the rest of the possible angles. The V-shaped structures reflect all rays of one angular interval into the other, and vice versa, thereby mixing the directional components. Figures 11.3b and 11.3c show how the V-shaped microstructures mix the k_x and k_y components. Both structures mix the incident parallel light, but the structure in Figure 11.3c will reflect the rays twice while the structure of Figure 11.3b only reflects the incident rays once. This will lead to increased reflection losses for the structure of 11.3c.

The optical properties of the structured concentrators were evaluated using Monte Carlo ray tracing performed in ZEMAX, a commercial ray tracing package (ZEMAX 2005).

11.2 Changed illumination of the absorber

The main explanation for the relatively low gains from using stationary parabolic concentrators for photovoltaic applications is the highly non uniform irradiance distribution on the cells and this was one of the reasons for evaluating the structured reflectors. Figure 11.4 and Figure 11.5 show the resulting irradiance distribution of the cells facing the front and

back reflector for the three structures and for a smooth reference trough. The simulation was performed for an azimuth angle of 15° and a solar altitude of 40°.

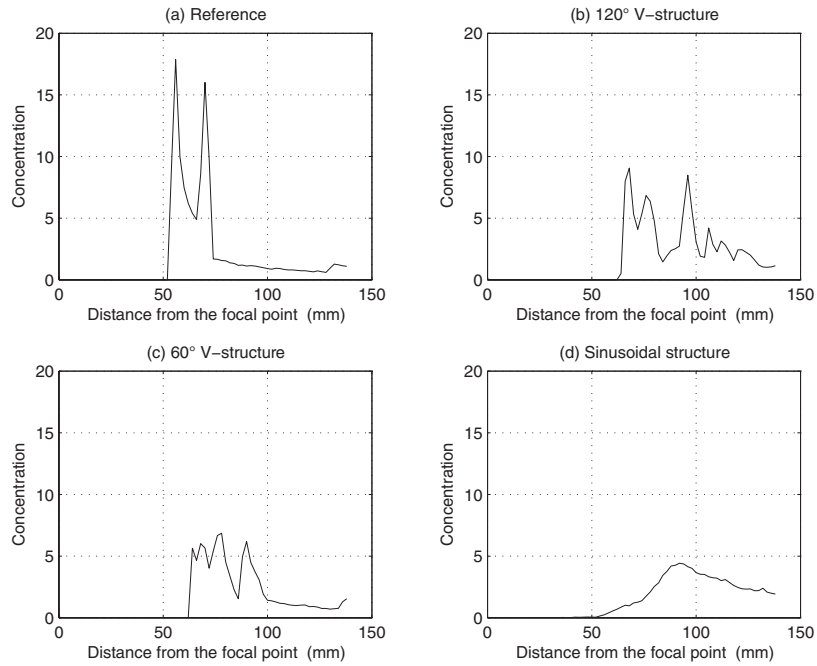

Figure 11.4 *Irradiance distribution on the cells facing the back reflector. The y-axis shows the intensity relative to the solar beam for an azimuth angle of 15° and a solar altitude of 40°.*

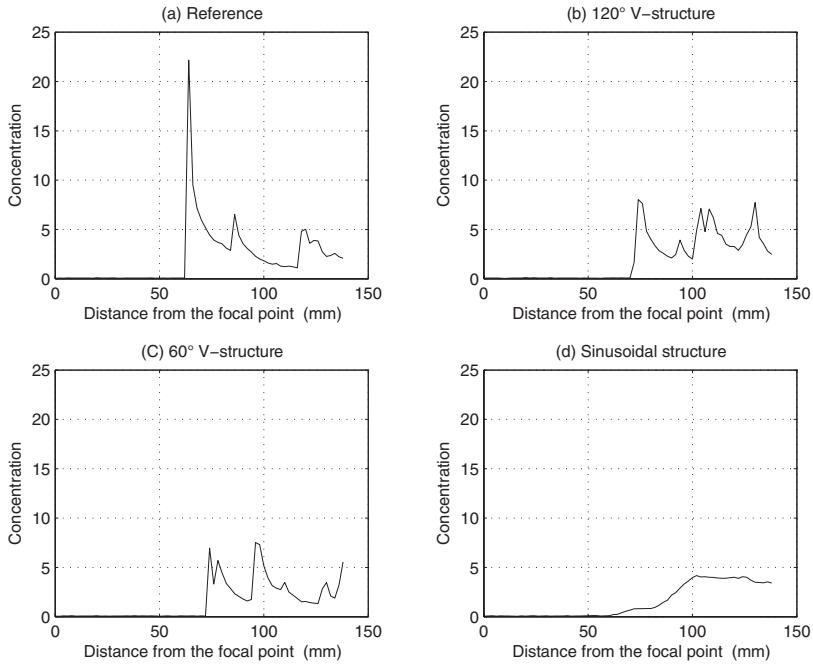

Figure 11.5 *Irradiance distribution on the cells facing the front reflector. The y-axis shows the intensity relative to the solar beam for an azimuth angle of 15° and a solar altitude of 40°.*

As can be seen from the figures, all structures considerably reduce the peak intensity on the cells and this will result in a higher fill factor, i.e. the resistive losses in the cells will be reduced. The effects of non-uniform illumination of the cells are described in more detail in Chapter 9. The sinusoidal structure clearly creates the greatest reduction in peak intensity, it never exceeds the beam intensity by more than a factor of five, and almost half the cell is illuminated. This makes the structure very interesting in combination with standard silicon cells, since they are sensitive to high irradiance spots due to their relatively high series resistance.

For the V-shaped structures, the reduction in intensity is slightly larger for the 60° structure, but this is due to the higher optical losses caused by a higher number of multiple reflections.

Previous measurements on a slightly diffusing reflector described in Chapter 8 showed that a slight reduction in peak intensity can improve the output of the cells considerably. However, the problem with that reflector is that the total reflectance of the reflector was lower than the reflectance of the standard aluminium reflector. If micro-structured reflectors are used,

the wider strip of light can be achieved without large reflection losses since a reflector with very high reflectance can be used.

11.3 Optical efficiency and annual output

The structured reflectors will introduce a higher average number of reflections at a given angle of incidence. Simulations were performed for a large interval of angles in the azimuth and solar altitude directions to study the optical efficiency of the three proposed troughs. A simulation of a smooth reference was also performed for comparison with the current design of the stand-alone MaReCo.

Figure 11.6 shows the optical efficiency as a function of the solar altitude when the source was in the meridian plane, the xz plane of Figure 11.1.

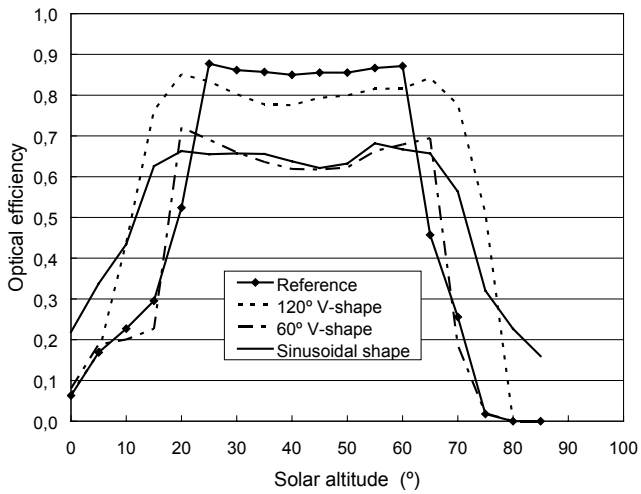

Figure 11.6 *Optical efficiency in the meridian plane. The sun is normal to the trough aperture at 60° solar altitude. The reflectance at normal incidence was 0.92 in the simulations.*

In the interval 25° to 60°, the reference shows a higher optical efficiency than any of the structured reflector troughs. This is due to the higher number of reflections for the structured reflectors. However, the difference between the 120° structure and the reference is small within the interval of acceptance. Outside the interval of acceptance (20° to 65°) all structured reflectors perform better than the reference. This means that the interval

of acceptance increases when structured reflectors are used as it is possible for light outside the interval of 20° to 65° to reach the absorber. The sinusoidal structure has the lowest optical efficiency inside the interval, but also the smallest decrease outside the interval.

Simulations for other angles of incidence show that the optical efficiency of the sinusoidal structured reflector and the 60° V-shaped structure has a local minimum in the meridian plane, the efficiency increases as the azimuth angle increases. This is shown in Figure 11.7 where the azimuth angle was varied while the solar altitude was constant at 40°.

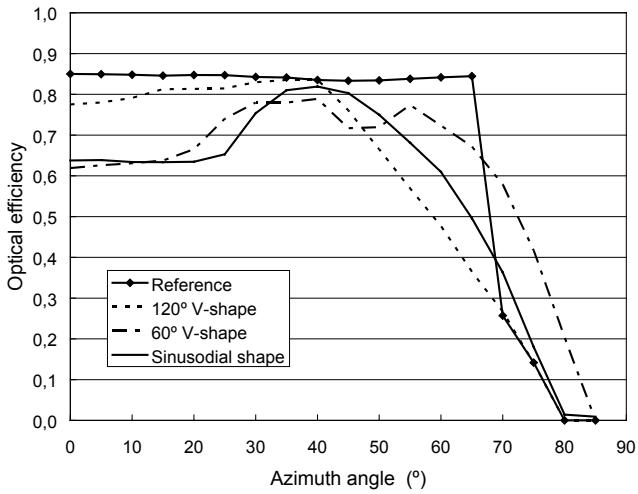

Figure 11.7 *Optical efficiency as a function of the azimuth angle at a constant solar altitude of 40°*

Using climate data for Lund, Sweden (55.75°N -13.22°E), the optical efficiency at different angles of incidence was weighted by the incident irradiation in each angular interval to get an evaluation of the different reflectors during a year of operation. Both direct and diffuse irradiation was included in the calculations. The diffuse irradiation was treated as completely isotropic, i.e. all parts of the sky were equally bright. The optical efficiency for diffuse irradiation was calculated according to Equation 11.1, where α is the solar altitude, γ is the azimuth angle, and θ_i is the angle of incidence on the aperture of the trough. $\mathrm{Cos}(\theta_i)$ represents the view factor and $\cos(\alpha)$ the fact that not all radiating elements are of the same size. η_{opt} is the optical efficiency for direct irradiation for a specific angle of incidence.

$$\eta_{opt,diff}(\alpha,\gamma)=\frac{\sum_{\alpha=0}^{\alpha=90}\sum_{\gamma=-180}^{\gamma=180}\eta_{opt}(\alpha,\gamma)\cdot\cos(\theta_i)\cdot\cos(\alpha)}{\sum_{\alpha=0}^{\alpha=90}\sum_{\gamma=-180}^{\gamma=180}\cos(\theta_i)\cdot\cos(\alpha)} \qquad \text{Equation 11.1}$$

The optical efficiency for diffuse irradiation for each of the systems is shown in Table 11.1

Table 11.1 Optical efficiencies for diffuse radiation for the micro-structured reflectors.

	Reference	120° V-shaped structure	60° V-shaped structure	Sinusoidal structure
Optical efficiency for diffuse irradiation	0.38	0.38	0.35	0.37

As the table shows, the optical efficiency for diffuse irradiation was approximately the same for all systems. The lower efficiency of the structured systems within the interval of acceptance of the smooth trough was compensated for by a wider interval of acceptance for the structured systems.

Table 11.2 shows the annual irradiation on the cells for the different cases compared with the reference.

Table 11.2 Relative annual irradiation incident on the cells

	Reference	120° V-shaped structure	60° V-shaped structure	Sinusoidal structure
Relative annual irradiation	1.0	0.91	0.89	0.90

Considering that the MaReCo was optimized for the climate of Sweden, it is not surprising that the cells in the smooth trough receive the largest annual irradiation. However, the 120° V-shaped structure and the sinu-

soidal structure show a mere 9-10% decrease. This indicates that small improvements in other system characteristics such as uniformity of the light distribution will improve the trough system using structured reflectors.

11.4 Increased concentration ratio

The increased concentration ratio given by the structured reflector can be exploited in two ways, either by reducing the cell area of the given system to get a lower system price, or by changing the shape of the trough to make use of the wider interval of acceptance that was shown in Figure 11.6. The interval of acceptance is directly connected to the size of the aperture. If the interval is smaller, the aperture is larger and vice versa. An interesting development would be to increase the trough aperture, creating a smaller angular acceptance interval for a smooth reflector system, but to use a structured reflector which makes the interval wider. This will make it possible to accept almost all the light in the interval 20°-65° while increasing the concentration ratio. This solution will be discussed in more detail in Chapter 13. The use of the sinusoidal structure would create the same possibilities as the V-shaped structures, but as the rays are more randomly reflected it would need a more thorough study of the geometry to use it optimally. It would probably also be more difficult to manufacture.

It is evident from Fig. 11.6 that the interval of acceptance in the simulations was approximately 10° larger for the 120° V-shaped structure. In principle, it should be possible to decrease the present angular interval from 20°-65° to at least 25°-60° using the structured reflector. This would increase the geometrical concentration ratio by 27% for an untruncated system.

11.5 Choice of structure

Of the three proposed structures, the 60° V-shaped structure receives the lowest annual irradiation. The 120° V-shaped structure has the highest optical efficiency for direct irradiation when the sun is in the meridian plane, but the annual irradiation on the cells is roughly the same as for the sinusoidal structure. This is due to two characteristics of the sinusoidal structure, the higher optical efficiency for direct irradiation at large azimuth angles, and the larger interval of acceptance. All three structures create a more uniform irradiance distribution on the cells which could be seen in Figure 11.4 and Figure 11.5. The sinusoidal structure has the

largest homogenizing effect, while the two V-shaped structures show a more moderate reduction in peak intensity.

If electricity generation during a few hours of the day has the highest priority, the choice would be the 120° V-shaped reflector structure as this has approximately the same optical efficiency for direct irradiation as the reference in the meridian plane, while still reducing the peak intensity on the cells. However, if the annual electricity generation is important, the sinusoidal structure should probably be chosen. The yearly irradiation on the cells is approximately the same as for the V-shaped structure, and the irradiance is considerably more uniform over the cells.

The best choice for a system that is intended to generate electricity all the year is to use sinusoidal or 120° V-shaped reflectors, and to change the size of the aperture to increase the concentration ratio. For a smooth reflector this would reduce the interval of acceptance, but as Figure 11.6 shows, the interval of acceptance widens when structured reflectors are used, and this would compensate for the increased aperture size.

12 A novel method for rapid design and evaluation of photovoltaic concentrators

It is difficult to develop new concentrators that address the problem of non uniform irradiance without tools to estimate the benefits of creating a more uniform distribution. As was found in Chapter 11; when the concentrator geometry is modified from the original parabolic form, this will inevitably lead to optical losses since the parabolic trough is thermodynamically ideal. It was found that the structured reflectors created considerably more uniform irradiance distribution, but it was difficult to estimate to what extent this improved the annual output of the concentrator. A new evaluation method has therefore been developed in order to enable development and optimization of new concentrators with higher efficiencies. The aim was to create a method that made comparisons between different designs easy.

12.1 Method

The method is completely based on simulations. It consists of three steps. Figure 12.1 shows a flowchart describing these steps.

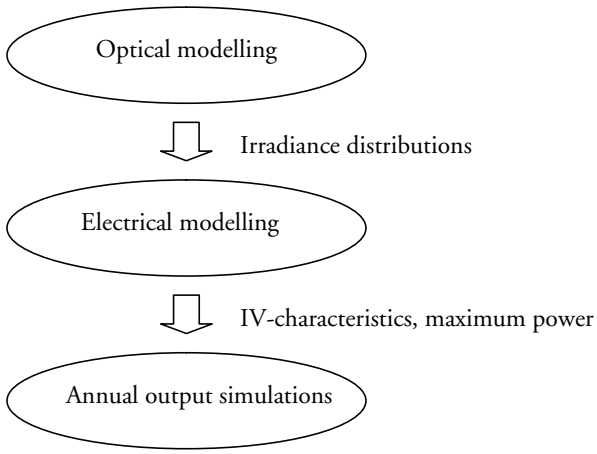

Figure 12.1 Description of the three-step simulation method.

The first step is to perform optical simulations, ray tracing, of the new system to evaluate its optical properties. The light distribution on the cells is simulated for a large number of angles of incidence using a commercial ray tracing software. The next step is to perform electrical simulations of the solar cells based on the light distributions generated by the optical simulations. A numerical solar cell model which has been developed for this purpose calculates the current-voltage characteristics of the cells at each angle of incidence. The last step is to simulate the annual output for a specific site based on the current-voltage characteristics from the electrical simulations. The system being studied is modelled by a matrix of efficiency coefficients where each element in the matrix represents the system efficiency at a certain angle of incidence. The efficiency coefficients were calculated using the maximum power point of each IV-characteristic. Since annual output estimates can be obtained, systems at different geographical locations can be easily compared.

12.1.1 Optical simulations

The optical efficiency of a stationary solar concentrator always depends on the angle of incidence. Both the total irradiation and the irradiance distribution are dependent on this angle. In order to perform annual output simulations, and to make it possible to simulate different locations,

it is necessary to simulate the light distribution on the cells for all angles of incidence.

Using ZEMAX (ZEMAX 2005), a commercial ray tracing package, the light distribution on the cells at an incoming irradiance of 1000 W/m^2 was simulated for angles of 0-90° in the azimuth direction and from 0-90° in the zenith direction. The sun was modelled as a light source with an angular spread of 0.27° (Duffie and Beckman, 1980). The incidence angle dependent reflectance of the reflector material and the incidence angle dependent absorptance of the solar cells were taken into account since this can have an important influence on the output. The number of rays traced for each system was set depending on the physical size of the system, and on the desired accuracy.

12.1.2 Electrical simulations

Since the main aim of a new design is to create a more uniform irradiance distribution on the cells, it is important to study how the light distribution influences the electrical output. A new model has therefore been developed based on a model by Foss (Foss et. al. 2005). The model is described in detail in Chapter 6.

Using this model the IV-characteristics were simulated based on the light distribution from each angle of incidence simulated in the previous step.

12.1.3 Annual output simulations

The most complete comparison between two systems at a specific site is to study the annual output, and its distribution over the year. The most reliable method is to build prototypes and conduct measurements for at least a year to compare the systems side by side. However, this is very time consuming, which makes a simulation of the annual output an interesting option. In the method presented here, the annual output is calculated based on a climate data file for a specific site. This file consists of hourly direct and diffuse irradiation on the system aperture. The file can contain either measured data or simulated data as long as it consists of hourly values. For the simulations performed in this thesis, the climate data was obtained from a Meteonorm simulation of the specific site (Meteonorm 2007).

The electricity generated by the diffuse and direct irradiation was calculated separately. The total annual electrical output was calculated as the sum of the electrical output generated by direct irradiation and the annual output generated by diffuse irradiation.

The direct irradiation on the aperture was divided into a matrix in angular space, where each element in the matrix represented the direct irradiation from a specific segment of the sky. The angles represented in the matrix were the solar altitude and the solar azimuth angle. The irradiation each hour was divided into 6 equal parts, each representing the irradiation incident on the system for a period of 10 minutes. The solar altitude and solar azimuth angle were calculated for the middle of each interval, and the irradiation incident during the period was added to the matrix element corresponding to the calculated solar angles. This was done for the whole year which resulted in a direct irradiation matrix consisting of angular resolved irradiation on the aperture.

The system efficiency for direct irradiation for each angle of incidence was calculated in a similar matrix. The system efficiency, $\eta_{\text{direct}}(\alpha,\gamma)$, was derived from the maximum power point, P_{max} resulting from the electrical simulations for each angle of incidence. α represents the solar altitude and γ represents the solar azimuth angle. The efficiency was calculated according to Equation 12.1.

$$\eta_{direct}(\alpha,\gamma) = \frac{P_{\max}}{1000 \cdot \cos(\theta_i) \cdot A_{cell}} \qquad \text{Equation 12.1}$$

θ_i represents the angle of incidence at the concentrator aperture. The maximum power was divided by the incident irradiation, $1000*\cos(\theta_i)*A_{cell}$ since this was the total irradiation incident on the cell in the optical simulations. By calculating the system efficiency in this way, $\eta_{\text{direct}}(\alpha,\gamma)$ represents the system efficiency per cell area as opposed to efficiency per aperture area. This means that when different systems were compared, the comparison was made for systems with equal numbers of solar cells. Since the solar cell is by far the most expensive component of the system, this was considered the most relevant comparison.

The total electrical output generated by direct irradiation was calculated as the sum of the products of each element of the direct irradiation matrix and the corresponding element of the system efficiency matrix.

For the diffuse irradiation, the sky was treated as an annual isotropic light source, i.e. all parts of the sky were assumed to be equally bright, or Lambertian. The electrical output generated by diffuse irradiation was calculated as the total diffuse irradiation on the aperture multiplied by the system efficiency for diffuse irradiation. This efficiency, $\eta_{diffuse}$, was calculated according to Equation 12.2 using the calculated optical efficiency for each angle of incidence. The optical efficiency was derived from the optical simulations, i.e. it does not contain the electrical losses in the cell due to different illumination conditions.

$$\eta_{diffuse} = \eta_{electric} \cdot \frac{\sum_{\alpha=0}^{\alpha=90} \sum_{\gamma=-180}^{\gamma=180} \eta_{opt}(\alpha,\gamma) \cdot \cos(\theta_i) \cdot \cos(\alpha)}{\sum_{\alpha=0}^{\alpha=90} \sum_{\gamma=-180}^{\gamma=180} \cos(\theta_i) \cdot \cos(\alpha)} \quad \text{Equation 12.2}$$

In Equation 12.2, $\eta_{electric}$ represents the electrical efficiency of the solar cell under standard test conditions, $\cos(\theta_i)$ the view factor, and $\cos(\alpha)$ the fact than not all elements on the isotropic sky are of equal size.

The system efficiency for diffuse irradiation can be derived either from the optical efficiency or from the system efficiency for beam irradiation, which was calculated using Equation 12.1. On days with a high fraction of direct irradiation, the system efficiency for diffuse irradiation will be overestimated if it is derived from the optical efficiency since the efficiency of the cell for each angle of incidence will be determined by the system efficiency for direct irradiation. On days with a lower fraction of direct irradiation, however, the light will be distributed evenly over the cell surface and the system efficiency will not suffer from the fill factor reduction due to non uniform irradiance. Since most of the diffuse irradiation at northern latitudes such as Lund is collected when the direct fraction is low, the best choice is to derive the system efficiency for diffuse irradiation from the optical efficiency. At locations where the fraction of direct irradiation is larger, the system efficiency for diffuse irradiation should be derived from the system efficiency for direct irradiation according to Equation 12.3.

$$\eta_{diffuse} = \frac{\sum_{\alpha=0}^{\alpha=90} \sum_{\gamma=-180}^{\gamma=180} \eta_{direct}(\alpha,\gamma) \cdot \cos(\theta_i) \cdot \cos(\alpha)}{\sum_{\alpha=0}^{\alpha=90} \sum_{\gamma=-180}^{\gamma=180} \cos(\theta_i) \cdot \cos(\alpha)} \quad \text{Equation 12.3}$$

Another possible source of errors in this method of calculating the electrical output from diffuse irradiation is that the sky is assumed to be completely isotropic. On days with a slight haze or thin clouds, the part of the sky closest to the sun is brighter than the rest of the sky, and this is not taken into consideration in the method. Since this contribution to the total annual diffuse irradiation is small for northern latitudes, as was discussed in the previous section, this error is considered acceptably small.

13 Design of two new photovoltaic concentrators for homogenized irradiance distribution

As has been discussed in previous chapters, the largest obstacle for stationary solar concentrators with standard solar cells is the non uniform irradiance distribution on the cells. One possible solution to the problem, to introduce structured reflectors, was discussed in Chapter 11. When structured reflectors were used in a MaReCo trough, it was found that the irradiance distribution became considerably more uniform, but the system output was not improved compared to the smooth reference system. One of the reasons why the new systems failed to achieve any performance improvements was that it was difficult to estimate the electrical gains due to the more uniform illumination of the cells. The second reason why there were no performance improvements was that the total collected irradiation was smaller for the structured systems. The conclusion of the study in Chapter 11 was that new designs had to be investigated in order to make optimum use of the new reflector technology.

In order to take the irradiance uniformity into consideration when new concentrators are designed, a new evaluation method was developed in Chapter 12. Using this method, it was possible to compare the annual electrical output of different designs for a specific climate.

The method was used to develop two new structured photovoltaic concentrators. One of the concentrators was designed for integration into flat roofs and one for integration into facades. Both systems were equipped with standard solar cells, which made irradiance homogenization an important factor.

13.1 Reference systems

The aim was to design one system for roof integration and one system for wall integration. The roof system was based on the MaReCo design, and the wall system was based on the geometry of the Solar Window (Fieber et. al. 2004). These systems are shown in Figure 13.1.

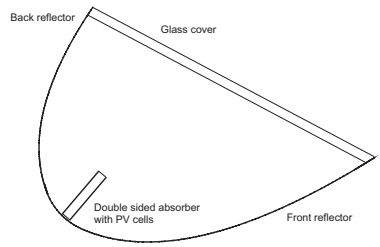

Figure 13.1a *Reference MaReCo concentrator with double sided absorber.*

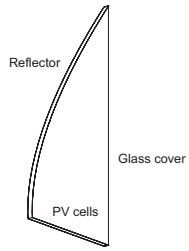

Figure 13.1b *Reference system for wall reflector.*

The systems were designed to use standard solar cells. The IV-characteristics of the cell that was used is shown in Figure 13.2.

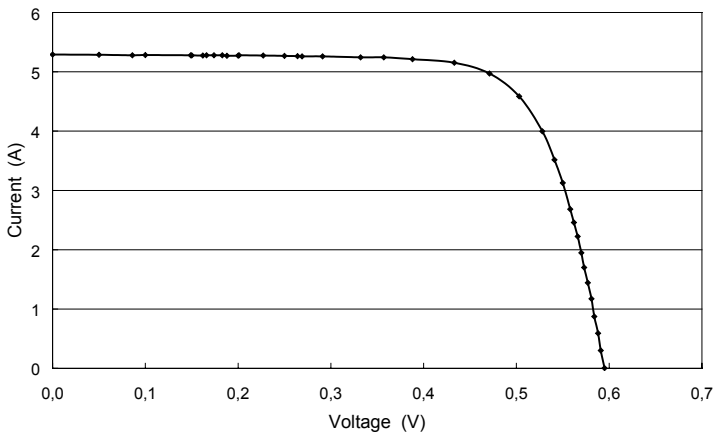

Figure 13.2 *IV-characteristics of the cell used in the design of the two new concentrators, measured under standard conditions. The measurement was performed on a 125 mm x 125 mm cell.*

As the figure shows, the short-circuit current of the cell was 5.29 A, the open-circuit voltage 0.60 V, and the fill factor 0.74 under standard conditions.

The reflector material used in the design was anodized aluminium, a highly specular reflector material which has a reflectance of 85 % for the solar spectrum. The reference systems had smooth reflectors, and the new systems were given a V-shaped structure. The structure is shown in Figure 13.3. It is identical to the 120° structure which was discussed in Chapter 11.

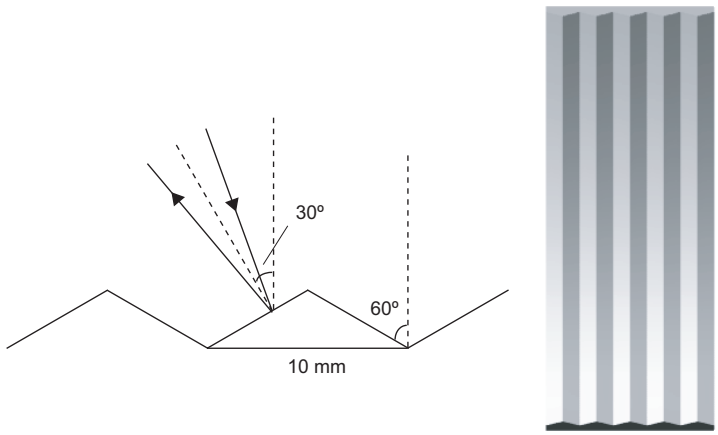

Figure 13.3 *Reflector structure used in the design of the new concentrators. The left of the figure shows the V-shaped structure with a half angle of 60°, and on the right a part of the reflector with several Vs is shown. The ridge of each V extends from the outer limit of the reflector to the absorber.*

The half angle of the V-shaped structure is 60° as can be seen in the left of the figure. The left of the figure also shows the structured reflector's effect on a skew ray. When the ray is incident at an angle smaller than 30°, it is reflected at an angle greater than 30° and vice versa. The right of the figure shows a section of the reflector with several Vs. The ridge of each V extends from the edge of the solar cells to the outer rim of the reflector.

13.2 Design of a new roof system

The acceptance interval of MaReCo is from 20° to 65°. When the structured reflectors were applied in Chapter 11 this resulted in a change in this interval of acceptance; it became wider and less distinct. In order to make optimum use of the structured reflectors, it was found that the tilt of the parabolas had to be changed. The tilt of the parabolas was therefore the design parameter that was altered in the new design. The original tilt of the parabolas, 20° and 65° from the horizontal was changed in steps of 2.5° which meant that the acceptance interval was reduced by 5° in each step while the centre of the interval remained unchanged. The cells of the reference system are mounted on a double sided absorber in order to increase the thermal output but the prototype systems were fitted with a wedge absorber since they were intended for electricity generation only. This slightly reduced the required reflector area.

One of the characteristics of a CPC concentrator is that it is possible to truncate it heavily without losing much of the collectable energy. When the MaReCo concentrator was designed, it was truncated to optimize the reflector surface area in relation to the collected energy. When the tilt of the reflectors was changed for the prototypes in order to find the most suitable structured reflector design, the aperture increased. Compared to a full CPC, the original truncation would mean a substantial reduction of the aperture when the tilt was increased. For this reason, the size of the reflectors had to be increased slightly.

The reference system was designed for 125 × 125 mm cells. When the tilt of the parabolas was changed, the concentrator became larger. Since it was intended to be integrated onto a flat roof where space can be limited, the size of the system is not an unimportant parameter. In order to reduce the size of the system, the cell size was therefore reduced to 62.5 × 125 mm which meant that the whole system could be down scaled to half its original size. In order to make the comparison with an existing concentrator, the cell size was kept at 125 mm × 125 mm for the reference.

Four new designs with different mirror tilts were investigated. The parameters for each of the prototypes, as well as for the reference, are shown in Table 13.1.

Table 13.1 Physical characteristics of the evaluated systems.

System	Back parabola tilt	Front parabola tilt	Aperture width	Cell width	Geometrical concentration ratio	Reflector structure
Reference	20°	65°	626 mm	125 mm	2.50	Smooth
Roof prototype 1	22.5°	62.5°	333 mm	62.5 mm	2.66	V-structure
Roof prototype 2	25°	60°	350 mm	62.5 mm	2.80	V-structure
Roof prototype 3	27.5°	57.5°	368 mm	62.5 mm	2.94	V-structure
Roof prototype 4	30°	55°	384 mm	62.5 mm	3.07	V-structure

As the table shows, the geometrical concentration ratio of the reference system was 2.5, and for the largest prototype it was 3.07.

13.2.1 Optical simulations of the roof concentrator

The light distribution on the cells for all angles of incidence was simulated for all the five systems. The irradiance distribution was found to be considerably more uniform in the structured systems in Chapter 11. Figure 13.4 shows the light concentration on the cells at a solar altitude of 40° and a solar azimuth angle of 15°. The distribution above the x-axis in the figure represents the distribution on the cells facing the back reflector, and that below the x-axis represents the cells facing the front reflector.

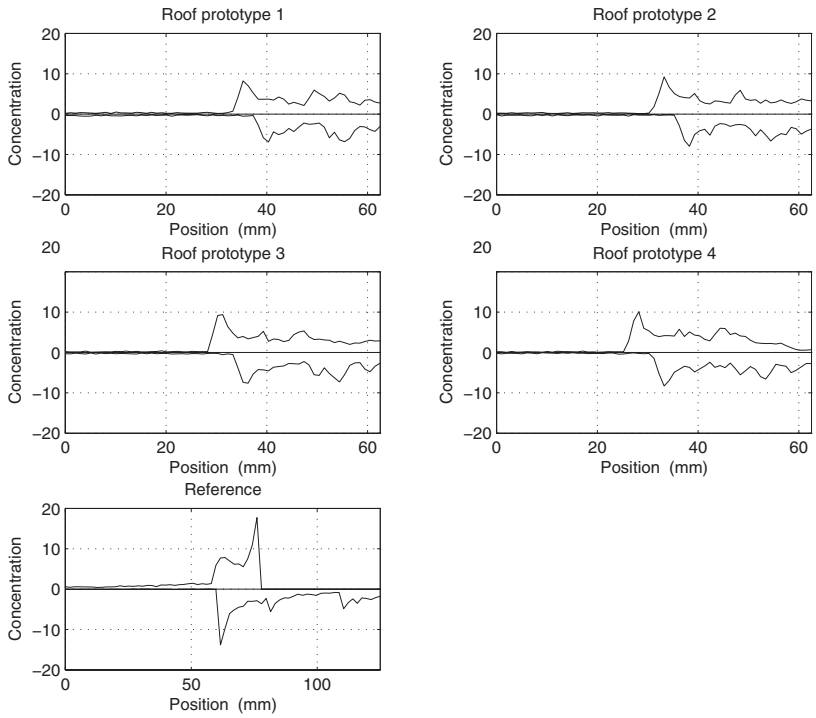

Figure 13.4 *Light concentration on the cells at a solar altitude of 40° and a solar azimuth angle of 15° for the five studied systems. The distribution above the x-axis in the figure represents the distribution on the cells facing the back reflector, and that below the x-axis represents the cells facing the front reflector.*

The figure shows that the irradiance distribution became more uniform when the structured reflectors were used. All prototype systems displayed similar irradiance homogenization. This indicates that it is an effect of the reflector structure rather than of the mirror tilt.

13.2.2 Electrical simulations of the roof concentrator

Using the light distributions from all angles of incidence, the current-voltage characteristics of the five systems were simulated. Since the geometrical concentration ratio was higher for the prototype systems, and since the light distribution was more homogeneous for these systems, both the current density and the fill factor of the cells in the prototypes were expected to

be higher. The result of such a simulation for the reference and for Roof prototype 2, for the light distributions shown in Figure 13.4, can be seen in Figure 13.5.

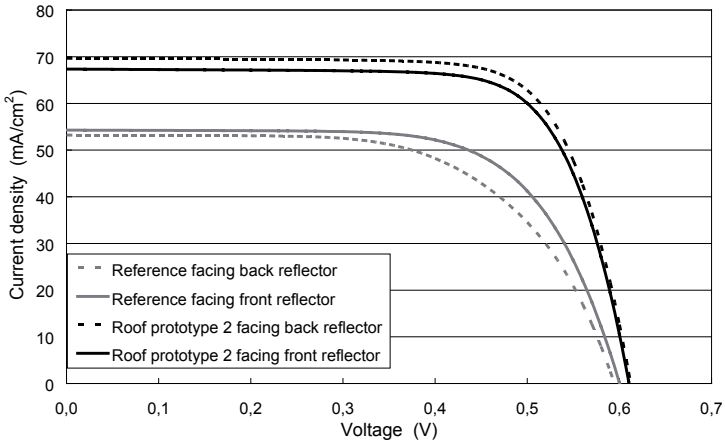

Figure 13.5 *Current-voltage characteristics for the reference system and for Roof prototype 2 for a solar azimuth of 15° and a solar altitude of 40°.*

The figure shows that both the short-circuit current and the fill factor were higher, as expected. The short-circuit current of the cells facing the back reflector was 31 % higher, and for the cells facing the front reflector, it was 24 % higher. The maximum power was 62 % and 38 % higher for the cells facing the back and front reflector respectively. The power increase was larger than the increase in short-circuit current since the fill factor was increased, which can also be seen in the figure.

13.2.3 Annual output simulations of the roof concentrator

The annual output was simulated for Lund (Lat. 55.72N, Long. -13.22) using the system efficiencies calculated according to Equation 12.1 and Equation 12.2. According to the Meteonorm simulations, the annual diffuse irradiation on the system aperture was 583 kWh/m^2, and the direct irradiation on the aperture was 568 kWh/m^2.

Figure 13.6 shows contour plots of the system efficiency for direct irradiation for Roof prototype 2 and for the reference system. The contour lines connect angles of incidence with equal efficiency.

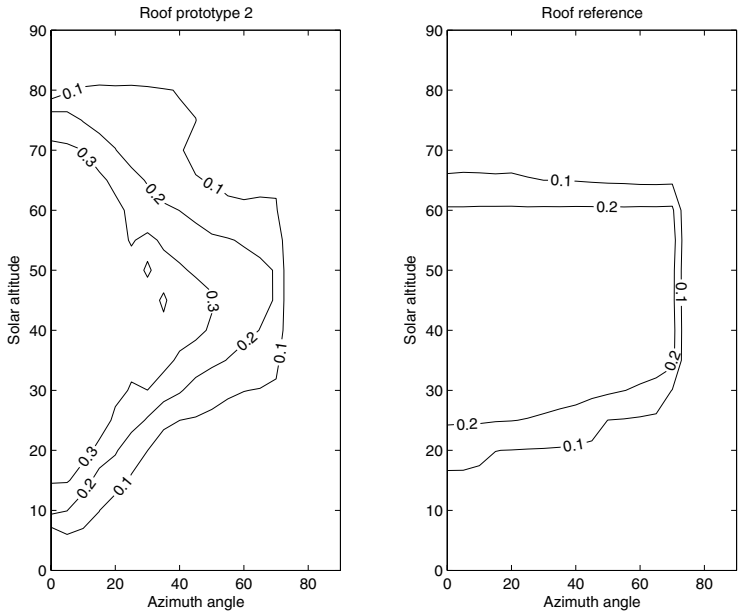

Figure 13.6 *Contour plot of the system efficiency for direct irradiation for Roof prototype 2 and for the reference. The contour lines connect angles with equal efficiency.*

The figure shows that, within the meridian plane, the interval of acceptance for the structured prototype was larger than the interval of acceptance for the reference. The efficiency was lower for the prototype at large azimuth angles close to the acceptance limits. This agrees well with previous results. Another important observation from the figure is that the system efficiency is larger within the interval of acceptance for the prototype.

The results of the annual output simulations are shown in Table 13.2.

Table 13.2 Results of the annual output simulations for the roof systems.

System	Annual output from direct irradiation	Annual output from diffuse irradiation	Total annual output per m^2 cell surface	Annual output increase compared to reference
Reference	67 kWh	96 kWh	163 kWh	1.00
Roof prototype 1	74 kWh	120 kWh	194 kWh	1.19
Roof prototype 2	73 kWh	121 kWh	194 kWh	1.20
Roof prototype 3	73 kWh	120 kWh	193 kWh	1.19
Roof prototype 4	72 kWh	119 kWh	191 kWh	1.17

As the table shows, all prototypes perform better than the reference system. The system with the highest annual output was Roof prototype 2 which is shown in Figure 13.7. It had a system efficiency for diffuse irradiation of 4.5%, compared to 4.4% for the reference. The annual output of both direct and diffuse irradiation was larger for this prototype. Roof prototype 2 showed a 20 % increase in annual output per cell surface area compared to the reference. The geometrical concentration ratio of the system is only 12 % higher than the concentration ratio of the reference system. This shows that both the increased concentration ratio and the increased fill factor are instrumental in increasing the annual electrical output.

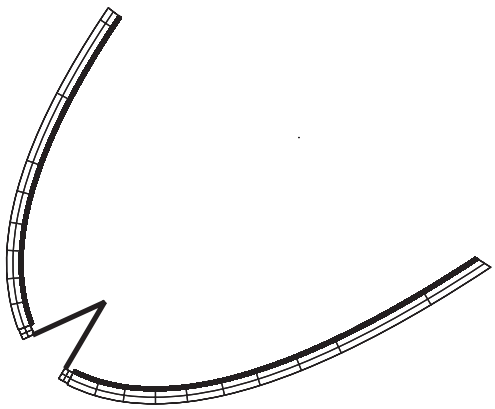

Figure 13.7 *Roof prototype 2 with reflectors tilted 25° and 60° from the horizontal.*

13.3 Design of a new wall system

In order to increase the concentration ratio of the new wall design, the tilt of the parabola was changed. The reference had its parabolic mirror tilted 15° from the horizontal, and this tilt was increased in steps of 5° to a maximum tilt of 50° for the prototype systems. The angle between the absorber and the reflector was constant which meant that the tilt of the absorber was changed along with the reflector. Table 13.3 shows the characteristics of the studied systems.

Table 13.3 Physical characteristics of the reference system and the eight prototypes.

System	Optical axis tilt	Absorber tilt	Aperture width	Cell width	Geometrical concentration ratio	Reflector structure
Reference	15°	20°	307 mm	125 mm	2.46	Smooth
Wall prototype 1	15°	20°	303 mm	125 mm	2.42	V-structure
Wall prototype 2	20°	20°	330 mm	125 mm	2.64	V-structure
Wall prototype 3	25°	15°	375 mm	125 mm	3.00	V-structure
Wall prototype 4	30°	10°	434 mm	125 mm	3.47	V-structure
Wall prototype 5	35°	5°	509 mm	125 mm	4.07	V-structure
Wall prototype 6	40°	0°	611 mm	125 mm	4.89	V-structure
Wall prototype 7	45°	-5°	748 mm	125 mm	5.98	V-structure
Wall prototype 8	50°	-10°	935 mm	125 mm	7.48	V-structure

As the table shows, the geometrical concentration ratio was increased significantly when the tilt of the parabola was changed. The geometrical concentration ratio of the largest system, Wall prototype 8, was more than three times greater than the concentration ratio of the reference. The wall system was designed for 125 mm x 125 mm cells.

13.3.1 Optical simulations for the wall system

When the light distribution on the cells in the wall systems was simulated, it was found that the homogenization seen in the simulations of the roof concentrators occurred for the wall concentrators as well. However, due to the significantly increased geometrical concentration ratio of the wall prototypes, the irradiance was observed to be high even though structured reflectors were used. For the largest system, Wall prototype 8, the peak irradiance was 50 times the solar beam. At such high irradiance levels, performance degradation in the electrical simulations can be expected.

As was shown in Chapter 11, the interval of acceptance increased when structured reflectors were applied. This is illustrated in Figure 13.8, which shows the optical efficiency as a function of the angle of incidence in the meridian plane. The optical efficiency was calculated according to Equation 13.1 as the collected irradiation divided by the incident irradiation.

$$\eta_{opt} = \frac{G_{collected}}{G_{incident}} \qquad \text{Equation 13.1}$$

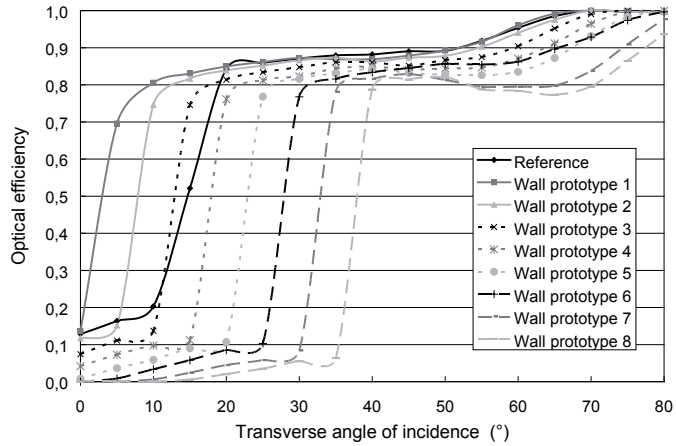

Figure 13.8 *Optical efficiency in the meridian plane, i.e. at a solar azimuth of 0°. The optical efficiency was calculated as collected irradiation divided by incoming irradiation.*

Wall prototype 3, which has its optical axis tilted 25° from the horizontal, displayed the same interval of acceptance as the reference system with a tilt of 15°. All prototypes with a greater axis tilt showed a smaller interval of acceptance, and all systems with a lower tilt showed a larger interval.

13.3.2 Electrical simulations for the wall reflector

The current-voltage characteristics for three of the systems at solar azimuth 15°, solar altitude 35°, can be seen in Figure 13.9. As expected, the short circuit currents of the structured prototypes were higher, but increased optical losses were seen since the difference in geometrical concentration ratio between the prototypes and the reference was greater than the difference in short-circuit current. The fill factor was observed to decrease for the structured systems due to the high local currents caused by the high concentration ratios. This is in agreement with the findings in Section 13.3.1.

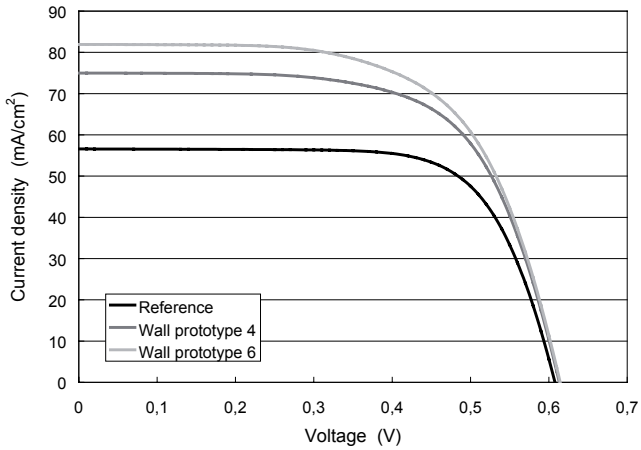

Figure 13.9 *Current-voltage characteristics for the reference system and for wall prototypes 4 and 6 for a solar azimuth of 15° and a solar altitude of 35°.*

13.3.3 Annual output simulations of the wall concentrator

The annual direct irradiation on the vertical aperture was 397 kWh, and the annual diffuse irradiation was 375 kWh. The system efficiency for direct irradiation was calculated from the electrical simulations. The system efficiency for direct irradiation of Wall prototype 6 and of the reference is shown as a contour plot in Figure 13.10.

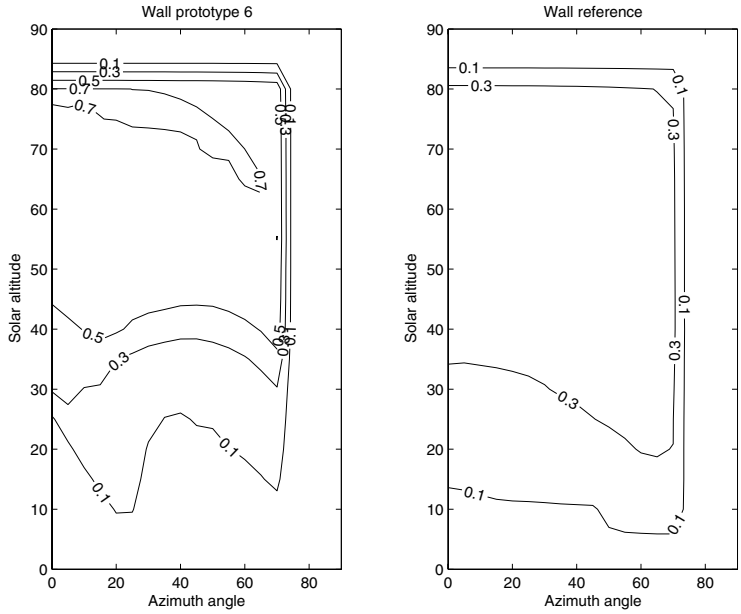

Figure 13.10 *System efficiency for direct irradiation as a function of the solar angles. The contour lines connect angles with equal efficiency.*

The system efficiency of Wall prototype 6 was low for low solar altitudes due to the large tilt of its optical axis; it was tilted 40° from the horizontal. Within its interval of acceptance, however, the efficiency of the prototype system was much larger than that of the reference.

The annual outputs of the wall prototypes and of the reference were simulated. The results are shown in Table 13.4.

Table 13.4 Estimated annual output for the investigated wall concentrators.

System	Annual output from direct irradiation	Annual output from diffuse irradiation	Total annual output per m^2 cell surface	Annual output increase compared to reference concentrator
Reference	101 kWh	93 kWh	194 kWh	1.00
Wall prototype 1	101 kWh	88 kWh	190 kWh	0.98
Wall prototype 2	104 kWh	89 kWh	192 kWh	0.99
Wall prototype 3	107 kWh	89 kWh	196 kWh	1.01
Wall prototype 4	110 kWh	89 kWh	199 kWh	1.03
Wall prototype 5	111 kWh	88 kWh	199 kWh	1.03
Wall prototype 6	120 kWh	93 kWh	213 kWh	1.10
Wall prototype 7	106 kWh	86 kWh	192 kWh	0.99
Wall prototype 8	101 kWh	85 kWh	186 kWh	0.96

As the table shows, the output was increased for most of the structured systems, but not at all to the extent of the increased concentration ratios. The best system, Wall prototype 6, was estimated to generate 10% more electricity compared to the reference concentrator. The system efficiency for diffuse irradiation of this prototype was 5%. For the reference it was 10%. It was estimated to generate approximately the same electrical energy from diffuse irradiation as the reference concentrator due to its higher concentration ratio. The electrical energy from direct irradiation for the prototype system was estimated to increase by 19% compared to the reference. The geometry of Wall prototype 6 is shown in Figure 13.11.

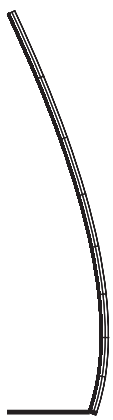

Figure 13.11 Wall prototype 6 with horizontal absorber and mirror tilt 40°.

13.4 Optimal designs

According to the simulations, the optimal roof system was Roof prototype 2. The parabolas of this system were tilted 25° and 60° from the horizontal. The estimates show that this system will generate 20 % more electricity compared to the reference system. As was shown in Section 13.2.2, both the short-circuit current and fill factor were improved when the structured reflectors were applied.

Another benefit of the more homogeneous irradiance distribution is that the local temperatures on the cell surface where the light is concentrated will be lower. The reference has been designed for the cells to be cooled by water from the back of the absorber. This makes the system produce heat as well as electricity which is a benefit if the investor is interested in both heat and electricity. If heat is uninteresting, however, it is useless. Furthermore, the temperature at the centre of the irradiance distribution will increase dramatically if the water circulation in the system stops and this may lead to breakage of the cells thus making the system sensitive to malfunction. Since the peak irradiance at the cell surface will be reduced when structured reflectors are used, this problem might be avoided. If so, it will be possible to manufacture stationary PV concentrators without active cooling. This will be a very interesting option for users that are not interested in heat since it will reduce the installation cost considerably and make the systems easier to integrate into a building.

Wall prototype 6 was found to be the most optimal wall concentrator solution. Its absorber was horizontal, and the optical axis of the reflector was tilted 40° from the horizontal. Compared to the reference, this system was estimated to generate 10% more electricity. The geometrical concentration ratio of this prototype was almost a factor of two higher than that of the reference, which shows that the geometrical concentration ratio has to be increased considerably in order to improve the reference system. The most important reason why the performance improvements were as small as they were is that the reference system shows very good fill factors even though the concentration ratio is 2.46. The reason for this is that the absorber is tilted 35° from the optical axis which causes the light to be out of focus when it strikes the cells. Since it is out of focus, the peak irradiance is considerably lower, and the fill factor thus increases.

The structured reflector is in itself 15% larger than a smooth reflector due to the Vs. When the tilt of the parabolas is changed in order to increase the concentration ratio, this increases the required reflector area even further as was discussed in Section 13.2. When more material is needed, the system cost is increased. It is therefore important to analyse at what prices for solar cells and reflector materials we can expect the energetic

gains to be economic gains as well. The ratio between reflector cost and solar cell cost at which the generation cost of the prototype equals the generation cost of the reference has been calculated. The results of these calculations are shown in Table 13.5. The cost of the glazing covering the system aperture has been included in the reflector cost.

Table 13.5 Ratio between reflector cost, including cover glazing, and solar cells cost at which the reference system and the prototype system generate electricity at equal costs.

Concentrator	Reflector cost/cell cost at which the generation cost of the prototype equals the generation cost of the reference system
Roof prototype 2	0.20
Wall prototype 6	0.04

As the table shows, the roof system becomes profitable at a reflector price 5 times higher than that of the wall system. This is due to the large reflectors in the system which has a concentration ratio almost a factor of two higher than the reference.

As an example, assume that the current cost of 1 m^2 of reflector including cover glazing is €27, and that the current cost of 1 m^2 of solar cells is €500. This would mean a ratio of 0.05. At these costs, Roof prototype 2 would be profitable and produce 14% more electricity per Euro. The wall system in this example would not be profitable; it would generate electricity at approximately the same cost as the reference system.

14 Measurements on a CPC with structured reflectors

Two new trough designs, one for a wall concentrator and one for a roof concentrator, were described in Chapter 13. The roof concentrator consists of two parabolic mirrors and a wedge absorber. The optical axes of the parabolas are tilted at 25° and 60°, which gives it a geometrical concentration ratio of 2.80 after truncation. In order to give it a larger interval of acceptance, and to create a more homogeneous irradiance distribution on the cells, a structured reflector was used. The reflector structure was a V-structure with an opening angle of 120°. The system was intended for building integration, which made the size and the geometry an important issue. For this reason, it was designed for 125 mm × 62.5 mm cells instead of the full size 125 mm × 125 mm cells. The system was developed through simulations, and the annual output estimates were simulated. In order to verify the simulation results, a prototype was constructed. This prototype is shown in Figure 14.1.

As the figure shows, the absorber was fitted with one cell facing each reflector. By having only one cell on each side of the absorber, the system properties were easier to measure. If more cells had been used, shading effects from the sides due to the short reflector and electrical losses due to cell mismatch would have influenced the measurements. A full scale system with a length of 3-4 m would not have cells on the outermost parts of the absorber in any case since its performance would deteriorate owing to the shading effects. Each reflector consisted of approximately 100 wooden prisms that were glued together. The reflecting material was an adhesive plastic film with a vacuum evaporated aluminium coating which had a reflectance of 85% in the solar spectrum.

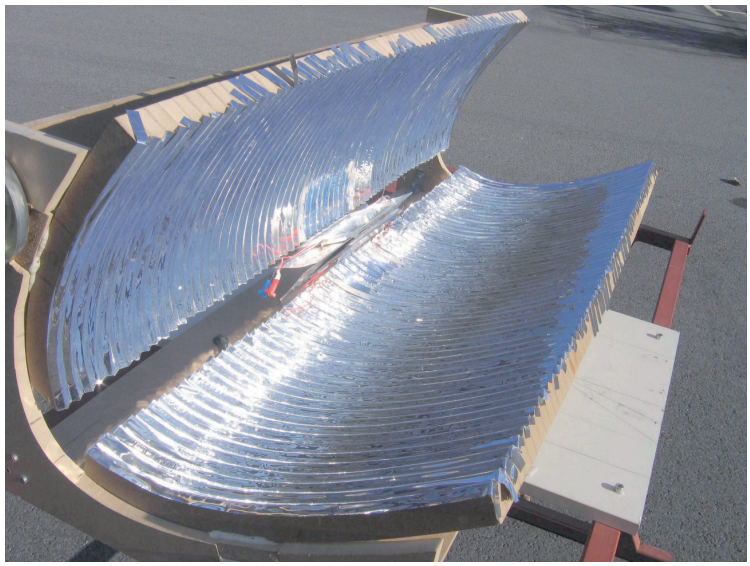

Figure 14.1 *Evaluated prototype system with V-structured reflectors where the Vs have an opening angle of 120°. The geometrical concentration ratio of the system is 2.8.*

In order to characterize the system, the current-voltage (IV) characteristics and irradiance distribution on the cells were measured for different angles of incidence.

The new prototype was intended to have a higher electrical output than the MaReCo concentrator with smooth reflectors. The results of the measurements were therefore compared with the measurements on this concentrator presented in Chapter 8. Throughout this chapter, the MaReCo with smooth aluminium reflectors and 125 mm × 125 mm wide cells will be referred to as the reference. Figure 14.2 shows the current-voltage characteristics of a cell used in the smooth MaReCo, and a cell used for the new prototype.

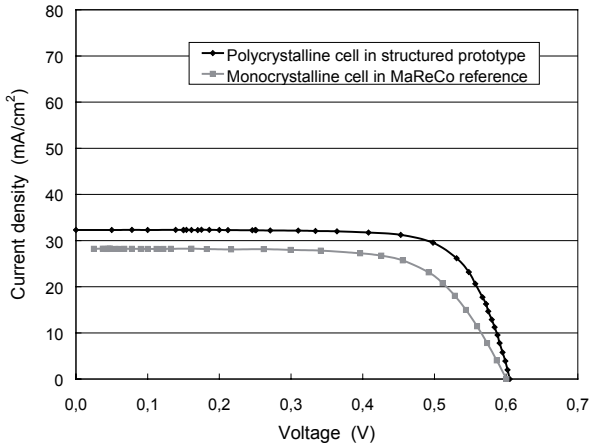

Fig 14.2 *Current-voltage characteristics of the two different cells used in the concentrators.*

The cell in the smooth reference system was a monocrystalline silicon cell and that in the new prototype system was a polycrystalline silicon cell. As the figure shows, the short-circuit current was higher for the cell in the prototype system. This can be explained by the fact that the monocrystalline cell is slightly older than the polycrystalline cell, and the efficiency of standard cells has increased considerably in recent years. The increased efficiency can also be seen from the fill factor which is 0.69 for the reference and 0.75 for the cell of the prototype.

14.1 Measurements of the irradiance distribution

The irradiance distribution was measured as described in Section 7.3. It was measured as a function of the solar altitude and the solar azimuth angle. The solar altitude was varied from 0° to 70° in steps of 5° for solar azimuth angles of 0°, 15°, and 30°.

Figure 14.3a shows the measured irradiance distributions on the cells facing the back reflector for the structured prototype and the smooth MaReCo at a solar altitude of 30° in the meridian plane. This altitude was chosen since the back reflector has a high efficiency for both concentrators here. Figure 14.3b shows the light distribution on the cells facing the front reflector for a solar altitude of 60° in the meridian plane. At this angle, the

cells facing the front reflector receive high irradiation for both concentrators. Note that the distributions for the reference were measured on a 125 mm wide cell and the distributions on the prototype were measured on a 62.5 mm wide cell. The x-axis of the reference is therefore above the graph, and the x-axis of the prototype is below the graph.

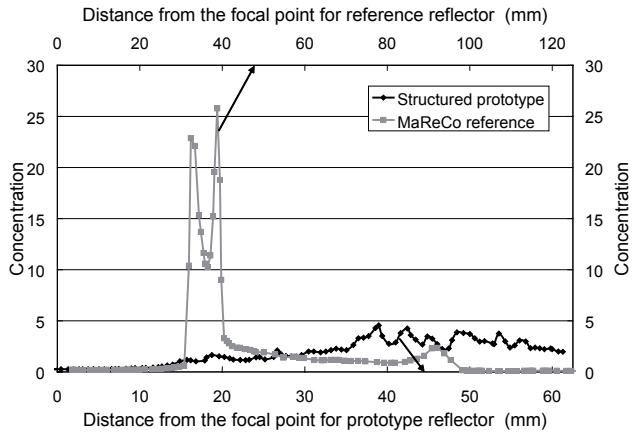

Figure 14.3a Light distribution on the cells facing the back reflector at a solar altitude of 30° at a solar azimuth angle of 0°.

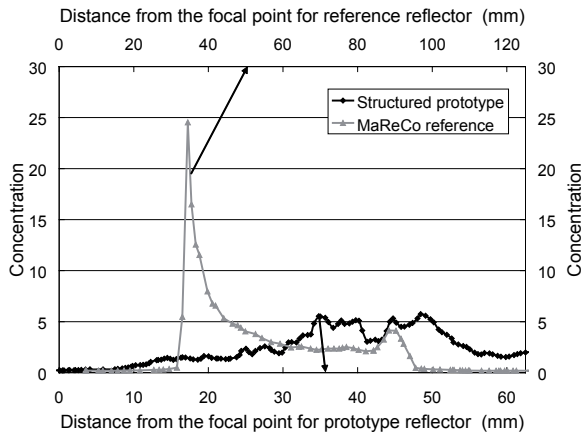

Figure 14.3b Light distribution for the cells facing the front reflector at a solar altitude of 60° at a solar azimuth angle of 0°.

The figures show that considerably more homogeneous light distributions were obtained in the structured prototype. The peak irradiance was close to 5 suns at both solar altitudes compared to almost 25 suns for the reference MaReCo. Integrations of the light distributions on the cells reveal that the cell in the prototype system and the cell in the reference system received approximately equal average irradiance. In Figure 14.3a, the average irradiance was 8 % higher for the cells in the prototype, and for Figure 14.3b, equal average irradiance was found. The geometrical concentration ratio of the prototype was 12 % higher than the concentration ratio of the reference. It was found in Chapter 11 and Chapter 13 that structured reflectors increase the optical losses. The optical losses found in the measurements, which were between 4 % and 12 %, have to be considered acceptable for angles within the meridian plane.

Figure 14.4 shows the light distributions for the cells facing the back and front reflectors at solar altitudes of 30° and 60° respectively for a solar azimuth angle of 30°.

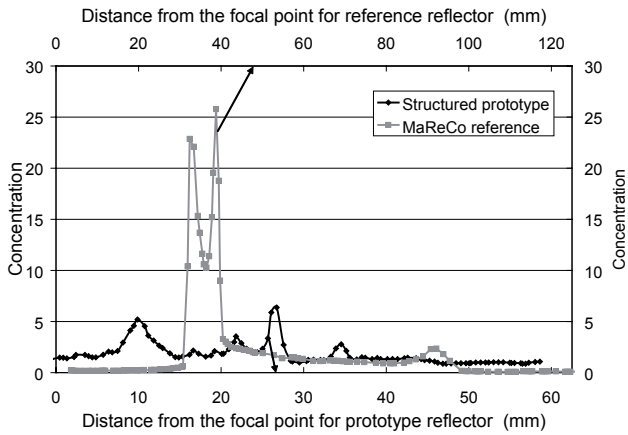

Figure 14.4a *Light distribution on the cells facing the back reflector at a solar altitude of 30° and a solar azimuth angle of 30°.*

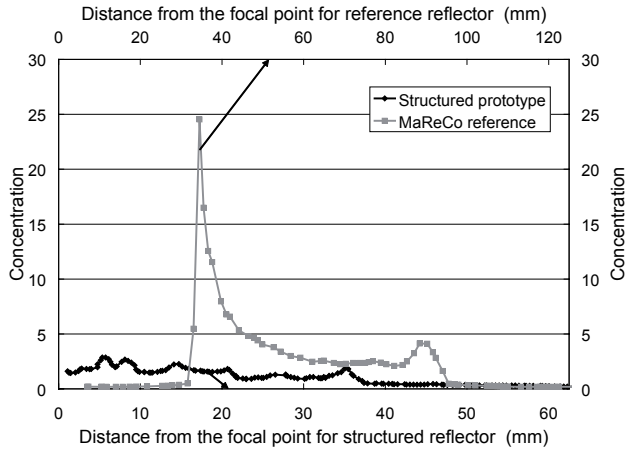

Figure 14.4b Light distribution on the cells facing the front reflector at a solar altitude of 60° at a solar azimuth angle of 30°.

Figure 14.4a and Figure 14.4b show that the light distributions on the cells in the prototype concentrators are homogeneous. However, the optical losses have increased considerably. The light distributions in the reference MaReCo were similar to the distributions of Figure 14.3. This is explained by the transverse projected angle of incidence which was almost the same for the two cases. Since the optical characteristics of a translationally symmetric concentrator are independent of the longitudinal angle, the light distributions will be similar. By integrating the light distributions it was found that for Figure 14.4a, the average irradiance was 20 % lower for the cells in the prototype system compared to the reference. In Figure 14.4b the average irradiance was 44 % lower for the cells in the prototype system. The irradiance at the focal point was not zero and this indicates that some of the rays were reflected above the cells and out of the system since the absorber ends at this point. For the cells in the reference MaReCo, this does not seem to be the case.

14.2 Measurements of the current-voltage characteristics

The current-voltage characteristics were measured for the same angles of incidence as the irradiance distributions. Since the light distribution in

the structured prototype was more uniform, fill factor improvements for the structured prototype were expected.

Figure 14.5a shows the current-voltage characteristics for the cells facing the back reflector at a solar altitude of 30° in the meridian plane. This means that they are the current-voltage characteristics corresponding to the light distributions in Figure 14.3a. The IV-characteristics corresponding to Figure 14.3b are shown in Figure 14.5b.

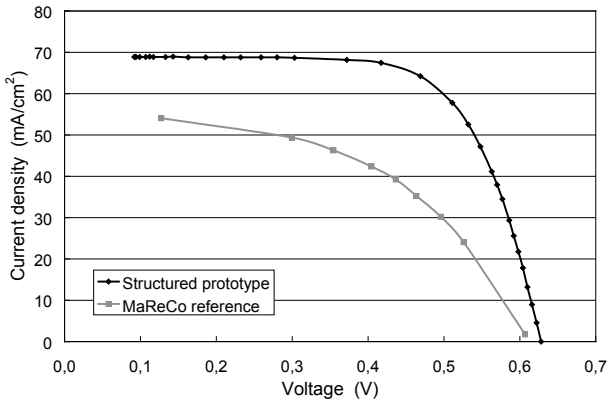

Figure 14.5a Current-voltage characteristics of the cells facing the back reflector for solar azimuth 30° and solar altitude 30°.

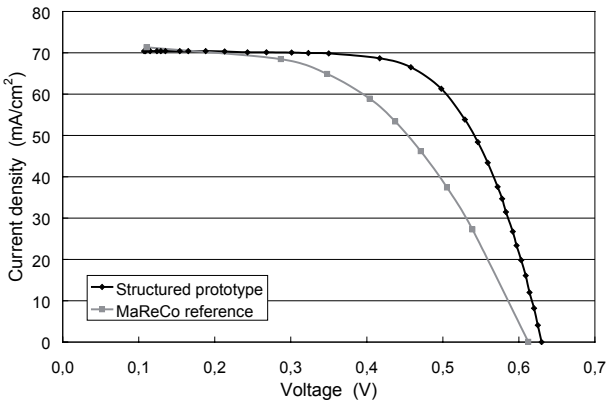

Figure 14.5b Current-voltage characteristics of the cells facing the front reflector for solar azimuth 30° and solar altitude 60°.

The figures clearly show that the problems regarding fill factor decline were reduced. For the reference MaReCo, the fill factor at uniform 1000 W/m^2 irradiance was 0.69. For Fig. 14.5a, the fill factor was reduced to 0.50 and for Fig. 14.5b; the fill factor was reduced to 0.54. This meant that the fill factor was decreased by 28 % for the cells facing the back reflector, and by 21 % for the cells facing the front reflector. For the cells in the structured prototype, the fill factor decreased from 0.75 to 0.70 and 0.68 respectively. This gave a fill factor decrease of 7 % for the back, and of 9 % for the front reflector cells.

For the cells facing the front reflector in Figure 14.5b, the short-circuit current density of the cells in the MaReCo concentrator was equal to the short-circuit density of the cells in the structured prototype. Considering that the short-circuit current of the cell in the prototype system was 14 % higher under standard test conditions, which was shown in Figure 14.2, this suggests that the optical efficiency of the prototype was slightly lower. However, the maximum power output density was 38 % higher for the cells in the prototype system due to the decreased fill factor reduction. For the cells facing the back reflector, the short-circuit current density of the cell in the prototype system was 23 % higher than for the cell in the reference system. The maximum power output density of the prototype system cell was 75 % higher than that of the reference.

Figures 14.3 and 14.5 clearly show that the system performance in the meridian plane can be improved by using a structured reflector. For angles outside the meridian plane, Figure 14.4 suggests that the same increases will not be obtained. Figure 14.6a shows the IV-characteristics for the cells facing the back reflector at a solar altitude of 30° and an azimuth angle of 30°. Figure 14.6b shows the characteristics for the cells facing the front reflector at a solar altitude of 60° and a solar azimuth angle of 30°. These are the current-voltage characteristics corresponding to the irradiance distributions shown in Figure 14.4.

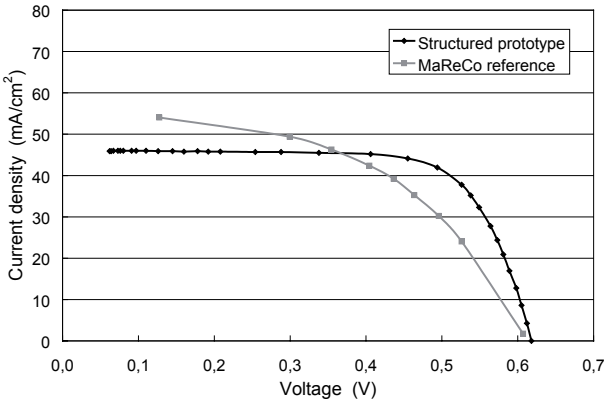

Figure 14.6a Current-voltage characteristics of the cells facing the back reflector for solar azimuth 30° and solar altitude 30°.

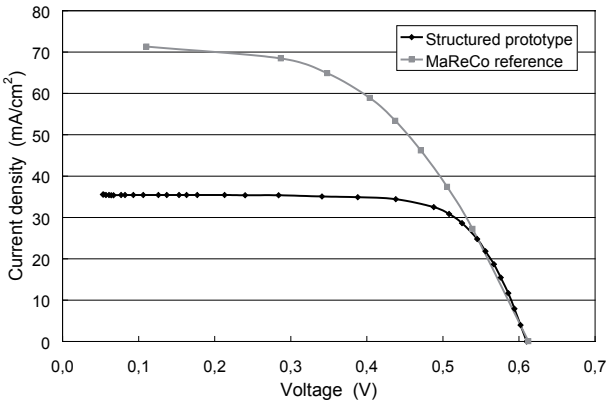

Figure 14.6b Current-voltage characteristics of the cells facing the front reflector for solar azimuth 30° and solar altitude 60°.

The figures show the same optical losses that were seen in Figure 14.4. The short-circuit current of the cells facing the back reflector in the prototype system was 18% lower than for the reference. For the cells facing the front reflector, the short-circuit current was 49% lower. The maximum power of the cells facing the back reflector was 21% higher for the prototype, but it

was 33% lower for the prototype in the cells facing the front reflector. At this angle of incidence, it is not possible to show any considerable increase in electrical output for the structured concentrator.

14.3 Discussion

The measurements have indicated large optical losses since the short-circuit currents were not as high as could have been expected from the higher short-circuit current of the new cells and from the increased concentration ratio of the new prototype. When the results of the optical simulations in Chapter 13 were examined, these large optical losses were not seen, which indicates that it might have to do with the construction of the prototype. When the sun was in the meridian plane, the losses were acceptable and considerable performance improvements could be seen. The higher standard test efficiency of the cells in the prototype system is one of the reasons why the output increased, but this cannot account for a power increase between 38% and 75%. This shows that structured reflectors have a large potential for increasing the system output of stationary concentrators. However, at larger azimuth angles, considerable performance improvements could not be shown even though the simulations anticipated such improvements.

By a visual inspection of the prototype, several flaws can be seen. The largest error is due to the manufacturing of the trough. A systematic error was introduced when the prisms were glued together which caused each segment to be translated slightly from its predecessor. This resulted in a twisted reflector. The outcome of this was that in order for the reflector to be straight along the absorber, it had to be truncated here. Close to one of the gables, almost two centimetres had to be removed, whereas the other edge of the reflector was left almost untouched. This obviously affects the optical properties of the system. A point that is on the optical axis of one of the edges corresponds to a point two centimetres from the focal line on the other side of the reflector. When measurements were performed in the meridian plane, this effect was relatively small since the difference between the left edge and the right edge of the cell was relatively small. When larger parts of the reflector became active at larger azimuth angles, however, the difference between the different parts of the reflector became considerable. This is one explanation of the larger optical losses. Another problem resulting from the truncation of the reflector close to the absorber was that the tilt of the absorber was changed. Since the innermost part of the reflector was removed, the angle between the two absorber halves increased in order to prevent a gap between the cells and the truncated

reflector. This also had an effect on where the cell became illuminated. The most important observation from Figure 14.5 regarding the optical losses was that the distribution was non zero at the focal point. The effects discussed above show partly why this happened.

The comparison in this study was made between a reference MaReCo with smooth reflectors and the new structured prototype. One obvious source of error in the comparison is the different characteristics of the two cells. The structured prototype was fitted with new standard polycrystalline cells whereas the smooth reference had slightly older monocrystalline cells. As was shown in Figure 14.2, the fill factor of the new polycrystalline cells was 9 % higher than the fill factor of the cell in the reference concentrator under standard test conditions. The short-circuit current was 14 % higher for the new cell. This resulted in a 26 % higher power output of the new polycrystalline cell under standard test conditions. This makes a comparison on equal terms difficult. The rationale for choosing these particular cells for the prototype was that when the new prototype was constructed, it was important to use currently available standard cells in order to illustrate how well the system can perform with current technology cells. Another reason to use these cells was that the simulations in Chapter 13 were performed for a currently available cell and this should make a comparison with the simulations easier. However, due to the low manufacturing precision, comparisons with the simulations are of little relevance.

The maximum power output increase of the prototype system from Figure 14.5 and Figure 14.6 is shown in Table 14.1. The 26 % higher power output of the newer cells was compensated for by multiplying all the reference system outputs by 1.26.

Table 14.1 Power output increase before and after compensation for the difference under standard test conditions.

Cell orientation	Solar altitude	Solar azimuth	Power increase before compensation	Power increase after compensation
Facing back reflector	30°	0°	75 %	39 %
Facing back reflector	30°	30°	21 %	- 3 %
Facing front reflector	60°	0°	38 %	10 %
Facing front reflector	60°	30°	- 33%	- 47 %

The table shows that within the meridian plane, the structured system outperformed the reference system, but at larger azimuth angles the optical losses became too large.

To make the system smaller in order to simplify building integration, the prototype was fitted with 62.5 mm wide cells instead of 125 mm wide cells. This will in itself yield a better fill factor since the smaller system will collect less irradiation and thus will have lower currents. This complicates the comparison even further.

Attempts were made to insert a smooth reflector into the prototype trough for comparison. But due to the skew trough, and to the slightly different prism sizes, it was impossible to obtain a smooth parabolic surface. When the irradiance was measured in the meridian plane for this system, the peak irradiance level at a solar altitude of 60° for the cells facing the front reflector was 7 suns. Based on previous measurements on smooth parabolic reflectors, the peak irradiance should probably have been around 25-30 suns for this mirror if it were completely parabolic.

One effect that was seen during the measurements was the non uniform irradiance distribution along the length of the absorber. In a translationally symmetric system, the distribution is completely uniform in this direction but this is not the case for structured troughs. Figure 14.7 shows a photo of the light distribution on the absorber taken during the measurements.

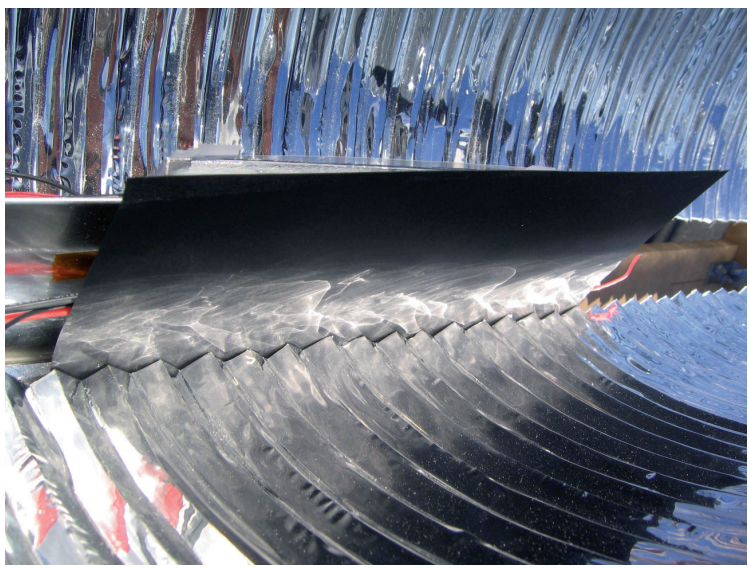

Figure 14.7 *Non uniform irradiance distribution along the absorber created by the relatively large prisms.*

The pattern that is seen in the picture probably has no influence on the electrical output since the irradiance peaks are small. If these non uniformities are considered a problem for any reason, they can be removed

by making the structure smaller. In the current design, each prism is approximately 10 mm wide. By making them smaller, the irregular pattern on the absorber would fade.

14.4 Conclusions

Due to the low manufacturing precision, it was difficult to draw conclusions about the measurements. What can be said is that the structured reflector performed well within the meridian plane where the more homogeneous light distribution increased the electrical output considerably. For angles outside the meridian plane, the optical losses became too large. The simulations show that the optical losses will increase in a structured trough, but not at all to the extent seen here. If structured reflectors are to be used in new designs, more care has to be taken when constructing the system. It is of the utmost importance to improve the shape of the reflectors and to mount the cells in their appropriate place. This was difficult to do for this prototype due to the lack of proper tools and equipment, as well as the lack of experience working with this technology. If a better prototype can be made, however, the measurements in the meridian plane indicate that this technology will make it possible to increase the electrical output of stationary concentrators with standard cells.

15 Improving the design of stationary solar concentrators

The main goal of this thesis has been to improve the efficiency of stationary concentrators with standard solar cells. There are many possible changes that can be made to the system in order to achieve this, and some of these have been investigated while some others have been left out. In this chapter, I will discuss some of the possible changes to the system, and the way they will affect the annual electrical output.

15.1 Reflector materials with a higher reflectance

One of the most obvious improvements to a mirror based stationary concentrator is to improve the reflectance of the mirrors. The most commonly used material for the reflectors is anodized aluminium, which has a reflectance of approximately 85%. Its main advantage is its low cost and its relatively good mechanical properties. If a thin reflector film is used for a reflector, it has to be supported by another material to give the reflector its shape. However, when aluminium is used for the reflector, it can be used both as reflector surface material and as supporting structure for the mirror. This makes aluminium one of the most cost-effective materials for solar mirrors.

The disadvantage of aluminium is the relatively low reflectance of 85%. It is possible to find materials with considerably higher reflectance; several manufacturers have reflectors with a reflectance of 96%. The price of such mirrors is higher than the cost of aluminium mirrors, but since the cost of the mirror is only a small fraction of the total system cost due to the high price of solar cells, it might be an interesting alternative anyway.

A small study was performed on a MaReCo concentrator with standard PV cells. One trough was fitted with a standard anodized aluminium mirror with a reflectance of 85%, and one trough was fitted with a mirror with a reflectance of 96%. This meant that the reflectance of the second system was 13% higher than the reflectance of the first trough. Using the method outlined in Chapter 12, the annual output of both systems was simulated. It was found that the system with the new reflector material would generate 13% more annual electricity than the reference with aluminium reflectors. Since the reflectance increased by 13 % as well, this shows that the output increase is directly proportional to the increased reflectance.

The conclusion is therefore that if the increase in system cost is lower than the increase in reflectance, it is a good idea to use the new reflector material when new systems are constructed.

15.2 Change the tilt angle of the absorber

For an ideal parabolic system with 100% reflectance and with cells that do not suffer from reduced efficiency due to non uniform irradiance, the best option is to have the absorber along the optical axis from the focal point to the mirror edge. Such a two dimensional system is thermodynamically ideal and therefore has the maximum theoretical concentration ratio. However, this is never true in practice, especially for stationary low concentrating systems with standard cells where it is important to keep the system cost as low as possible. Changing the tilt angle of the absorber is in this case an interesting design parameter since it will change the light distribution and the number of reflections (Baum et. al. 1986).

Consider a wall reflector such as the solar window geometry discussed in Chapter 13. When the absorber is tilted upwards from the optical axis, this results in a lower geometrical concentration ratio for a given absorber width. This is negative in the sense that less light will be collected on the solar cells. On the other hand, the decreased concentration ratio will lead to lower irradiance on the cells, which can have a positive effect on the fill factor. Other positive effects that can be expected when the absorber is tilted is that more light strikes the cells directly without being reflected, and that the light incident along the optical axis will be slightly out of focus when it strikes the cell surface. Since all the reflected light will be somewhere between the focal point and the reflector when it strikes the absorber, no light will miss the absorber due to the change of tilt.

In order to analyse the effects of tilting the reflector, the annual output of one wall reflector with tilted absorber and one wall reflector with the absorber along the optical axis was simulated. The optical axis of the para-

bolic mirror was tilted 25° from the horizontal, which made the system accept light with a solar altitude greater than 25°. The absorber was tilted 15° upwards from the horizontal in the case with tilted absorber, which made the difference in absorber tilt 40° between the two cases. The system with the absorber along the optical axis had a concentration ratio of 3.46, which was 13% higher than the concentration ratio of the system with a tilted absorber.

The simulations show that the system with the absorber tilted 15° from the horizontal would yield 5% more annual electricity for the same solar cell surface area.

There are mainly two reasons why the system with the absorber tilted 15° outperformed the system with a higher concentration ratio. The first reason is the increased efficiency for diffuse light. The system with the absorber along the optical axis does not collect any irradiation at solar altitudes below 25° whereas the other system collects light directly on the absorber due to its tilt. For solar altitudes above 25°, the system with the tilted absorber exhibited a lower average number of reflections since more light would hit the cell directly without being reflected off the reflector. The system efficiency for diffuse light calculated according to Eq. 12.2, for the system with the absorber along the optical axis, was 6.6% and for the system with 15° tilt it was 8.1%.

The second reason for the increased output was that the peak irradiance for light incident just inside the interval of acceptance was reduced since some of the light hit the cells directly. This resulted in an increased fill factor. The increased fill factor can be seen in Figure 15.1, which shows the current-voltage characteristics of the cells at a solar altitude of 30° in the meridian plane.

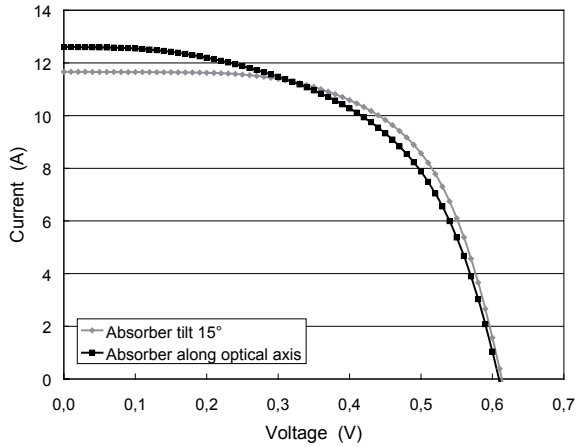

Figure 15.1 *Current-voltage characteristics for the cells at solar altitude 30°, solar azimuth 0°.*

The figure shows that the short-circuit current was 7% lower for the cell at 15° tilt, but the maximum power was 6% higher. When larger solar altitudes were studied it was found that it is only close to the acceptance angle that we can expect gains due to defocusing. At higher solar altitudes, the higher concentration ratio is more important since the light is more evenly distributed over the cells anyway.

The results from the comparison show that tilting the absorber can be a good idea to increase the efficiency for diffuse light, and to improve the performance around the acceptance angle. The simulations showed that the system with an absorber at 15° tilt performed better at low solar altitudes, and the system with the absorber tilted along the optical axis performed better at higher solar altitudes.

The conclusion is that for systems that already have a high efficiency for diffuse irradiation, tilting the absorber is of little use. This is also true if a system is designed in such a way that the irradiation around the acceptance angle is low, since it is at this angle that the flux concentration ratio is high and thus the largest gains can be made.

15.3 Double sided versus single sided absorber

In Chapter 13, simulations were performed to estimate the annual electrical output of a new roof concentrator and a new wall concentrator. MaReCo was used as a reference for the roof system, and the geometry of the solar window as a reference for the wall concentrator. Both reference systems had a geometrical concentration ratio of approximately 2.5. The total irradiation on the MaReCo aperture tilted at 30° from the horizontal was 1113 kWh/m^2. The total irradiation on the vertical wall system aperture was 772 kWh/m^2 which shows that 44% more irradiation is available for collection at the aperture tilted at 30°. The simulations estimated the annual output of the MaReCo concentrator at 163 kWh, and that of the wall concentrator at 194 kWh. Considering that the roof system receives more annual irradiation, it is somewhat surprising that it is estimated to yield 16% less annual electricity.

One of the reasons for this result is the double sided absorber of the MaReCo concentrator. MaReCo was originally developed as a solar thermal concentrator where the aim was to generate as much heat as possible from the direct irradiation. Due to the double sided absorber, the system performs very well for this application since a thermal absorber is double sided by nature. For photovoltaic applications however, the double sided absorber costs twice as much as a single sided absorber, and this considerably reduces the system efficiency per absorber surface area. The result is that the MaReCo concentrator performs slightly worse than a wall concentrator during the winter, and slightly worse than a horizontal concentrator during the summer. The outcome is that compared to a flat PV module mounted at 30° tilt, it only produces 25% more annual electricity.

Due to the high cost of solar cells, it is not wise to optimize the output for a double sided absorber. Too many compromises have to be made in order to get reasonable output from both sides. It is more profitable to optimize two side-by-side systems. One system could be optimized to maximize the collection during the winter and the other to maximize summer collection in order to get a system that can generate electricity all the year round.

15.4 Design for increased efficiency for diffuse irradiation

Another reason why the wall reflector performed better than the MaReCo was that the wall concentrator produced considerably more electricity from diffuse irradiation, 93 kWh compared to 67 kWh.

By looking at Figure 15.2, it is evident that the wall concentrator has a higher optical efficiency for almost all angles of incidence compared to the roof concentrator.

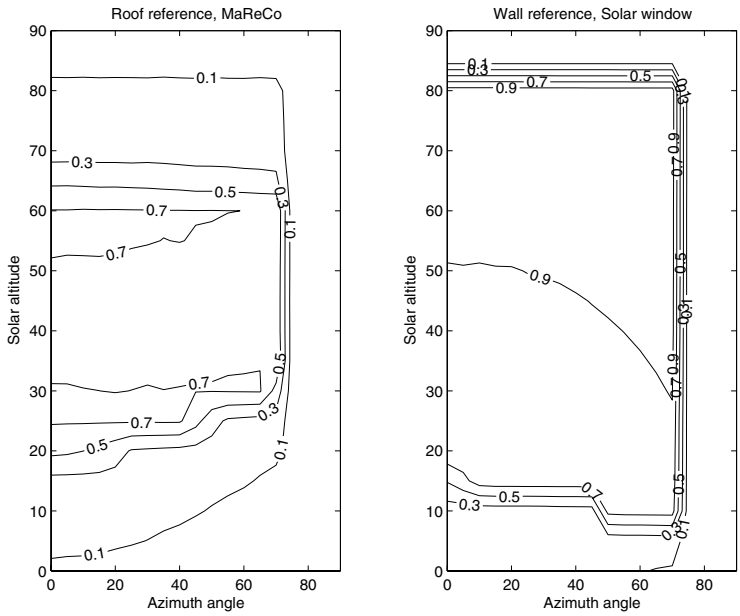

Figure 15.2 *Optical efficiency for all angles of incidence for the roof reference system and for the wall reference system. The contour lines connect angles of equal efficiency.*

As was shown in Figure 10.7, very little direct irradiation is received above 65° or below 20°. This was the basis for the design of the MaReCo, which has a low efficiency outside its interval of acceptance. For diffuse irradiation, however, it makes a difference. And since the diffuse irradiation is almost equal to the direct irradiation for both a vertical and a tilted surface for northern latitudes such as Lund, it is costly to exclude this part of the total irradiation on the aperture. If we calculate the optical efficiency for diffuse irradiation by using Equation 12.2 without $\eta_{electric}$

since it was optical efficiency and not system efficiency, we find that the optical efficiency for diffuse irradiation was 67% for the wall reflector, and 30% for the MaReCo. This shows why the wall reflector is so successful at collecting diffuse irradiation. If the same equation is used to calculate the optical efficiency for diffuse irradiation of a planar PV module, the efficiency is 93%, but considering that the concentration ratio of the wall system is 2.46, we can expect the wall system to generate considerably more electricity from diffuse irradiation.

When concentrators are discussed, the diffuse light is often discarded since it is such a small part of the irradiation on the cells. This is true for systems with a high concentration ratio, or systems in a climate with a high fraction of direct irradiation. For low concentrating systems in climates with a high fraction of diffuse irradiation, however, care must be taken not to overlook the possibility of maximizing the collection of diffuse irradiation.

15.5 Micro-structured reflectors

The use of micro-structured reflectors was thoroughly discussed in Chapter 11 and Chapter 13. Micro-structured reflectors mainly give two advantages for concentrators with standard solar cells, a more homogeneous light distribution and the possibility to increase the geometrical concentration ratio while maintaining the same acceptance interval. The disadvantage of micro-structured reflectors is increased optical losses due both to a higher number of reflections and to light being reflected out of the system.

In order to illustrate how the homogenization of the light distribution affects the system output, the annual output of one MaReCo with smooth reflectors and one with V-structured reflectors was simulated. Since the global shape of the mirrors and absorber was the same for both cases, it is a good example of how the V-structure affects the system output. The analysis showed that the structured system would generate 6% more electricity over the year. The increased output was due to the homogenization of the irradiance on the solar cells for most, but not all, angles of incidence. This is seen in Fig. 15.3 which shows the light distribution on the cells facing the front and back reflector when the light is incident normal to the system aperture, i.e. at a solar altitude of 60° in the meridian plane.

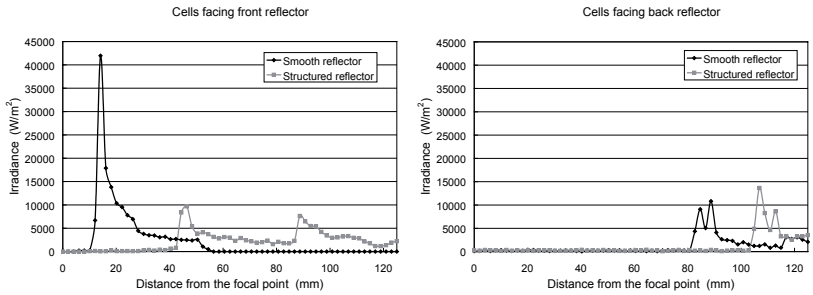

Figure 15.3 *Light distribution on the cells facing the front reflector (left) and the cells facing the back reflector (right) at a solar altitude of 60°, solar azimuth 0°.*

As can be seen in the figure, the light distribution on the cells facing the front reflector was significantly improved by the structured reflector. However, this was not the case for the cells facing the back reflector. Here we can even see a slight increase in peak irradiance but not at all on the same level as the irradiance peak of the cells facing the front reflector. The resulting IV-characteristics of the cells for the light distributions in Figure 15.3 are shown in Figure 15.4.

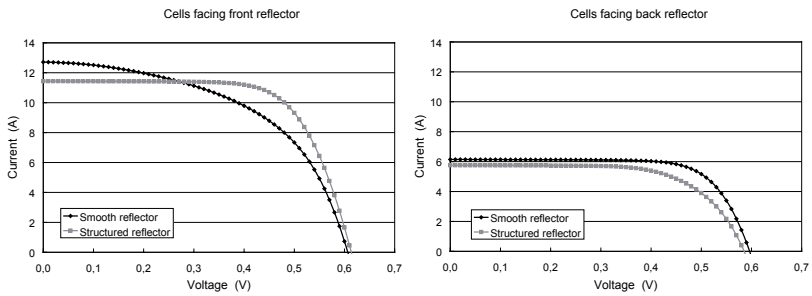

Figure 15.4 *Current-voltage characteristics of the cells facing the front (left) and back (right) reflector at a solar altitude of 60°, solar azimuth 0°.*

Figure 15.4 illustrates the benefits and problems of the structured reflector well. The peak irradiance of the smooth reflector in Figure 15.3 was very high, approximately 42 times the solar beam. This yields a low fill factor and thus a low maximum power output. The reduced short-circuit current shows that the optical losses are larger for the structured reflector. Figure

15.4 shows that the homogenized light distribution of the structured reflector improves the maximum power output by 22% even though the short-circuit current is 10% lower. For the cells facing the back reflector, the power output decreases for the structured reflector.

The structured reflector will improve the performance of the concentrator for some angles of incidence, and worsen the performance at some angles and this is the reason for the small annual output increase.

The other beneficial effect of the structured reflectors was that the concentration ratio of the system could be increased. One of the findings in Chapter 11 was that new geometries had to be investigated in order to make optimum use of the possibility to increase the concentration ratio. If it is used to make a design with a larger aperture but with the same interval of acceptance it is possible to improve the performance of the system. As was found in Chapter 13, where two new designs were developed, it was possible to increase the annual output of the MaReCo concentrator by 20% if the tilt angles of the optical axes of the trough were changed to increase the system aperture.

If standard cells are used in a stationary concentrator, it is therefore recommendable to consider using structured reflectors when a new design is developed in order to reduce the otherwise problematic irradiance peaks.

15.6 Scattering reflectors

Another possible solution to the problem of non uniform irradiance distribution on the cells is to use scattering reflectors. The scattering has to be limited to a small angular interval so as not to create unnecessary optical losses, but if such a material is used it is possible to get a more favourable light distribution.

One such material is lacquered rolled aluminium which has been laminated on a PET substrate (Brogren 2004). The rolling process creates grooves in the reflector during manufacture which makes the material scatter light more in one of the directions. The scattering of the material is shown in Figure 15.5.

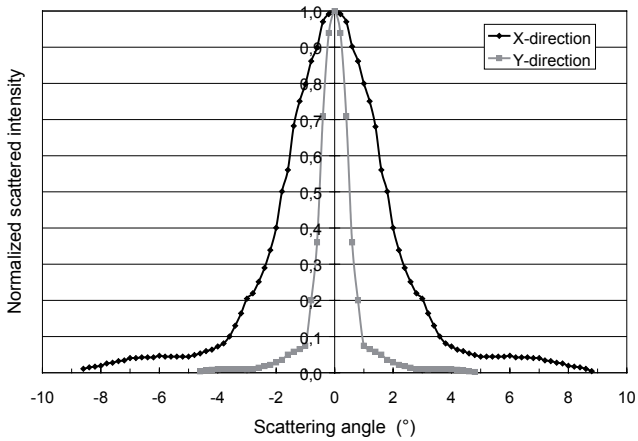

Figure 15.5 Scattering from lacquered rolled aluminium.

The scattering is highest perpendicular to the grooves, in the X-direction in the figure. Since the scattering is non-symmetric, it will affect the system performance differently depending on whether the grooves are oriented along the cross section of symmetry of the concentrator, or whether they are oriented perpendicular to the cross section of symmetry.

In order to study these effects, the annual output of one MaReCo with the grooves oriented along the axis of symmetry and one MaReCo with the grooves oriented in the plane of the cross-section was simulated. The total reflectance was 85% for all cases.

The simulations show that the system with the grooves in the plane of the cross section would generate 3% more annual electricity than a MaReCo with smooth reflectors. For the system with the grooves oriented perpendicular to the cross section, the annual output increase was 4 %. Closer examination of the details of the simulations reveals that the improvement is found in the system efficiency for direct irradiation, while the system efficiency for diffuse irradiation is approximately the same for all three systems.

Figure 15.6 shows the light distribution (left) and current-voltage characteristics of the cells facing the front reflector in the three systems at a solar altitude of 60° in the meridian plane.

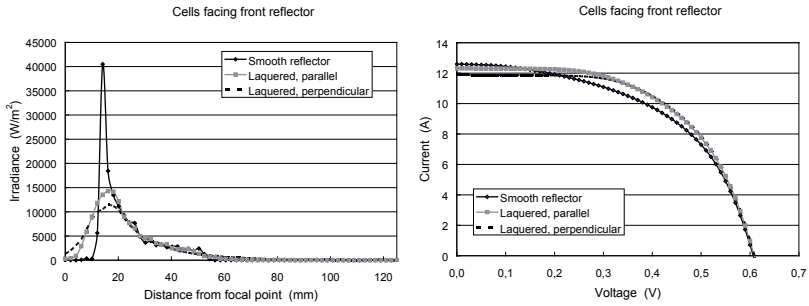

Figure 15.6 *Comparison between a smooth reflector and a lacquered reflector in a MaReCo trough at a solar altitude of 60° in the meridian plane*

When the grooves were oriented parallel to the cross section of symmetry, the optical losses were negligible which can be seen by the small difference in short-circuit current between the smooth reflector and the lacquered reflector in Figure 15.6. The peak irradiance for this case was only 35% of the peak irradiance of the smooth reflector, and this resulted in a 7% increase in maximum power output.

For the reflector with the grooves perpendicular to the cross section of symmetry, the peak irradiance was 25% of that of the smooth reflector and the maximum power was 8% higher. This means that for this particular reflector material and this particular geometry, the best option was to have the rolling grooves oriented perpendicular to the meridian plane.

To conclude; increased scattering can improve the system output. However, when the scattering increases, so do the optical losses. This is especially true if the scattering is high in the plane of the cross section, i.e. when the grooves are oriented perpendicular to the cross section which was seen by the lower short-circuit current in Figure 15.6.

This means that for reflector materials with a relatively high total reflectance and with a limited scattering such as from rolling grooves, improved system output can be expected.

15.7 Conclusions

Among the different solutions discussed, there is one strategy that can improve the efficiency of existing stationary concentrators with standard cells independently of the system design. This is to use a reflector material with a higher reflectance. The study of the annual output shows that the

output increase is proportional to the increased reflectance. This means that as long as the increase in reflectance is higher than the increase in total system cost including the solar cells, the reflector material with the highest reflectance should always be used.

If a new stationary concentrator with standard PV cells is to be designed, consider the following points:

- Use micro-structured reflectors in a concentrator with standard PV cells. This will give a more homogeneous light distribution on the cells, and the concentration ratio will be increased. The homogenization becomes more important as the concentration ratio increases since this will lead to a higher flux concentration and thus higher electrical losses due to the non uniform irradiance distribution.
- Do not overlook the diffuse irradiation. The annual diffuse irradiation in northern latitudes such as Sweden can often be at least as high as the annual direct irradiation. A design where a large part of the sky is invisible to the cells can give a high concentration ratio, but if the diffuse light is discarded it might only be possible to collect half the annual irradiation
- Do not use a double sided absorber with PV cells. The cost of such an absorber is twice the cost of a single sided absorber and it is very difficult to design a double sided system that has a higher collection efficiency than an optimized design for a single sided absorber.
- A reflector with a small scattering interval will improve the system efficiency if the total reflectance is as high as for the more specular reflector. In the study in Section 15.6, a decrease in total reflectance from 85 % to 82 % would have meant that the output gain due to the slight homogenization of the light distribution would have been lost.
- Changing the tilt of the absorber will give a better system efficiency for diffuse light if it is tilted in order to collect more of the light directly, thus reducing the reflective losses. It will have a small effect in increasing the efficiency around the angles where the flux concentration ratio is at a maximum, but this will only have a marginal effect on the annual output.

16 Contributions to co-authored articles

Articles that are part of the thesis

In the following articles, the author has participated in writing a substantial part of the publication.

Article VII – PV performance of a multifunctional PV/T hybrid solar window

The photovoltaic section of the article was written by the author. This consisted of measurements of the optical efficiency, simulation of the annual electrical output, and a general analysis of the system.

Article VIII – A new model and method for determination of the incidence angle dependent g-value of windows and sunshades

The author simulated the sunshades in a ray tracing study. The analysis of the model and its application to sunshades was largely performed in cooperation with the author.

Articles or books outside this thesis

For the sake of completeness, I would also like to show the contributions to other articles and books that are not a part of this thesis. In the case of "Sustainable Solar Housing", a book is not a reasonable format for publication as part of the thesis. In some other cases, the work of co-authoring has not been of equal magnitude as for the articles that are part of the thesis.

Sustainable Solar Housing

(Hastings and Wall 2006)

The author wrote the overview chapter about photovoltaic-thermal hybrids and concentrating systems. The book was written as part of IEA Solar Heating and Cooling Task 28. The chapter describes the rationale for photovoltaic-thermal hybrids and solar concentrators. It compares co-generation of heat and electricity in a hybrid with side-by-side systems of solar panels and solar collectors. The chapter also discusses different PV-thermal technologies including stationary solar concentrators and building integrated systems.

Optical properties, durability, and system aspects of a new aluminium-polymer-laminated steel reflector for solar concentrators

(Brogren et. al. 2004)

Measurements on concentrators with different reflector materials were performed by the author.

Design, Building Integration and Performance of a Hybrid Solar Wall Element

(Fieber et. al. 2003)

The photovoltaic section of the article was written by the author. This consisted of measurements of the optical efficiency, simulation of the annual electrical output, and an analysis of the system in a photovoltaic perspective.

A new model and method for determination of the incidence angle dependence of the optical efficiency of solar concentrators

(Helgesson et. al. 2004b)

A ray tracing study of the optical efficiency of the three concentrators was performed by the author. The author took part in co-authoring large parts of the article focusing mainly on the optical characteristics and the biaxial model of the systems.

Building Integration of Solar Energy

(Fieber 2005)

A TRNSYS model of the Solar Window was developed by the author. This model calculates the annual output of hot water, electricity and passive gains in the building. The model made it possible to simulate different user strategies and their implications on the annual performance of the Solar Window. A ray tracing study of the optical performance of the solar window at different angles of incidence was also performed by the author.

Summary

The goal of this thesis has been to increase the electrical output of stationary solar concentrators.

In order to improve existing concentrators, it is important to identify the most significant losses. This was done by characterization of an asymmetrically truncated CPC fitted with standard solar cells. The current-voltage characteristics and the light distribution on the solar cells were measured at different angles of incidence. By calculating the optical efficiency as a function of the angle of incidence, the annual electrical and thermal output were simulated. It was found that having cells facing the front reflector yielded the highest annual electrical output, 205 kWh/m^2 solar cells. The system was estimated to generate 363 kWh of heat per m^2 absorber area. The non uniform irradiance distribution on the cells was identified as the single most important reason for electrical losses.

To obtain a more accurate measure of the losses due to non uniform irradiance distribution on the cells, measurements were performed on one monocrystalline standard cell and one polycrystalline standard cell. Different light distributions were created on the cells and the current-voltage characteristics were measured. It is common knowledge that the irradiation in a parabolic concentrator is concentrated to a line of high irradiance. It was found that for line widths below 15-20 mm, the losses increase exponentially when the line narrows. This will lead to large losses and should therefore be avoided. It was also found that the output is very dependent on the position of the line. Maximum power output is generated when the line is located close to, but not at, one of the bus bars.

Once a new system has been built, it is necessary to obtain a measure of its annual output in order to compare it to other systems, and to facilitate system sizing for installation. The most accurate method is to install the system and measure its output for a full year. However, to measure for a whole year is not always the most desirable situation. In many cases it would be beneficial to obtain the annual output faster. A new method for estimating the efficiency of translationally symmetric concentrators was therefore developed. It models the system efficiency at a particular angle of incidence as a product of the efficiency of the glazing and the efficiency

of the reflector and solar cells. The efficiency of the glazing was expressed as a function of the angle of incidence, and the efficiency of the reflector system was expressed as a function of the transverse projected solar altitude. The benefit of this model is that it is only necessary to measure the system output as a function of the transverse projected angle of incidence to obtain a good measure of the system efficiency. When the system efficiency is known, the annual output can be simulated in MINSUN, which is a simulation program for estimating the annual output of solar energy systems. The new method was shown to produce more accurate results than the previously used method of the system efficiency.

As a means of obtaining a more uniform irradiance distribution on the cells, a micro-structured reflector was introduced for the system that was characterized in the first part of the thesis. Three different structures were evaluated by simulation in order to find the one most suitable for this particular application. It was found that all structured reflectors created a more uniform irradiance distribution on the cells. Two of the structures showed promising results, a sinusoidal shaped structure and a V-structure with an opening angle of 120°. The V-structure showed the highest optical efficiency when the sun was close to the meridian plane of the concentrator and the sinusoidal structure yielded the most homogeneous light distribution on the cells. The annual collected irradiation was approximately the same for both structured reflectors. It was difficult to show any performance improvements compared to the smooth reference system in this study. In order to show this, a solar cell model that takes non uniform irradiance distribution on the cells into account when calculating the electrical output would have had to be used. It was also found that in order to maximize the benefits of the structured reflector, it is necessary to increase the concentration ratio of the system.

When a new photovoltaic concentrator is developed, many designs will be compared in order to find the optimum solution. If this involves construction of each of the prototypes, this is tedious work. Another possibility is to compare the measured electrical output of the different systems under some specific conditions. The problem with this approach is that it is difficult to estimate how the output under certain conditions will influence the annual output. Another issue is that all the prototypes have to be constructed and this will consume time and money. A new three step method was therefore developed where the simulated annual output of different systems can be compared. The first step of the method was to perform optical simulations of the concentrator in order to find the irradiance distribution on the cells for all angles of incidence. One of the findings of the study where the structured reflectors were applied in an existing concentrator was that it is necessary to take the irradiance distribution on the cells into account when the annual output is calculated.

Output simulations using such a solar cell model were therefore the second step of the method. Based on the irradiance distributions simulated in the previous step, the current-voltage characteristics were simulated for all angles of incidence. Using the maximum power point of each IV-characteristic, a matrix of the system efficiency for direct irradiation as a function of the solar altitude and solar azimuth angle was calculated. This matrix was used to calculate an estimate of the annual electrical output.

The new evaluation method was used in the design of two new concentrators. One of the concentrators was intended for wall integration, and the other for roof integration. Both systems were fitted with standard PV cells and structured reflectors. The reflector structure used was the V-structure with an opening angle of 120° that was used in the previous study with structured reflectors. The roof concentrator was based on the asymmetrically truncated CPC with a double sided absorber which was characterized in the first part of the thesis. The optimal wall concentrator was based on a system with a single sided absorber and a parabolic reflector above the absorber. The design parameter for both systems was to increase the tilt of the optical axis and thus the geometrical concentration ratio. It was found that the optimum roof concentrator had its optical axes tilted at 25° and 60° which gave it a geometrical concentration ratio of 2.8. It was estimated to generate 194 kWh of electricity per m^2 solar cells annually. This was 20 % higher than the annual output of the reference concentrator with smooth reflectors. The wall concentrator had its optical axis tilted at 40° from the horizontal, which gave it a geometrical concentration ratio of 4.9. This system was estimated to generate 213 kWh of electricity per m^2 solar cells annually, which was a 10% improvement compared to the reference wall concentrator.

In order to verify the simulation results, a prototype of the roof concentrator was constructed. Measurements on the prototype showed that a more uniform irradiance distribution was obtained. This resulted in considerably improved performance when the sun was in the meridian plane. However, due to low manufacturing precision, the optical losses of the prototype were substantial. This made it difficult to demonstrate any output gains from the structured reflector at large azimuth angles.

The last chapter of the thesis discusses different aspects of new concentrator designs. The aspects that are discussed are reflector materials, the tilt angle of the absorber, whether the absorber should be double sided or single sided, the importance of the diffuse irradiation, whether structured reflectors should be used, and whether scattering reflectors would improve the annual output. It was suggested that the use of a structured reflector, design for maximum possible acceptance of diffuse irradiation, and the use of a single sided photovoltaic absorber were the most important pa-

rameters in designing stationary photovoltaic concentrators for northern latitudes such as Sweden.

References

Adsten M., Helgesson A., Karlsson B. (2005) *Evaluation of CPC-collector designs for stand-alone for- or wall installation*. Solar Energy Vol. 79 (6), pp. 638-647

Baum H.P., Blanco M.E., Gomez-Leal E., Gordon J.M. (1986) *Optimal configurations of asymmetric CPC solar collectors with planar receivers.* Solar Energy Vol. 36 (2), pp. 187-189

Benítez P., Mohedano R. (1999) *Optimum irradiation of concentrated sunlight for photovoltaic energy conversion*. Applied Physics Letters. 74 (17), pp 2543-2545

Bortz J., Shatz N., Ries H. (1997) *Consequences of étendue and skewness conservation of nonimaging devices with inhomogeneous sources and targets*. Proceedings of SPIE Vol. 3139, pp 59-75

Bortz J., Shatz N., Winston R. (2001) *Performance limitations of translationally symmetric nonimaging devices, nonimaging optics: maximum efficiency light transfer VI*. Proceedings of SPIE vol. 4446.

Brogren M. (2004) *Optical Efficiency of Low-Concentrating Solar Energy Systems with Parabolic Reflectors.* Dissertation thesis. Uppsala, Sweden. ISBN 91-554-5867-X

Brogren, M., Wennerberg, J., Kapper, R., Karlsson, B. (2003) *Design of concentrating elements with CIS thin film solar cells for wall integration*. Solar Energy Materials & Solar Cells Vol. 75, 567-575.

Brogren M., Nostell P., Karlsson B. (2000) *Optical efficiency of a pv-thermal hybrid CPC for high latitudes*. Solar Energy Vol. 69(Suppl.), pp 173-185

Brogren M., Helgesson A., Karlsson B., Nilsson J., and Roos A. (2004) *Optical properties, durability and system aspects of a new aluminium-polymer-laminated steel reflector for solar concentrators.* Solar Energy Materials and Solar Cells Vol. 82, pp 387-412

Burgers A.R., Eikelboom J.A., Schonecker A., Sinke W.C. (1996) *Improved treatment of the strongly varying slope in fitting solar cell I-V curves.* Conference Record of the 25th IEEE Photovoltaic Specialists Conference

Carvalho M.J., Collares-Pereira M., Gordon J.M., Rabl A. (1985) *Truncation of CPC solar collectors and its effect on energy collection*. Solar Energy Vol. 35 (5) pp. 393-399

Chant V.G., Håkansson R. (1985) The *MINSUN simulation and optimisation program*. Application and users guide. IEA SH & C Task VII, Ottawa

Coventry J.S. (2005) *Performance of a concentrating photovoltaic/thermal solar collector*. Solar Energy Vol. 78(2), pp 211-222

Duffie, J.A., Beckman, W.A. (1980) *Solar Engineering of Thermal Processes*. Wiley Interscience, New York.

Feuermann D., Gordon J.M. (2001) *High-concentration photovoltaic designs based on miniature parabolic dishes*. Solar Energy Vol. 70(5), pp 423-430

Fieber A., Gajbert H., Håkansson H., Nilsson J., Rosencrantz T., Karlsson B. (2003) *Design, Building Integration and Performance of a Hybrid Solar Wall Element.* Proceedings of ISES Solar World Congress 2003, Gothenburg, Sweden

Fieber A. (2005) Building *Integration of Solar Energy – A Multifunctional Approach.* (Report EBD-T—05/3). Lund, Sweden: Div. Energy and Building Design, Dept. Construction and Architecture, Lund University

Foss S.E., Olaisen B.R., Marstein E.S., Holt A. (2006) *A new 2.5D distributed SPICE model of solar cells.* Proceedings of the 21st European Photovoltaic Solar Energy Conference an Exhibition, Dresden, Germany

Fraidenraich, N. (1998) *Design procedure of V-trough cavities for photovoltaic systems*. Progress in Photovoltaics: Research and Applications Vol. 6(1), pp 43-54

Franklin E.T., Coventry J.S. (2002) *Effects of Highly Non-uniform Illumination Distribution on Electrical Performance of Solar Cells*. Proceedings of ANZSES Conference, Newcastle, Australia.

Gordon J.M., Lasken M., Ries H. (1996) *Upper bounds for the yearly energy delivery of stationary solar concentrators and the implications for concentrator optical design*. Solar Energy Vol. 58 (4-6), pp. 197-202

Green M.A. (1998) *Solar Cells – Operating principles, Technology and System Applications*. University of New South Wales

Hastings R., Wall M. (2006) *Sustainable Solar Housing.* Edited by Robert Hastings and Maria Wall, Earthscan, London.

Helgesson A., Krohn P. Karlsson B. (2004a) *Development of a MaReCo-Hybrid for Hammarby Sjöstad, Stockholm*. Proceedings of Eurosun 2004, Freiburg, Germany

Helgesson A., Nilsson J., Karlsson B. (2004b) *A new model and method for determination of the incidence angle dependence of the optical efficiency of solar concentrators*. Accepted for publication after revision in Solar Energy Materials & Solar Cells.

Hollands K.G.T. (1971) *A concentrator for thin-film solar cells*. Solar Energy Vol. 13 (3), pp. 149-163

IEA-PVPS Task 7 (2005) *Designing with Solar Powe*r. Edited by Prasad D. and Snow M. IEA-PVPS Report

IEA-PVPS (2006) *Trends in photovoltaic applications*. Report IEA-PVPS T1-15:2006, IEA-PVPS, St. Ursen, Switzerland

IEA-PVPS (2007) *Annual report 2006*. IEA-PVPS, St. Ursen, Switzerland

Karlsson B., Wilson G. (1999) *MaReCo – A large asymmetric CPC for high latitudes*. Proceedings of ISES Solar World Congress, Jerusalem, Israel

Leutz R., Suzuki A., Akisawa A., Kashiwagi T. (1999) *Design of a nonimaging Fresnel lens for solar concentrators.* Solar Energy Vol. 65(6), pp 379-387

Lorenzo E., Sànchez E., Luque A. (1980) *Experimental verification of the illumination profile influence on the series resistance of concentrator cells*. J. Appl. Phys. 52 (1) pp. 535-536

Leutz R., Ries H. (2005) *Microstructured light guides overcoming the two-dimensional concentration limit.* Applied Optics Vol. 44 (32) pp. 6885-6889

Leutz R., Ries H. (2003) *Squaring the Circle – The Use of Microstructures for Converting and Homogenizing Beam Cross-sections*. Proceedings of SPIE Vol. 5186

Luque A. (1989) Solar Cells and Optics for Photovoltaic Concentration. Adam Hilger, Bristol

Luque A., Sala G., Arboiro (1998) *Electric and thermal model for non-uniformly lluminated concentration cells.* Solar Energy Materials & Solar Cells Vol. 51 (3), pp. 269-290

Mallick, T.K., Eames, P.C., Hyde, T.J., Norton, B. (2004) *The design and experimental characterisation of an asymmetric compound parabolic photovoltaic concentrator for building facade integration in the UK*. Solar Energy Vol. 77(3), pp 319-327

McIntire, W. R. (1982) *Factored approximations for biaxial incident angle modifiers*. Solar Energy Vol. 29(4), pp 315-322

McMahon T.J., von Roedern B. (1997) *Effects of light intensity on current collection in thin-film solar cells*. Proceedings of 26th PVSC conference, Anaheim, USA

METEONORM Version 5.1 (November 2004)

Mills D.R. (1978) *The place of extreme asymmetrical non-focussing concentrators in solar energy utilization*. Solar Energy Vol. 21 (5), pp. 431-434

Mills D.R., Giutronich J.E. (1978) *Asymmetrical non-imaging cylindrical solar concentrators*, Solar Energy Vol. 20, pp 45-55

Miñano J.C., González J.C., Benítez P. (1995) *A high-gain, compact, nonimaging concentrator: RXI.* Applied Optics Vol. 34(34), pp 7850-7856

Perers B., Karlsson B. (1993), *External reflectors for large solar collector arrays, simulation model and experimental results.* Solar Energy Vol. 51(5), pp 327-337

Piszczor M.F. Jr., O'Neill M.J., Fraas L.M. (1993) *A novel space photovoltaic module using a linear Fresnel lens and a line-focus tandem cell receiver*. Proceedings of the 23rd Photovoltaic Specialists Conference, Louisville, KY, USA

Rabl A. (1976a) *Comparison of Solar Concentrators*. Solar Energy Vol. 18 (2), pp. 93-111

Rabl A. (1976b) *Optical and thermal properties of compound parabolic concentrators.* Solar Energy Vol. 18, pp 497-511.

Rönnelid M., Karlsson B. (1997), *Irradiation distribution diagrams and their use for estimating the collectable energy.* Solar Energy Vol. 61, pp 191-201

Rönnelid M., Karlsson B. (1998) *Optical Acceptance Function of Modified Compound Parabolic Concentrators with Linear Corrugated Reflectors.* Applied Optics Vol. 37 (22) pp. 5222-5226

Rönnelid M., Karlsson B. (2003) *Optimised truncation of a wide acceptance angle CPC*. Proceedings of ISES Solar World Congress 2003 in Gothenburg, Sweden.

Sala G., Arboiro J.C., Luque A, Zamorano J.C., Minano J.C., Dramsch C., Bruton T., Cunningham D. (1996) *The EUCLIDES prototype: An efficient parabolic trough for PV concentration*. Proceedings of the 25th Photovoltaic Specialists Conference, Washington D.C. USA

Schmitz M., Schwarzbözl P., Buck R., Pitz-Paal R. (2006) *Assessment of the potential improvement due to multiple apertures in central receiver systems with secondary concentrators*. Solar Energy Vol. 80 (1), pp. 111-120

Schramek P., Mills D.R. (2003) *Multi-tower solar array*. Solar Energy Vol. 75(3), pp 249-260

Schroder D.K., Meier D.L. (1984) *Solar cell contact resistance – A review*, IEEE transactions on Electron Devices Vol. 31, pp. 637-647

Souka, A.F., Safwat, H.H. (1966) *Optimum orientations for the double exposure flat-plate collector and its reflectors*. Solar Energy Vol. 10, pp 170-174

SPICE, http://bwrc.eecs.berkeley.edu/Classes/IcBook/SPICE/

Swanson R.M. (2000) The Promise of Concentrators. Progress in Photovoltaics: Research and Application Vol. 8 (1), pp. 93-11

Vant-Hull L.L, Hildebrandt A.F. (1976) *Solar thermal power system based on optical transmission*. Solar Energy Vol. 18(1), pp 31-39

Wenham S.R., Green M.A., Watt M.E., *Applied Photovoltaics*, Centre for Photovoltaic Devices and Systems, University of New South Wales, Australia

Williamson D.E. (1952) *Cone channel condenser optics.* Journal of the Optical Society of America Vol. 42, pp 712-715

Winston R. (1974) *Principles of solar concentrators of a novel design*. Solar Energy Vol. 16 (2), pp. 89–95.

Winston R., Hinterberger H. (1975) *Principles of cylindrical concentrators for solar energy*. Solar Energy Vol. 17, pp 225-258

Winston R., Miñano J.C., Benítez P., Shatz N., Bortz J.C. (2005) *Non-imaging optics,* Elsevier Academic Press, London, UK

Würfel P. (2005) *Physics of Solar Cells*. Wiley-VCH, Weinheim

ZEMAX version February 3, 2005, ZEMAX Development Corporation, San Diego, California, USA

Appendix A

Basic function of the electronic load

The electronic load is schematically shown in Figure A.1. A more detailed description is shown in Figure A.2.

An operational amplifier compares the actual voltage over the electronic load connected to the solar cell with a control voltage from the logger. If the voltage over the electronic load is higher than desired, the output voltage from the op-amplifier is increased, and this increases the current through the power transistor (T1). This causes the voltage over the load to be reduced as the current from the cells increases and the measuring point on the IV-curve is moved towards lower voltage.

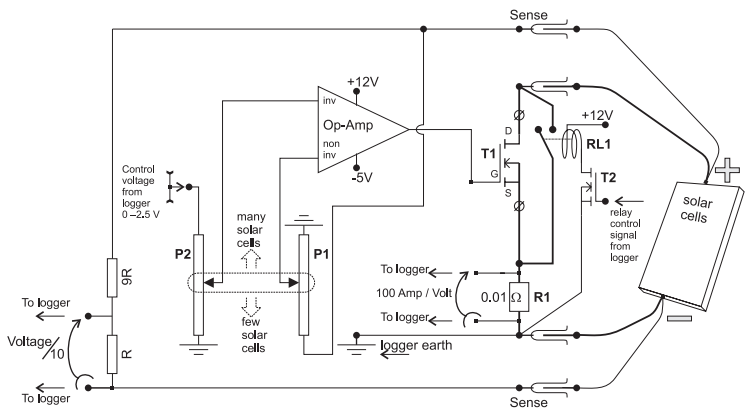

Figure A.1 *Layout drawing of the electronic load for measuring IV-characteristics.*

Voltage ranges

The logger produces excitation voltages up to 2.5 V. To make it possible for the electronic load to measure at higher voltage ranges, a potentiometer acting like a voltage divider is connected to the solar cells. This is the potentiometer P1 shown in the figure.

To be able to measure on solar cell arrays with less than 2.5 V maximum voltage, another potentiometer is added in the control circuit (P2). The two potentiometers are mechanically connected in opposition as the figures show. When the left potentiometer is moved up in the figure to compensate for a higher open circuit voltage, the right potentiometer will use a larger part of the 2.5V control signal to further compensate for the higher voltage.

Measurement of current

A four terminal shunt resistance, R1, of 0.01 Ω is used for the current measurements. With a 4 wire arrangement, the voltage drop in the two wires conducting the current has no effect on the voltage measured by the other two wires. The tolerance of the resistor is ±1%. The maximum power is 2 W according to the specifications, which allows for 14 A continuous current through R1.

Low resistance

To reduce the resistance for the short circuit measurement, a relay, RL1, is used for this measurement point. When the relay closes the circuit, most of the current goes through the switch. To further minimise the internal resistance, attention has been paid to reducing the wire length between the connections, relay, and shunt resistance. The (Ø 4 mm) connectors on the front panel can also be doubled if two wires in parallel are used to reduce the resistance.

Sense input

In order to exclude the resistance of the connecting wires that carry the current in the I-V-measurements, the voltage is measured with separate wires connected to the sense input on the front panel of the electronic load. When voltage sensing wires are not used, two 3 Ω resistances connect the sense input to the voltage of the connectors on the front panel. If the voltage sensing wires are connected to an active panel before the wire for current measurements is connected, a large current will pass through the 3 Ω resistance causing overheating. By choosing resistors with a high positive temperature coefficient this potential overheating is prevented.

1:10 voltage reduction

The resistors in the voltage divider are constructed from an integrated (thick film) resistor network with fifteen resistors of the same value. Nine resistors are connected in parallel together with one single resistor in series. In this way a 1:10 voltage divider is realized. The advantages of constructing the voltage divider in this way is that it is simple to make and that all resistors are expected to have the same temperature coefficient. It has also proved to be accurate. Finally the voltage divider can be tested with a voltage source and a voltage meter. If the precision demands are not met, the resistor network can be easily discarded and replaced.

Prevention of oscillations

An electronic load should be able to produce a very low and stable resistance. This is especially important for solar panels with few cells and high irradiance. This requires a large amplification of the control voltage to current and if a high amplification is used there could be a tendency to oscillation. The power transistor is prevented from amplifying and radiating high frequencies by using a ferrite bead connected close to the drain terminal and also by a capacitor between drain and gate for negative feedback.

A 10 nF/3 kΩ network is connected to the output of the operational amplifier to help compensate for the phase shift caused by the internal capacitance of the power transistor.

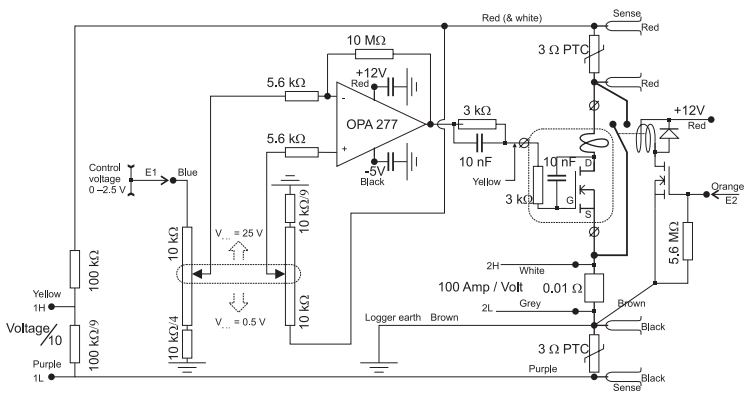

Figure A.2 Detailed drawing of the electronic load.

Article I

Available online at www.sciencedirect.com
ScienceDirect
Solar Energy 81 (2007) 917–928
SOLAR ENERGY
www.elsevier.com/locate/solener

Electrical and thermal characterization of a PV-CPC hybrid

Johan Nilsson *, Håkan Håkansson, Björn Karlsson

Division of Energy and Building Design, Department of Architecture and Built Environment, Lund University, P.O. Box 118, Lund SE-22100, Sweden

Received 27 July 2005; received in revised form 21 September 2006; accepted 27 November 2006
Available online 26 December 2006

Communicated by: Associate Editor Hansjörg Gabler

Abstract

Long term evaluation of an asymmetric CPC PV-thermal hybrid built for high latitudes, MaReCo (MaximumReflectorCollector), is performed in Lund, lat 55.7°, and this paper discusses output estimates and characteristics of the system. The output estimates are calculated using the MINSUN simulation program. To get the input for MINSUN, measurements were performed on two MaReCo prototypes. These measurements show that the front reflector collects most of the irradiation in the summer, and the back reflector in the spring and fall. Two different reflector materials were used, anodized aluminium and aluminium laminated steel. The steel based reflector was selected for its rigidness. The output estimates show no difference in yearly output between the two reflector materials, both back reflectors deliver 168 kW h/(m^2 cell area) of electricity compared to 136 kW h/m^2 cell area for cells without reflectors. The cells facing the front reflector deliver 205 kW h/(m^2 cell area) of electricity. The estimated output of thermal energy was 145 kW h/(m^2 glazed area) at 50 °C. The estimates show that the optimal placement of the photovoltaic cells is facing the front reflector, but having cells on both sides is in most cases the best option.

Keywords: Solar concentrators; PV/T; Characterization; Annual output estimates

1. Introduction

In view of the high costs of photovoltaic modules, it is necessary to find ways to reduce the cost of a PV system considerably to generate more extensive use. One approach is to use concentrating reflectors to increase the irradiation on the photovoltaic cells. This approach is promising due to the low cost of the reflectors, which is significantly lower than the cost of the cells and this has been shown to reduce the energy cost (Perers and Karlsson, 1993). The electricity generation is impeded by high temperatures, and cooling the cells actively with water is one efficient way to increase the yield (Rönnelid et al., 2000). Another benefit from cooling the cells with water is the possibility to use the hot water for heating provided that the produced heat fulfils a demand and replaces heat from other sources. By rising the temperature of the cooling water it can be utilized for heating, however at the expense of lower electrical yield.

In Sweden, and other high latitude countries, the solar radiation over the year is asymmetric because of the high cloud coverage during the winter months and thus concentrated to a small angular interval of high irradiation. This makes the use of stationary reflectors or concentrators attractive.

An asymmetric compound parabolic reflector system with two truncated parabolic reflectors, MaReCo (MaximumReflectorCollector) has been built considering the conditions of high latitude (Adsten et al., 2005), and the aim of our current project is to evaluate this system for a PV/T hybrid. The theory of symmetric two-dimensional parabolic concentrators was developed in Winston (1974); Rabl (1976); Rabl et al. (1979). The modification

* Corresponding author. Tel.: +46 46 2227606; fax: +46 46 2224719.
E-mail address: johan.nilsson@ebd.lth.se (J. Nilsson).

0038-092X/$ - see front matter © 2007 Elsevier Ltd. All rights reserved.
doi:10.1016/j.solener.2006.11.005

Nomenclature

b_0	incidence angle modifier coefficient	$\eta(\theta_T)$	incidence angle modifier in the solar altitude direction
C_g	geometrical concentration ratio of the system	η_{0b}	optical efficiency for beam irradiation used in heat calculations
C_{gf}	geometrical concentration ratio of the front reflector	η_{0d}	optical efficiency for diffuse irradiation used in heat calculations
$f(\theta)$	optical efficiency	ΔT	difference between the ambient temperature and the temperature of the collector (K)
$g(\theta_L)$	incidence angle modifier in the azimuth direction	Θ	angle of incidence (°)
G	incident irradiation (W/m^2)	θ_L	longitudinal projected angle of incidence (°)
I_{1000}	reference short circuit current at 1000 W/m^2 (A)	θ_T	transverse projected angle of incidence (°)
I_{SC}	short circuit current (A)	$dT_f/d\tau$	time derivative of the temperature of the cooling media (K/s)
k_1	loss coefficient per collector area (W/m^2 K)		
$K_{\tau\alpha}$	planar incidence angle modifier		
$(mC)_e$	heat capacity of the collector (J/m^2)		

into asymmetric parabolic concentrators was discussed in Mills and Giutronich (1979a). Other examples of building integrated concentrators are discussed in Tripanagnostopoulos et al. (2000), and in Mallick et al. (2004).

The system is described in Fig. 1. The transverse interval of acceptance of the system is 20–65° and the glazed aperture is tilted in 30° from the horizontal. The photovoltaic cells used are standard monocrystaline silicon cells for non concentration applications for keeping the cost of the system low. The aperture of the front reflector is tilted 2° from the horizontal and has a geometrical concentration ratio (aperture area/cell area) of 3.5. The aperture of the back reflector is tilted 8° from the vertical and the geometrical concentration ratio is 2.5.

2. The evaluated system

Two different MaReCo prototypes were characterized, MaReCo1 and MaReCo2. Table 1 shows data for the systems. The third prototype, MaReCo3 was used for long term outdoor measurements.

The cells used were 12.5 × 12.5 cm BP585L monocrystalline silicon cells, but the study is valid for all standard silicon cells regardless of size. The cells were laminated onto an aluminium profile that was eloxidized to a dark colour to improve its heat absorbing properties. One of the variants had cells on one side of the absorber only, and the other side was just absorbing heat. The series connected cells were matched to generate equal current, and

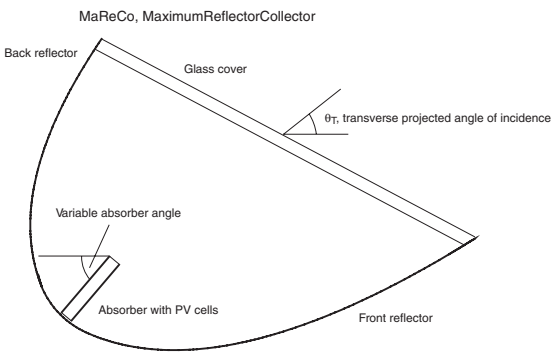

Fig. 1. The MaReCo PV-thermal hybrid. Both parabolic reflectors have the same focal point, at the top of the absorber. The photovoltaic cells are laminated on the absorber. The glass cover tilted in 30° is for weather protection. The absorber angle is the angle between the absorber and the horizontal. Also shown is the transverse projected angle of incidence.

Table 1
Evaluated prototypes

	MaReCo1	MaReCo2	MaReCo3
Cells facing back reflector	2	12	0
Cells facing front reflector	3	0	20
Absorber angle	45	20	65
Trough material	Anodized aluminium	Steel with aluminium coating	Anodized aluminium
Length (m)	1	2	3.5

The absorber angle and the placement of the reflectors are defined by Fig. 1.

since no by-pass diodes were used, it was possible to use the short circuit current as a measure of the incident irradiation.

MaReCo1 and MaReCo2 were not of full length, the full size MaReCos have a length of 3–5 m. One effect that will be more pronounced in the small scale evaluations compared to the full size systems is the shading of the outermost cells by the trough gables. In the mornings and evenings, the part of the absorber closest to the gables will be shaded. In the full size system, the photovoltaic cells will be placed a longer distance from the gables to prevent shading of the cells. This is not possible in the short prototype systems. The effects of the shading have therefore to be corrected for when the performance of long collectors is simulated.

3. Reflector materials

Two of the troughs had reflectors made of anodized aluminium, and one had reflectors of aluminium laminated steel (Brogren et al., 2004). The advantage of the steel based reflector is its mechanical properties, i.e. its rigidness. A stainless steel parabolic reflector can be made with less mechanical support than an aluminium reflector. The disadvantage with the laminated steel reflector is its relatively low specular reflectance. Fig. 2 shows a comparison between the reflectance of anodized aluminium and aluminium laminated steel. The steel based reflector has very low reflectance below 400 nm since its plastic coating absorbs light below 400 nm. The reflectance of the steel based reflector is slightly lower in the wavelength interval where the solar cells operate.

By visual inspection, there was a considerably larger number of imperfections in the aluminium reflector troughs, which shows the difference in rigidness between the steel reflector and the aluminium reflector.

An interesting aspect of the steel based reflector is its slightly higher scattering of the light. It has been shown previously that more evenly distributed light over the cells increases the efficiency of the cell (Benítez and Mohedano, 1999).

4. Measurements

4.1. General measurements

The electrical performance and the irradiance distribution on the cells was measured for different transverse projected angles of incidence.

To measure the characteristics at different transverse projected angles, the trough was manually rotated along its axis of symmetry and a potentiometer placed at the axis recorded the tilt of the trough. The potentiometer was calibrated in the beginning of the measurement by manually observing the angle of incidence with a graduated arc mounted on the side of the trough. A very fast *I–V* tracker for monitoring the current and voltage from the cells at

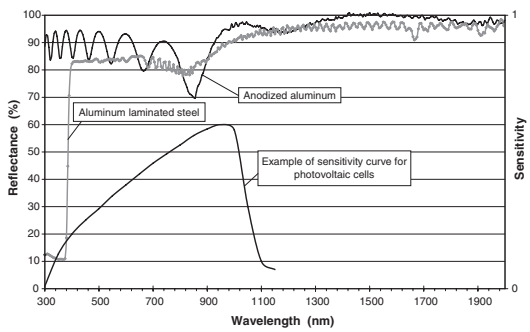

Fig. 2. Reflectance as a function of wavelength for the two reflector materials. The sensitivity curve shows an example of the wavelength interval where the silicon cell is working.

different loads was constructed to facilitate the measurements. The tracker consists of a fast electronic load, and by controlling the input voltage to the load with a datalogger it was possible to measure the complete current–voltage relationship for a certain angle of incidence in less than a second. This made it possible to obtain the *I–V* characteristics and the fill factor for all transverse angle of incidence in a short period of time. Only a fraction of the measured data is presented here.

The irradiance distribution on the cells was measured using a photodiode. The diode was placed on a rotating lever which was moved from the top to the bottom of the cell. The lever was rotated in a plane very close to the cell surface, and the angle of rotation was measured by a potentiometer. The photodiode aperture area was reduced by a plate with a 1 mm diameter hole to increase the spatial resolution.

The total incident irradiation was measured using a pyranometer that was mounted normal to the solar beam.

4.2. Short circuit current

Figs. 3 and 4 show the short circuit current (I_{SC}) and the fill factor as a function of transverse projected angle for the cells facing the back and front reflector. The short circuit current of the cell is approximately proportional to the irradiance and the fill factor is a measure of the resistive losses in the cells, a low fill factor corresponding to high losses (Green, 1982).

At low transverse projected angles, the back reflector is providing most of the light on the cells. The back aluminium reflector has its best electrical performance in the interval between 25° and 55° transverse angle as seen in Fig. 3. At higher transverse projected angles, in the summer, the front reflector contributes to the majority of the irradiation onto the cells. The optimal angle for this reflector is according to Fig. 4 between 40° and 65°. This system will thus collect irradiation between a transverse projected angle of incidence of 25° and 65° efficiently. The two local minima of the curves, at 27° and 55° in Fig. 4, occurs when the strip of concentrated light, which is only approximately 2 cm wide in practice, falls on one of the two conducting fingers on the surface of the cell. This finger shades a part of the cell and less photons are absorbed.

The MaReCo concentrator consists of two asymmetric concentrators, the front reflector has an acceptance interval of 0–65°, and the back reflector has an acceptance interval of 20–100° (Mills and Giutroich, 1979b). The aperture of both concentrators is from the focal point to the edge of the reflector. The aperture of the back concentrator is close to vertical and the aperture of the front reflector is horizontal. When the two concentrators are combined, they form an asymmetrically truncated CPC with an acceptance interval of 20–65°. As can be seen in Figs. 3 and 4, both have a maximum flux concentration ratio at the limiting angles (20° and 65°) where all of the light is concentrated to the focal point. Due to the fact that the cells are slightly smaller than the absorber and thus not covering the whole absorber area, the peaks are shifted slightly in the figures.

The short circuit current of the two back reflectors differ slightly. The maximum short circuit current of the aluminium reflector is higher than that of the steel based reflector, and the steel based reflector is more efficient at higher angles where the short circuit current is approximately 1.5 A higher. The lower peak current of the steel based reflector is due to its lower specular reflectance.

The absorbers of the characterized MaReCos were placed at different tilt angles, as defined in Fig. 1. The absorber angle of the aluminium trough was 45° and the absorber angle was 20° for the steel trough. The higher efficiency at high transverse angles of the steel based reflector system is due to its lower absorber angle, which decreases

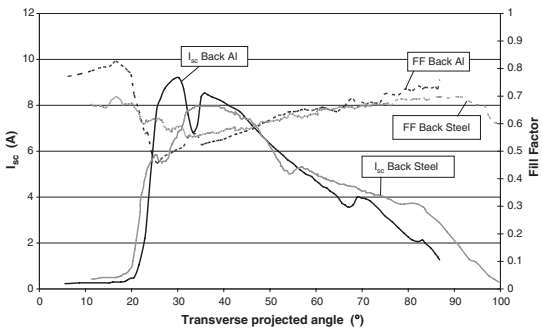

Fig. 3. Short circuit current and fill factor for back reflectors of MaReCo1 and MaReCo2.

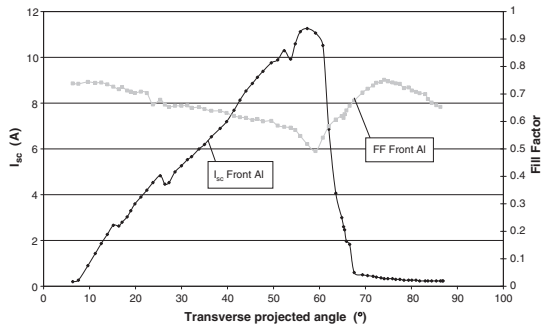

Fig. 4. Short circuit current and fill factor for the front reflector of MaReCo1.

the number of reflections and thus the reflection losses. For a discussion on the effects of absorber angle, refer to Section 4.6.

Both figures show that the fill factor is low, 0.5–0.6, when the short circuit current is high, i.e. when the light is concentrated more, it is utilized less. This is visible in Fig. 3 which shows that the fill factor is 20% higher for the steel based reflector cells at maximum concentration. The internal losses in the cell are proportional to the square of the current, RI^2, and the output power of the cell is proportional to the current, UI, where U's dependence on the irradiance can be neglected. As the current increases when the irradiation on the cell increases, the relative losses increase more than the delivered power, and the fill factor decreases. Another aspect of this, visible in Fig. 3, is that when the light is concentrated onto the finger of the cell (at 33° and 57° transverse projected angle of incidence), the short circuit current is significantly lower, and the fill factor is higher. This is explained by the fact that the electrical losses are reduced when light is concentrated close to the fingers and the current has less resistance to the conductor. This indicates that it is desirable to have the intensity maximum close to, but not on, the fingers (Benítez and Mohedano, 1999).

4.3. I–V characteristics

The most important measure of the power delivered from the cells is the *IV*-plots, the relationship between the output current and the output voltage. Fig. 5 shows these relationships at two different transverse projected angles, 35°, and 57°, close to the flux concentration maximum of the back and front reflectors respectively.

The figure indicates that the aluminium reflector has slightly better performance than the steel based. The difference in fill factor between the steel and aluminium reflectors is small and the short circuit current is higher for the aluminium reflector. The fill factor for the cells in the steel trough is 0.56 and for the aluminium trough cells 0.53. The figure also shows that the front reflector collects more light as the short circuit current is higher for this reflector.

The maximum power point for each curve was calculated by a parabolic fit to three discrete measured *I–V* points. The maximum power was 2.7 W/cell for the back aluminium reflector, and 2.6 W/cell for the steel based reflector at an angle of incidence of 35°. The front reflector had a maximum power output of 3.8 W/cell at an angle of incidence of 57°.

4.4. Irradiance distribution

The irradiance distribution over the cells varies with the angle of incidence. The distribution was measured for the two prototypes at the two transverse projected angles of 33° and 57° as can be seen in Figs. 6 and 7. The transverse angles were selected as 33° and 57° to be able to study the back and front reflector at angles were they have high efficiencies.

Fig. 6 shows the irradiance distribution at 33° transverse angle. The front reflector gives a low intensity at the cells in this case, but both back reflectors seem to be working in their optimum range, all of the light is concentrated onto the cells. The peak intensity of the aluminium reflector is higher than the peak of the steel based reflector, 25 times the beam intensity of the sun compared to 14 times in the case of the steel based reflector. This is due to the higher specular reflectance of the aluminium. The steel based reflector is more diffusing, and this makes the strip of concentrated light slightly wider and less intense. The slightly lower peak in this case is not of great importance, as seen in Fig. 3 the short circuit current is lower, but the fill factor is higher. The coupling of these two factors makes the

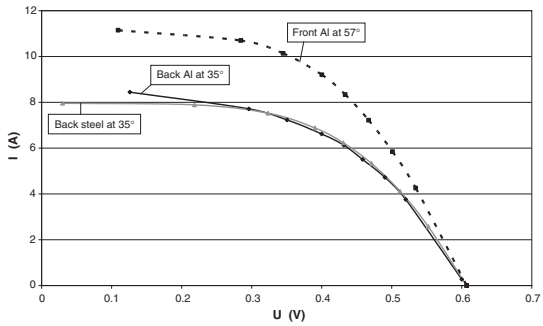

Fig. 5. *I–V* characteristics at 35° transverse projected angle of incidence for the back reflectors and at 57° for the front reflector. The voltage of one cell is shown to make a comparison possible. The voltage at open circuit condition is the same for all geometries.

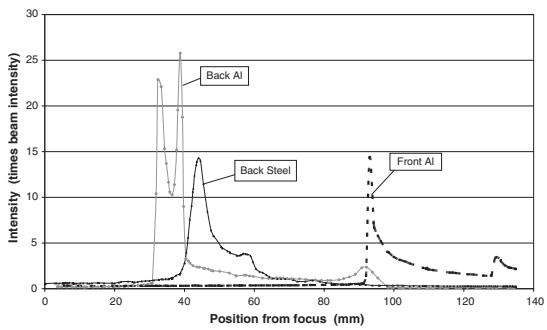

Fig. 6. Irradiation distribution at 33° transverse projected angle of incidence. The intensity is measured in times the beam intensity of the sun, and 0 at the position axis means on the end of the absorber, at the focal point.

difference in intensity less significant, which will be shown in Section 5. The peak intensity of the steel based reflector is shifted to the right of the aluminium one, and this is due to the different absorber angles of the two systems. The angle between absorber and the horizontal plane in the case of the steel based reflector is considerably smaller than the angle in the aluminium absorber case, and this shifts the peak towards the reflector. Section 4.6 discusses the influence of the absorber angle on the output.

Fig. 7 shows the distribution at a higher solar height, 57°. At this height, the front reflector is more optimal, refer to Fig. 4. The peak intensity is here 25 times the beam intensity of the sun, and all of the reflected light hits the cells. The back reflectors are less optimal in these conditions.

4.5. Optical efficiency and electrical output

Using the measured data as input, a simulation of the yearly output of heat and electricity was performed using MINSUN (Chant and Håkansson, 1985). This program was originally created for simulating solar heating systems, but it can be used to calculate the output of photovoltaic/thermal hybrids.

MINSUN uses hourly climate data, including direct and diffuse irradiation, from a large database to calculate the total annual irradiation on a specified surface. The irradiation data is used together with the incidence angle modifiers of the system to calculate the annual output. It is possible to use one of two different models of incidence angle modifier. The normal case for planar solar collectors

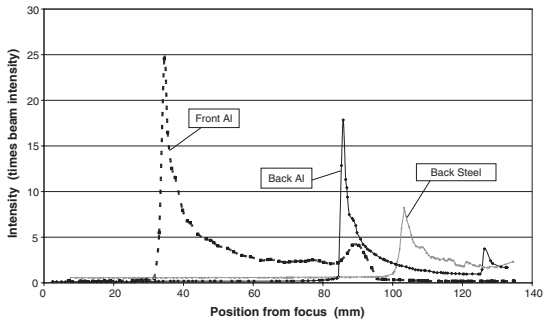

Fig. 7. Irradiation distribution at 57° transverse projected angle of incidence. The intensity is measured in times the beam intensity of the sun, and 0 at the position axis means on the end of the absorber, at the focal point.

and planar photovoltaic modules is to use $K_{\tau\alpha}$, which is defined in Eq. (1):

$$K_{\tau\alpha} = 1 - b_0\left(\frac{1}{\cos(\theta)} - 1\right) \quad (1)$$

b_0 is the incidence angle modifier which is supplied as input data to the simulation, and θ is the angle of incidence. The alternative is to have MINSUN calculate the product between the incidence angle modifier as a function of the transverse projected angle (in the meridian plane), $\eta(\theta_T)$, and the modifier in the east–west horizontal direction, $g(\theta_L)$ by supplying values of the two functions in intervals of 10°. The total incidence angle modifier, the optical efficiency (Nilsson et al., 2006), is then calculated according to Eq. (2):

$$f(\theta) = g(\theta_L) \cdot \eta(\theta_T) \quad (2)$$

$g(\theta_L)$ was represented by $K_{\tau\alpha}(\theta_L)$ with a b_0 of 0.23. This value has been obtained in previous measurements in our laboratory. $\eta(\theta_T)$ was calculated according to Eq. (3) for a surface with a 30° tilt, as the glazing is tilted 30°.

$$\eta(\theta_T) = \frac{I_{sc} \cdot 1000}{I_{1000} \cdot C_g \cdot G \cdot \cos(\theta_T - 60)} \quad (3)$$

I_{1000} is the short circuit current at an irradiance of 1000 W/m^2 on the module, which in this case was 4.55 A. C_g is the geometrical concentration of the concentrator system defined as the glazed aperture area divided by the cell area. θ_T is the transverse projected angle of incidence in degrees, and G is the total intensity normal to the sun. To get the efficiency relative to the incoming irradiation, the expression was divided by C_g. $G(\cos(\theta_T - 60))$ is the irradiance at the glazing. The measurements were performed on very clear days with a low fraction of diffuse irradiation, and the total irradiation was treated as a beam irradiation incident in the incidence angle of the beam.

The short circuit current plots in Figs. 3 and 4 were used to calculate the angular dependence of the short circuit current I_{sc}. Applying Eq. (3) to the measured data gives incidence angle modifiers according to Fig. 8. The MINSUN simulations were performed using a climate data file for Stockholm, Sweden (latitude 59.3°), as the small difference in the climate compared to Lund can be neglected in view of other assumptions made in the simulation.

Reference simulations with photovoltaic cells mounted with 30° tilt and horizontally were done for comparison.

The results of the simulations are shown in Table 2. The table shows that the result for the back aluminium laminated steel based reflector, MaReCo2, and the back anodized aluminium reflector, MaReCo1, are identical. The output increase from the reference simulation is 22.6%. Looking in detail at $\eta(\theta_T)$ in Fig. 8 reveals that the peak modifier for the aluminium reflector is higher than for the steel based reflector, but the incidence angle modifier is higher at high solar angles for the steel based reflector. These two effects cancels out in the simulation. The front reflector seem to be more suitable for photovoltaic cells, the output increase from the reference simulation is here 49.1%.

These simulations show that if the target is to maximize the ratio kW h/(cell area), the optimal placement of the cells is facing the front reflector.

4.6. Influence of absorber angle

The angle of the absorber, which was defined in Fig. 1, influences the irradiance distribution over the absorber. As discussed in the previous section, the irradiance distribution on the cells affects the electrical output. Using Eq. (3), the incidence angle modifier in the transverse direction was measured and calculated for three different absorber

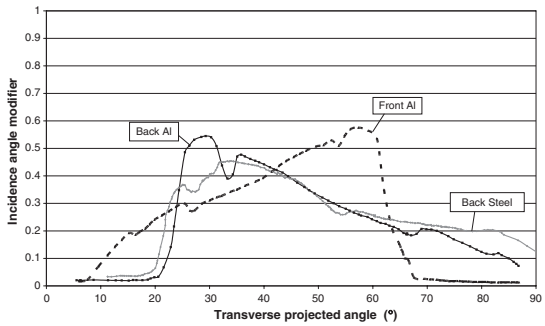

Fig. 8. Incidence angle modifiers in the meridian plane. The incidence angle modifier, $\eta(\theta_T)$, was calculated using Eq. (3) and the measurements of Figs. 4 and 5.

Table 2
Electrical output from different prototypes

Prototype	Yearly electrical output per m^2 cell area (kW h)	Improvement (%)
MaReCo1, back reflector	168	22.6
MaReCo2, back reflector	168	22.6
MaReCo1, front reflector	205	49.1
Reference in 30° tilt	136	0.0
Horizontal reference	103	−24

The cells without concentrators were placed horizontal or in 30° tilt for comparison.

angles, 20°, 45°, and 70° and the results can be seen in Fig. 9. The measurements were performed when the sun was in the meridian plane of the trough and this makes the incidence angle modifier equal to the total optical efficiency as the incidence angle modifier in the east–west direction is one for this case. MaReCo2 was used in the measurements, having cells facing both back and front reflector. What is shown in the figure is the total optical efficiency of the system where the electricity from both sides of the absorber has been combined. The absorber angle was changed, and the measurements were performed as described in Section 4.2.

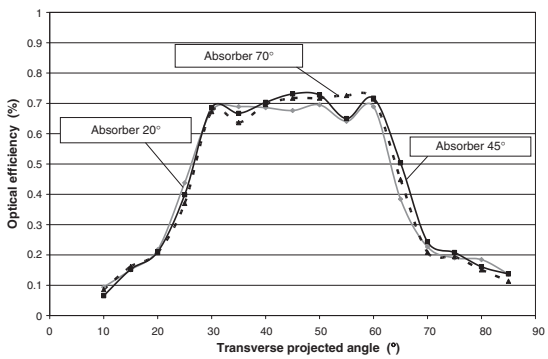

Fig. 9. Optical efficiency for the MaReCo when the absorber is mounted in three different angles.

As seen from the figure, all three cases have favourable angular intervals, but the total output on a yearly basis is approximately the same. The irradiation incident on the MaReCo between 20° and 65° is collected onto the absorber in all three cases, the difference originates from the different distribution of light over the absorber, see Figs. 6 and 7. These differences in distribution accounts for the small differences at each angle, but as can be seen from Fig. 9, there is no single angle which has better performance at all transverse projected angles. The distribution profile is shifted to the left or right when the absorber angle changes, but the profile stays the same. Since it is the intensity at a certain point that creates the output and the losses, the output change due to the angular shift is a small in comparison to other effects.

Yearly simulations show that the difference in output is approximately 3%, which is within the margin of error of the measurements.

5. Outdoor measurements

A MaReCo hybrid with aluminium reflectors and 20 cells facing the front reflector was placed outside for long term measuring. It is shown in Table 1 as MaReCo3. The absorber was tilted in 65° and had no cells facing the back reflector. The side facing the back reflector was untreated and had a relatively low absorptance. The thermal performance of this hybrid was evaluated by multiple linear regression (MLR) analysis and the electrical performance by measuring the short circuit current.

5.1. Thermal evaluation

MINSUN was used to evaluate the annual thermal performance of the hybrid. In order to perform heat calculations, MINSUN uses Eq. (4) to calculate the heat gained.

$$P = \eta_{0b}(\theta) \cdot G_b + \eta_{0d}(\theta) \cdot G_d - k_1 \cdot \Delta T - (mC)_e \cdot \frac{dT_f}{d\tau} \qquad (4)$$

η_0 is the optical efficiency for beam (b) and diffuse (d) irradiation
k_1 [W/m^2 K] is the loss coefficient per collector area
ΔT [K] is the difference between the ambient temperature and the temperature of the collector
$(mC)_e$ [J/m^2] is the heat capacity of the collector
$dT_f/d\tau$ [K/s] is the time derivative of the temperature of the cooling media
θ is the angle in incidence

The parameters were calculated for MaReCo3 doing an MLR analysis on measurement data for three summer months. The resulting values were $\eta_{0b} = 0.474$, $\eta_{0d} = 0.334$, $k_1 = 3.85$ W/m^2 K, and $(mC)_e = 10691$ J/m^2. Different fluid temperatures, ΔT, gives different delivered energy, and to be able to use the water for tap water or heating, it must be at least 50 °C. When this temperature of the fluid was selected, the annual energy yield of the system was 145 kW h/(m^2 glazed area). To demonstrate the difference, if a fluid temperature of 25 °C was accepted, the yield would have been 264 kW h/m^2 glazed area.

A thermal MaReCo with a standard absorber has $\eta_{0b} = 0.6$, $\eta_{0d} = 0.40$, and $k_1 = 2$. The high k_1 for the hybrid is due to the high emittance of the photovoltaic cell as it is without the selective coating of a standard thermal absorber. The low η_{0b} can be explained by two factors. The first factor is that absorber is untreated on the side facing the back reflector, it gives a shiny impression. This decreases the absorption of the back side. The second factor is due to problems in the manufacturing of the prototypes. The absorber is designed to make it possible to do the assembly in place when the system is erected, but the manufacturing precision is too low. The copper pipe containing the heat collecting fluid has a bad thermal contact with the absorber profile, and the losses due to this is considerable as there will be a gap of air reducing the heat flow. In future prototypes, this has to be solved, or a less flexible absorber has to be used to increase the thermal output and reduce the overheating of the photovoltaic cells.

5.2. Electrical evaluation

To validate the experimental electrical measurements, the short circuit current was measured for MaReCo3 during three summer months. As comparison, the same type of absorber with the same type of cells was placed horizontally beside the MaReCo. The reason for having a horizontal reference is that as the trough only has cells facing the front reflector, the aperture is almost horizontal.

The measurements in Fig. 10 show that the short circuit current at high transverse angles (around noon) is similar for the reference and the concentrating system apart from the concentration factor, i.e. the concentrating system has the same angular dependence. This is an important observation, at the conditions where the irradiation has its maximum, the performance of the MaReCo is optimal. Important to note about the figure are the cut-offs on the MaReCo graph are due to the small size of the concentrator trough. The gables are shading the cells as the sun is east or west of the trough glass surface, before 9:30 and after 14:30, as discussed in Section 2.

Fig. 11 shows measurements on clear days between 10.00 and 14.00. This figure clearly indicates a linear dependence between reference current and MaReCo current. The time interval of the measurements is to avoid the shading effects discussed earlier, effects that could be seen in Fig. 10.

The measurements were performed on a clear day with a high percentage of direct insolation, but these ideal condition are not always present. Most days at the Swedish latitude have a high percentage of diffuse, isotropic irradiation. Fig. 12 shows the collection efficiency, i.e. short circuit current, of the MaReCo compared to the reference on a day with low direct irradiation, an almost isotropic sky. The short circuit current of the MaReCo is in this case

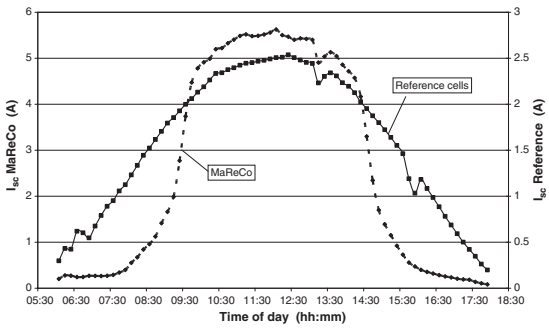

Fig. 10. Short circuit current for horizontally mounted cells and the MaReCo with identical cells. The measurements were taken outdoors on a clear day with a very high percentage of direct irradiation. The current drop at 9:30 and 15:00 is due to shading from the trough gables.

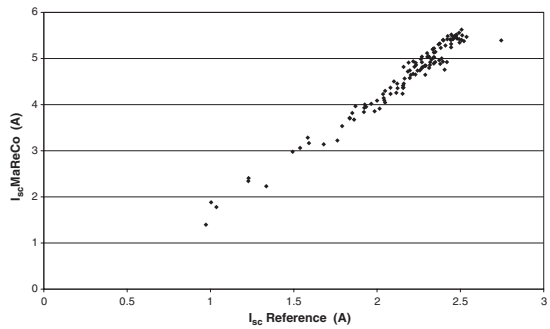

Fig. 11. Short circuit current of MaReCo versus reference cells on clear days between 10.00 and 14.00 when no shading from the gables takes place.

the same as the short circuit current of the reference cells all day apart from the reduction due to the reflectance of aluminium in the reflectors, and the reflections on the cover glass. The optical efficiency can be derived from the figure to approximately 0.8. Due to the laws of thermodynamics, light concentration can only be achieved by increasing the divergence of the light. Since the light has maximum divergence on a day with isotropic sky, it is not possible to concentrate the diffuse light, and this explains the fact that no light gain is obtained on cloudy days.

The relationship between the short circuit current of the reference and the short circuit current of the MaReCo under a longer period with changing weather conditions is shown in Fig. 13. The current of the reference can be seen as a measure of the amount of diffuse irradiation. Low short circuit current of the reference means low amounts of direct irradiation. The linear dependencies at high amounts of direct irradiation, and high amounts of diffuse isotropic irradiation can clearly be seen in this figure.

6. Conclusions

The objective was to estimate the annual electrical and thermal energy output from the MaReCo hybrid. This system is optimized for high latitudes such as Lund, Sweden, where the long term monitoring is to be performed. The *I–V* characteristics and the irradiance distribution on the cells of the hybrids were measured, with the back and front reflectors. Changing the back reflector from anodized aluminium to aluminium laminated steel did not change the

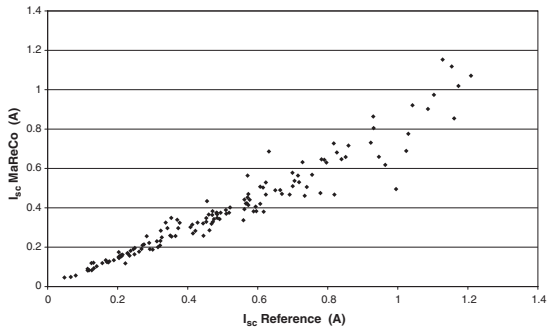

Fig. 12. The short circuit current of the MaReCo versus the reference cells. Measurements taken on a cloudy day with high percentage of diffuse isotropic irradiation.

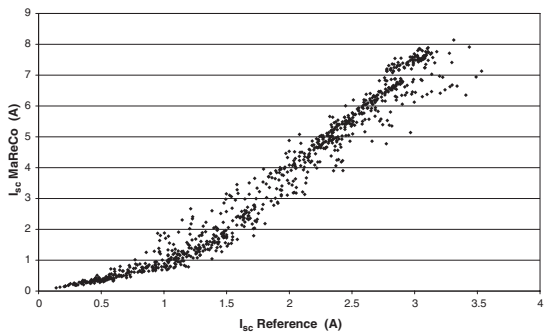

Fig. 13. Short circuit current of MaReCo versus reference cells in all weather conditions. Measurements were taken under a period of one and a half months between 10.00 and 14.00.

energy output. This makes the steel based reflector an interesting option. The annual thermal output estimate for the MaReCo system was 145 kW h/m^2 of hot water at 50 °C. If the absorber is improved, this can be significantly increased. The estimated output of electricity was compared with cells mounted in 30° tilt without reflector, and the MINSUN simulation show a 49% output increase for the front reflector and a 23% increase for the back reflector of MaReCo1, and 23% increase of the back reflector in MaReCo2. This shows that the optimal placement of the photovoltaic cells is facing the front reflector. This could also be seen from the measurement of the short circuit current, where the front reflector had considerably better performance.

The MaReCo is designed to collect most of the irradiation incident on the system during a year. The back reflector collects the light at low transverse angles, and the front reflector collects light at higher transverse angles. If the absorber has photovoltaic cells on one side only, the electricity production will be more unevenly distributed over the year. As the system is intended to be integrated into residential buildings, having an even electricity production is an important factor. Having cells on both sides will also increase the total electricity production considerably, another important factor in integration into residential buildings where roof space is normally limited. If the space is unlimited, and the most important parameter is to produce electricity at the lowest price, the best choice is to have

the cells on the absorber facing the front reflector. In all other cases, photovoltaic cells should be placed on both sides of the absorber; the price of adding cells to the other side of the absorber is relatively low once a trough with cells on one side of the absorber is constructed.

The outdoor measurements show that a two fold increase in output can be expected at noon on a clear day, but the losses at higher azimuth angles and losses due to less direct irradiation makes the estimates given by the MINSUN simulations more probable.

Nevertheless, these results presented here clearly show the possibility to lower the cost of PV-electricity and hot water using the MaReCo hybrid.

References

Adsten, M., Helgesson, A., Karlsson, B., 2005. Evaluation of CPC-collector designs for stand-alone for- or wall installation. Solar Energy 79 (6), 638–647.

Benítez, P., Mohedano, R., 1999. Optimum irradiation of concentrated sunlight for photovoltaic energy conversion. Applied Physics Letters 74 (17), 2543–2545.

Brogren, M., Helgesson, A., Karlsson, B., Nilsson, J., Roos, A., 2004. Optical properties, durability and system aspects of a new aluminium-polymer-laminated steel reflector for solar concentrators. Solar Energy Materials and Solar Cells 82, 387–412.

Chant, V.G., Håkansson, R., 1985. The MINSUN simulation and optimisation program. Application and User's Guide. IEA SH&C Task VII, Ottawa.

Green, M., 1982. Solar Cells. Prentice-Hall Inc., USA.

Mallick, T.K., Eames, P.C., Hyde, T.J., Norton, B., 2004. The design and experimental characterization of an asymmetric compound parabolic photovoltaic concentrator for building façade integration in the UK. Solar Energy 77 (3), 319–327.

Mills, D.R., Giutronich, J.E., 1979a. New ideal concentrators for distant radiation sources. Solar Energy 23 (1), 85–87.

Mills, D.R., Giutroich, J.E., 1979b. Symmetrical and asymmetrical ideal cylindrical radiation transformers and concentrators. Journal of the Optical Society of America 69 (2), 325–328.

Nilsson, J., Brogren, M., Helgesson, A., Roos, A., Karlsson, B., 2006. Biaxial model for the incidence angle dependence of the optical efficiency of photovoltaic systems with asymmetric reflectors. Solar Energy 80 (9), 1199–1212.

Perers, B., Karlsson, B., 1993. External reflectors for large solar collector arrays, simulation model and experimental results. Solar Energy 51 (5), 327–337.

Rabl, A., 1976. Comparison of solar concentrators. Solar Energy 18 (2), 93–111.

Rabl, A., Goodman, N.B., Winston, R., 1979. Practical design considerations for CPC solar collectors. Solar Energy 22 (4), 373–381.

Rönnelid, M., Perers, B., Karlsson, B., Krohn, P., 2000. Cooling of PV modules equipped with low-concentrating CPC reflectors. In: Proceedings ISES 1999 Solar World Congress 1999, Jerusalem, Israel, vol. 3. Elsevier Science, pp. 400–404.

Tripanagnostopoulos, Y., Yianoulis, P., Papaefthimiou, S., Zafeiratos, S., 2000. CPC solar collectors with flat bifacial absorbers. Solar Energy 69 (3), 191–203.

Winston, R., 1974. Principles of solar concentrators of a novel design. Solar Energy 16 (2), 89–95.

Article II

MEASUREMENTS OF THE EFFECTS OF NON-UNIFORM IRRADIANCE DISTRIBUTION ON STANDARD PV CELLS

Johan Nilsson, Håkan Håkansson, Björn Karlsson
Div. of Energy and Building Design, Lund University
P.O. Box 118, Lund, SE-22100, Sweden
Phone: +46 46 2227606, Fax: +46 46 2224719, E-mail: johan.nilsson@ebd.lth.se

ABSTRACT: Stationary parabolic trough systems with standard pv cells often exhibit low outputs compared to the theoretical optical efficiency. This is due to the non uniform irradiance distribution on the cells, which causes large resistive losses. In order to improve the output of the concentrators, it is important to understand and characterize this effect. Presented here are measurements of the effects of non uniform irradiance on the output of one monocrystalline and one polycrystalline Silicon cell. The influence of the width and position of the strip of high irradiance have been measured.
We show that the width of the strip has a large impact on the fill factor and power output when the width is below 10-15 mm. The position of the strip of high irradiance is of lower importance, but the maximum power output is obtained when the strip is close to the busbar. These findings suggest that higher efficiencies can be obtained in new parabolic trough concentrators by widening the irradiance peak while maintaining the same total collected irradiation.
Keywords: Characterisation, Solar Cell Efficiencies, Concentration

1 INTRODUCTION

Medium and high concentrating systems, systems with a concentration ratio above 10, rely on concentrator cells due to the high irradiance levels obtained in the systems. The reason why standard cells cannot be used is that such cells are designed for 1 sun illumination. If the irradiance is much higher than 1 sun, the efficiency decreases rapidly due to the relatively high series resistance of the cells, something that can be seen even in low concentration systems. Concentrator cells are considerably more expensive than standard PV cells due to the fact that most such cells are made in laboratories, or in small volumes. However, it could be possible to use standard cells in low concentration systems, systems with a concentration ratio less than 5, due to the low total irradiation. If feasible, it will lower the price of the system considerably.

The existing low concentrating systems where standard cells could be used are mostly based on two dimensional CPCs in some form [4] and [6], but other geometries such as V-troughs have also been considered [2]. Unfortunately, the electrical output of low concentrating systems with standard cells is often half of what could be expected if concentrator cells were used. This is due to a characteristic that is common to all parabolic mirrors; the incident light is concentrated onto a narrow line of high irradiance. Even though the geometrical concentration ratio is 3-4, irradiance levels of 25-30 times the solar beam are common [7]. The high irradiance level on a small part of the cell has a large negative impact on the electric output. If standard cells are to be used in low concentrating systems, this problem has to be solved by redesigning the concentrator trough in order to get a more uniform illumination on the cells. But, as the parabolic mirror is a thermodynamically ideal concentrator, altering this design will inevitably result in a lower optical efficiency. The optimal system should thus reduce the concentration ratio of the ideal parabolic concentrator as little as possible, while at the same time smoothen the illumination of the cells enough to make the resistive losses acceptable.

In order to perform such a reflector optimization, it is necessary to measure or model the effects of non uniform illumination of standard cells. In the work presented in this article, we have measured the effects on two standard cells, one monocrystalline Silicon cell and one polycrystalline Silicon cell. Two effects have been characterized, the effect of varying the width of the irradiance profile with a constant total irradiation, and the effect of changing the position of the line of high irradiance. At each measurement, the IV-characteristics and the irradiance profile have been measured. The effects are quantified and the impact of the different illumination conditions on the electrical output is discussed. Finaly, basic rules on how to design low concentration systems with standard cells are presented.

2 MATERIALS AND METHODS

2.1 Photovoltaic cells

Two 125 x 125 mm standard cells were used in the measurements, one monocrystalline Silicon cell and one polycrystalline Silicon cell. The IV-characteristics at uniform irradiance of 1000 W/m^2 for the two cells are shown in Figure 1.

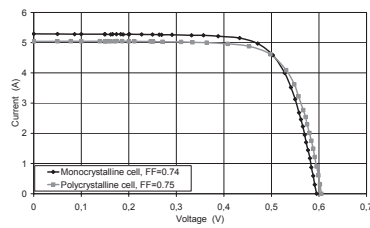

Figure 1 IV-characteristics for the two cells at standard conditions.

To remove the effect of increasing cell temperature during measurement series, the cells were glued to an aluminium plate. The plate was 4 mm thick and 30 cm x 40 cm wide, sufficient to ensure good heat transport from

the cell. The glue used was Wacker Elastosil N10 viscous silicone. It has good thermal conductivity, 0.2 W/mK, and is electrically insulating. A fan was mounted with metallic contact to the plate directly underneath the cells to further increase the cooling.

2.2 Output measurements

The cell output was measured as a function of two different irradiance distribution variations. The total irradiance was kept constant in the first set of measurements while the width of the distribution was varied. In the second set, the position of the strip of high irradiance was varied. Each set of measurements consisted of one IV-measurement and one measurement of the irradiance distribution.

The light source for both measurement sets was a cylindrical halogen lamp that was placed in the focal point of an elliptical reflector trough. The cell was placed as close to the second focal point as possible to achieve maximum concentration. A reflective screen with a 5 mm aperture was placed at the second focal point to screen off stray light.

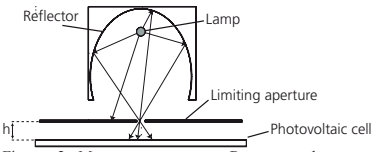

Figure 2 Measurement setup. Rays are drawn to demonstrate the elliptical mirror and limiting aperture. h indicates the distance between the light source aperture and the PV cell.

In the first set h, the distance between the light source aperture and the cell, was varied in order to change the width of the light strip. Figure 3 shows the light distribution at the cell surface at two different distances, 4 mm and 12 mm.

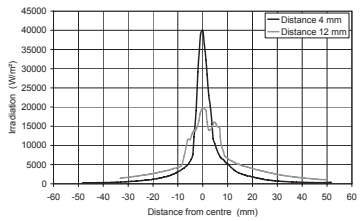

Figure 3 Light distribution on the cell surface when the source was placed 4 mm from the cell and when the source was placed 12 mm from the cell.

As the distance between the source and the cell increased, a small fraction of the light in the direction of the trough axis of symmetry missed the cell. This is the light that would come out of the paper in Figure 2. Using a ray tracing model of the experimental setup, the amount of lost light was calculated. Since the fraction was small, the error could be compensated by multiplying the current measurements with a correction factor. The width of the peak was calculated as the full width at half maximum (FWHM).

In the second set of measurements the light source was kept at 4 mm. This resulted in the light distribution that could be seen in Figure 3. The cell was then moved in order for the strip of high irradiance to move from one edge of the cell to the other, always having the line of high irradiance parallel to the busbars.

The IV-characteristics were measured for both cases using a data logger with electronically controlled relays. The relays changed the cell load. The current and voltage were measured simultaneously. The irradiance distribution on the cell was measured using a photodiode placed on a rotating lever which moved from one edge of the cell to the other. The lever was rotated in a plane very close to the cell surface, and the angle of rotation was measured by a potentiometer. The photodiode aperture area was reduced by a plate with a 1 mm diameter hole to increase the spatial resolution.

3 RESULTS

3.1 Different irradiance distributions at constant flux

13 sets of measurements were performed for each cell to determine what changes occurred in the irradiance distribution and IV-characteristics as the distance between the cell and the source aperture was varied. The first measurement was taken at a distance of 4 mm, which resulted in a width of 6.6 mm and a peak irradiance of 40 kW/m^2, and the last measurement was taken at a distance of 28 mm when the width was 31 mm and the peak irradiance was 6 kW/m^2. The resulting IV-characteristics from two of the measurements can be seen in Figure 4. As expected, the figure clearly shows the influence of the illumination conditions on the series resistance [5].

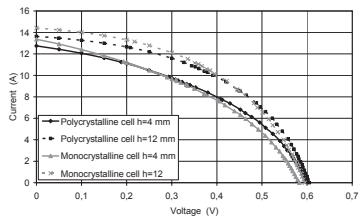

Figure 4 Measured IV-characteristics as a function of h, the distance from the light source aperture to the cell as was shown in Figure 2.

It is important to point out that the total irradiation on the cell was higher than 1 sun since the short-circuit currents measured were almost 3 times the short-circuit current at 1000 W/m^2.

The measured data was used to calculate the maximum output power of the cells, which is shown as a function of the irradiance peak width in Figure 5.

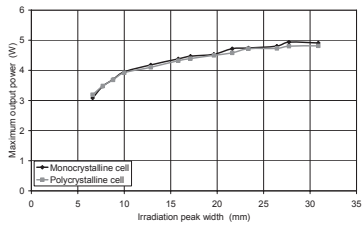

Figure 5 Maximum power output from the cell as a function of the peak width. The data was obtained from the current-voltage measurements.

Starting from the right in figure 5, a decrease in open-circuit voltage and an increase in short-circuit current was observed when the peak width was decreased. This is in agreement with data published by Franklin and Coventry [3]. This resulted in a linear decrease of the maximum power output since the decrease in open-circuit voltage was dominating. At small peak widths, a decrease of short-circuit current occurred, and this yielded an exponential decrease of power.

The cell was well cooled from the back, resulting in an average cell temperature very close to the ambient, but it was impossible to cool the cell locally at the strip of high irradiance. This resulted in high local temperatures as long as the light source was on, and this explains the decrease of open-circuit voltage. When the strip was widened, the local maximum irradiance was lower, which resulted in lower local temperatures and higher open-circuit voltage.

3.2 Influence of the position of the strip of high irradiance

The light source was moved from edge to edge of the cell in steps of 10 mm and current-voltage measurements were taken at each step. The width of the irradiance peak was 6.6 mm. No measurements were taken at the edges since some of the light would miss the cell in that case. Using the measured current-voltage characteristics, the fill factor was calculated. Figure 6 shows the the calculated fill factors and maximum power output for the cells.

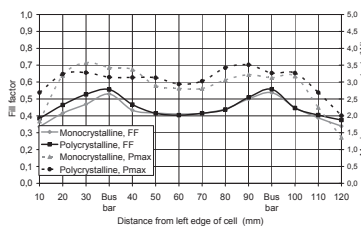

Figure 6 Calculated fill factor and maximum power output as a function of the position of the strip of high irradiance.

Due to the high series resistance of the cells, the fill factor improved significantly when the light was focused close to the busbars. This is in agreement with previously presented results by Benítez and Mohedano [1]. However, the busbar shades the cell partially and this results in lower power output.

4 DISCUSSION

We have shown that the irradiance distribution should be kept as wide as possible for maximum power output of standard cells irrespective of cell type. Due to the large finger spacing of the cells, the ideal irradiance distribution is homogenous. Since uniform irradiance distribution is impossible to achieve in existing concentrators, the decision has to be made on what can be considered as acceptable losses. The losses are linearly dependent on the irradiance width as long as the strip is wider than 10-15 mm. If the peak becomes narrower, the losses will increase rapidly and this has to be avoided. The width of the peak of high irradiance is often around 10 – 20 mm for low concentration parabolic systems [7]. This is on the limit of the linear decrease in power output, and if it is possible to widen the distribution, the output power would certainly benefit.

One characteristic of stationary concentrators is that the light will be distributed differently over the cell at different solar angles of incidence. As Figure 6 shows, the output power can change by 15% when the strip of high irradiance moves over the cell during the day. This has to be considered when new stationary concentrators are designed.

Our measurements clearly show that the challenge in developing low concentrating systems for photovoltaic applications is to increase the irradiance peak width while at the same time maintaining the high collection efficiency. This contradicts the idea of concentration somehow since maximum irradiance is the aim of concentration, but if a choice can be made between two different cases with equal total irradiation, the case with the widest irradiance peak width should be selected to maximize the electrical output.

Our findings show that a parabolic reflector might prove to be an interesting option if the width of the peak can be increased slightly in order for the cells to be working in the linear section seen in Figure 5.

The irradiance distribution can be widened by using a diffusing reflector, or by introducing reflector with a periodic microstructure [8]. Using a diffusing reflector is a low cost solution to the distribution problem. It reduces the peak irradiance and widens the peak, but it has the disadvantage of randomizing the reflected light. This will lead to a higher fill factor at the cost of increased optical losses. Another option is to use microstructured reflectors to achieve the peak widening. As opposite to the diffuse reflector, the structured reflector is not random in nature and a controlled reduction of the peak irradiance can be obtained by using the correct structure. Widening of the irradiance distribution will then be achieved without considerable optical losses.

The ideal concentrator system for photovoltaic applications has a high concentration ratio, low peak irradiance, and focus the light close to the busbars. A system that is able to achieve this at a concentration ratio greater than 2.5X will at least double the power output per cell surface area. If this can be achieved without a large increase in cost, such a system has great economic potential.

5 REFERENCES

[1] Benítez P., Mohedano R. (1999) *Optimum irradiation of concentrated sunlight for photovoltaic energy conversion*. Applied Physics Letters. 74 (17), pp 2543-2545

[2] Fraidenraich, N. (1998) *Design procedure of V-trough cavities for photovoltaic systems*. Progress in Photovoltaics: Research and Applications Vol. 6(1), pp 43-54

[3] Franklin E.T., Coventry J.S. (2002) *Effects of Highly Non-uniform Illumination Distribution on Electrical Performance of Solar Cells*. Proceedings of ANZSES Conference, Newcastle, Australia.

[4] Karlsson B., Wilson G. (1999) *MaReCo – A large asymmetric CPC for high latitudes*. Proceedings of ISES Solar World Congress, Jerusalem, Israel

[5] Lorenzo E., Sånchez E., Luque A. (1980) *Experimental verification of the illumination profile influence on the series resistance of concentrator cells*. J. Appl. Phys. 52(1) pp. 535-536

[6] Mallick, T.K., Eames, P.C., Hyde, T.J., Norton, B. (2004) *The design and experimental characterisation of an asymmetric compound parabolic photovoltaic concentrator for building facade integration in the UK*. Solar Energy Vol. 77(3), pp 319-327

[7] Nilsson J., Håkansson H., Karlsson B. (2003) *Electrical and thermal characterization of a PV-CPC hybrid*. Proceedings of ISES Solar World Congress, Gothenburg, Sweden

[8] Nilsson J., Leutz R., Karlsson B. (2005) *Improving asymmetrical CPCs for photovoltaics by using microstructured reflectors*. Proceedings of the 19th European Photovoltaic Solar Energy Conference, Paris, France

Article III

Available online at www.sciencedirect.com
SCIENCE DIRECT®
Solar Energy 80 (2006) 1199–1212
SOLAR ENERGY
www.elsevier.com/locate/solener

Biaxial model for the incidence angle dependence of the optical efficiency of photovoltaic systems with asymmetric reflectors

Johan Nilsson [a,*], Maria Brogren [b], Anna Helgesson [c], Arne Roos [b], Björn Karlsson [a,c]

[a] *Division of Energy and Building Design, Department of Construction and Architecture, Lund University, P.O. Box 118, 221 00 Lund, Sweden*
[b] *Division of Solid State Physics, Department of Engineering Sciences, Uppsala University, Box 534, 751 21 Uppsala, Sweden*
[c] *Vattenfall Utveckling AB, 814 26 Älvkarleby, Sweden*

Received 18 February 2004; received in revised form 31 August 2005; accepted 2 September 2005
Available online 2 November 2005

Communicated by: Associate Editor Brian Norton

Abstract

The optical efficiency of concentrating solar thermal and photovoltaic systems with cylindrical geometries is asymmetrical about the optical axis. Biaxial models, based on projected incidence angles, are often used to estimate the annual performance of asymmetric concentrators. However, the use of projected angles tends to underestimate optical losses in the cover glass. In this work, a biaxial model for the incidence angle dependence of the optical efficiency, which uses the transverse projected incidence angle for determining the influence of the reflector and the real incidence angle to determine the influence of the glazing is proposed. The model gives an absolute value of the optical efficiency and it is valid for concentrating systems with translational symmetry, as well as for flat plate collectors and planar photovoltaic modules. The model is validated for a system with an east–west aligned parabolic reflector without a cover glass and it is shown that the dependence on the optical efficiency of the reflector on the longitudinal angle of incidence is negligible. The model is compared with the commonly used biaxial model and it is found that the difference is a couple of percentage points when the difference between the longitudinal projected incidence angle and the real incidence angle is large and the angle of incidence on the glass is high.

Keywords: Solar concentrators; Optical efficiency; Incidence angle dependence; Biaxial incidence angle modifier

1. Introduction

1.1. Background

The use of solar concentrators for increasing the output from solar collectors and photovoltaic modules is often cost-effective. However, before

* Corresponding author. Tel.: +46 46 2227606; fax: +46 46 2224719.
E-mail address: johan.nilsson@ebd.lth.se (J. Nilsson).

0038-092X/$ - see front matter © 2005 Elsevier Ltd. All rights reserved.
doi:10.1016/j.solener.2005.09.008

Nomenclature

a	absorber width (m)	K_L	longitudinal incidence angle modifier according to McIntire
β	inclination of the module (°)	K_T	transverse incidence angle modifier according to McIntire
b_0	incidence angle modifier coefficient	$\langle n \rangle$	average number of reflections
C_g	geometrical concentration ratio	η_n	optical efficiency at normal incidence for a planar isotropic system
f_L	optical efficiency of the glazing	η_{opt}	optical efficiency of the system
f'_L	optical efficiency of the system with glazing measured at constant transverse projected angle	ν	inclination of the optical axis (°)
f'_T	optical efficiency of the system with glazing measured at constant longitudinal angle	ξ	angle between module and optical axis (°)
h	aperture height (m)	R_T	optical efficiency of the reflector
I_{SC}^{conc}	short circuit current of the concentrator system (A)	ρ	reflectance of the reflector
$I_{SC}^{reference}$	short current of the reference system (A)	S_L	shading function of the gables
k	normalization constant for the simple numerical model of optical efficiency of the reflector	θ_i	angle of incidence (°)
$K(\theta_L, \theta_T)$	biaxial incidence angle modifier according to McIntire	θ_L	longitudinal projected angle of incidence (°)
		θ_T	transverse projected angle of incidence (°)
		φ	angle between module and aperture (°)

investment in a concentrating solar energy system is made, it is appropriate to calculate the annual thermal or electrical energy output. Predicting the annual output at a specific location requires knowledge of the incidence angle dependence of the optical efficiency of the system. Measurements of the angular dependent performance of concentrators are time-consuming. Therefore, using a model for the incidence angle dependence of the optical efficiency is helpful. Furthermore, if the system is not yet constructed, measurements cannot be performed and a model for predicting the angular dependence is necessary.

For planar isotropic solar energy systems, an incidence angle modifier is often used to describe the incidence angle dependence of the optical efficiency. At a given angle of incidence, θ_i, the optical efficiency, η_{opt}, is given by the product of the optical efficiency at normal incidence, η_n, and the incidence angle modifier according to

$$\eta_{opt}(\theta_i) = \eta_n \left(1 - b_0 \left(\frac{1}{\cos\theta_i} - 1\right)\right), \quad (1)$$

where b_0 is the incidence angle modifier coefficient (Souka and Safwat, 1966; Duffie and Beckman, 1980). The incidence angle modifier coefficient is found by a fit to measurement data or it can be estimated. A commonly used value for glazings and flat plate solar thermal collectors is 0.2.

1.2. Measurements of the optical efficiency of photovoltaic systems

The short-circuit current of a CIGS cell is independent on the illumination distribution on the cell as long as the strip of light is larger than half a millimetre, which is the case for the studied system (McMahon and von Roedern, 1997). This was also shown by Wennerberg et al. (2000). As for the temperature dependence of the short-circuit current, previous studies have shown that for the temperature increases that we can expect in our measurements, this dependence can be neglected (Brogren et al., 2003).

Since the short-circuit current of a photovoltaic module, at a constant temperature, in a concentrating system depends only on the irradiance on the module, which is determined solely by the optical efficiency of the concentrator, measurements of the short-circuit current as a function of real or projected incidence angles can be used to determine the optical efficiency if the current that is generated in the concentrating system is compared with the current from an identical module without concen-

trator and the result is divided by the geometrical concentration ratio, C_g. Hence, the optical efficiency is given by

$$\eta_{opt} = \frac{1}{C_g} \frac{I_{SC}^{conc}}{I_{SC}^{reference}}, \quad (2)$$

where I_{SC}^{conc} is the current from the module in the concentrator and $I_{SC}^{reference}$ is the current from the planar module mounted on the system aperture.

For methods for determining the optical efficiency of solar thermal and photovoltaic-thermal systems from measurements of the thermal output, the reader is referred to earlier work by the authors (Brogren et al., 2000; Helgesson and Karlsson, 2001).

The main source of error in the measurements is the system alignment. It is difficult to align the system and the reference to have their aperture normals facing exactly south. The error in alignment is estimated to approximately 3°. The current was measured as a voltage over a shunt resistance with a very high accuracy. The reference module and the module in the concentrator were calibrated before the measurements to give equal current, but there might be dynamic effects affecting the two modules differently. The dominant error is due to alignment errors and we estimate the total worst-case error of the short-circuit current due to misalignment to be approximately 0.1 A. This would occur at noon if the sun has an altitude between 20° and 30°.

1.3. Biaxial models for the incidence angle dependence of the optical efficiency

The optical efficiency of asymmetric concentrating systems has different incidence angle dependence in different directions. For asymmetric systems with translational symmetry, it is often convenient to define the projected transverse and longitudinal angles of incidence. These angles are defined in Fig. 1.

McIntire presents a biaxial incidence angle modifier, K, for the optical efficiency of asymmetric concentrating systems:

$$K(\theta_L, \theta_T) \approx K_L(\theta_L, 0) K_T(0, \theta_T), \quad (3)$$

which is obtained from measurements in the perpendicular transverse and longitudinal directions (McIntire, 1982). A disadvantage of this model is that it, like the uniaxial incidence angle modifier in Eq. (1), has to be normalized, i.e. that the optical efficiency is the product of the optical efficiency at

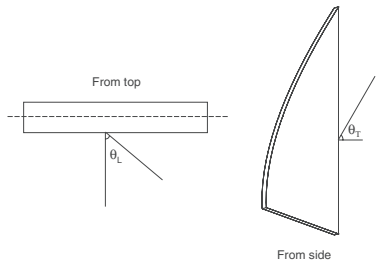

Fig. 1. Definition of the transverse and longitudinal incidence angles for the concentrating system. The left drawing is seen from the top of the system and the right is seen from the side.

normal angle of incidence and the biaxial incidence angle modifier, according to

$$\eta_{opt}(\theta_i) = \eta_n K(\theta_L, \theta_T). \quad (4)$$

Furthermore, it is not always possible to determine the factor K_L at $\theta_T = 0$, depending on how the projected angles of incidence are defined. However, the aspect of this model that may have the largest practical implications is that it underestimates the optical losses in the glazing, due to its utilisation of the projected longitudinal incidence angle to determine the transmittance of the cover glass, which leads to large errors at high angles of incidence (Rönnelid et al., 1997). On the other hand, the angular dependence of the glass is accounted for twice, both in the K_T and K_L, which reduces this effect.

The relationship between the real, the longitudinal, and the transverse angles of incidence is given by

$$\tan^2\theta_i = \tan^2\theta_T + \tan^2\theta_L \quad (5)$$

and is shown in Fig. 2. The lines are iso-incidence angles. However, all these combinations of the real and the projected incidence angles are not found for a concentrating system. The combinations of angles are determined by the celestial movement and the system geometry. As an example of the combinations that can be found, Fig. 3 shows the incidence angle of the direct solar radiation against a south wall in Älvkarleby (60.5° N, 17.4° E), Sweden, as well as the transverse and longitudinal projected incidence angles on the same wall, as functions of the time of the day on the 15th July and 23rd September. At noon, the transverse and the real incidence angles coincide with the solar altitude.

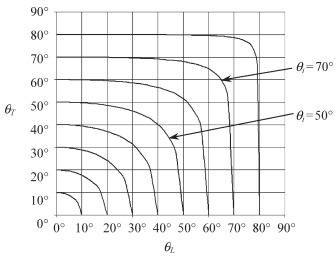

Fig. 2. Angular relationships between the projected angles θ_T and θ_L and the real incidence angle θ_i. The curves represent constant real incidence angle contours.

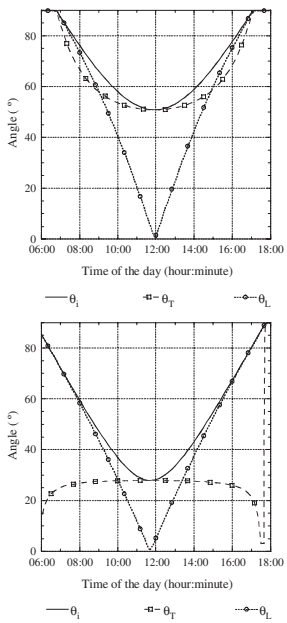

Fig. 3. The incidence angle of the direct solar radiation on a south-facing vertical wall, as well as the transverse and longitudinal projected incidence angles on the same wall, as functions of the time of the day on the 15th July (upper) and 23rd September (lower), in Älvkarleby (60.5° N, 17.4° E), Sweden.

1.4. Transverse projected angle and the orientation of translational symmetric reflector systems

The optical performance of a translational symmetric reflector system, such as the studied system, is determined solely by the transverse projected angle of incidence. As can be seen in Fig. 3 (lower), the transverse projected angle of incidence is constant during the day at equinox. A translational symmetric reflector system with the axis of symmetry aligned in the east–west direction will around the equinox have constant optical efficiency all day. This makes it possible to evaluate the angle dependencies of the cover glass and the absorber during equinox. Another option is to rotate through 90° counterclockwise and tilt it to the latitude angle. When the system is in this setup, the sun will move in the plane perpendicular to the system axis of symmetry all day, and it is possible to measure the optical performance as a function of the transverse projected angle of incidence.

When not stated otherwise in this article, the system is always aligned with the axis of symmetry parallel to the east–west axis, facing south. The transverse projected angle of incidence is then the angle of incidence on the glazing projected into the meridian plane.

1.5. Objectives

The objective of this work is to present and validate a biaxial model for the optical efficiency of asymmetric concentrating solar energy systems. The model is based on separate measurements of the effects on the optical efficiency of the reflector and the glazing.

1.6. The studied system

Fig. 4 shows a photograph of the prototype system that was used to conduct the investigation of the incidence angle dependence of the optical efficiency. The system includes an off-the-shelf thin film ST-50 CIGS module from Siemens and a parabolic over edge reflector of anodised aluminium with a solar reflectance of approximately 80% at near normal angle of incidence. The module consist of series connected cells that are extended perpendicular to the reflector. This ensures that all individual cells receives the same illumination in the translational symmetric reflector system. The characteristics of CIGS cells in concentrating systems have been dis-

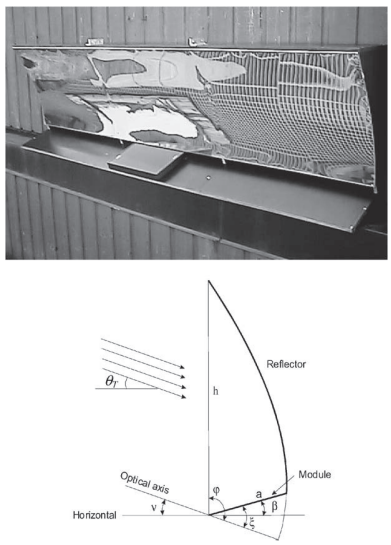

Fig. 4. Photograph of a 3X concentrating façade-mounted concentrating system with parabolic over edge reflector and thin film photovoltaic module (upper) and a schematic showing the cross-section of the concentrator (lower). The transverse incidence angle, θ_T, is defined in the schematic. φ is the internal angle between the glazing and the optical axis, and is in this case 115°.

cussed in earlier work by Brogren et al. (2003) and Wennerberg et al. (2000). A cross-section of the system is shown in the lower figure. The optical axis of the system is inclined at $v = 25°$, which means that all irradiance incident on the parabolic reflector at angles less than 25° will be reflected back out of the system without reaching the cells. The module plane has an inclination of, $\beta = 20°$, and the angle between the module plane and the optical axis is given by $\xi = \beta + v = 20° + 25° = 45°$. This results in a geometrical concentration ratio, C_g of

$$C_g = \frac{h}{a} = \frac{\cos^2\left(\frac{\xi}{2}\right)}{\cos^2\left(\frac{v+90°}{2}\right)} = 2.95, \quad (6)$$

where h is the height of the vertical aperture and a is the width of the module plane, as indicated in Fig. 4. In its original design, the system does not include a glazing. The height of the vertical aperture, h, is 974 mm and the width of the module, a, is 330 mm. This 3X concentrating photovoltaic system is further described elsewhere (Brogren et al., 2001a,b, 2003). For discussions about other low concentrating systems refer to Zacharopoulos et al. (2000) and Tripanagnostopoulos et al. (2002).

2. New biaxial model

The biaxial model that is proposed in this paper is based on separate measurements of the influence of the reflector and glazing. This requires that the glazing can be removed from the system or that the measurements are performed before the glazing is applied. It is possible, however, to determine the contribution of the reflector from measurements with the glazing present, using a compensation for the glazing in the expression for the effect of the reflector. This procedure is described in Section 4.3. The proposed biaxial model can be written

$$\eta_{opt} = R_T(\theta_T) f_L(\theta_i), \quad (7)$$

where $R_T(\theta_T)$ describes the dependence on the optical efficiency of the system on the reflector as a function of the transverse incidence angle, and $f_L(\theta_i)$ describes the dependence on the optical efficiency of the system on the glazing as a function of the real incidence angle. Note that, unlike in Eq. (3), it is the real incidence angle that is used to describe the longitudinal dependence in Eq. (7).

2.1. Incidence angle dependence of the optical efficiency of the reflector

We will show that the optical efficiency of the reflector is independent of the longitudinal angle of incidence by measuring $f_L(\theta_L)$ without a glazing. For our system, measuring the optical efficiency at $\theta_T = 0$ makes no sense, since the lower acceptance angle is 25°, all light falling on the reflector below this angle of incidence is reflected out of the system. However, measurements of the optical efficiency as a function of the longitudinal angle of incidence at constant θ_T can be used to show that the reflector function, R_T, is independent of θ_L. Measurements of the current generated in the concentrating system on the 6th and 17th September 2003, close to the autumn equinox, were compared with the current generated in a vertical module mounted on the aperture using Eq. (2) and the resulting optical efficiency as a function of the time of the day is shown in Fig. 5. Around the equinoxes, the transverse

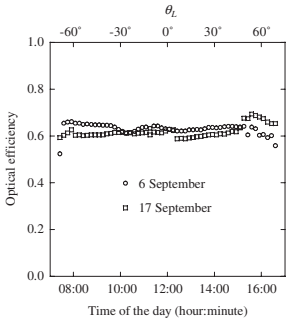

Fig. 5. Optical efficiency of the parabolic over edge reflector as a function of the time of the day on two days close to the autumn equinox, when θ_T is constant. The global irradiance was around 800 W/m^2 at noon and the diffuse fraction was about 10% during the whole day on both dates.

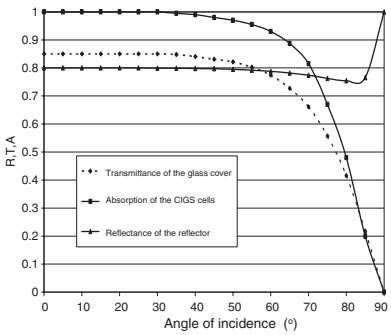

Fig. 6. Calculated optical properties of aluminium and glass, and the normalised conversion efficiency of a CIGS module, as a function of incidence angle.

incidence angle, θ_T, is constant at about 30° (90°-latitude) during the entire day, which is shown in the lower graph in Fig. 3. The longitudinal angle, however, changes from −90°, at 06:00 in the morning to 90° at 18:00 in the evening, and the change is +15° per hour.

Fig. 5 shows that the optical efficiency of the reflector is independent of θ_L as it is constant when the longitudinal angle changes during the day.

Assuming that the reflectance of the reflector material is independent of the angle of incidence, the influence of the reflector on the optical efficiency of the system is largely determined by the average number of reflections, $\langle n \rangle$, in the reflector, and the optical efficiency of the reflector, η^R_{opt}, can be described by

$$\eta^R_{opt} = \rho^{\langle n \rangle}, \tag{8}$$

where ρ is the reflectance of the reflector. For a reflector of aluminium, the assumption that the total solar reflectance is independent of the angle of incidence is valid within a few percent for incidence angles below 80°. This is shown in Fig. 6, which also displays the angular dependent transmittance of a 3 mm glass, as well as the measured normalised incidence angle dependent conversion efficiency of the thin film CIGS module, which is used in the 3X concentrating system. The incidence angle dependent conversion efficiency of the module was obtained from outdoor measurements and the angular dependent reflectance and transmittance values were obtained from Fresnel calculations, using tabulated complex indices of refraction.

The number of reflections, $\langle n \rangle$, is determined solely by the projected transverse incidence angle and the system geometry. Thus, the influence of the reflector on the optical efficiency of a translational symmetric concentrating system with a specific geometry can be formulated by an equation with the transverse incidence angle θ_T as the only parameter. This function can be a theoretical function that is derived from the geometry and the measured solar reflectance, or it can be obtained from measurements or ray tracing.

The optical efficiency of the 3X concentrating over edge parabolic reflector was obtained from measurements of the short-circuit currents as a function of the transverse incidence angle. The measurements were performed close to the autumn equinox, when the longitudinal angle changes by +15° per hour and the transverse incidence angle is constant. As discussed in Section 1.4, if the system is placed appropriately (rotated 90° clockwise and tilted to the latitude angle), the sun moves in the transverse plane of the system. It is thus possible to monitor the optical efficiency as a function of the transverse angle of incidence θ_T as the sun moves across the sky. The effect on the optical efficiency of the reflector, R_T, was determined using the expression:

$$R_T(\theta_T) = \frac{1}{C_g} \frac{I_{SC}^{conc}(\theta_T)}{I_{SC}^{reference}(\theta_T)}. \quad (9)$$

The result is shown in Fig. 7. With the system mounted as described above, high positive transverse incidence angles corresponds to the morning hours, 90° represents 6:00 a.m., and the transverse incidence angle is negative after 12:00 p.m.

If it is not possible to mount the system as described above, a comparison between the current that is generated in the concentrating system and the current that is generated in a module without a concentrator can still be performed by calculating θ_T at each point. However, in this kind of measurement, the longitudinal incidence angle is not zero, but changes with the time of day. Thus, in order for the comparison to give the influence of the reflector as a function of the transverse angle alone, the longitudinal incidence angle dependence of the reflector has to be the same as for the reference module. This is the case for the concentrating system without a glazing, which was shown in Fig. 5.

Fig. 8 shows the measured short-circuit currents as functions of the time of day for the vertical module and for the module with a reflector mounted as the system is described in Fig. 4, as well as the resulting optical efficiency.

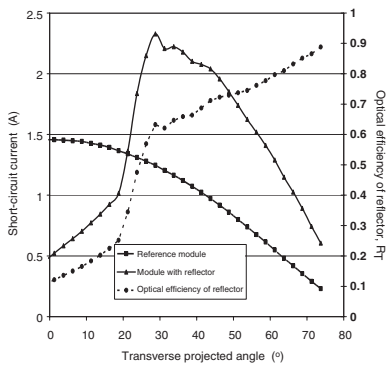

Fig. 7. Short-circuit currents for the module in the concentrating system and a reference module of the same size without a reflector, as functions of the transverse projected angle on 24th September 2003.

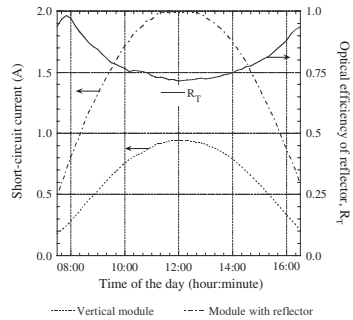

Fig. 8. Measured short-circuit currents for the module in the concentrating system and a vertical module of the same size without a reflector, and the optical efficiency of the reflector, as functions of the time of the day on 15th July 2003.

2.2. Formulation of a simple numerical model for R_T and a comparison with ray-tracing

An analysis of the geometry of the concentrating system shown in Fig. 4 gives that at transverse incidence angles below 25°, no radiation that is reflected in the reflector will reach the module. However, at $\theta_T < 25°$, direct radiation reaches the module at an angle of incidence of $70° - \theta_T$. The θ_T dependence of the optical efficiency of the system, compared to the optical efficiency of a vertical module, is thus given by

$$R_T(\theta_T) = \frac{a \cdot \cos(70° - \theta_T)}{h \cdot \cos(\theta_T)} \quad (10)$$

for θ_T below the lower acceptance angle. For θ_T higher than 25°, part of the beam radiation reaches the module directly and part is reflected in the reflector before reaching the module and the expression for the θ_T dependence of the optical efficiency can be formulated as

$$R_T(\theta_T) = \frac{k \cdot [h \cdot \cos(\theta_T) - a \cdot \cos(70° - \theta_T)] + a \cdot \cos(70° - \theta_T)}{h \cdot \cos(\theta_T)}$$
$$= k + (1 - k) \frac{a \cdot \cos(70° - \theta_T)}{h \cdot \cos(\theta_T)}, \quad (11)$$

where k is dependent on the reflectance of the reflector. Using numerical values of a and h, and a curve fit to the measured θ_T dependence of the optical efficiency in Figs. 7 and 8, a parametric expression for $R_T(\theta_T)$ was formulated:

$$R_T(\theta_T) = \begin{cases} 0.33784\frac{\cos(70^\circ-\theta_T)}{\cos\theta_T} \\ \quad \text{for } \theta_T < 25^\circ, \\ 0.45 + 0.1864\frac{\cos(70^\circ-\theta_T)}{\cos\theta_T} \\ \quad \text{for } \theta_T \geqslant 25^\circ. \end{cases} \quad (12)$$

The normalisation constant, k, that is used to get a good fit to measurement data was 0.45. In an ideal system without resistive losses in the photovoltaic cell, no angular dependence of the absorption of the cells, and with a perfect geometry, this constant would be equal to the reflectance of the reflector as the average number of reflections is close to unity. The reflector of the measured system contains dents and other imperfections due to the manufacturing process. These imperfections will cause undesired reflections, some of the light incident within the interval of acceptance will be reflected out of the system, and some of the light will be reflected in a slightly different direction generating multiple reflections etc. The electrical losses that has significance for the normalization constant are discussed in Section 6.2.

The model for R_T is shown in Fig. 9, together with the measured R_T. The model was also compared with results from ray-tracing, using a three-dimensional CAD model of the system and the commercial ray-racing program ZEMAX (ZEMAX, 2004). No cover glass was used in the simulations and the source of the rays was placed at the vertical aperture. The angle of incidence was chosen as the transverse projected incidence angle, and it was varied from 0° to 90° in steps of 5°. The source generated 10,000 rays for each angle of incidence. The error in each simulated angular optical efficiency was less than 3% for all angles of incidence. The results from ray-tracing, using reflectance values of 0.8 are included in Fig. 9. As the measured values are divided by the current of the reference module that is mounted on the aperture, the ray-tracing values in the figure are divided by the absorption of the cells at the angle of incidence from Fig. 6 to enable a comparison. The absorber is mounted in 20° from the horizontal in the studied system, i.e. when the transverse angle of incidence is 70° and the sun is in the meridian plane all of the light incident on the system aperture is absorbed at normal incidence at the absorber resulting in maximum absorption. The angle of incidence on the reference cells will in this case be 70°, an angle where the absorption has dropped almost 20% as can be seen in Fig. 6. This explains why R_T reaches 1 before 70° and can have a value >1.

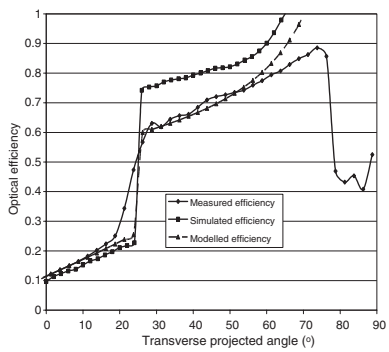

Fig. 9. Comparison between the measured R_T, the simple parametric model, and normalized ray-tracing.

At low θ_T, only light that reaches the module directly contributes to the optical efficiency. At θ_T above 25°, the optical efficiency increases rapidly with increasing θ_T due to the fact that all light that is reflected in the parabolic mirror reaches the module. At even higher θ_T, a larger fraction of the light reaches the module directly, due to a reduced effective reflector area and an increased effective module area at high θ_T. At $\theta_T > 70$, no direct radiation is reflected in the parabolic mirror, as all of it reaches the module directly. The dips in the optical efficiency that can be seen in the curves from ray-tracing are due to multiple reflections in the parabolic mirror at high θ_T. At $\theta_T = 60°$, the average number of reflections is 1.5. The lower optical efficiency due to the multiple reflections is only noticeable at a small angular interval. In this interval, the influence is small, and this indicates that multiple reflections can be neglected in the model.

3. Validation of the model for R_T

3.1. Comparison between model and measurements for single days

Fig. 10a shows the measured optical efficiency of the reflector on a summer day (15th July 2003) and Fig. 10b an autumn day (6th September 2003, close to equinox) together with the model predictions for

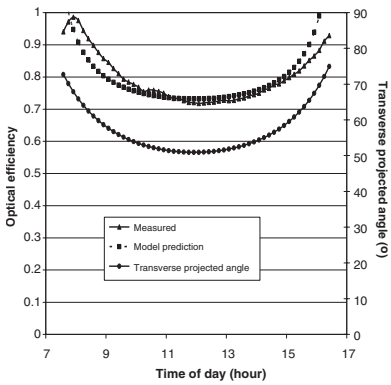

Fig. 10a. Comparison between our model prediction and the measured optical efficiency on the 15th July 2003.

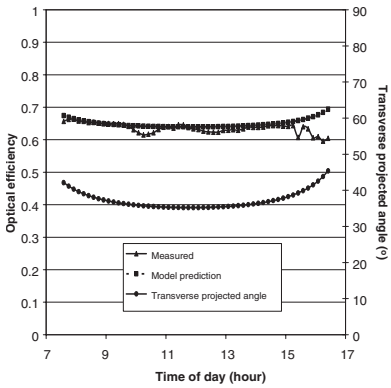

Fig. 10b. Comparison between our model prediction and the measured optical efficiency on the 6th September 2003.

the optical efficiency (Eq. (12)), using $k = 0.45$. The figures show that there is a good agreement between the model and the measured optical efficiency, both for high and moderate projected transverse incidence angles. The flat optical efficiency on 6th September, is due to a constant $\theta_T = 36°$ during this day.

3.2. Comparison between model and measurements for long periods of time

Fig. 11 shows a comparison between the measured short-circuit currents for the vertical module and the module with a parabolic over edge concentrator for the period 10th July to 12th September 2003. Data for every 10th minute for 7:30–16:30 is included in the graph. It can be seen that the concentrating module produces approximately twice the current of the vertical module of the same size. Furthermore, there is a knee in the function at low and moderate currents. The knee, which is indicated in Fig. 11, can be explained by the fact that low and moderate currents are mostly generated in the mornings and in the afternoons, when direct radiation reaches the module in the concentrating system at a more favourable angle of incidence than for the vertical module, since the module in the concentrating system is tilted 20° from the horizontal. This results in a high optical efficiency at the high transverse incidence angles in the mornings and in the afternoons, which was shown in Fig. 10a.

In order to study how well the model describes long-term system efficiency, the measured short-circuit currents for the vertical module during the period 10th July to 12th September 2003 were used in the parametric model (Eq. (12)), together with the geometrical concentration ratio and the calculated θ_T, to predict the generated short-circuit current

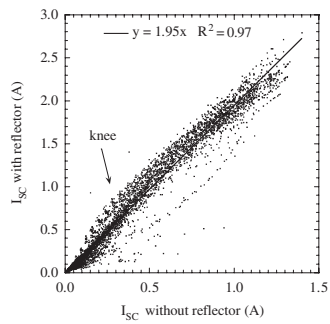

Fig. 11. Comparison between measured short-circuit currents from the module with 3X reflector and the module without reflector, during the period 10th July to 12th September 2003.

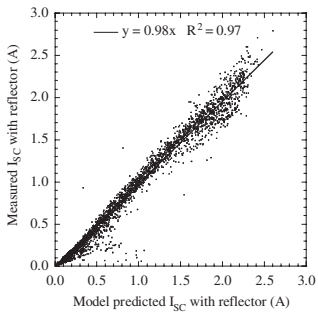

Fig. 12. Comparison between model predictions of the short-circuit current from the module in the concentrator, based on the R_T function and the measured short-circuit current from the vertical module, and the measured short-circuit current from the module with reflector, during the period 10th July to 12th September 2003. One data point for every tenth minute, 7:00–17:00, is included in the graph.

from the module with the 3X reflector during this period. The predicted and the measured short-circuit currents are shown in Fig. 12. The comparison indicates that the model describes the optical efficiency well. There is a tendency that the measured values are lower than the model predictions and the difference is largest at high currents. This is discussed in Section 6.2.

4. Formulation of the complete model

4.1. The effect of a cover glass

The influence of the reflector was measured without a glazing. However, the unsatisfying long-term durability outdoors of most inexpensive reflector materials often necessitate that a cover glass is used, although this reduces the optical efficiency of the system significantly. To a first approximation, the addition of a cover glass will not, per definition, influence the function R_T. Neither does the reflector have any effect on the longitudinal incidence angle behaviour, which was shown above. Thus the angular dependence of the optical efficiency due to the glazing can be assessed separately. In this work, we have chosen to use the incidence angle dependent transmittance of a 3 mm glass, obtained from Fresnel calculations, for the f_L function. The calculated angular transmittance of the glass as a function of incidence angle was shown in Fig. 6. However, for any given cover glass, the angular dependent transmittance can be measured using for instance spectrophotometry. It is also possible to use an incidence angle modifier (Eq. (1)), for example with $\eta_n = 0.9$ and $b_0 = 0.2$, to model the angular dependent transmittance of the glass.

4.2. The effect of the angular dependence of the cell absorption

The absorption of the pv cells as a function of the angle of incidence is described in Fig. 6. As can be seen from the figure, the absorptance is almost constant up to 70°, where it starts reducing rapidly. As the cells are used for measuring the incidence angle dependence of the reflector, this effect will to a small extent introduce an error in the measurements as the transverse projected angle of incidence differs from the angle at which the light is incident on the cells. A ray tracing simulation was performed to study this effect and to be able to estimate the size of error introduced. Fig. 13 shows the result of this simulation, performed for the same date as Fig. 8, July 15. The reflectance was set to 1 in order to remove the effects of the aluminium mirror. As can be seen from the figure, the error is 2–3% during the part of the day when the irradiation is high, and we conclude that the effects can be neglected in the model as they are less than other errors in the measuring

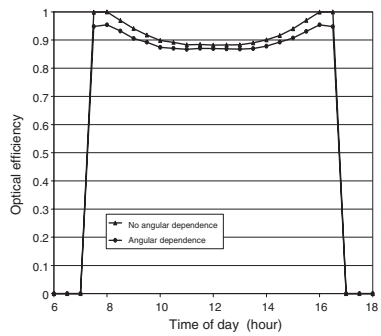

Fig. 13. The influence of the angular dependence of the absorber on the ray tracing results. The reflectance of the reflector was set to 1.

process. The errors will be further discussed in Section 6.2.

4.3. Measurement of the R_T function with a cover glass present

The expressions for R_T and f_L were obtained by performing separate measurements and calculations on the reflector and the glazing, respectively. If the cover glass cannot be removed from the system, this procedure cannot be followed and the R_T function has to be obtained in some other way. R_T can be found by measuring the incidence angle dependence of the optical efficiency of the entire system (including glass and reflector) in the longitudinal and transverse directions, while keeping the other projection of the incidence angle as close to zero as possible in at least one of the measurements. (For the 3X system with a parabolic over edge reflector with a lower acceptance angle of 25°, it makes little sense to measure at $\theta_T < 25°$.) This gives the functions f'_L and f'_T, for the longitudinal and transverse incidence angle dependence of the optical efficiency. The R_T function is then obtained as the ratio between these functions for $\theta_L = 0$, according to

$$R_T(\theta_T) = \frac{f'_T(\theta_T)}{f'_L(\theta_T)}. \quad (13)$$

4.4. Graphical representation of the model

When R_T and f_L have been obtained from measurements, modelling, or ray tracing, the biaxial model for the incidence angle dependence of the optical efficiency can be formulated. Fig. 14 shows the factors f_L and R_T that determine the optical efficiency of the studied 3X concentrating system. Since the functions f_L and R_T depend on different angles of incidence (θ_i and θ_T, respectively) and these angles have a relationship that changes with the time of day and the time of the year, it is not relevant to present their product, η_{opt}, graphically. The optical efficiency at any given moment in time is obtained by taking the product of $f_L(\theta_i)$ and $R_T(\theta_T)$, using the real angle of incidence and the transverse projection angle at that time.

4.5. Application of the model on flat plate collectors and planar pv modules

A flat plate collector or planar module is symmetrical in the transversal and longitudinal directions by measuring the incidence angle dependence in both directions it can be shown that f'_T and f'_L are identical functions. The R_T function will in this case according to Eq. (13) be equal to 1 for all angles of incidence. The model, formulated by Eq. (7), will in this case be reduced to Eq. (14):

$$\eta_{opt} = R_T(\theta_T) f_L(\theta_i) = [1] \cdot f_L(\theta_i) = f_L(\theta_i). \quad (14)$$

This shows that the same methodology and model can be used for concentrator systems as well as for more simple systems such as the flat plate collector or the planar module.

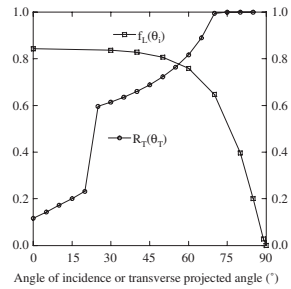

Fig. 14. The factors f_L and R_T that determine the optical efficiency of the 3X concentrating system with a parabolic over edge reflector and a vertical glazing.

5. Comparison between the proposed model and the previous biaxial model

Fig. 15 shows a comparison between the model predictions obtained by the proposed and McIntire's biaxial models for a summer day and a day close to the autumn equinox. Since it is not possible to measure the longitudinal dependence of our system at $\theta_T = 0$, and our system does not include a glass in its original design, we have used a simulated glass, which is the same as the glass for which the transmittance is shown in Fig. 6, in the calculations. Our model is thus the model presented in Fig. 14 above. Our interpretation of McIntire's model is equal to our model for the reflector function, but it uses the projected longitudinal incidence angle for determining the influence of the cover glass. The comparison shows, that there is little difference between the models at the autumn equinox (lower figure), when the difference between the real and

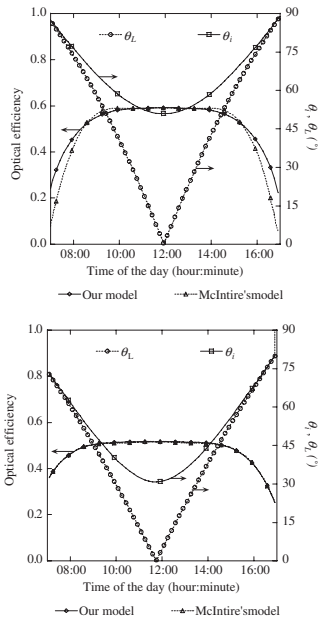

Fig. 15. Optical efficiency as a function of the real (our model) and the projected longitudinal (McIntire) angle of incidence on the 15th July (upper) and the 19th September (lower). The real and the projected longitudinal incidence angles are included in the graphs.

the longitudinal incidence angles never exceeds 30°. However, in summer, when the real incidence angle is high during the entire day and there is a significant difference between the real and the projected angles in the mornings and in the afternoons, a difference between the two models is noticeable, and this difference increases with increasing incidence angle. This is explained by the fact that, at angles of incidence above 50°, the transmittance of the glass drops fast with increasing angle of incidence. The difference between the two models is visible, for example at 14:30 in the upper diagram below. At 14:30 on 15th July, the real angle of incidence is 62.5°, while the projected longitudinal angle is 51.0°, and McIntire's model gives an optical efficiency that is too high, underestimating the transmission losses in the glass.

6. Discussion

6.1. Effects of diffuse radiation

Fig. 16 shows the optical efficiency of the 3X over edge parabolic reflector on a day with little direct radiation. The optical efficiency is obtained using Eq. (2), i.e. it is measured in comparison to a planar module that is mounted vertically beside the concentrating system. The observed optical efficiency for diffuse radiation is 65%, which is almost as high as for direct radiation. The fact that the system seems to concentrate diffuse radiation can be explained by the anisotropy of the diffuse radiation at the test site, the low concentration ratio, which allows the module to see a wide angular interval of the sky, and the low lower acceptance angle (25°) of the studied system. Where the systems are mounted, on a wall that faces south and approximately 1.2 m above the ground, the diffuse radiation that is incident at angles below 25° is negligible.

If the reflector would be ideal ($R = 1.0$) then the isotropic diffuse irradiance on the concentrator module should be equal to the diffuse irradiance on a module tilted 20° from the horizontal and almost twice as high as the irradiance on a vertical module. This effect is further increased by shadow

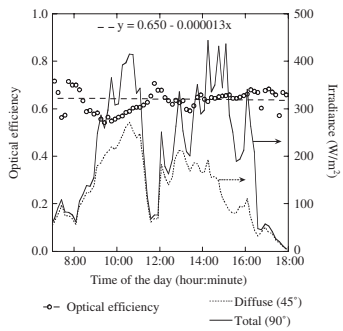

Fig. 16. The optical efficiency of the 3X concentrating over edge parabolic reflector, the total irradiance on the south vertical, and the diffuse irradiance on a surface inclined at 45° towards south, on 15th September 2003, as a function of the time of the day.

effects on the irradiance from angulars below $\theta_T = 25°$.

Fig. 12 which compare model values and measurements also indicate that the efficiency of the concentrator is similar for diffuse and beam irradiance.

6.2. Effects of concentration on cells designed for one sun's illumination

A comparison between the measured optical efficiency, the results from ray-tracing simulations, and the parametric model shows that the measured, the simulated, and the modelled curve are identical below $\theta_T = 25°$. However, when θ_T exceeds 25°, radiation is focussed at the front edge of the module. The module that is used in the test system is designed for one sun's illumination. Furthermore, the contacts are placed on the edge of the module closest to the reflector, and the series resistance of the cell increases with the distance from the contacts to the point where the electron is generated. As the light image from the reflector moves from the reflector edge to the focal point as the sun moves from a transverse angle of 90–25°, the series resistance increases. The voltage drop given by the series resistance will slightly increase the shunt current, and thus decrease the short circuit current, when the series resistance increases with the decreasing transverse projected angle.

These effects are introduced in the model through the normalisation constant, k, and explain the low measured optical efficiency for θ_T above 25°, which was shown in Fig. 9.

6.3. Effects of gables

It has been assumed that the east–west aligned reflector is long in comparison to the photovoltaic module and that there are no edge effects. In the case of a concentrating system with gables that shadows the cells or thermal absorber in early mornings and late evenings, a function $S_L(\theta_L)$, which is essentially a step-function that is 1 without shading and 0 when the module or absorber is shaded, can be introduced in the expression for the optical efficiency.

6.4. Measurement errors

The reference is mounted in the plane of the concentrator aperture. If the plane of the reference is not completely parallel with the plane of the concentrator aperture, it will introduce an error. The analysis is sensitive to this error, an error of 3° will e.g. mean a shift of 10 min in the measured data. This could mean that instead of using the measured reference current for 11:00, the current for 11:10 should be used in order to get correct model predictions. Fig. 10a shows exactly this kind of error, the graphs have the same shape, but there is a clear shift between them. Another error is introduced if the system normal is not pointing perfectly south. As with the previous example, a 3° angle between the south axis and the aperture normal equals 10 min. Looking at Fig. 9, a 3° shift would clearly create a large error compared to the simulated case around the angle of acceptance.

7. Conclusions

A new biaxial model for the incidence angle dependence of the optical efficiency for solar energy systems, $\eta_{opt} = R_T(\theta_T) f_L(\theta_i)$, was proposed. The model uses as parameters the transverse projected incidence angle for determining the effect of the reflector and the real incidence angle to determine the effect of the glazing. The model is valid for all translational symmetric concentrating systems, as well as for flat plate solar collectors and planar photovoltaic modules. Furthermore, the model gives an absolute value of the optical efficiency, i.e. it does not have to be normalised. The model was applied on a system with an east–west aligned asymmetric parabolic reflector without a cover glass and it was shown that the dependence of the optical efficiency of the reflector on the projected longitudinal angle of incidence was negligible. The new model was compared with the commonly used biaxial model, $\eta_{opt} = \eta_n K_T(\theta_T) K_L(\theta_L)$, and it was found that the difference between the models can be a couple of percentage points.

Acknowledgments

This work was supported by Elforsk AB and carried out under the auspices of the Swedish national Energy Systems Programme, which is financed by the Swedish Energy Agency, the Swedish Foundation for Strategic Research, and Swedish industry. The Swedish Energy Agency's Solar heating programme (FUD) is acknowledged for financial support.

References

Brogren, M., Nostell, P., Karlsson, B., 2000. Optical efficiency of a PV-thermal hybrid CPC module for high latitudes. Solar Energy 69 (1–6), 173–185.

Brogren, M., Karlsson, B., Håkansson, H., 2001a. Design and modelling of low-concentrating photovoltaic solar energy systems and investigation of irradiation distribution on modules in such systems. In: Proceedings of 17th EUPVSEC, Munich, Germany.

Brogren, M., Wennerberg, J., Kapper, R., Karlsson, B., 2001b. Design of concentrating elements with thin film solar cells for wall integration. In: Proceedings of 12th PVSEC, Cheju, Korea.

Brogren, M., Wennerberg, J., Kapper, R., Karlsson, B., 2003. Design of concentrating elements with CIS thin film solar cells for wall integration. Solar Energy Materials and Solar Cells 75, 567–575.

Duffie, J.A., Beckman, W.A., 1980. Solar Engineering of Thermal Processes. Wiley Interscience, New York.

Helgesson, A., Karlsson, B. 2001. Study of incidence angle dependence on optical efficiency based on outdoor measurements, modelling of incidence angle dependence of non-symmetrical collectors. In: Proceedings of NorthSun, Holland.

McIntire, W.R., 1982. Factored approximations for biaxial incident angle modifiers. Solar Energy 29 (4), 315–322.

McMahon, T.J., von Roedern, B., 1997. Effects of light intensity on current collection in thin-film solar cells. In: Proceedings of 26th PVSC Conference, Anaheim, USA.

Rönnelid, M., Perers, B., Karlsson, B., 1997. The factorisation of incidence angle modifiers for CPC collectors. Solar Energy 59 (4–6), 281–286.

Souka, A.F., Safwat, H.H., 1966. Optimum orientations for the double exposure flat-plate collector and its reflectors. Solar Energy 10, 170–174.

Tripanagnostopoulos, Y., Nousia, T.H., Souliotis, M., Yianoulis, P., 2002. Hybrid photovoltaic/thermal solar systems. Solar Energy 72 (3), 217–234.

Wennerberg, J., Kessler, J., Hedström, J., Stolt, L., Karlsson, B., Rönnelid, M., 2000. Thin film pv modules for low-concentrating systems. Solar Energy 69 (Suppl.), 243–255.

Zacharopoulos, A., Eames, P.C., McLarnon, D., Norton, B., 2000. Linear dielectric non-imaging concentrating covers for pv integrated building facades. Solar Energy 6 (5), 439–452.

ZEMAX version November 1, 2004. ZEMAX Development Corporation, San Diego, California, USA.

Article IV

Available online at www.sciencedirect.com
ScienceDirect
Solar Energy Materials & Solar Cells 91 (2007) 525–533
Solar Energy Materials and Solar Cells
www.elsevier.com/locate/solmat

Micro-structured reflector surfaces for a stationary asymmetric parabolic solar concentrator

Johan Nilsson[a,*], Ralf Leutz[b], Björn Karlsson[a]

[a]Division of Energy and Building Design, Department of Architecture and Built Environment, Lund University, P.O. Box 118, Lund SE-22100, Sweden
[b]Physics Department, Philipps-University, Renthof 5, 35037 Marburg, Germany

Received 4 January 2006; accepted 3 November 2006
Available online 18 December 2006

Abstract

One of the main problems in using parabolic concentrators with standard photovoltaics (PV) cells is the highly non-uniform illumination of the cells. The non-uniform irradiation causes high resistive losses in the standard cells due to their relatively high series resistance. This results in a considerably lowered efficiency. To solve the problem, we introduce three different structured reflectors that will create a more uniform illumination, and also increase the concentration ratio in certain cases. The structures were evaluated in an existing trough system by Monte Carlo ray tracing, and it was found that structures improve the system performance mainly by homogenizing the light on the cells. The yearly irradiation collected in the evaluation system is slightly lower than for a reference with smooth reflectors, but the more uniform illumination of the cells will generate a net increase of the total system performance compared to a system that was optimized with smooth reflectors. The benefit of the increased concentration ratio is increased flexibility in designing new systems with concentration ratios surpassing the limit of existing trough concentrators.

Keywords: Solar concentrators; Photovoltaics; Structured reflectors; Optical design

1. Introduction

In view of the high costs of photovoltaics (PV) modules, it is necessary to find ways to reduce the cost of a PV system considerably to facilitate more extensive use. Using concentrating reflectors to increase the irradiance on the cells, expensive PV cell area can be exchanged by considerably less expensive reflector area. This has been shown to reduce the cost of the electricity produced [1]. Many reflector systems are based on compound parabolic concentrator reflectors, or CPCs [2].

Parabolic reflectors are ideal concentrators for distant sources; all light incident parallel to the optical axis of the reflector is reflected into the focal point.

The sun is an extended source with a half-angle $\theta_s = 0.27^\circ$ [3]. Sunlight produces a focal line in a parabolic trough concentrator. The geometrical concentration ratio C of the parabolic trough of unit width and a rim angle ψ defines the half-width of the focal line r_t on a flat absorber. Note that θ_s in Eq. (1) is in radians and not degrees:

$$r_t = \frac{1}{C} = \frac{\theta_s}{\cos(\psi)\sin(\psi)}. \quad (1)$$

For $\theta_{max} = \pi/4$, i.e. a rim angle of 45°, the average geometrical concentration ratio of the parabolic trough reaches its maximum of 104, with a peak at $C_{max} = \sin\theta_{max}/\sin\theta_s = 144$. A parabolic shape will concentrate sunlight into a hot spot of high geometrical concentration, independent of the acceptance half-angle θ_{max} [2] of the system.

The high local intensities on the PV cells in parabolic troughs often make the use of concentrator cells necessary to reduce the losses due to the high local currents [4]. These cells are expensive and are produced in small series, but if the light could be more uniformly distributed over the cells, it would be possible to use standard silicon cells in the systems, and this would reduce the system price significantly. To address this problem, we evaluated three

*Corresponding author. Tel.: +46 46 2227606; fax: +46 46 2224719.
E-mail address: johan.nilsson@ebd.lth.se (J. Nilsson).

0927-0248/$ - see front matter © 2006 Elsevier B.V. All rights reserved.
doi:10.1016/j.solmat.2006.11.003

Nomenclature

C	geometrical concentration ratio	η	optical efficiency
C_{max}	maximum theoretical concentration ratio	Θ_i	flux at detector i
k_x	X direction cosine	θ_{exit}	angle between exit aperture normal and exit ray
r_t	half width of focal line	θ_i	angle of incidence
α	solar altitude	θ_{max}	acceptance half angle of concentrator
γ	solar azimuth angle	θ_s	angular spread of the solar beam
		θ_t	angle of incidence in the meridian plane
		ψ	rim angle of trough

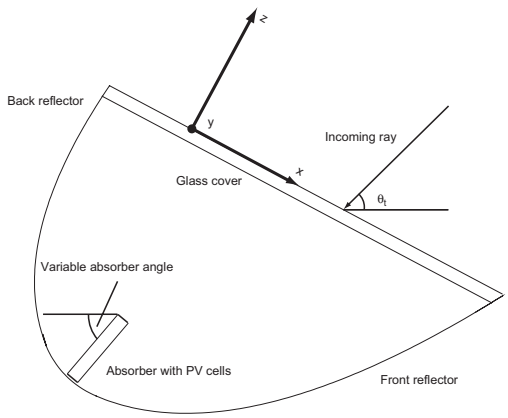

Fig. 1. System layout of the asymmetric parabolic trough concentrator. Shown is the local coordinate system.

different structured reflectors that creates a more uniform light distribution.

Stationary asymmetric CPC systems such as the MaReCo, MaximumReflectorCollector, which is shown in Fig. 1 [5] are suitable for northern latitudes such as Sweden due to the relatively low solar altitude and the high cloud coverage during the winter. It consists of two parabolic aluminium mirrors with their respective optical axis tilted in 20° and 65° from the horizontal. The absorber is an aluminium profile with copper pipes in the middle to collect heat, and standard monocrystalline silicon cells are laminated on the profile. The system is designed to accept all irradiation between 20° and 65° in the meridian plane. The angle is shown as θ_t in Fig. 1.

The system has an average concentration ratio of 3.5 for the lower reflector and 2.4 for the upper reflector. This system was chosen as the evaluation platform for the proposed reflectors.

Even though the concentration ratio is low for the system, local intensities of 30 times the solar beam have been measured on the cells due to the parabolic shape of the mirrors [5]. The high local intensity at the focal point creates high local currents in the illuminated part of the cells, and the relatively high resistance of standard cells that are used in this system causes large losses. The large difference between 3.5, the concentration ratio, and 30, the real intensity at the centre of the strip of light, indicates that rational changes to the geometry of the reflectors have a large potential for performance improvement.

2. Theory

The étendue of an optical system is a measure of the power that can be accepted by the system. The principle of étendue conservation states that a translational symmetric two-dimensional compound parabolic reflector (CPC) system has a maximum concentration ratio of $1/\sin(\theta_{max})$, where θ_{max} is the half-angle of acceptance in the symmetry plane for $y = 0$. For a three-dimensional (3D) concentrator such as the CPC of rotational symmetry, the maximum concentration ratio is $1/\sin^2(\theta_{max})$ accordingly. Independently conserved quantities in the translational symmetric

system are the two-dimensional étendues in the symmetry planes [6]:

$$\Delta x \Delta k_x = \text{const},$$
$$\Delta y \Delta k_y = \text{const}. \quad (2)$$

This limits the part of the phase space that is filled with light at the exit aperture of the system [7]. Maximum concentration ratio is achieved when the angular phase space is completely filled at the exit aperture, i.e. when the rays are exiting at all angles in three dimensions into a hemisphere. If the angular space is not completely filled at the exit aperture, it limits the concentration ratio by a factor $\sin(\theta_{exit})$, where θ_{exit} is the angle between exit aperture normal and exit ray. For translational symmetric systems, k_y is not affected by reflections and this dictates that both k_y and Δy are constant.

The angles opened by the directional vector components k_x, k_y are small for sources with small angular spread and concentrators with smooth reflectors. Breaking the symmetry of the reflector surface will selectively mix the directions of the reflected rays. While for smooth reflectors the étendues in the symmetry planes (Eq. (2)) are independently conserved, selective mixing leads to the conservation of total étendue

$$\Delta x \Delta k_x \Delta y \Delta k_y = \text{const}. \quad (3)$$

By breaking the symmetry of the trough's smooth reflectors, i.e. affecting the directional components of the reflected rays, it is possible to achieve concentration ratios greater than the limit of two-dimensional concentrators $1/\sin(\theta_{max})$, approaching the 3D limit $1/\sin^2(\theta_{max})$ [8,9]. Breaking the symmetry can thereby lead to an increase of the light throughput (étendue) of the concentrator. The ideal concentrator is characterized by rays of all possible directions at the exit aperture. This tells us that complete mixing of the different angles is desirable. Three different micro-structures were proposed as possible solutions for breaking the symmetry, all shown in Fig. 2 (2d shows the trough cross-section, which is in the xy-plane). All structures are oriented perpendicular to the translational symmetry axis.

Selective mixing of the direction components can be obtained by creating a V-shaped structure on the reflector with an angle of 120°(a) or 60°(b) according to Fig. 2 [10]. Structure (c) in the figure is a sinusoidal wave. The sinusoidal shaped structure has all possible surface normals from $-45°$ to $45°$ depending on the position on the reflector. This creates randomization of the angles of the rays after reflection.

Fig. 3(a) shows the two-dimensional étendue of incidence projected onto a half-circle. The étendue limited by the angular interval $-30° < \theta < = 30°$ is equal to the étendue comprising the rest of the possible angles. The V-shaped structures reflect all rays of one angular interval into the other, and vice versa, thereby mixing the étendue.

The two V-shaped structures mix the étendue in different ways. The structure in Fig. 2(a) with an angle of 120° will create this in one reflection, and the 60° structure in Fig. 2(b) will produce the same result by reflecting every ray twice. As can be seen in Fig. 3, the angle with the trough cross section after reflection will be the same, but the rays might travel in different directions along the axis of symmetry after being reflected. The obvious drawback of the 60° structure is the lower optical efficiency due to the double reflection. All reflected rays will have a lower intensity in this case compared to the 120° structure. The behaviour of the sine-shaped structure was evaluated using a statistical method, Monte Carlo ray tracing.

3. Method

The proposed changes to the structure of the MaReCo reflectors were evaluated by Monte Carlo ray tracing. Four sets of simulations were performed, one for each structured reflector, and one reference simulation with smooth reflectors. 3D models of the four systems were constructed and simulated in ZEMAX, a commercial ray tracing package [11].

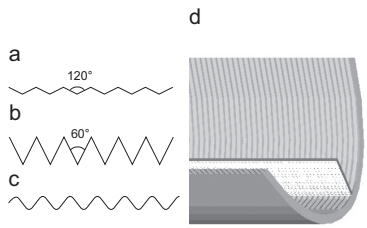

Fig. 2. Different micro-structures. The structure (a) has an opening angle of 120°, the structure, (b) has an angle of 60°, and the structure, (c) is sinusoidal shaped to obtain complete randomization. The MaReCo with structured reflectors is shown in an artist's view (d).

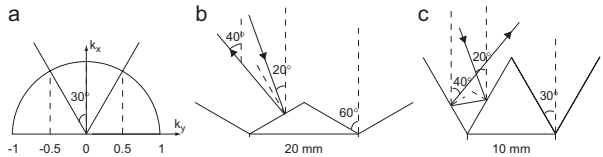

Fig. 3. Selective mixing of reflected rays in the two-dimensional phase-space. The étendue limited by the angular interval-$30 < \theta < = 30$ is equal to the étendue comprising the rest of the possible angles. The V-shaped structures reflect all rays of one angular interval into the other, and vice versa, thereby mixing the étendue.

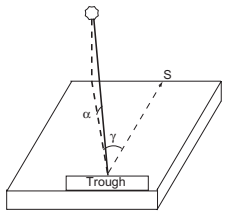

Fig. 4. Definition of the angles used in the simulations, α is the solar altitude and γ is the azimuth angle. The trough is aligned with the axis of symmetry in the east–west direction and the aperture faces south.

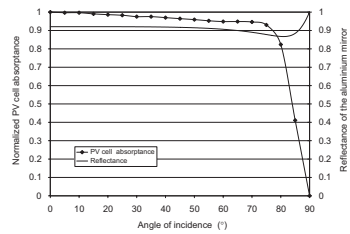

Fig. 5. Normalized absorptance of the PV cell and reflectance of the aluminium mirror, used to model the incidence angle dependency of the system [11].

The cover glass of the system was omitted in all cases, and the source of the rays was placed vertically in front of the system aperture. The source generated 25,000 rays at a specific angle at random locations, and the rays were detected at the trough aperture as a measure of the incident flux, as well as on the front and back side of the absorber. The angle of incidence was varied in both azimuth direction and solar altitude from 0° to 85° in steps of 5° and one simulation was done for each angle resulting in 324 simulations for each reflector type. Fig. 4 defines these angles of incidence, where α is the solar altitude and γ is the azimuth angle.

The normalized absorptance of the PV cells was modelled according to Fig. 5 [12].

The detectors on the aperture and on the absorber consisted of one bin each to detect the incident flux. The optical efficiency of the system was calculated according to

$$\eta_{\text{opt}}(\alpha,\gamma) = \frac{\Theta_{\text{FrontAbs}} + \Theta_{\text{BackAbs}}}{\Theta_{\text{Aperture}}}, \quad (4)$$

where Θ_i is the detected flux at a detector i.

The reflector material was aluminium with a specular reflectance of 92% at normal incidence. Its reflectance as a function of the angle of incidence can be seen in Fig. 5. The maximum error in flux detected by the detectors for each angle is estimated to 2%.

The detectors were later fitted with 70 bins in the y direction of the absorber in order to be able to analyse the uniformity of the irradiance distribution on the cells. This second round of simulations was performed for certain angles of incidence, now using 500,000 rays for higher spatial resolution.

4. Results

4.1. Changes in the light distribution

One of the main challenges in improving low concentration CPC systems such as the MaReCo is the highly non-uniform irradiance distribution on the PV cells. Solving this problem is the main objective when introducing the structured reflectors.

Some of the results from the simulations are shown in Figs. 6 and 7 where the former illustrates the irradiation distribution on the cells facing the upper reflector for an azimuth angle of 15° and a solar altitude of 40°. The latter shows the irradiation distribution on the cells facing the lower reflector at the same angle of incidence.

As can be seen from the figures, all three structural changes reduce the peak intensity of the light incident on the absorber. This will result in a higher fill factor of the cells, i.e. the resistive losses in the cells will be lower. The highest peak reduction is obtained by using the sinusoidal micro-structure. Figs. 6 and 7 show a maximum intensity

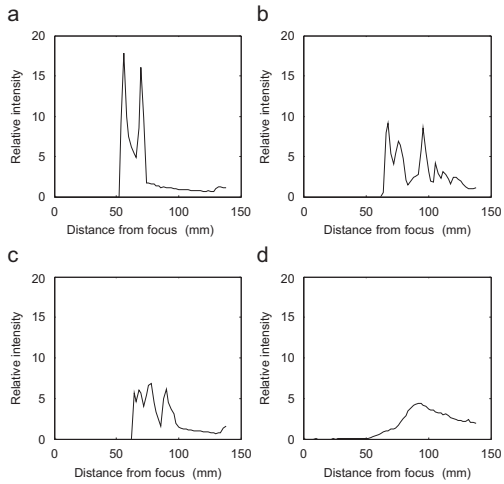

Fig. 6. Irradiance distribution on the cells of the upper absorber for $\alpha = 40^\circ$, $\gamma = 15^\circ$. The four different reflector structures are shown in a–d. (a) Reference, (b) 120° V-shape, (c) 60° V-shape, (d) sinusoidal shape.

of 5 times the sun for this reflector. This intensity should be low enough for the standard cells in the MaReCo system. For the V-shaped structures, the 60° structure seems to reduce the peaks slightly more than the 120° structure, but on the other hand, the overall irradiation on the cell (the integrated intensity profile) is larger for the 120° structure which could explain the greater reduction of the peaks. The peaks for the V-shaped structures can reach levels of almost 10 times the sun. At these intensities, the high resistance of the standard cell becomes a problem, even though it will cause considerably less losses than for the case of the reference reflector where the intensity can be as much as 25 times the beam of the sun. An important point to make about Figs. 6 and 7 is that the absorber connects to the reflector at $x = 140$ mm. If the light distribution is non-zero at the parabola's focus, $x = 0$ in the figures, it can be an indication that some of the light is reflected outside the absorber and lost.

4.2. Comparison of the optical efficiency of the systems

The optical efficiency of the system is defined as the ratio between the incident and the absorbed flux, as described by Eq. (4). The micro-structured reflectors change the path of the rays, and will in some cases cause the rays to miss the absorber. On the other hand, the increased flux concentration ratio of the structured reflectors will make the system absorb irradiation outside the acceptance interval of the reference system, i.e. outside the angular interval of 20° and 65° in the meridian plane. Fig. 8 shows the optical efficiency of the four reflector systems when the solar altitude is changed at a constant azimuth angle of 0°, i.e. in the cross-sectional plane of the trough facing south (the *xz*-plane).

The optical efficiency of the reference system is high between 20° and 65°, but drops rapidly outside this interval. The efficiency does not drop exactly at 20° and 65° in the figure, but this is due to the choice of interval in the simulations. If the interval was smaller, this effect would be more clear. The well-defined interval of acceptance is a characteristic of compound parabolic trough concentrators. The shape of the trough was designed to accept all light in this interval as a compromise considering the yearly irradiation incident on a south facing surface tilted in 30°, as the trough aperture. The 120° structured reflector has a slightly lower peak efficiency, around 7% lower, but the acceptance angle interval is larger, around 10° at both ends. The wider interval is due to the mixing of the direction components of the rays, and the slightly lower peak efficiency is due to the fact that the randomization of the reflected rays in some cases will cause multiple reflections. The sinusoidal-shaped reflector and

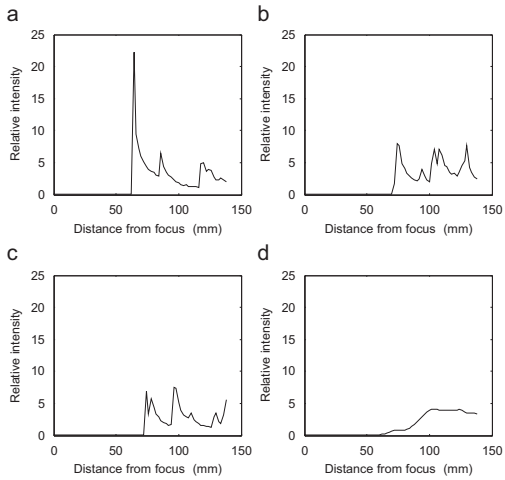

Fig. 7. Irradiance distribution on the cells of the lower absorber for $\alpha = 40^\circ$, $\gamma = 15^\circ$. The four different reflector structures are shown in a–d. (a) Reference, (b) 120° V-shape, (c) 60° V-shape, (d) sinusoidal shape.

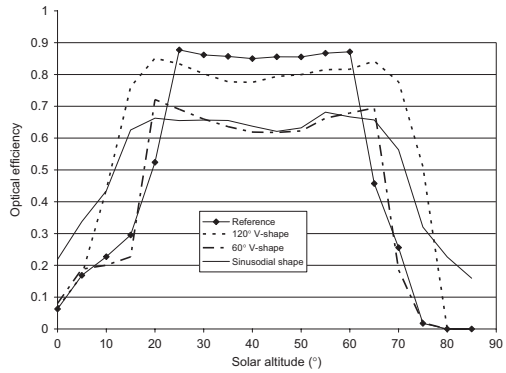

Fig. 8. Optical efficiency as a function of solar altitude in the *xz*-plane. Normal incidence is equal to a solar altitude of 60°.

the 60° structure show considerably lower peak efficiencies, most of the rays are reflected more than once. For the 60° structure this effect can be explained with Fig. 3c, where most rays incident on the reflector are reflected twice. The higher number of multiple reflections for the sinusoidal structured reflector is due to the large randomization of the reflected rays, which is evident in the figures of light distribution on the cells where the light is more evenly

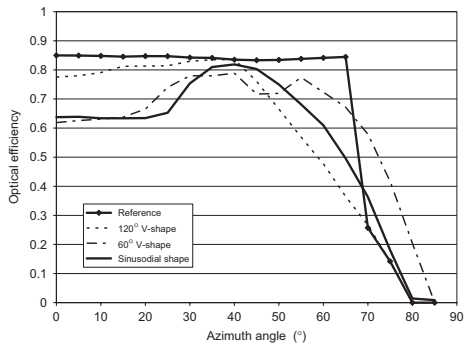

Fig. 9. Optical efficiency as a function of the azimuth angle at a constant solar altitude of 40°.

distributed in spite of the fact that the mirror's global shape is parabolic.

Fig. 9 shows the optical efficiencies of the four reflector systems at changing azimuth angle. The solar altitude in the simulation was kept constant at 40°, within the interval of acceptance for the smooth reference trough.

As expected, the reference reflector shows an almost constant optical efficiency at all angles up to 70°, where the acceptance limit of a transverse angle of 65° is exceeded. The transverse angle is the angle of the solar vector projected into the *xz*-plane. As the solar altitude was constant at 40° throughout the simulation, the transverse angle became 65° at an azimuth angle of approximately 67°. As can be seen from Fig. 8, the optical efficiency of the reference drops considerably once this angle is reached. Another aspect that can be seen from Fig. 8, is that the efficiency is almost constant in this interval which explains the constant efficiency of Fig. 9. The 120° structured reflector has an efficiency close to the reference up to azimuth angles of 45°, where it starts to drop. At large azimuth angles, more and more of the rays are reflected outside the absorber. The efficiency of this reflector never exceeds the reference in the simulated case. The 60° structure and the sine-shaped structure have a 25% lower efficiency at low azimuth angles, but as the angle increases, the efficiency follows suit. At angles of around 70°, both structures have a higher efficiency than the reference, the 60° structure having the highest efficiency.

4.3. Evaluation of the MaReCo using different reflectors in Lund, Sweden

Insolation is not equal for all angles of incidence, it is highest in the middle of the day, around 0° azimuth angle. The yearly direct insolation in Lund, Sweden, 55.73°N, 13.22°E was divided into angular intervals of 5° in the solar altitude and azimuth directions. The optical efficiencies at different angles were multiplied by the irradiation values to get a local evaluation of the concentrator performance. This is not equal to the annual output, but it allows for a comparison of the four reflectors at this specific site.

Table 1
Optical efficiencies of the micro-structured reflectors for diffuse radiation

	Reference (smooth)	120° V-shapes	60° V-shapes	Sinusoidal shape
η_{diffuse}	0.38	0.38	0.35	0.37

The diffuse part of the yearly insolation was treated separately. The diffuse sky was treated as isotropic all year, i.e. the different parts of the sky were assumed to radiate equally strong, or lambertian. The efficiencies of the troughs for diffuse radiation were calculated according to Eq. (5), where α is the solar altitude, γ is the azimuth angle, and θ_i is the angle of incidence on the aperture of the trough. Cos(θ_i) accounts for the view factor and cos(α) accounts for the fact that not all radiating elements are of the same size:

$$\eta_{\text{diffuse}}(\alpha,\gamma)=\frac{\sum_{\alpha=0}^{\alpha=90}\sum_{\gamma=-180}^{\gamma=180}\eta_{\text{direct}}(\alpha,\gamma)\cos(\theta_i)\cos(\alpha)}{\sum_{\alpha=0}^{\alpha=90}\sum_{\gamma=-180}^{\gamma=180}\cos(\theta_i)\cos(\alpha)}. \quad (5)$$

Table 1 shows the result of these calculations. The optical efficiencies for diffuse radiation are very similar for all cases even though the structured reflectors create more multiple reflections. The reason for this can be seen in Fig. 6, as the interval of acceptance is smaller for the reference case. As smaller interval of acceptance practically means that the cells see a smaller part of the sky.

The optical efficiency for diffuse radiation was multiplied by the total diffuse radiation on a surface tilted 30°, modelling the aperture. The diffuse irradiation was then

Table 2
Annual irradiation on the PV cells of the system relative to the reference

	Reference (smooth)	120° V-shapes	60° V-shapes	Sinusoidal shape
Relative irradiation	1.0	0.91	0.89	0.90

added to the direct irradiation from the previous calculations. Table 2 shows the result of the irradiation calculations.

Considering the fact that the MaReCo was optimized for climate of Lund, it is not surprising that the smooth reflector receives the highest yearly irradiation. The 120° structure and the sinusoidal-shaped structure show a mere 9–10% decrease in accepted irradiation over the year.

5. Discussion

5.1. The 120° V-shaped reflector structure

The 120° structure has the highest overall optical efficiency of the three evaluated structures. The simulations show that 9% less irradiation reaches the cells over a year, when compared to a reference concentrator with smooth reflectors. The main advantage of this reflector compared to the other two structured reflectors is that it has roughly the same average number of reflections as the smooth reference. This can be seen in Fig. 8 where the optical efficiency is close to the reference inside the interval of acceptance as long as the azimuth angle is small. When the azimuth angle increases, more rays are reflected out of the concentrator, and the efficiency drops as Fig. 9 shows. At small azimuth angles, this structure would be preferred to the reference as the interval of acceptance is wider for the structured reflector and this gives a higher degree of freedom in designing the system. However, it is less efficient as the azimuth angle increases.

Considering the irradiance distribution, this reflector shows the lowest peak reduction of the three structures, although uniformity is still considerably better than for the reference case.

This reflector would be the best choice when the irradiation is concentrated within small azimuth angles, or for east–west tracking. The small 9% reduction in total yearly irradiation shows that it could improve stationary concentrators as well due to the more homogenous irradiation distribution. If the generated electricity is more valuable in the middle of day, this would be another reason for choosing this reflector.

5.2. Sinusoidal reflector structure

The sine structured reflector has almost the same overall optical efficiency as the 120° structured reflector, only 10% less irradiation reaches the absorber in this case compared to the reference. At small azimuth angles, the efficiency is considerably lower compared to the reference. As the interval of acceptance is less pronounced, the efficiency decreases slowly outside the 20–65° interval rather that showing the step characteristic of the reference. As the azimuth angle increases, Fig. 9 shows an increasing optical efficiency, and at larger azimuth angles, the sinusoidal structure shows a similar or slightly higher efficiency than the reference.

Of the three proposed micro-structures, this one shows the most uniform irradiation profile on the absorber, most of the peaks are removed, and the intensity in Figs. 6 and 7 is never higher than 4.5 times the intensity of the sun.

This reflector shows an overall efficiency similar to the 120° V-shaped reflector in the evaluation with the local climate, but the more uniform irradiation distribution generated by the sinusoidal micro-structure makes it a promising candidate for use in the stationary MaReCo system, especially if the irradiation is evenly distributed over the azimuth angles.

Important for this reflector is the ratio between the length of the period of the structure and the amplitude. As it was chosen in the studied case, the slope of the reflector at $y = 0$ is somewhere between the slope of the 120° structure and the 60° structure. Had the amplitude been larger, more multiple reflections would have resulted in an increased randomization of the reflected rays and a decreased optical efficiency. A more detailed study of the optical effects of different ratios between period and amplitude of sinusoidal micro-structures is beyond the scope of this article.

5.3. The 60° V-shaped reflector structure

The 60° structured reflector showed the lowest annual output. This is due to the fact that, compared to the reference case and the 120° structure, more rays are reflected twice before reaching the absorber. These reflection losses are the reason for the 11% reduction in yearly irradiation on the cells. This is evident from Fig. 8 as the optical efficiency is 25% lower than the reference inside the interval of acceptance at zero azimuth angle. As the azimuth angle increases, the efficiency of this reflector system increases. At large azimuth angles, the efficiency is higher than the efficiency of the reference. The interval of acceptance in the meridian plane, shown in Fig. 8, is the same as for the reference, clearly showing that this reflector system has a lower efficiency at small azimuth angles.

The intensity peak reduction on the absorber generated by this micro-structure is similar, or slightly larger than at the 120° structured reflector but as less light is collected at the absorber, this is to be expected.

This reflector shows some of the features of the 120° structured reflector, and some of the sinusoidal structured reflector, but of the three, it has the least benefits.

6. Conclusions

6.1. Illumination of the cells

The two goals of introducing structured reflectors were to increase the concentration ratio and to get a more uniform illumination distribution on the PV cells. By breaking the symmetry, the system became an actual 3D concentrator system, and a new illumination distribution was created. As was seen in Figs. 6 and 7, all three structures reduced the peak irradiation, creating a more uniform distribution. However, reducing the peak illumination by accepting less irradiation on the cells is not the solution to the problem, but it was shown that during a year in Lund, the reflector system with a 120° angle received 9% less irradiation on the cells, 11% less for the 60° structured reflector, and 10% less for the sine structured reflector.

In a previous measurement study on the MaReCo reflector system [5], three reflector materials were tested. One of these materials, aluminium laminated steel, was slightly diffusing, reducing the peaks of high irradiation. When this material was used in the system, the fill factor of the cells was increased by as much as 12% even though the peak reduction was smaller than for any of the reflectors tested here. This tells us that the introduction of structured reflectors has a large potential for increasing the fill factor, and thus the power output of the system in parabolic trough systems such as this, since the reduction of yearly illumination is only 9% or 10% in the best cases.

We conclude that the small decrease in total irradiation is acceptable considering the larger gains in fill factor.

6.2. Increased concentration ratio

The increase of concentration ratio achieved by the phase space mixing due to the structured reflector can be exploited in two ways: either by reducing the cell area of the given system to get a lower system price, or by changing the shape of the trough to make use of the wider interval of acceptance seen in Fig. 8. The MaReCo trough is designed to accept as much irradiation as possible in an interval of 20–65° in the meridian plane of incidence, thereby discarding almost all of the irradiation outside this interval. This interval is connected directly to the size of the aperture, if the interval is smaller, the aperture can be larger and vice versa. In future studies on the structured reflectors, the trough aperture will be increased, creating a smaller angular interval for a smooth reflector system. As could be seen from Fig. 8, the interval of acceptance widens when a structured reflector is used. This will make it possible to accept almost all light in the interval of 20–65° while increasing the concentration ratio. The use of the sinusoidal structure would create similar possibilities as the V-shaped structures, but due to the randomness of the reflections, a more thorough study on the geometry would have to be performed to make the best use of it.

6.3. Robustness of the system

The MaReCo trough was created for PV/thermal hybrids that have PV cells laminated on a thermal absorber using a copper pipe inside the absorber for collecting the heat. The fluid keeps the cells at a lower temperature, and this increases the electricity output as well as produces hot water. A known problem with this type of hybrids is destruction of the cells if the circulation pump stops working when the trough is collecting at peak irradiation. Hot spots occur on the cell surface due to the high intensity peaks, and without the cooling of the cells the heat can not be dissipated at an adequate rate. The results are delamination of the cells or cracking of the cells due to the thermal expansion of the different materials in the module. Reducing the intensity peaks with structured reflectors, this problem will almost certainly be solved as the cell will have a much more uniform temperature distribution. This will make the performance less restricted by heat conductivity and cooling.

References

[1] B. Perers, B. Karlsson, Sol. Energy 51 (5) (1993) 327.
[2] W.T. Welford, R. Winston, High Collection Nonimaging Optics, Academic Press Inc., New York, 1989.
[3] J.A. Duffie, W.A. Beckman, Solar Engineering of Thermal Processes, Wiley Interscience, New York, 1980, p. 288.
[4] A. Luque, G. Sala, J.C. Arboiro, Sol. Energy Mater. Sol. Cells 51 (1998) 269.
[5] J. Nilsson, H. Håkansson, B. Karlsson, Monitoring of electrical and thermal performance of PVCPC hybrids, in: Proceedings of ISES 2003 Solar World Congress, Göteborg, Sweden, June 2003.
[6] R. Leutz, H. Ries, Micro-structured light guides overcoming the two-dimensional concentration limit, Appl. Optics 44 (32) (2005) 6885.
[7] J. Bortz, N. Shatz, R. Winston, Performance limitations of translationally symmetric nonimaging devices, nonimaging optics: maximum efficiency light transfer VI, in: Roland Winston (Ed.), Proceedings of SPIE, vol. 4446, 2001.
[8] M. Rönnelid, B. Perers, B. Karlsson, Optical properties of nonimaging concentrators with corrugated reflectors, in: C.M. Lampert (Ed.), Optical Materials Technology for Energy Efficiency and Solar Energy Conversion XIII, Volker Wittwer, Claes G. Granquist, 1994, pp. 595–602 (Proceedings of the SPIE 2255).
[9] M. Rönnelid, B. Karlsson, Appl. Opt. 37 (22) (1998) 5222.
[10] R. Leutz, H. Ries, Squaring the circle—the use of microstructures for converting and homogenizing beam cross-sections, in: Proceedings of SPIE International Symposium on Optical Science and Technology; Design of Efficient Illumination Systems, vol. 5186, San Diego, CA, August 2003.
[11] ZEMAX version November 1, 2004, ZEMAX Development Corporation, San Diego, CA, USA.
[12] M. Brogren, P. Nostell, B. Karlsson, Sol. Energy 69 (Suppl.) (2000) 173.

Article V

A NEW SIMULATION BASED EVALUATION METHOD FOR PHOTOVOLTAIC CONCENTRATORS

Johan Nilsson
Division of Energy and Building Design, Lund University,
Box 118
221 00 Lund, Sweden
johan.nilsson@ebd.lth.se

ABSTRACT
The electrical output of low concentration systems with standard pv cells is heavily impaired by non uniform irradiation distribution on the cells. In order to design new concentrators that improve the system efficiency by homogenizing the light, a new method of evaluation has been developed. It is based on simulations, and generates an estimated annual output. The method consists of three steps, optical simulations of the concentrator, electrical simulations of the cells in the concentrator at certain solar angles of incidence, and system simulations of the annual output. As an example, the method is used in the design of a stationary roof concentrator.

1. INTRODUCTION

A promising approach to concentrating photovoltaics is to design concentrators for standard pv cells. A well designed concentrator with a concentration ratio of 3 should in theory be able to halve the cost of the produced electricity compared to standard photovoltaic panels. However, one of the necessary requirements for using standard cells is that the irradiation distribution on the cells has to be almost uniform, and this is not the case for parabolic reflectors that are the most common choice for this type of concentrator. Instead, the reflector creates a highly non uniform irradiation distribution with peaks of 25-30 times the solar beam [1]. At locations on the cell where the irradiance is high, this results in high local currents, currents that can be 25-30 times higher than the currents at homogenous illumination conditions. Due to the high series resistance of the standard cell, this causes large losses.

We have presented a solution to the problem of non uniform irradiation from parabolic reflectors by introducing micro-structured reflectors [2]. These reflectors increase the concentration ratio and smoothens the light distribution on the cells. However, it was found that in order to utilize the technique at its maximum potential, it is necessary to redesign the geometry of the concentrator trough. The trough used in the study was an asymmetrically truncated translational symmetric CPC with a distinct interval of acceptance [3]. When the micro-structured reflectors were used, this interval became wider and less pronounced.

The distinct interval of acceptance for the ideal two dimensional CPC makes it easy to design a system for a specific climate and location [4]. The problem when designing non ideal three dimensional concentrators, such as a translational symmetric CPC with micro-structures, is that the optical efficiency will depend on the angle of incidence in three dimensions instead of two. This makes it difficult to use analytical design methods. Another problem is that it is difficult to estimate the power losses due to non uniform irradiation distribution on the standard cells. Since the main reason for introducing the micro-structured reflector is to obtain a more homogenous illumination of the cells, it is imperative to have a measure of cell output as a function of the irradiation distribution on the cells. Furthermore, it is important to evaluate the new design for a full year since the main objective of the design is to maximize the annually generated electricity.

To solve the problem of the non-trivial optimization, a method for simulating the system in the design process has been developed to enable optimizations for a specific climate. The method consists of three steps, ray tracing of the optical properties of the proposed design, electrical simulations of the solar cell output at different irradiation distributions, and finally, system simulations to estimate the annual output for the specific site.

2. METHOD

The three steps of the method are shown as a flow chart in Figure 1.

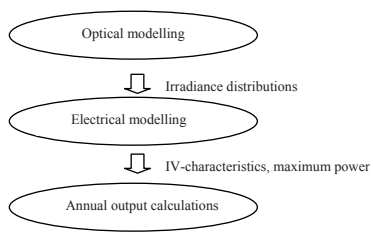

Figure 1 Flow chart showing the three steps of the proposed method.

As the figure shows, the first step was to perform optical simulations. The objective was to simulate the irradiation distribution on the cells for all incidence angles. In the second step, electrical simulations of the solar cell output were performed. Based on each light distribution simulated in the previous step, the IV-characteristics of the cell were calculated using a detailed numerical model that accounts for the light distribution on the cell. In the last step, the maximum power point for each IV-characteristic (and thus for each angle of incidence) was calculated and used to calculate the system efficiency for each angle of incidence. The resulting matrix of efficiencies was used together with climate data for the specific site to obtain an annual estimate of the electrical output.

2.1 Optical modelling

The optical efficiency of all realizable concentrators is depending on the angle of incidence. The irradiance and its distribution on the cells will be different for all angles of incidence. In order to perform annual system simulations, and to make it possible to simulate different locations, it is necessary to ray trace the system for all possible angles of incidence.

In this method, the light distribution on the cells at an incoming irradiation of 1000 W/m^2 normal to the beam was simulated for azimuth angles from 0º to 90º and solar altitudes from 0º to 90º in steps of 5º. The software used for the simulations was ZEMAX, a commercial ray tracing package [5]. The sun was modelled as a source of parallel light with an angular spread of 0.27º [6], and the incidence angle dependence and reflectance of the reflector material was specified. The angular dependence of the absorptance of the solar cells was also taken into account. The number of traced rays was set depending on the desired accuracy of the light distribution, and on the physical size of the system.

2.2 Electrical modelling

The total irradiance and the distribution of light on the solar cell both have a large impact on the output. Standard pv cells are designed for an irradiance of 1 sun, but function well up to 3 or 4 suns if the irradiation is uniform over the cell. This means that if the irradiance on parts of the cell is greater than 3-4 suns, it will result in undesirable losses. Since one of the most important aims for a new design was to create a more uniform irradiation distribution on the cells, it was important to study how the distribution affected the power output. This was done by detailed modelling of the electrical characteristics of the cell.

The model used was originally developed by Foss [7] and was modified to take into account non uniform irradiation on the cell. The model can be seen in Fig. 2.

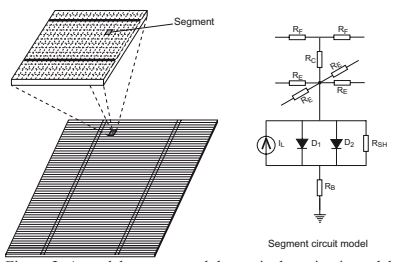

Figure 2 A model segment and the equivalent circuit model of a solar cell used in the simulations.

The cell was divided into many small segments, which can be seen in the top left part of the picture where the space between two fingers is divided into numerous segments.

Each segment was modelled with the segment circuit model shown in Fig. 2. Each segment consisted of a 2-diode model of the cell, which was connected to the back of the cell through the base resistance R_B. R_B represented the bulk resistivity. The segment was connected to adjacent segments through R_E. Each segment was connected to 2-4 adjacent segments depending on where the segment was located. The segments closest to the fingers were connected to the finger though R_C and each part of the finger was modelled with R_F. The light distribution was incorporated into the model by modelling I_L as a function of the irradiance on the segment. The cell parameters for the two diode model were obtained using IVFit [8], a program specifically designed to extract solar cell parameters from current-voltage measurements for a solar cell at standard test conditions. The other parameters were taken from literature [7,9,10].

The current-voltage characteristics for the complete circuit, i.e. the whole cell, were simulated using SPICE [11]. SPICE is a commonly used numerical tool for basic circuit analysis. One simulation was performed for each light distribution generated in the previous step which resulted in 361 simulations. A C++ program was written to generate the SPICE input file using the simulated irradiation distribution and the cell parameters as input. One of the benefits of using ZEMAX for the ray tracing simulations is that it can run scripts. Once the light distributions were simulated, the C++ program was called by the script and the equivalent circuit model resulting from the light distribution was generated automatically.

Figure 3 shows a comparison between measured data and data simulated from the light distribution of the measured case. The reason for the very low fill factor in the figure is that the irradiation distribution measured for this case was highly non uniform, with a peak concentration of 36X.

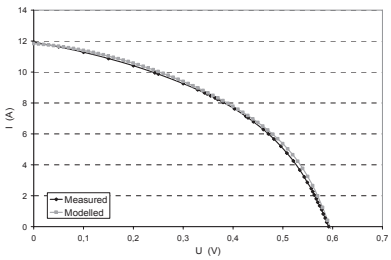

Figure 3 Comparison between measurements and electrical simulations under highly non uniform irradiation

As the figure shows, the simulation agrees well with the measured data at a light distribution that results in a low fill factor. Considering that the model parameters were obtained from a reference measurement of uniform 1 sun illumination of the cells, the figure demonstrates that the model performs well for cases of highly non uniform irradiation distribution and low fill factors and not only for light distributions and currents close to the reference case.

2.3 System modelling of the annual output

The annual electrical output was simulated using climate data for a specific site consisting of hourly diffuse and direct irradiation on the system aperture. The climate data was taken from a yearly Meteonorm[12] simulation of the specific site, but can also be taken from measurements.

By studying the annual output, it was possible to optimize the annual electricity production of the different systems.

The electric energy generated by the direct and diffuse irradiation was calculated separately. The total annual electrical output was calculated as the sum of the electrical output generated by direct irradiation and the annual output generated by diffuse irradiation.

The annual direct irradiation on the system aperture was separated into a matrix in angular space where each element was represented by the solar azimuth angle and solar altitude. In order to increase the angular resolution of the matrix, each hourly value was divided into smaller intervals of equal irradiation. For each of these intervals, the solar altitude and solar azimuth was calculated in the middle of the interval and the irradiation component was added to the corresponding matrix element. The full matrix thus described the annual direct irradiation as an inhomogeneous light source in angular space.

The efficiency for direct irradiance at each angle of incidence, $\eta_{direct}(\alpha,\gamma)$, was derived from the maximum power point, P_{max}, of each IV-characteristic from the electrical simulations. In the expression for the efficiency, α represented the solar zenith angle and γ represented the solar azimuth angle. The efficiency matrix element was calculated according to Eq. 1.

$$\eta_{direct}(\alpha,\gamma)=\frac{P_{\max}(\alpha,\gamma)}{1000\cdot\cos(\theta_i)\cdot A_{cell}} \qquad \text{Eq. 1}$$

A_{cell} was the surface area of the cell, and the maximum power was divided by $1000*\cos(\theta_i)$, which was the irradiance on the plane of the aperture since the ray tracing simulations were performed at a beam irradiance of 1000 W/m^2. θ_i was the angle of incidence on the aperture. The efficiency for direct irradiation was depending on both the optical efficiency and the electrical efficiency since it was derived from the electrical simulations that were based on the results of the optical simulations.

The total annual electrical contribution from the direct irradiation was calculated by multiplying each element of the annual direct irradiation matrix with the corresponding direct efficiency element.

The diffuse part of the annual irradiation was treated separately. The diffuse sky was treated as an annual isotropic light source, i.e. the different parts of the sky were assumed to be equally bright, or lambertian. The system efficiency for diffuse radiation, $\eta_{diffuse}$, was calculated according to Eq. 2, using the optical efficiency, η_{opt}.

$$\eta_{diffuse}(\alpha,\gamma)=\eta_{electric}\frac{\sum_{\alpha=0}^{\alpha=90}\sum_{\gamma=-180}^{\gamma=180}\eta_{opt}(\alpha,\gamma)\cdot\cos(\theta_i)\cdot\cos(\alpha)}{\sum_{\alpha=0}^{\alpha=90}\sum_{\gamma=-180}^{\gamma=180}\cos(\theta_i)\cdot\cos(\alpha)} \qquad \text{Eq. 2}$$

The diffuse efficiency was derived from the optical simulations, i.e. it does not contain the electrical losses in the cell due to different illumination conditions. To get system efficiency instead of optical efficiency, the expression was multiplied with the electrical efficiency at standard test conditions, $\eta_{electrical}$. The angle θ_i represented the angle of incidence on the aperture of the concentrator, The $\cos(\theta_i)$ factor accounted for the view factor and $\cos(\alpha)$ accounted for the fact that not all radiating elements were of the same size.

The annual electrical contribution from diffuse irradiation was calculated by multiplying the total annual diffuse irradiation on the system aperture with the efficiency for diffuse irradiation.

It is possible to derive the diffuse efficiency either from the optical efficiency for direct irradiation, η_{opt}, or from the system efficiency for direct irradiation, η_{direct}. On almost clear days, with a significant fraction of beam irradiance, the diffuse efficiency is overestimated if it is derived from the optical efficiency since the cell efficiency will be determined by the uniformity of the direct irradiation. On the other hand, it will be a very good estimate on days where the sky is isotropic and has a low fraction of direct irradiance. This method was developed mostly to be used for northern latitudes such as Sweden. Most of the diffuse irradiation at these latitudes is from days with an isotropic sky, only a small fraction can be collected at almost clear days and the optical efficiency was therefore chosen as the optimal variable for deriving the diffuse efficiency. If the method is to be used in climates where a larger fraction of the annual diffuse irradiation is incident on days with significant direct irradiation, the best choice might be to derive the efficiency from the system efficiency for direct irradiation. In this case, $\eta_{electric}$ has to be removed from the equation since it is already represented in η_{direct}.

Both the diffuse and direct efficiency was in this method expressed per cell surface area which means that the method compares electricity generation for equal amounts of solar cells and not systems of equal aperture area. Since the cost of the cells is considerably higher than the cost of the reflectors, a comparison per cell area is the best option for comparing different systems. If generation per aperture area was compared, the cost of the cells and reflectors would become a more important part of the comparison.

3. APPLICATION OF THE METHOD

In order to demonstrate the method, it was applied to an asymmetrically truncated CPC for roof integration. Because of the parabolic shape of the mirrors, it is an ideal concentrator, i.e. it is designed to accept all incoming irradiation with a solar altitude of more than 20º and less than 65º in the meridian plane. The geometry is shown in Figure 4.

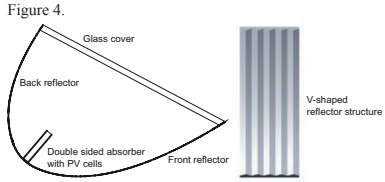

Figure 4 The asymmetrically truncated CPC with a concentration ratio of 2.50 (left). V-shaped micro-structured reflector used to homogenize the light distribution (right).

Previous measurements on this system have shown large losses due to the non uniform irradiation distribution on the cells. Therefore, a similar system with a micro-structured reflector was simulated to investigate if it could be expected to improve the system performance. The micro-structured reflector is shown to the right in Fig. 4.

The pv cells used in the study were 12.5x12.5 cm standard monocrystalline Silicon cells with a fill factor of 0.74, an efficiency of 15%, and a maximum power of 2.3W at reference conditions. The electrical model parameters derived for this cell are shown in Table 1.

TABLE 1: CELL CHARACTERISTICS USED IN THE ELECTRICAL SIMULATIONS

Model parameter	Value
J_{D1}	1.79E-12 A/cm^2
n1	1
J_{D2}	7.14E-8 A/cm^2
n2	2
R_{SH}	11.72 Ω
ρ_B	1.5E-4 Ωcm^2
ρ_E	38 Ω/□
ρ_C	10E-3 Ωcm^2
ρ_F	0.6 Ω/cm

3.1 Optical simulations

As the first step, ray tracing simulations were performed for both systems to create the matrices of light distributions. The simulated reflector material was anodized aluminium with a specular reflectance of 85 %. Figure 5 shows the simulated light distributions on the cells facing the front reflector for both systems at a solar altitude of 60º in the meridian plane. This particular angle of incidence was chosen since the light is incident normal to the system aperture.

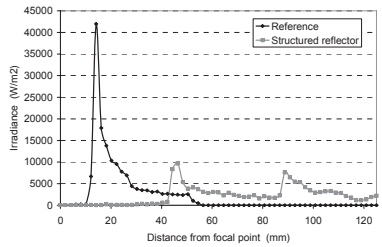

Figure 5 Simulated light distributions for the reference and the structured system at a solar altitude of 60º and a solar azimuth of 0º.

It is clear from the figure that the structured reflector design creates a far more uniform distribution at this angle of incidence. The light distribution was integrated to obtain a measure of the total collected irradiation and it was found that compared to the reference, 10% less irradiation was collected by the cells in the new structured design for this angle of incidence. This agrees well with the previous study on the use of structured reflectors [2]. The reason for the higher optical losses is that the structures will cause some of the light to be redirected above the focal point and out of the system.

3.2 Electrical simulations

The next step was to simulate the current-voltage characteristics for one solar cell using the simulated light distributions. Shown in Figure 6 are the current-voltage characteristics for the two systems as a result of the light distributions from Figure 5.

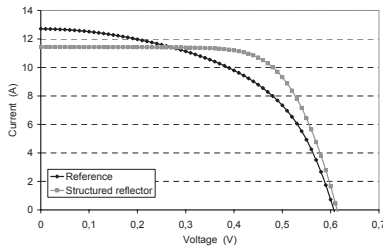

Figure 6 IV-characteristics for azimuth angle 0º, solar altitude 60º

The figure illustrates both the benefits and the problems of the micro-structured reflectors. The short circuit current, which is a measure of the total collected irradiation, was 11% lower for the new design which indicates that some of the light is directed outside the cells. However, the maximum power was found to be 22 % higher for the new design due to the higher fill factor resulting from the more uniform light distribution.

3.3 System simulations

The last step was to simulate the annual output for a specific site. Figure 7 shows a plot of the efficiency for direct irradiation as a function of the solar angles for both systems. The lines in the plot connect solar angles of equal efficiency.

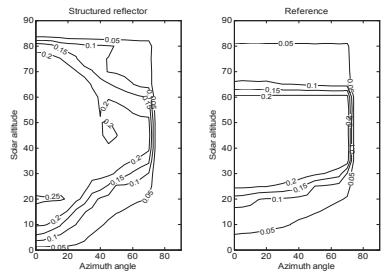

Figure 7 Contour plot of the efficiency for direct irradiation for the structured reflector and for the reference. The contour lines connect angles with equal efficiency.

The figure shows the characteristics of the structured reflector. The efficiency is higher, and the interval of acceptance is wider, close to the meridian plane. At large azimuth angles, the efficiency is higher for the smooth reference.

The efficiency for diffuse irradiation calculated using Eq. 2 was 4.6% for the smooth reference and 4.9% for the structured system.

The evaluation of the two systems was made for Lund, Sweden (Lat. 55.72N, Long. -13.22). The result of the comparison between the two systems can be seen in Table 2.

TABLE 2: ANNUAL ELECTRICAL OUTPUT PER M² SOLAR CELLS

	Reference	Structured reflector
Annual electrical output	163kWh	172 kWh

As the table shows, the structured concentrator was estimated to generate 6% more electricity over the year.

4. DISCUSSION

We know that a more uniform irradiation distribution on the cells will increase the electrical output. Despite this, it was difficult to show any significant output improvements in a previous study on the effect of using structured reflectors for this particular CPC concentrator [2]. With the model presented here it was possible to show a 6% increase in electrical output when structured reflectors were used. The output increase was relatively small, but as was shown in the previous study, new geometrical designs have to be developed to make optimum use of the new technique.

The results from the integration of the light distribution in sect. 3.1 agree well with the differences in short circuit current in sect. 3.2. For both cases, the cells in the structured trough received approximately 10 % less irradiation. Additionally, the two IV-characteristics shown in Fig. 3 indicate only marginal differences between measurements and simulations at highly non uniform irradiation conditions. Both factors show that the electrical output as a function of the irradiation distribution was modelled with good accuracy.

The new model is now being used in the design of two new concentrators. One will be a stand-alone concentrator for flat roofs. It will consist of two reflectors and a wedge absorber. The other new concentrator will be a wall integrated system with one reflector above the cells.

5. REFERENCES

1. J. Nilsson, H. Håkansson, B. Karlsson, “Electrical and thermal characterization of a PV-CPC hybrid”, Solar Energy, 81(7) 2001, pp. 917-928
2. J. Nilsson, R. Leutz, B. Karlsson, “Micro-structured reflector surfaces for a stationary asymmetric parabolic solar concentrator”, Solar Energy Materials and Solar Cells, 91(6) 2007, pp. 525-533
3. M. Adsten, A. Helgesson, B. Karlsson, ”Evaluation of CPC-collector designs for stand-alone roof- or wall installation”, Solar Energy, 79(6) 2005, pp. 638-647
4. M. Rönnelid, B. Karlsson, “Irradiation distribution diagrams and their use for estimating collectable energy” Solar Energy, 61(3) 1997, pp. 191-201
5. ZEMAX, Optical Design Program. User’s Guide, February 3, 2005
6. J.A. Duffie, W.A. Beckman, “Solar Engineering of Thermal Processes”, Wiley Interscience, New York, 1980, p. 288
7. S. E. Foss, B. R. Olaisen, E. S. Marstein, A. Holt, ”A new 2.5D distributed SPICE model of solar cells”, *EUPVSEC 2006, September 4-8 2006*, Dresden, Germany
8. A.R Burgers., J.A. Eikelboom, A. Schonecker, W.C. Sinke, “Improved treatment of the strongly varying slope in fitting solar cell I-V curves”, Photovoltaic Specialists Conference 1996, Conference Record of the Twenty Fifth IEEE
9. D.K. Schroder, D.L. Meier, “Solar cell contact resistance – A review“, IEEE transactions on Electron Devices 31, 637-647 (1984)
10. E. Franklin, J. Coventry, “Effects of highly non-uniform illumination distribution on electrical performance of solar cells”, Proceedings of ANZSES Solar Conference 2002, Newcastle, Australia
11. http://bwrc.eecs.berkeley.edu/Classes/IcBook/SPICE/
12. METEONORM Version 5.1 (November 2004)

Article VI

DESIGN OF STATIONARY PHOTOVOLTAIC CONCENTRATORS FOR HOMOGENIZED IRRADIANCE DISTRIBUTION

Johan Nilsson, Björn Karlsson
Div. of Energy and Building Design, Lund University
P.O. Box 118, Lund, SE-22100, Sweden
Phone: +46 46 2227606, Fax: +46 46 2224719, E-mail: johan.nilsson@ebd.lth.se

ABSTRACT: The light distribution in stationary concentrators is non uniform which results in relatively high losses when standard photovoltaic cells are used. By using structured reflectors, it is possible to create a more uniform distribution on the cells. We have developed two new stationary photovoltaic concentrators with structured reflectors, one intended for wall integration and one intended for roof integration. Both systems have been optimized using a newly developed evaluation method based on simulations of the optical and electrical characteristics of the system. The new wall system is estimated to improve electricity generation on facades by 10 % comparing to the reference system with smooth reflectors. For the roof system, the estimates show that 20 % more electricity will be generated by this system compared to a reference roof system.

1 INTRODUCTION

Stationary concentrators designed for standard photovoltaic cells are a promising alternative for reducing the cost of solar electricity. However, large scale introduction of the systems have yet to be achieved. One of the reasons for this is that the systems are unable to perform as well as could be expected. Theoretically, the electrical output of a system with a concentration ratio of 3 should at least be 2-2.5 times the output of a system without reflectors. For the current systems existing today, this is not reached.

The main reason why stationary compound parabolic concentrators (CPCs) with standard solar cells do not generate at their theoretical potential is the highly non uniform irradiance distribution on the solar cells. Standard cells are designed for homogenous 1 sun irradiance. As long as the irradiance is uniform, the cells should probably be able to withstand 2-4 times the solar irradiance. However, the highly non uniform irradiance distribution that is a characteristic of the parabolic concentrator is not compatible with the cells. In previous measurements, we have shown that the peak irradiance in existing CPC systems reach 25-30 times the solar beam [1]. At locations on the cell where the irradiance is high, this results in high local currents that can be 25-30 times higher than the currents at homogenous illumination conditions. Due to the high series resistance of the standard cell, this causes large losses. Since the CPC is the most common choice for stationary low concentrating systems, it is important to address the problem of non uniform irradiance distribution on the cells if we want to achieve the goals of improved performance. If we want to use thin-film solar cells which have even higher series resistance, it is imperative that the irradiance distribution becomes more uniform.

One possible solution to the problem of non uniform irradiance in CPCs is to use micro-structured reflectors. Previous studies have shown that structured reflectors increase the concentration ratio of the system and homogenize the irradiance on the cells [2-4].

We have previously presented a simulation study where micro-structured reflectors were used in an existing asymmetrically truncated CPC [5]. The conclusion of this study was that a much more uniform irradiance distribution was achieved, but there was no significant increase in total irradiation collection on the cells. In the study, we were unable to estimate the gains of the more uniform irradiance distribution due to lack of good solar cell models taking the non uniform irradiance distribution into account. This partly explains why the results of the simulations did not show improved performance. Furthermore, it was also found that the geometry which was designed for smooth reflectors was not ideal for structured reflectors.

The findings of the previous study have lead to the development of a new three-step method where the influence of the irradiance distribution on the solar cell is taken into account [6]. The method is completely based on simulations and yields an annual electrical output estimate. Due to the high level of detail in each of the three steps, the new method can be expected to yield highly accurate output estimates.

The aim of the current study is to develop two new stationary concentrators that show significantly improved performance by using the new evaluation method. Both will be stationary systems for standard cells, one is intended for installation on flat roofs, and one for wall integration.

2 STRUCTURED REFLECTORS

The main reason for introducing structured reflectors is to obtain a more uniform irradiance distribution on the cells. In the following section, the reasons for using structured reflectors are given.

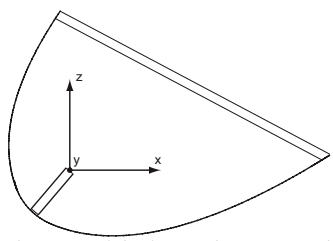

Figure 1. Translational symmetric concentrator with local coordinate system

Consider the local coordinate system in Figure 1 where k_x, k_y, and k_z are the directional components of the incoming light along each axis. In a translational

symmetric system such as in Figure 1, the two-dimensional étendues in the symmetry planes (at x=0 and y=0), are independently conserved [4]. This yields:

$$\Delta x \cdot \Delta k_x = \boldsymbol{constant} \qquad \text{Eq. 1}$$
$$\Delta y \cdot \Delta k_y = \boldsymbol{constant}$$

This limits the concentration ratio to $1/\sin(\theta_{max})$, where θ_{max} is the half-angle of acceptance. If the translational symmetry is broken, the system becomes a 3D concentrator where k_x and k_y can be mixed. The conservation of étendue then states:

$$\Delta x \cdot \Delta k_x \cdot \Delta y \cdot \Delta k_y = \boldsymbol{constant} \qquad \text{Eq. 2}$$

The system then becomes a 3D concentrator for which the fundamental limit of concentration is $1/\sin^2(\theta_{max})$.

By using a structured reflector in the translational symmetric system, the symmetry is in fact broken, and this makes it possible to increase the concentration ratio beyond the limit of 2D concentrators [7]. Another desirable effect obtained by the mixing of the directional components k_x and k_y is that the light distribution becomes more uniform on the cells. The size of the structures is of little importance as long as they are small in comparison to the size of the concentrator. Reasonable sizes are around 5 mm to 20 mm for a full size concentrator of 2-5 meters.

3 METHOD

A three-step simulation method was developed in order to find the most suitable design. The method is illustrated in Figure 2.

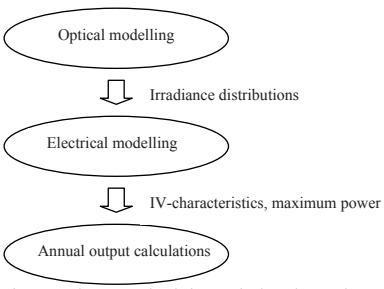

Figure 2. Three-step simulation method used to evaluate the new prototypes

The first step of the method was to simulate the irradiance distribution on the cells for all incidence angles. This was done using a commercial ray tracing software. In the second step, electrical simulations of the solar cell output were performed using a newly developed solar cell model. Based on each light distribution simulated in the previous step, the IV-characteristics of the cell were simulated using a detailed numerical model that accounted for the light distribution on the cell. In the last step, the maximum power point for each IV-characteristic (and thus for each angle of incidence) was used to calculate the system efficiency for each angle of incidence. The resulting angular dependence of the efficiency was given in a matrix in angular space which was used to obtain an estimate of the annual electrical output at a specific site.

3.1 Optical simulations

The irradiance distribution on the solar cells was simulated for a large number of incidence angles. Since the optical efficiency of all realizable concentrators is depending on the angle of incidence, both the irradiance and its distribution on the cells will change. In order to perform annual system simulations, it was necessary to ray trace the system for all possible angles of incidence. To do this, the light distribution on the cells at an incoming irradiance of 1000 W/m^2 normal to the beam was simulated for azimuth angles from 0º to 90º and zenith angles from 0º to 90º in steps of 5º. The software used for the simulations was ZEMAX, a commercial ray tracing package [8]. The sun was modelled as a source with an angular spread of 0.27º [9], and the incidence angle dependence and reflectance of the reflector material was specified. The angular dependent absorptance of the solar cells was also taken into account. The number of traced rays was set depending on the desired accuracy of the light distribution, and on the physical size of the system to be designed.

3.2 Electrical simulations

A new numerical model of a solar cell was used to simulate the current-voltage characteristics at different illumination conditions. The model used was a distributed circuit model originally developed by Foss [10] which was modified to take into account non uniform irradiance distribution on the cell [6]. The model divides the cell into many small elements. Each element consists of a two diode circuit model, where the diode circuit is connected to the back of the cell, adjacent elements, and in applicable cases to the fingers or bus-bars. A model element is shown in Figure 3.

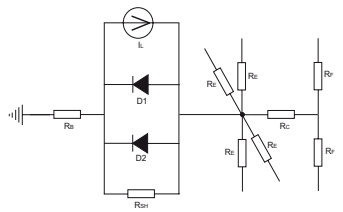

Figure 3. Circuit used to model one cell element.

The simulated light distribution on the cell was used to determine the light generated current of the current generator in each individual model element.

To identify the model parameters, a tool was used to extract this information from a reference measurement on the particular solar cell being used at reference conditions, i.e. 1000 W/m^2 homogenous irradiance on the cell at 20ºC. The tool used was IVFit [11]. The model parameters that could not be obtained from IVFit were taken from literature [10,12-13].

The full circuit with all elements connected was simulated in a numerical circuit simulation software to obtain the current voltage characteristics. The software

used was SPICE [14]. To be able to model the concentrating system at all angles of incidence, one simulation was run for each light distribution from the optical simulations which resulted in 361 simulations of the current-voltage characteristics for each concentrator.

3.3 Annual output simulations

The annual electrical output was calculated using climate data for Lund, Sweden (Lat. 55.72N, Long. -13.22) consisting of hourly diffuse and direct irradiation on the trough aperture simulated from Meteonorm [15]. By studying the estimated annual output, it was possible to compare different systems at conditions close to reality.

The electric energy generated by the direct and diffuse irradiation was calculated separately.

The annual direct irradiation on the trough aperture was separated into a matrix in angular space where each element was represented by the solar azimuth angle and solar altitude. In order to increase the angular resolution of the matrix, each hourly value was divided into smaller time periods of equal irradiation. For each of these intervals, the solar altitude and solar azimuth was calculated in the middle of the interval and the irradiation component was added to the corresponding matrix element. This yielded a matrix of efficiencies for direct irradiance as a function of the solar angles. This matrix describes the annual direct irradiation as an inhomogeneous light source in angular space.

The efficiency for direct irradiance at each angle of incidence, $\eta_{direct}(\alpha,\gamma)$, was derived from the maximum power point, P_{max}, of each IV-characteristic from the electrical simulations, where α represented the solar zenith angle and γ represented the solar azimuth angle. The efficiency matrix element was calculated according to Eq. 3.

$$\eta_{direct}(\alpha,\gamma) = \frac{P_{\max}(\alpha,\gamma)}{1000 \cdot \cos(\theta_i) \cdot A_{cell}} \qquad \text{Eq. 3}$$

A_{cell} was the surface area of the cell, and the maximum power was divided by $1000*\cos(\theta_i)$, which was the irradiance in the plane of the aperture since the optical simulations were performed at a beam irradiance of 1000 W/m^2. θ_i was the angle of incidence on the aperture. Since the efficiency for direct irradiation was calculated from the results of the optical and electrical simulations, it is depending both on the optical efficiency of the reflector system and on the electrical efficiency of the cell. Notable is that the efficiency describes the system efficiency per cell area, which means that it compares electricity generation for equal amounts of solar cells and not systems of equal aperture area.

The total annual electrical contribution from direct irradiation was calculated by multiplying each element of the annual direct irradiation matrix with the corresponding direct efficiency element.

The diffuse part of the annual irradiation was treated separately. The diffuse sky was treated as an annual isotropic light source, i.e. the different parts of the sky were assumed to be equally bright, or lambertian. The efficiencies of the troughs for diffuse radiation were calculated according to Eq. 4, where θ_i is the angle of incidence on the aperture of the trough. The $\cos(\theta_i)$ factor accounts for the view factor and $\cos(\alpha)$ accounts for the fact that not all radiating elements are of the same size. $\eta_{electric}$ is the cell efficiency at standard test conditions, and η_{opt} is the optical efficiency of the system derived from the optical simulations.

$$\eta_{diffuse} = \eta_{electric} \cdot \frac{\sum_{\alpha=0}^{\alpha=90}\sum_{\gamma=-180}^{\gamma=180} \eta_{opt}(\alpha,\gamma)\cdot\cos(\theta_i)\cdot\cos(\alpha)}{\sum_{\alpha=0}^{\alpha=90}\sum_{\gamma=-180}^{\gamma=180} \cos(\theta_i)\cdot\cos(\alpha)} \qquad \text{Eq. 4}$$

The annual electrical contribution was then calculated by multiplying the annual diffuse irradiation on the trough aperture with the efficiency for diffuse irradiation, $\eta_{diffuse}$.

By calculating the efficiency for diffuse irradiation from the optical efficiency instead of from the efficiency for direct radiation, the low fill factor due to non uniform irradiance will not deteriorate the performance. On cloudy days where the diffuse irradiation is dominant, the fill factor of the cells in the concentrator will be equal to the fill factor of a standard pv module. Using the beam efficiency from Eq 3 would in this case underestimate the efficiency. However, on clear days when the diffuse irradiation is only a small fraction superposed on the larger direct non uniform irradiation, the diffuse efficiency will be overestimated when using Eq 4 since the fill factor often is low in this case. For northern latitudes such as for Sweden for which the method was developed, most of the annual diffuse irradiation on a surface arrives on cloudy days, which justifies the choice of using the optical efficiency. For climates where diffuse irradiation on relatively clear days gives the largest contribution to the annual diffuse irradiation, the diffuse efficiency should be derived from the efficiency for direct irradiation, substituting η_{opt} in Eq 4 with η_{direct} from Eq 3, and by removing $\eta_{electric}$.

Adding the two contributions yielded the annual output estimate.

Since the cost of the cells is considerably higher than the cost of the reflectors, a comparison per cell area is the best option for comparing the different systems. If generation per aperture area was compared, the cost of the cells and reflectors would become a more important part of the comparison.

3.4 Reference systems

The aim was to design one system for flat roofs and one system for wall integration. The roof system was based on an asymmetrically truncated CPC designed for northern latitudes [16]. It has been designed to accept all incoming irradiation between 20º and 65º in the meridian plane. The cross section of the system is shown in the left part of Figure 4. As can be seen in the figure, the absorber has cells on both sides.

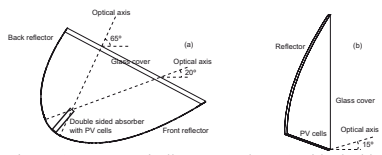

Figure 4. Asymmetrically truncated CPC with double sided absorber designed for northern latitudes, consisting of two parabolas connected by a circular section (left). Reference wall reflector (right).

The wall system was based on a parabolic mirror design where the reflector is located above the cells [17]. This system can be seen in the right part of Figure 4. The wall reflector reflects all the irradiation with an incidence angle in the meridian plane greater than 15º onto the PV cells. The cells are tilted 20º from the horizontal.

The new systems were designed for standard monocrystalline solar cells. The current voltage characteristics of the cell used in the design are shown in Figure 5.

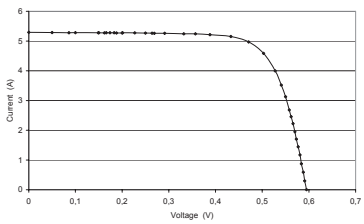

Figure 5. Current voltage characteristics at reference conditions, homogenous 1000 W/m^2 irradiance, for the cell used in the design process.

The cell used has a short circuit current of 5.29 A, open circuit voltage of 0.60 V, and a fill factor of 0.74. Its efficiency was 15 % at standard conditions.

Anodized aluminium, a highly specular reflector material with a specular reflectance of 85% was used for the reflectors of both reference systems as well as for the prototypes.

3.5 Reflector structure

The structure used to break the symmetry was a V-shaped structure with a half angle of 60º. The left part of Figure 6 shows the cross section of the structure. The width of one V was 10 mm as can be seen in the figure.

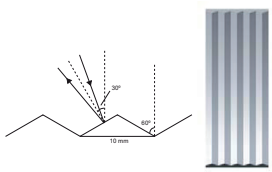

Figure 6. Reflector structure used in the design of the two new concentrators. The V-shape has a half angle of 60º (left). The right part shows a section of the reflector where several Vs can be seen. The Vs extend from the top of the concentrator to the solar cells.

The right part of the figure shows a section of the reflector with several Vs. The Vs are oriented from the cells to the upper and lower edges of the concentrators in order to change the directional component of the light parallel to the axis of symmetry. The left part of the figure shows the mixing of the directional components. Light incident at an angle less than 30º exit at an angle greater than 30º and vice versa. This yields complete mixing of the incident light [4].

4 RESULTS

4.1 New roof system

The main design parameter for the roof system was to change the tilt of the optical axis of the parabolas. The previous study of applying structured reflectors to the asymmetrically truncated CPC showed that the acceptance interval became larger and less distinct. In order to make optimum use of the technique, the tilt of the optical axis of the parabolas of the original design was changed. This yielded a system with wider aperture and thus higher geometrical concentration ratio. The reference system has been designed for a double sided absorber, but the new prototypes were fitted with a wedge absorber to reduce the reflector material used. In the original system shown in the left part of Figure 4, the optical axis if the back reflector was tilted 20º from the horizontal, and the optical axis of the front reflector was tilted 65º from the horizontal. This created a system that accepted all light where the projected angle of incidence in the meridian plane was between 20º and 65º. In the new designs, this interval was made smaller by changing the tilt of the optical axes of the parabolas. When the reference system was developed, it was truncated to reduce the reflector size while maintaining a high aperture area. Comparing to a full CPC, the original truncation would mean a substantial reduction of the aperture when the mirror tilt was increased. For this reason, the size of the reflectors had to be increased slightly.

The new systems were designed for 62.5 x 125 mm cells. The original system was designed for 125 x 125 mm cells but since the system became larger when the optical axis tilt was altered in the new design, the new systems were made for smaller cells in order to reduce the size of the systems. Since the systems are intended for integration into flat roofs, the size is an important parameter. Very large system can be difficult to integrate into small roofs.

Four new designs were evaluated. The tilt of the optical axis of the parabolas and the aperture width of the evaluated systems can be seen in Table 1.

Table 1. Description of the evaluated roof systems.

System	Back parabola axis tilt	Front parabola axis tilt	Aperture width	Cell width	Geometrical concentration ratio	Reflector structure
Reference	20º	65º	626 mm	125 mm	2.50	Smooth
Prototype 1	22.5º	62.5º	333 mm	62.5 mm	2.66	V-structure
Prototype 2	25º	60º	350 mm	62.5 mm	2.80	V-structure
Prototype 3	27.5º	57.5º	368 mm	62.5 mm	2.94	V-structure
Prototype 4	30º	55º	384 mm	62.5 mm	3.07	V-structure

The axis tilt of the parabolas was gradually changed in steps of 2.5º for both parabolas which meant that the centre of the acceptance interval remained unchanged. As the tilt was changed, the geometrical concentration ratio was increased from 2.5 for the reference case to 3.1 for Prototype 4.

4.1.1 Optical simulations

The light distribution on the cells was simulated for all angles of incidence for the five systems. As expected, the light distribution on the cells was more uniform in the new prototypes with structured reflectors. Figure 7 shows the light concentration for both absorbers. The distribution above the x-axis in each figure represents the cells facing the back reflector, and the distribution below the x-axis represents the cells facing the front reflector. The distributions were simulated for an azimuth angle of 15º and a solar altitude of 40º.

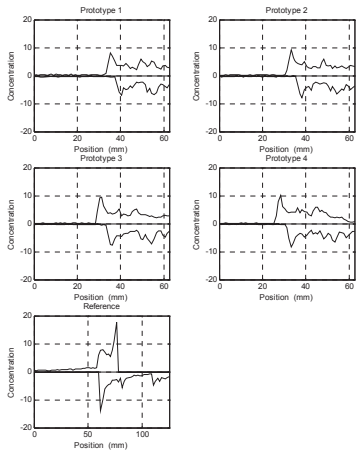

Figure 7. Light concentration on both absorbers for all evaluated systems at an azimuth angle of 15º and a solar altitude of 40º.

As the figure shows, the light distribution is very similar for all four prototypes. This shows that the distribution is dependent mostly on the reflector structure, and only slightly on the tilt angle of the optical axis of the parabolas. It indicates that the difference in light distribution, and therefore the electrical output, between the different prototypes will only be depending on the concentration ratio, and on the amount of light that is lost as reflections outside the absorber due to the change in tilt.

4.1.2 Electrical simulations

The main reason for introducing the structured reflectors was to make the irradiance distribution on the cells more uniform and thereby increase the maximum power output of the cells. Figure 8 shows the current-voltage characteristics of the reference system and of Prototype 2. Since all prototypes generated similar light distributions, the same trends can be seen for all prototypes.

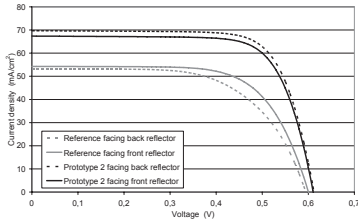

Figure 8. Current-voltage characteristics for a solar cell in Prototype 2 and in the reference system at an azimuth angle of 15º and a solar altitude of 40º.

The figure clearly shows the higher short-circuit current and the improved fill factor for the cells in Prototype 2. For the reference system, the fill factors are 0.62 and 0.67 for the cell facing the back and front reflector respectively. For the prototype system, the corresponding fill factors are 0.74 and 0.73. The current density is also larger for the cell in the prototype system, 67 mA/cm^2 and 70 mA/cm^2 compared to 55 mA/cm^2 for the cells in the reference system.

As a result of the increased current density and fill factor, the maximum power per cm^2 cell area was increased for the prototype system. The maximum power for the reference system was 19.5 mW/cm^2 and 21.9 mW/cm^2 for the cell facing the back reflector and front reflector respectively. For the prototype system, the maximum power was 31.5 mW/cm^2 and 30.2 mW/cm^2 for the same cells. This yielded a 62% power increase for the cells facing the back reflector, and a 38% power increase for the cells facing the front reflector.

4.1.3 Annual output

The main goal of the study was to increase the annual electrical output. Using all the simulated maximum power points from the previous step, the annual output was calculated for all five systems at an equal solar cell surface area of 1 m^2. The annual diffuse irradiation on the system aperture was 583 kWh/m^2, and the direct irradiation on the aperture was 568 kWh/m^2.

Figure 9 shows a contour plot of the calculated efficiency for direct irradiation for Roof prototype 2 and for the reference. As the figure shows, the efficiency of the prototype is higher for almost all angles of incidence, and the interval of acceptance in the meridian plane is wider. This illustrates one of the important characteristics of the structured reflectors, the increased concentration ratio. The efficiency of the reference is only higher at low solar altitudes in combination with large azimuth angles.

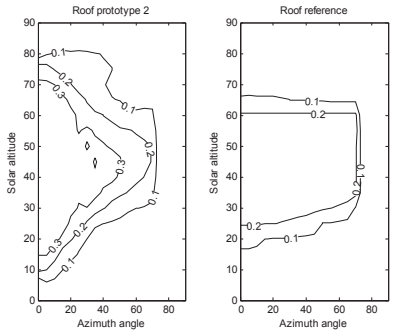

Figure 9. Contour plot of the efficiency for direct irradiation for Roof prototype 2 and for the reference. The contour lines connect angles with equal efficiency.

The results of the annual output simulations can be seen in Table 2.

Table 2. Results of annual output simulations for the 5 systems all consisting of 1 m^2 of solar cells. The last column shows annual electrical output increase compared to the reference

System	Annual output per m^2 cell surface	Annual output increase compared to reference
Reference	162 kWh	1.0
Roof prototype 1	194 kWh	1.19
Roof prototype 2	194 kWh	1.20
Roof prototype 3	193 kWh	1.19
Roof prototype 4	191 kWh	1.17

.

The table shows that all 4 prototype systems produce 18-20% more electricity compared to the reference system. The difference between the different prototypes is not very large, but the optimum system was found to be Prototype 2, which has its optical axes of the reflectors tilted in 25º and 60º. This system, which has an electrical efficiency for diffuse irradiation of 4.4%, will produce 20% more electricity per year compared to the reference.

4.2 New wall system

The tilt of the optical axis of the parabola and the tilt of the absorber were changed for the wall prototype systems based on the wall reflector shown in Figure 4b. The original tilt of the optical axis of the parabola was 15º and the tilt was changed in steps of 5º to a tilt of 50º. The tilt of the absorber was changed along with the axis tilt of the parabola. Additionally, four other cases were included where the absorber angle was changed for some of the first 8 prototypes. The system parameters for all systems are shown in Table 3. The tilt angles are explained in Figure 10.

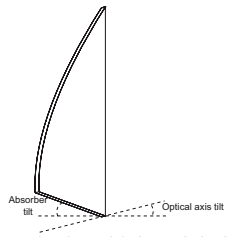

Figure 10. Angles changed during optimization

The wall system was designed for 125 mm wide cells. The roof system was developed for 62.5 mm wide cells due to space constraints. The space constraint for the wall system is that it cannot be too wide if it is to be integrated into a wall, but since the system width is determined by the width of the cell, which is only 125 mms, this does not influence integration.

Table 3 Description of the evaluated wall systems.

System	Optical axis tilt	Absorber tilt	Aperture width	Cell width	Geometrical concentration ratio	Reflector structure
Reference	15º	20º	307 mm	125 mm	2.46	Smooth
Wall prototype 1	15º	20º	303 mm	125 mm	2.42	V-structure
Wall prototype 2	20º	20º	330 mm	125 mm	2.64	V-structure
Wall prototype 3	25º	15º	375 mm	125 mm	3.00	V-structure
Wall prototype 4	30º	10º	434 mm	125 mm	3.47	V-structure
Wall prototype 5	35º	5º	509 mm	125 mm	4.07	V-structure
Wall prototype 6	40º	0º	611 mm	125 mm	4.89	V-structure
Wall prototype 7	45º	-5º	748 mm	125 mm	5.98	V-structure
Wall prototype 8	50º	-10º	935 mm	125 mm	7.48	V-structure
Wall prototype 9	30º	0º	461 mm	125 mm	3.69	V-structure
Wall prototype 10	30º	20º	405 mm	125 mm	3.24	V-structure
Wall prototype 11	45º	0º	721 mm	125 mm	5.77	V-structure
Wall prototype 12	50º	0º	869 mm	125 mm	6.95	V-structure

4.2.1 Optical simulations

Since the same structure was used for the wall reflector as was used for the roof system, the same smoothening of the light distribution was obtained for all the wall prototypes. As expected, the interval of acceptance changed when the axis tilt of the parabolas was changed. This is illustrated in Figure 11 which shows the optical efficiency for angles between 0º and 90º in the meridian plane.

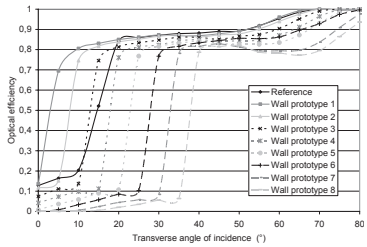

Figure 11. Optical efficiency in the meridian plane calculated as absorbed irradiation divided by incoming irradiation.

As can be seen in the figure, Wall prototype 4 which has its optical axis tilted 30º from the horizontal has approximately the same interval of acceptance as the reference system. All systems with a lower optical axis tilt have a wider interval of acceptance and vice versa.

One finding from the optical simulations was that the higher geometrical concentration ratios of the wall concentrator prototypes compared to the roof system increased the irradiance levels on the cells considerably. For the prototypes with the highest optical axis tilt angles, irradiance levels of 50 times the solar beam were observed and this will certainly affect the fill factor in the electrical simulations.

4.2.2 Electrical simulations

The electrical simulations were performed for all wall prototypes. Figure 12 shows the current-voltage characteristics for the reference and two of the wall prototypes to illustrate the influence of the structured reflectors.

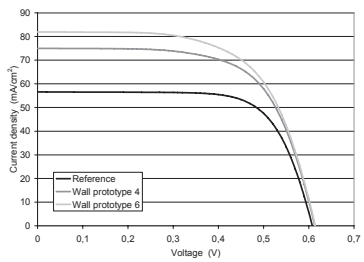

Figure 12. Current-voltage characteristics for three wall systems at an azimuth angle of 15º and a solar altitude of 35º.

The figure shows that the short-circuit current is higher for the two prototypes, but not at all at the extent that could be expected when considering the much higher concentration ratio. The concentration ratio of Wall prototype 4 is 41% higher than the reference, and the concentration ratio of Wall prototype 6 is 99% higher than the reference. However, the maximum power is only 23% higher for Wall prototype 4, and only 30% higher for Wall prototype 6. This illustrates that the optical and electrical losses increase significantly when the tilt of the parabola's optical axis is increased, which was also seen in Figure 11. Also visible in the figure is the decreased fill factor as the tilt, and thereby concentration ratio, increases as was predicted in the optical simulations. For the cells used in the current evaluation, the fill factor is relatively good at concentration ratios such as for the reference, but when the concentration ratio increases even further, the high irradiance levels cause significant fill factor losses.

4.2.3 Annual output

Annual output calculations for Lund, Sweden, were performed for all prototypes using the efficiency factors derived from Eq. 3 and Eq. 4. The annual diffuse irradiation on the aperture was 375 kWh/m^2, and the direct irradiation was 397 kWh/m^2.

A contour plot of the resulting efficiency matrices of Wall prototype 6 and of the reference is shown in Figure 13.

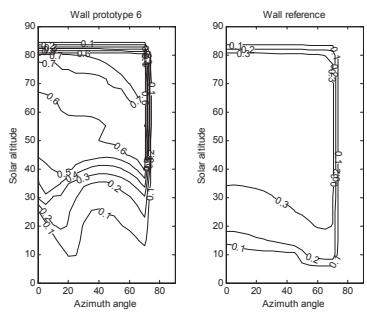

Figure 13. Contour plot of the efficiency for direct irradiation for Wall prototype 6 and for the reference. The contour lines connect angles with equal efficiency.

As the figure shows, the efficiency of the prototype system is considerably higher than the reference when the solar altitude exceeds 30º. These results agree with the results shown in 4.1.3; the concentration ratio is increased when structured reflectors are used.

The estimated annual outputs of the 13 systems are shown in Table 4.

Table 4 Estimated annual output of the different wall systems in Lund, Sweden. The annual output is shown per m^2 cell surface area.

System	Annual output per m^2 cell surface	Annual output compared to reference
Reference	194 kWh	1.00
Wall prototype 1	190 kWh	0.98
Wall prototype 2	192 kWh	0.99
Wall prototype 3	192 kWh	1.01
Wall prototype 4	198 kWh	1.03
Wall prototype 5	199 kWh	1.03
Wall prototype 6	213 kWh	1.10
Wall prototype 7	192 kWh	0.99
Wall prototype 8	186 kWh	0.96
Wall prototype 9	197 kWh	1.02
Wall prototype 10	197 kWh	1.02
Wall prototype 11	194 kWh	1.00
Wall prototype 12	190 kWh	0.98

As can be seen in the table, most prototype systems produce more electricity than the reference concentrator. The highest annual output is for Prototype 6, which has its optical axis tilted 40º from the horizontal, and its absorber horizontal. It has a diffuse efficiency of 5.1% and produces approximately 10 % more electricity over the year.

5 DISCUSSION

5.1 New designs

The result of the optimization for a new roof concentrator was that Prototype 2 gave the highest output increase, 20% more electricity was produced compared to the reference. For this prototype, the optical axis of the front reflector was tilted 60º from the horizontal, and the axis of the back reflector was tilted 25º from the horizontal. The system is shown in Figure 14.

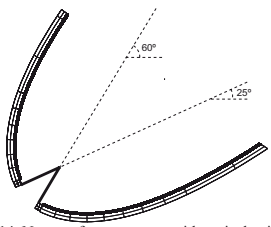

Figure 14. New roof concentrator with optical axis tilts of 25º and 60º.

It has a geometrical concentration ratio 12 % greater than the concentration ratio of the reference, which shows that both the increased concentration ratio and the more homogenous light distribution improve the system output. This was also seen in Figure 8 where the fill factor, current density, and maximum power point all were higher for the prototype system. Due to the smaller cell size of this system compared to the reference, it will be easy to use this system on a flat roof.

Another benefit of the more homogenous light distribution is that the local temperatures on the cell surface will be lower due to the lower local intensities. The reference system was designed to be cooled by water from the back of the absorber, but the lower local temperatures will probably make it possible to run Prototype 2 without cooling. This will make the system less complicated and thus easier to accept for the potential users that are not interested in hot water. If the user is interested in hot water however, this system will produce more heat than the reference because of its higher concentration ratio, but without the local hot spots that deteriorates the electrical performance.

The optimization for a wall concentrator showed that the most suitable wall system was Wall prototype 6. It was estimated to generate 10% more electricity compared to the smooth reference system. This system is shown in Figure 15.

Figure 15. Proposed wall concentrator design, Wall prototype 6. The parabolic reflector has its optical axis tilted 40º from the horizontal and the solar cells are horizontal.

The optical axis of the parabolic mirror is tilted 40º from the horizontal, and it has a horizontal solar cell absorber. The geometrical concentration ratio is almost a factor of two higher than the concentration ratio of the reference, which indicates that the optical and electrical losses are a problem. The main reason why the system performs only 10% better than the reference is that the reference system yields good fill factors even with smooth reflectors. This is due to the tilt of the absorber, it is tilted 35º from the optical axis which means that the light is never completely focused. We therefore conclude that improving the electrical output by 10% was a good result considering the low losses of the reference system.

The simulations used to derive the efficiency for direct irradiation were performed at 1000 W/m^2 direct irradiance. At such high irradiance levels, the electrical losses are at a maximum. For lower irradiance levels, slightly lower losses can be expected. A sensitivity analysis was therefore performed, where the same simulations were run at 500 W/m^2 direct irradiance. The result of these simulations was that the electrical output increased slightly for all systems. The reference systems exhibited the highest performance gains since they had the largest electrical losses due to high irradiance, which made the performance gains of Roof prototype 2 decrease from 20% to 13%. The performance of Wall prototype 6 in relation to the wall reference was unchanged. Since most of the direct irradiance in Lund, Sweden, is collected on days with a high fraction of direct irradiance, much higher than 500 W/m^2, we conclude that modeling the efficiency at 1000 W/m^2 is an acceptable approximation.

5.2 Economical considerations

Whether the increased electrical output decreases the total cost per generated kWh depends on the cost of the cells, reflectors, and cover glazing. Comparing to the smooth references, both the new roof concentrator and new wall concentrator have larger reflector surface area per solar cell surface area. Whether an investment into the proposed concentrators is good or not depends on the ratio between the square meter price of the reflector and the square meter price of the solar cells. We have calculated the ratio at which the systems show equal cost per generated kWh of electricity. The cost of a glazing covering the concentrator aperture was included in the price of the reflector. The ratio for the roof design was 0.13 and the ratio for the wall design was 0.03. At a reflector cost lower than this ratio, the new design will generate electricity at a lower cost compared to the reference concentrator. The new roof concentrator will be economical at a higher reflector cost compared to the new wall concentrator. This is due to the high tilt angle of the optical axis in the wall prototype which makes the reflector large and therefore more expensive.

6 REFERENCES

[1] Nilsson J., Håkansson H., Karlsson B. (2007) *Electrical and thermal characterization of a PV-CPC hybrid.* Solar Energy 81(7), pp. 917-928

[2] Rönnelid M., Perers B., Karlsson B. (1994) *Optical properties of nonimaging concentrators with corrugated reflectors*, in: Proceedings of the SPIE 2255, C.M. Lampert (Ed.), Optical Materials Technology for Energy Efficiency and Solar Energy Conversion XIII, Volker Wittwer, Claes G. Granquist, pp. 595–602

[3] Bortz J., Shatz N., Winston R. (2001) *Performance limitations of translationally symmetric nonimaging devices, nonimaging optics: maximum efficiency light transfer VI.* in: Roland Winston (Ed.), Proceedings of SPIE, vol. 4446

[4] Leutz R., Ries H. (2005) *Micro-structured light guides overcoming the two dimensional concentration limit.* Applied Optics 44, pp. 6885-6889

[5] Nilsson J., Leutz R., Karlsson B. (2007) *Micro-structured reflector surfaces for a stationary asymmetric parabolic solar concentrator.* Solar Energy Materials and Solar Cells 91, pp. 525-533

[6] Nilsson J. (2007) *A novel method for rapid design and evaluation of photovoltaic concentrators.* in: Proceedings of ISES Solar World Congress 2007, September 18-21 2007, Beijing, China

[7] Rönnelid M., Karlsson B. (1998) *Optical Acceptance Function of Modified Compound Parabolic Concentrators with Linear Corrugated Reflectors.* Applied Optics 37, pp. 5222-5226

[8] ZEMAX, Optical Design Program. User's Guide, February 3, 2005

[9] Duffie J.A., Beckman W.A. (1980) *Solar Engineering of Thermal Processes*, Wiley Interscience, New York, p. 288

[10] Foss S.E., Olaisen B.R., Marstein E.S., Holt A. (2006) *A new 2.5D distributed SPICE model of solar cells*. in: Proceedings of EUPVSEC 2006, September 4-8 2006, Dresden, Germany

[11] Burgers A.R., Eikelboom J.A., Schonecker A., Sinke W.C. (1996) *Improved treatment of the strongly varying slope in fitting solar cell I-V curves*. Photovoltaic Specialists Conference 1996, Conference Record of the Twenty Fifth IEEE

[12] Schroder D.K., Meier D. L. (1984) *Solar cell contact resistance-A review.* IEEE transactions on Electron Devices 31, pp. 637-647

[13] Franklin E., Coventry J. (2002) *Effects of highly non-uniform illumination distribution on electrical performance of solar cells*. in: Proceedings of ANZSES Solar Conference 2002, Newcastle, Australia

[14] http://bwrc.eecs.berkeley.edu/Classes/IcBook/SPICE/

[15] METEONORM Version 5.1 (November 2004)

[16] Adsten M., Helgesson A., Karlsson B. (2005) *Evaluation of CPC-collector designs for stand-alone, roof- or wall installation*, Solar Energy 79, pp. 638-647

[17] Fieber A., Gajbert H., Håkansson H., Nilsson J., Rosencrantz T., Karlsson B. (2003) *Design, Building Integration and Performance of a Hybrid Solar Wall Element*. in: Proceedings of ISES Solar World Congress 2003, Gothenburg, Sweden

Article VII

PV PERFORMANCE OF A MULTIFUNCTIONAL PV/T HYBRID SOLAR WINDOW

Andreas Fieber, Johan Nilsson and Björn Karlsson
Div. of Energy and Building Design, Dept. of Construction and Architecture, Lund University
P.O. Box 118, S-221 00, Sweden

ABSTRACT: A multifunctional wall element has been developed, with a PV/T absorber with concentrating reflector screens behind an insulation window. The system provides PV electricity besides hot water and daylight, and the reflector screens provide sunshade for the window. The reflectors have a geometrical concentration factor of 2.45, which decreases the required PV cell area. The hybrid strategy has synergetic effects such as cooling the PV cells for increased performance, and to simultaneously make use of the heat generated in the cell. The climate protected system is a visible element in the exterior and particularly in the interior, and its performance is directly connected to the operation of the reflectors, which can be switched between a closed, concentrating mode or an open, transparent mode.
This paper deals with the monitoring of a prototype of the system, concerning its photovoltaic performance. Out of an estimated annual energy gain via the window of 609 kWh/m^2, approximately 69 kWh is expected to be power from the PV modules.
The results will be used as a guideline for further investigation on the potential of implementing the system, with possible modifications of concentrating geometry or operating strategy, in glazed office façades.
Keywords: Building Integration, Concentrators, Hybrid

1 INTRODUCTION

1.1 Background

Building integrated photovoltaics (BIPV) offer a way to reduce installation cost of PV power by ascribing the PV panels additional functions. However, there is a challenge in meeting energy demands with the supply from the photovoltaic cells. One building application is to integrate PV panels as solar shading devices into the façades of a growing number of glazed office buildings. Hence, the production of PV electricity can simultaneously contribute to reducing the energy demand for cooling the building.

1.2 Concentrating systems in buildings

Using low-concentrating technologies for increasing the cost-efficiency of solar energy systems is a promising strategy, especially if the reflectors can be used for multiple purposes. In this case, the reflectors can be used as flexible solar shading devices. By placing the system behind the exterior glazing of the building, the glazing serves as a climate shell, both for the interior space and for the PV/T system.

2 DESIGN CONCEPT

2.1 Windows in BIPV

By using the window's light transmitting property for integrating solar energy systems, an architectural quality is obtained, since the window has a more penetrable character than i.e. the roof. This has been used mainly in partially transparent PV modules, where the PV cells are mounted between glass panes, with a distance that permits light to enter between the cells. Our alternative design suggests a way to put the cells together with reflectors behind the window glass, in order to protect it from the outer climate.

2.2 Concentrating reflectors

By using a low-concentrating technology, the cell area can be reduced and more efficiently used, leading to lower investment costs. The reflectors can be designed as pivoted sunshades. This also makes it possible to separate the PV modules with intermediate reflector area, thus allowing daylight to enter the interior when the reflectors are not used. Hence, the integration into glazed facades is a promising option for a low-concentrating system.

2.3 Hybrid system

Concentrating irradiation onto the PV cell generates high local temperatures, which demands cooling. Therefore, a PV/T absorber is designed in order to cool the cell for better performance, and simultaneously produce hot water for hygienic demands. This active thermal part of the system also contributes to cooling the interior space behind the window.

2.4 Design of the Solar Window

An initial design from this concept has been developed for application in residential housing, where heating demand is the most important design factor for a temperate climate, from an energy perspective [1]. For this application, the reflectors are made in a sandwich construction with a core of polystyrene and serve as added internal insulation in the closed mode. For the office application, they only serve as reflectors, and therefore they can be made in a thinner and harder material. In consequence with its integration into a glazed façade, it was suggested to make the reflectors out of glass. Anodized aluminum or sheet steel with an aluminized surface are other alternatives. The reflector geometry is a parabolic curve with a geometric concentration factor of 2.45, determined by a tilt of the optical axis of 15°, and a tilt of the fixed PV/T absorber of 20°, see figure 1.

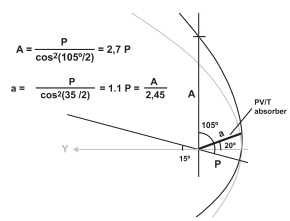

Figure 1: Geometry of the optical design.

The reflectors are pivoted along the upper edge of the absorber, and can hence be switched between a closed, active mode, and an open mode to let the sunlight directly into the building, according to figure 2.

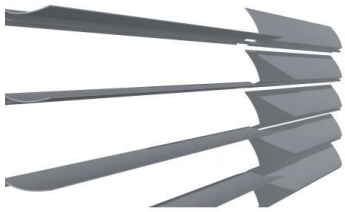

Figure 2: Illustration of the reflectors from the interior with one section in an opened mode (left) and one in a closed mode (right).

3 BUILDING INTEGRATION

3.1 Passive gains and daylight

For the residential house application, a main advantage was the option to gain passive heat from the sun at low irradiance levels. This is not desired in double skin office buildings, where the inner an outer glazing should have different properties. For the outer skin, mainly serving a wind-protection function, a high level of transmittance is required. For the inner layer, a low-E and sun shade coating is suggested to prevent from overheating and glare in the interior. However the transmittance can be relatively high due to the solar-shading effect of the reflectors at high irradiation levels.

Figure 3: Illustration of integration of the Solar Window into the glazed façade of a staircase of an ecological exhibition building in Malmö.

3.2 Aesthetics

The curved shape of the reflector expresses the collecting character of the hybrid solar window, why it deserves an exposure towards the exterior and the interior of the building. The shift between the two modes of operation, in combination with the changing appearance of the mirror-like concave side of the reflectors, offer a wide variety of façade expressions. The convex side of the reflectors facing the interior can be given any suitable surface.

3.3 Operating strategy

The option to operate the Solar Window as a Venetian blind makes it a complex task to predict the output of the active systems. To be able to make predictions, an operating strategy is described, that combines demands on energy performance and user comfort. The strategy must also be applicable for automation. For a residential house, it is suggested that the reflectors are opened during mornings, late afternoons and evenings to allow for daylight, view and passive heating while the house is actively occupied. During the middle of the day, the house is assumed to be mainly empty, why the reflectors can be closed and work optimally. During the nights they can also be closed, to prevent view inside and to insulate from thermal losses through the window. This corresponds fairly well to a suggested automation procedure where the reflectors are closed at irradiance levels below 50 W/m^2 and above 300 W/m^2. At intermediate levels, the reflectors are opened. For the application to an office façade, the control strategy will be determined in order to obtain an optimal combination between PV performance, daylight sufficiency and solar shading to prevent overheating.

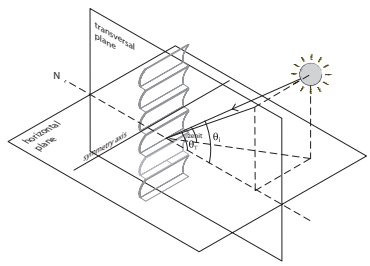

Figure 4: The geometry of the closed Solar Window with the angle of incidence in the transversal plane, θ_T, defined.

4 PHOTOVOLTAIC PROPERTIES

A prototype with an aluminum absorber laminated with polycrystalline silicon photovoltaic cells was built for measurements. The absorber contains water pipes for cooling the PV cells, and the reflector was made of anodized sheet aluminum with a reflectance of 0.87.

The optical efficiency of the reflector in the transversal plane (see figure 4), $R_T(\theta_T)$, is defined as the electricity generation of the system divided by the electricity generation from a system with identical cells mounted on a vertical surface of the same area as

the concentrator system aperture

For a 2-dimensional translational symmetric system such as this, the efficiency is determined solely by the irradiation projected in a plane normal to the symmetry axis, and it is enough to measure the performance at different solar heights when the sun is in this plane, see figure 4. By determining this efficiency at different angles of incidence, we obtain a complete description of the system's characteristics and it makes it possible to perform simulations to evaluate its true performance. The optical efficiency at different angles of incidence θ_T was monitored by measuring the short circuit current, I_{SC}, as a function of θ_T in the transversal plane The optical efficiency was calculated according to Eq. (1):

$$R_T(\theta_T) = \frac{I_{sc} \cdot 1000}{I_{1000} \cdot C_g \cdot G} \qquad \text{[Eq. (1)]}$$

I_{1000} is the short circuit current of the module at 1000W/m^2 at normal incidence, C_g is the geometrical concentration of the concentrator system, and G is the global intensity perpendicular to the glazing.

The geometrical concentration, C_g, was calculated as the aperture area divided by the PV cell area. Figure 5 shows the calculated values for the optical efficiency.

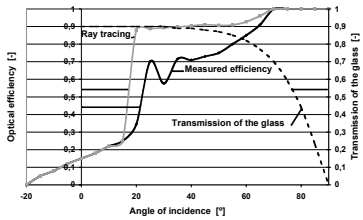

Figure 5: Optical efficiency $\eta(\theta_T)$ at different angles of incidence projected in the plane normal to the axis of symmetry

The measurements were performed during high irradiance and with a diffuse fraction of approximately 10%. The optical system accepts irradiance in all angles above 15º, with the correction for reflection losses. This can be seen from the curve labeled Ray Tracing in Figure 5. At 70º, all of the irradiance hits the cells without reflections, thus yielding an efficiency of 1. It was not possible to measure at incidence angles above 50º due to a construction limitation of the prototype, the efficiencies at these angles were derived from the ray tracing simulations. The large drop in efficiency around an incidence angle of 30º occurs when the strip of concentrated light falls on the conducting finger of the cell. This finger shades the cell considerably when the strip of concentrated light hits it. The measured efficiency evens out around 0.7 while the ray traced efficiency evens out around 0.9. The main reason for this is that the cells have losses due to their relatively large series resistance. The light is concentrated to a narrow strip of high irradiance, and this creates high local currents in the cell. The losses increase with increasing current, and thus results in a lower efficiency.

The optical efficiency was used to estimate the annual output of electricity for this system in Stockholm, Sweden, (lat 59.33). The simulations were performed in MINSUN [2]. Inputs to the simulations were the incidence angle modifier of the system concerning diffuse and beam irradiance. The model used to describe the incidence angle dependence of the optical efficiency as

$$\eta_{opt} = R_T(\theta_T) f_L(\theta_i) \qquad \text{[Eq. (2)]}$$

R_T describes the behaviour of the reflector only and f_L the transmission of the window glass. θ_T is the transversal component of the incident light and θ_i is the angle of incidence relative to the glass normal.

This model has previously been shown to describe the performance of similar systems well [3]. The glass component of the efficiency, $f_L(\theta_i)$, is shown in figure 5.

The calculation of the system efficiency for diffuse irradiance including the glass performance, the view factor of the sky, and the reflectance of the aluminum reflector was estimated to be 70% of the beam efficiency.

The results of the simulation were compared with a reference, which has identical cells of the same area as the prototype cells, and these cells are mounted on a vertical wall. The results show a 93% increase in electrical output compared to the reference. This means that one square meter of window would generate 69 kWh of electricity annually. A reference tilted in 20º from the horizontal would generate considerably more electricity, and comparing to this reference, the prototype produced 43% more electricity annually.

One factor that has to be taken into account if an economical comparison is to be performed is that only 90% of the window area is active. The rest is necessary to allow for the movement of the reflectors and the pipes for the thermal transport.

5 DISCUSSION

5.1 Variations of concentrating geometry

When varying the solar height, one interesting phenomena can be observed. When the sun is close to the acceptance angle of 15º, the strip of concentrated light is narrow and placed at the focal point at the outer end of the absorber. When the solar height is increasing, this strip is quickly moving over the absorber, and gets wider as it travels. This observation shows that the outer part of the absorber receives considerably less irradiation than the inner part. The resistive losses are also highest for current generated on the edges of the cell.

The PV cells are the most expensive part of the system, hence the system price per kWh of electricity produced would drop considerably if the electricity output per PV cell area could be increased. This can be obtained if the cell area can be reduced while accepting most of the irradiance. By using the observations in the previous paragraph, this can be obtained by making two modifications to the existing geometry, i.e. rotating the parabolic reflector and decreasing the size of the absorber. The parabolic reflector in the existing prototype is rotated 15º from the horizontal plane, which gives the system a minimum angle of

acceptance of 15º. By rotating the reflector 5º towards the horizontal, the light would hit the absorber closer to the reflector than what would be the case in the current geometry. At an angle of incidence at 25º the semi focus occurs in the center of the cell, as illustrated in figure 6. This means that the cell can be reduced by a factor of two and still accept all irradiation above 25º, corresponding to the time period between the equinoxes in the south of Sweden. This solution would generate a smaller annual output per glazed area but a higher output per cell area and a lower capital investment per delivered kWh. This geometry also has an advantage that the peaks of the highest intensity on the cell are avoided since the focus fall outside the cell. This however requires a modified technical design, since the reflector curvature will be wider than the cell, according tgo figure 6. Another alternative is to change the optical axis to 25º. This gives a similar concentration factor but also very local intensities on the edge of the cell. These alternatives will be further analyzed by detailed ray tracing.

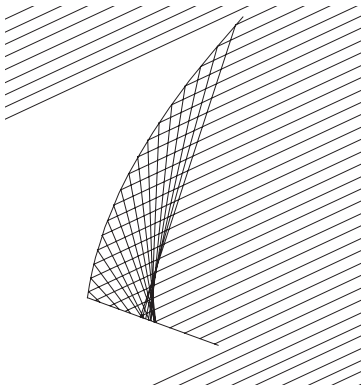

Figure 6: Ray tracing for the reflector with the optical axis at 15° and at a solar altitiude of 25°.

5.2 Operating strategy influence on PV performance

The photovoltaic performance of the Solar Window is dependent upon the chosen operating strategy. The calculated annual performance of 69 kWh applies for the reflectors in a continuously closed mode. The suggested operating strategy however implies that the reflectors should be opened for intensities below 300 W/m^2. Lower irradiation suggests the reflectors being opened. Since the PV/T absorber is in a fixed position, it is exposed to the non-concentrated irradiation even in the opened mode. It can then be regarded as a conventional PV cell mounted in a 20° tilt angle, with a 35 % aperture covering. For estimating the annual output due to the suggested operating strategy, the hours with an irradiation level below 300 W/m^2 towards the south-facing window were identified. The output was then calculated for every hour, as a concentrating system or as a conventional solar panel, depending on the mode. A more accurate annual performance is hence obtained.

In choosing the most suitable control strategy, it is suggested to compare PV performance with the amount of working hours with adequate daylight, and the thermal shading effect by the reflectors, which both should be maximized. Figure 7 below shows the relation between the PV output and the number of daily hours when the reflectors are opened, as functions of the maximum irradiance level for the reflectors being opened. The figure shows that regulating at 300 W/ m^2 annually gives 65 kWh/m^2 of electricity and 3700 hours of daylight, while regulating at 100 W/m^2 gives 75 kWh/m^2 of electricity and 2700 hours of daylight. As mentioned, a continuously closed reflector would deliver 69 kWh/m^2, and no daylight. In finding the optimal breaking point in order to determine a suitable maximal irradiance level, it is suggested to complete the parametric study with the shading effect of the reflectors in various operating. The shading effect when regulating at 300 W/m^2 is according to simulations around 240 kWh/m^2 annually.

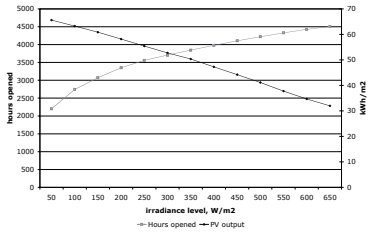

Figure 7: Annual number of hours with an opened reflector and annual output of the PV-module as a function of the irradiance level, where the reflector is closed. The dark hours are amitted.

CONCLUSION

Integrating low-concentrating PV/T systems into glazed façades might be a promising architectural feature, due to its many functions. However, there is a challenge in the complexity in finding an optimal control strategy, and future modifications of the concentrating geometry could be made in order to reduce investment cost.

REFERENCES

[1] Fieber A. et al, 2003, *Design, Construction and Performance of a Multifunctional Solar Wall*, in the proceedings of ISES 2003, Gothenburg

[2] Chant V.G. and Håkansson R., 1985. *The MINSUN simulation and optimisation program. Application and users guide*. IEA SH&C Task VII, Ottawa.

[3] Brogren M. et al. Biaxial model for the incidence angle dependence of the optical efficiency of photovoltaic and solar thermal systems with asymmetric reflectors. Submitted to Solar Energy Journal.

Article VIII

A NEW MODEL AND METHOD FOR DETERMINATION OF THE INCIDENCE ANGLE DEPENDENT G-VALUE OF WINDOWS AND SUNSHADES

Tobias Rosencrantz, Johan Nilsson, Björn Karlsson
Energy and Building Design, Lund University, P.O. Box 118, Lund, SE-221 00, Sweden,
Phone Number +46 46 22 48 51, Fax +46 46 222 47 19, e-mail: tobias.rosencrantz@ebd.lth.se

Abstract – The development of a new method for modelling the incidence angle dependent g-value of asymmetric sunshades is described. The new model is tested by monitoring the g-value of four different sunshades and also by performing ray tracing. For asymmetric components, an overall biaxial incidence angle modifier can be used in order to model the optical efficiency properly. One example of this is a product model, where the incident angle modifier is approximated by factoring it into two components $g(\theta_L,\theta_T)=g_L(\theta_L, 0)g_T(0, \theta_T)$. In the equation above, the index T denotes the transverse and L the longitudinal planes. The longitudinal plane is the plane including the surface normal and a line along the window extension, and the transverse plane is the plane including the surface normal and perpendicular to the longitudinal plane. This means that the model described by equation 1 is strictly correct only when radiation is incident in either of the analysis planes. In order to better characterise the incidence angle dependence of asymmetric components, an alternative method is suggested in this paper. In this model, the influence of the glazing and of the sunshade on the system is studied separately: $g_{sys}(\theta_t,\theta_T) = g_w(\theta_t)g_{sh}(\theta_T)$. In this equation, the factor $g_w(\theta_t)$ basically gives the influence of the glazing and $g_{sh}(\theta_T)$ gives the influence of the sunshade. This equation is, in principle, different from the product above since θ_L is not used. $g_{sh}(\theta_T)$ is obtained as a ratio between $g_{sys}(0,\theta_T)$ and $g_w(0,\theta_T)$: $g_{sh}(\theta_T) = g_{sys}(\theta_L=0,\theta_T)/g_w(\theta_L=0,\theta_T)$. This equation is also valid for plane windows having $g_{sh}(\theta_T) = 1$ resulting in g being a function only of θ, just as expected. In the T plane, the incoming radiation is first transmitted through the sunshade and then transmitted through the glass. Geometric effects and multiple reflections in the sunshade affect the system g-value. In the L direction, the properties of the glass are important. This means that the incidence angle dependence in the L direction of a window with a sunshade device should be similar to the dependence in the overall direction for a plane window.

1. INTRODUCTION

1.1 Background

Solar shading devices are used in buildings to lower the energy consumption for cooling and to increase the indoor comfort by preventing overheating (Bülow-Hübe, 2001). Today there is no standard procedure for the characterisation of exterior sunshades which are not parallel to the glazing surface. The standard ISO 15099 only accounts for internal and interpane solar shadings situated parallel to the panes with intimate thermal-optical contact. We suggest a method for this characterization by applying a new biaxial incidence angle model for both a window and solar shading. This could also lead to improvement in understanding the optimized design and geometry of the solar shading. This could make it easier to choose the right solar shading device for a specific building.

1.2 Measurements of g-value

The g-value or the total solar energy transmittance is defined as the direct transmittance through the glazing system plus the energy absorbed in the system which is transmitted towards the room (ISO 15099). The g-value is thus a measure of the efficiency of the solar shading device.

The g-values of several shading devices on the market have been measured using both outdoor guarded twin-boxes and an indoor solar simulator in the Solar Shading project (Wall & Bülow-Hübe, 2001 & 2003). However, the g-value was for the most part not evaluated against the incidence angle of the solar radiation.

1.3 Objectives

The objectives of this paper are to apply an angle dependence model for external asymmetric solar shadings in combination with a window. Characterization of different external solar shadings and ray tracing simulations are performed in order to verify this new model.

1.4 Biaxial model for incidence angle dependence

For asymmetric components, an overall biaxial incidence angle modifier can be used in order to model the optical efficiency properly. McIntire presented a biaxial incidence angle modifier for the optical efficiency of asymmetric concentrating solar collectors. The incidence angle modifier was obtained from measurements in the perpendicular transverse and longitudinal directions (McIntire, 1982). Equation 1 defines this model.

$$G(\theta_L, \theta_T) = G_L(\theta_L,0)G_T(0, \theta_T) \quad (1)$$

In the equation above, θ_T and θ_L, denotes the angular of incidence projected in the transverse and the longitudinal planes. The longitudinal plane is the plane including the surface normal and a line along the window extension, and the transverse plane is the plane including the surface normal and perpendicular to the longitudinal plane, according to fig 1. In equation 1, the angular dependence of the window is determined from measurements made in two orthogonal planes, figure 1.

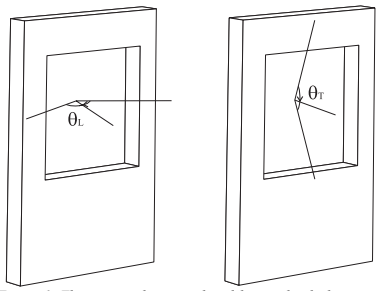

Figure 1. The projected traversal and longitudinal planes and the angles θ_T and θ_L projected in these planes.

$$\tan^2 \theta_i = \tan^2 \theta_L + \tan^2 \theta_T \quad (2)$$

Figure 1 and equation 2 shows the relation between the incidence angle (θ_i) and the two projected angles θ_T and θ_L. The model described by equation 1 is strictly correct only when radiation is incident in either of the analysis planes (Nilsson et al., 2005).

1.5 Sunshades studied

Four different solar shadings were studied; Venetian blind, Awning, Diffuse film, and Screen. The Venetian blind was characterized outdoors, while the others were measured indoor in the Solar Simulator of Energy and Building Design, Lund University. The awning and the Venetian blind are asymmetric shadings while the screen and the diffuse film are symmetric shadings.

2. THE NEW MODEL AND METHOD OF VALIDATION

2.1 New model

In order to systematically characterize the incidence angle dependence of asymmetric components, a new method and model is suggested in this paper. In this model, the influence of the glazing and of the solar shading on the system g-value is studied separately. If the sunshade has no edge effects and do not introduce any light scattering an optical model given by equation 3 is proposed.

$$g_{sys}(\theta_i,\theta_T)=g_w(\theta_i)g_{sh}(\theta_T) \quad (3a)$$

$$g_w(\theta_i)=g_w(\theta_L,\theta_T) \quad (3b)$$

$$g_{sh}(\theta_T)=g_{sys}(\theta_L=0,\theta_T)/g_w(\theta_T) \quad (3c)$$

g_{sys} is the measured g-value of the sunshade in combination with the window. g_w is the measured g-value of the bare window.

In this equation, the factor $g_w(\theta_i)$ basically gives the influence of the glazing and $g_{sh}(\theta_T)$ gives the influence of the solar shading. Equation 3 is, in principle, different from equation 1 since θ_L is not included. $g_{sh}(\theta_T)$ is obtained as a ratio between g_{sys} and $g_w(\theta_T)$. Equation 3 is also valid for plane windows having $g_{sh}(\theta_T) = 1$ resulting in g_{sys} being a function of only θ_i, just as expected. In the T plane, the incoming radiation is first transmitted through the solar shading and then transmitted through the glass. Geometric effects and multiple reflections in the sunshade affect the g-value. In the L direction, the properties of the glass are important. This means that the incidence angle dependence in the L direction of a window with a transparent solar shading device should be similar to the dependence in the overall direction for a plane window.

$$g_{sys}(\theta_L,\theta_T=C) \approx g_w(\theta_i) \quad (4)$$

Most sunshades introduce scattering. This means that the g-value functions will be affected and the function $g_{sh}(\theta_L,\theta_T=C)$ is expected to show a weaker angular dependence than $g_w(\theta_i)$. Many sunshades like awnings exhibit edge effects. This means that equation 3 has to be extended with an end effect function h (θ_L)

$$g_{sys}(\theta_i,\theta_T,\theta_L) = g_w(\theta_i)g_{sh}(\theta_T)h(\theta_L) \quad (5)$$

2.2 Outdoor measurements of external solar shadings

Four different types of external solar shading devices were characterized indoors and outdoors. The Venetian blind was measured outdoor in the hot box arrangement at Energy and Building Design, Lund University (M.Wall and H Bülow-Hübe, 2001). Two well insulated vertical boxes with constant temperatures measured the energy flow through windows and solar shading devices. Both boxes faced south direction. One box with a window only served as a reference box and the other box had both window and solar shading. The g-value of the solar shading was then defined as:

$$g_{sh} = g_{sys}/g_w \quad (6)$$

The windows were double glazing units with 4 mm clear glass and 12 mm space between the panes. The

measurement methodology and techniques are described in details elsewhere (Wall and Bülow-Hübe, 2001).

The Venetian blind was measured in both horizontal and vertical position. The angle of the lamellas of the Venetian blind was 0° for both the horizontal and vertical placement, seen in figure 2.

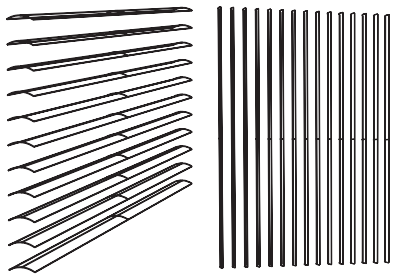

Figure 2. Drawing of the studied Venetian blind. a. Horizontal. b. Vertical.

The Venetian blind was measured near spring equinox when the transverse projected incidence angle (θ_T) is constant 34° at latitude 56°, see figure 3. When the blind was aligned vertical, fig 2b, the measurements gave the incidence angle dependence in the transverse plane at a constant longitudinal angle of 34°. By measuring both vertical and horizontal, it was possible to obtain the dependence in both longitudinal and transverse direction.

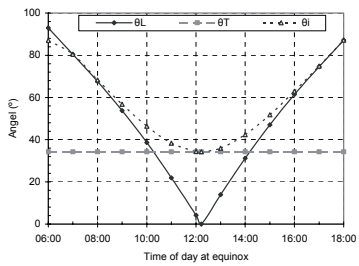

Figure 3. The projected transverse and longitudinal angles (θ_T) (θ_L) and the incidence angle (θ_i) at the equinox, when θ_T=(90-latitude)

2.3 Indoor measurements of external solar shadings

The measurements were performed with the solar simulator in the solar laboratory Energy and Building Design, Lund University see (Wall and Bülow-Hübe, 2003). The solar simulator makes indoor measuring possible for sunshades, windows and solar heating components in a standardized way. The irradiance incident on the window and calorimetric box was 950 W/m^2 at normal incidence. The measurements were performed for incidence angles corresponding to the equinox thereby making the comparison with the outdoor measurements convenient. The indoor measurements were performed for awning, diffuse film and screen, where the diffuse film and screen were mounted closely to the window.

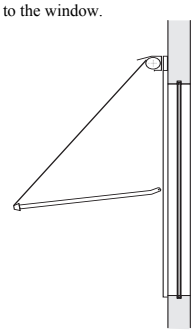

Figure 4. Principal drawing of the awning.

The calorimeter window was a double glazed unit (DGU) with 4 mm glass panes and 12 mm space between the panes, i.e. the same configuration as for the outdoor measurements.

2.4 Ray tracing simulations

The optical simulations were performed in a commercial ray tracing program, ZEMAX (ZEMAX, 2005).

The light incidents on the window system and the fraction of the light transmitted through the system were detected. The blind material was simulated by the optical properties of aluminium at a wavelength of 550 nm with a refractive indices of n=0.96093 and k=-6.6856. The reflectance at normal incidence was 85%. Five percent of the reflected light was reflected specularly and the remaining was supposed to be diffusely reflected with a Lambertian distribution. The simulated window consisted of two panes with 4 mm glass, with a total transmittance of 69% at normal incidence.

The source of 2 500 rays was placed vertically outside the external light detector and the angle of incidence was varied in each simulation. In one set of simulations, the longitudinal angle was kept at 34º and the transverse angle was varied from 0º to 88º in steps of 2º. This should be identical to the measurements performed at the spring equinox with the blind rotated 90º, fig 2b. The other set was performed at a constant transverse angle of 34º, equal to the transverse angle at the equinox in Lund, Sweden, fig 2a. The longitudinal angle was then varied

from 0º to 88º in steps of 2º. This gave a total of 88 simulations.

The estimated error in the derived transmittance of the system was 2% for each angle of incidence.

3. RESULTS, ANALYSIS AND MODELS

3.1 Results of outdoor measurements on a Venetian blind

The Venetian blind characterized outdoors is seen in figure 2. It was monitored in both horizontal and vertical position. In figure 5 results of measurements of the Venetian blind in the horizontal position is shown. The slat angle of the individual blinds is horizontal 0°. The g-values of the system, window and sunshade are plotted in the graph, where the g-value of the sunshade is calculated from equation 3c.

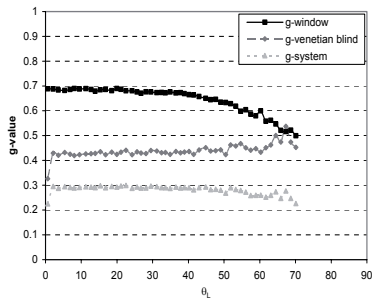

Figure 5. Outdoor measurements of g-values of system, window and Venetian blind as functions of longitudinal angle θ_L for a Venetian blind in horizontal position and 0° slat angle. θ_T=34°.

The measurement as function of the longitudinal angle (θ_L) ends at 75° since the measurement errors increases rapidly for high angles of incidence.

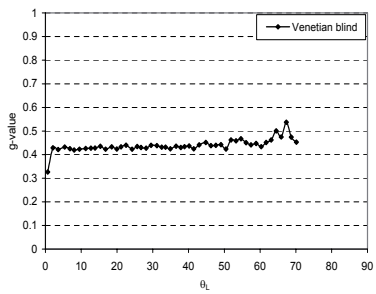

Figure 6 g_{sh}-value of Venetian blind as a function of longitudinal angle (θ_L). θ_T=34°.

In figure 6 the g_{sh}-value of the Venetian blind is shown separately as a function of longitudinal angles. As seen, the g_{sh}-values are nearly constant at angles up to 70°. This means that g_{sys} and g_w have a similar angular dependence in the longitudinal direction. Thus, equation 3 is valid for the blind. The g-value for a vertically placed Venetian blind, fig 2b, is shown in figure 7 as a function of the transverse incidence angle (θ_T).

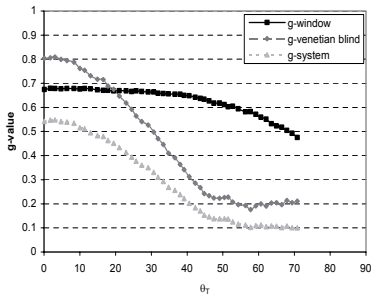

Figure 7. The g-value of the Venetian blind in vertical position as a function of transverse angle (θ_T). θ_T=34

In figure 7 there is as expected a considerably larger variation of the g-values compared to the measurements in the longitudinal direction position. Figure 8 shows only the g_{sh}-value of the Venetian blind as a function of the transverse angle. The g_{sh}-values decreases with increasing θ_T until complete shadowing occur and then it remains at a constant level, when the scattered light reaches the absorber.

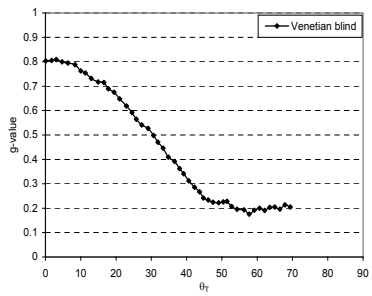

Figure 8 g_{sh}-value of the Venetian blind as function of transverse angle (θ_T). θ_T=34.

3.2 Comparison of measurements and ray tracing

Figure 9 shows the g_{sh}-*value* as a function of the transverse angle (θ_T) for a Venetian blind where the individual blinds is horizontal. The blinds are made of aluminum and the light reflected from the blinds is highly diffuse. Both the ray tracing and the measurements are included in the figure.

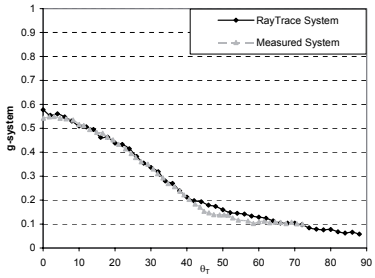

Figure 9. g_{sys}-value of both ray tracing and measurements for a Venetian blind with the window as function of the transverse incidence angle (θ_T).

The graphs differ at large transverse angles due to the reflecting surface of the blind. The simulation assumes a large diffuse component with a Lambertian distribution, but the graphs indicate that the near specular component of the reflected light is higher. The overall agreement between measurements and ray tracing is satisfying. When the light is incident from the horizon, all of the light is transmitted directly through the blind, and almost nothing is reflected. As the transverse angle increases, more and more light is reflected from the blind, and less is transmitted directly. This can be seen from the almost linear decrease in transmittance with increasing angle of incidence. At approximately 42º, no light is transmitted directly and all light is reflected from the blinds. Since the surface is assumed to be nearly Lambertian, the incidence angle has an influence only on the small specularly reflected component. This is also seen in the figure 9, where g_{sys} is almost constant above 42º.

Figure 10 shows the transmission as a function of the longitudinal angle of incidence at a constant transverse angle of 34º. For small and medium angles, the g_{sh} values are constant. At large longitudinal angles, the scattering of the reflected light decreases the reflectance of the window slightly and this results in an increasing transmittance of the system. The scattered light will suppress the angular dependence of the window.

At longitudinal angles below 60º, g_{sh} is constant and Equation 3a is valid. The ray tracing in figure 10 shows good agreement with the measurements in figure 6 for angles below 60°. For higher angles the ray tracing predict a higher g_{sh}. This is explained by larger scattering for high angles of incidence in the ray tracing simulation.

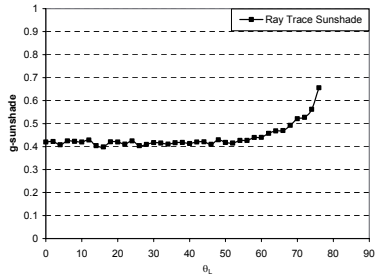

Figure 10. g_{sh}-value from ray tracing of Venetian blind as a function of the longitudinal angle (θ_L). θ_T=34°.

Figures 5-10 show that measurements of the transverse incidence angle dependence are enough to characterize the behavior of a Venetian blind for small and medium longitudinal angles. For very large longitudinal angles of incidence g_{sys} increases due to scattering. The irradiance for these high angles is however low. Figure 11 shows a comparison between the model defined by Equation 3a and ray tracing simulations of the system for angles where $\theta_T=\theta_L$. Equation 3c has been used to obtain $g_{sh}(\theta_T)$. The model approximates the g-value of the system well for small and large angles. For incidence angles in the range of 30º-60º the model tends to overestimate the g-value. This is due to the diffusing effect of the blinds, an effect that can not be described completely by incidence angle dependence in the transverse direction. The diffusivity tends to decrease the incidence angle at the glazing and this increases the transmittance of the glass for large angles of incidence.

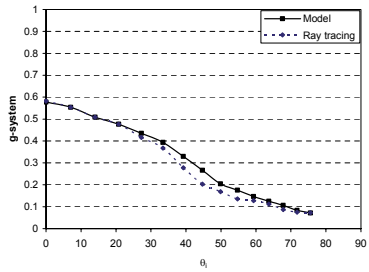

Figure 11. Comparison of g_{sys} from the model and ray tracing of the Venetian blind as a function of the angle of incidence in the plane where $\theta_T=\theta_L$.

3.3 Results of indoor measurements on an awning.

The measurements of the awning are described in this section. Figure 12 illustrates the results of the measurements of g_{sh} as a function of θ_T for a light and a dark short awning characterized in the solar simulator.

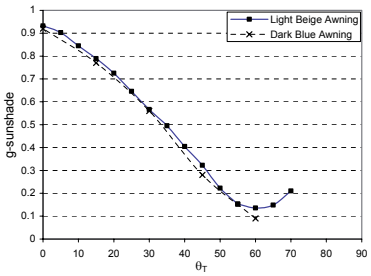

Figure 12. g_{sh}-values measured in the simulator of relatively short awnings as function of the transverse angle θ_T.

Figure 13 shows the measurements at constant transverse angle of 34°, corresponding to equinox for a fully extended awning with its arm turned 120° from the original upper position in figure 4. The measurements were performed for 0° to 80° in the longitudinal direction.

The awning has a more complex behavior than for example the Venetian blind since the awning exhibits edge effects at non zero angles in the longitudinal direction. As shown in figure 13 the g-value of the awning increases with increasing longitudinal angle, due to edge effects.

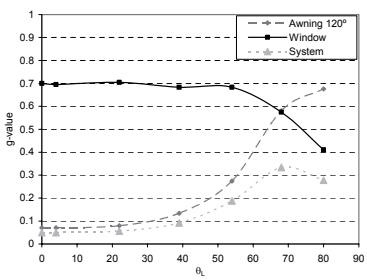

Figure 13 g-values of system, window and awning as functions of longitudinal angle θ_L. θ_T=34°.

For a very long awning compared to the window the shadow should have covered the window for all θ_L without any un-shaded edge effects. The g_{sys}-value would then have been 0.08 for all θ_L as indicated in figure 13. The g_{sh}-value of the awning is dependent on both the longitudinal and transverse angles. The model of the awning is given by the extended equation 5, where $h(\theta_L)$ gives the edge effect of the shading. The window dependency $g_w(\theta_i)$ is very small compared to the edge effect $h(\theta_L)$ and can be included in the $h(\theta_L)$-function. This means that the angular dependence of the awning can be written:

$$g_{sys}(\theta_i,\theta_T) = g_{Sh}(\theta_T)h(\theta_L) \quad (7)$$

3.4 Results of indoor measurements on a diffuse film and a screen.

The diffuse film and the screen are symmetric and have the same optical geometry in all directions. Figure 14 shows the g-values of the diffuse film, window and system as function of the longitudinal angle θ_L.

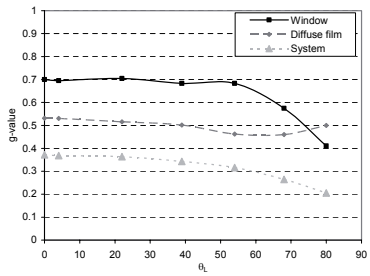

Figure 14. g-values of system, window and diffuse film as function of longitudinal angle θ_L. θ_T=34°.

The g_{sh} -values for the diffuse film is nearly constant. This means that g_{sys} for the diffuse film is similar to the window g_w for angles between 0° and 80°. The measurements of higher angles increase the measurement errors and the inaccuracy, therefore they are not shown here.

A screen fabric was measured in the same mode as the diffuse film with a constant transverse angle of θ_T=34°. The screen was very dense with only 3 % direct transmittance. Thus, most of the transmitted rays were diffusely scattered. In figure 15 the g-values of the system, window and screen are shown as a function of the longitudinal angle. The g-values of the screen g_{sh} are nearly constant and follow the angular dependence of the window g-value, g_w.

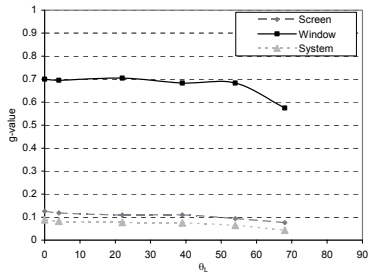

Figure 15. g-values of system, window and screen as a function of the longitudinal angle θ_L. θ_T=34°.

It can be concluded that the g-value of the diffuse film and the screen is almost independent of the longitudinal incidence angle. This means that angular dependence of the diffuse film and the screen can be written

$$g_{sys}(\theta_i,\theta_T) = g_w(\theta_i)g_{sh}(\theta_T) \quad (8)$$

and the shadow function $g_{sh}(\theta_T)$ is an angular independent constant.

In table 1 the models are summarized.

Table 1 Summary of equations presented in the paper.

Parameters / Shades	$g_w(\theta_i)$	$g_{sh}(\theta_T)$=	$h(\theta_L)$
1. Windows	$g_w(\theta_i)$	1	1
2. Shades without scattering	$g_w(\theta_i)$	$g_{sh}(\theta_T)$	1
3.Venetian blind	$g_w(\theta_i)$	$g_{sh}(\theta_T)$	1
4. Awning	1	$g_{sh}(\theta_T)$	$h(\theta_L)$
5. Screen / Diffuse film	$g_w(\theta_i)$	$g_{sh}(\theta_T)$=C	1

4 CONCLUSION

We have shown that the proposed model can be used for Venetian blinds, Awnings, Screens and Diffuse films. The model describes the incidence angle dependence of the Venetian blind well. In the case of the Awning, the model has to be extended to account for the effect of the edges at non zero longitudinal angles. For the symmetric Screen and Diffuse film, the shading devices can be modeled by a constant as the g_{sh} of the shading is independent of the angle of incidence.

Another effect that was observed was the increased g-value of the window at high angles of incidence when the solar shading devices tend to diffuse the irradiance. A window normally has low g-value at large angles of incidence, but since most of the shading devices diffuse the light as it is transmitted, some of the transmitted light is incident on the window at angles where the g-value of the window is higher. This means that the product model under estimate the g-value of the system, g_{sys} and the g-value of the shading device, g_{sh}, for high angles of incidence.

REFERENCES

Bülow-Hübe H. (2001) *Energy efficient window systems. Effects on energy use and daylight in buildings.* (Report TAB—01/1022), Lund, Sweden. Div. Energy and Building Design, Dept. Construction and architecture, Lund University.

McIntire, William R. *Factored approximations for biaxial incident angle modifiers, 1982 Solar* Energy, Vol 29 no 4 pp 315-322 1982

Nilsson J, Brogren M., Helgesson A, Karlsson B. and Roos A., (2005). B*iaxial model for the incidence angle dependence of the optical efficiency of photovoltaic systems with asymmetric reflectors,* Submitted to Solar Energy

ISO 15099:2003. Thermal performance of windows, doors and shading devices -- Detailed calculations.

Wall M. and Bülow-Hübe H. (2001) *Solar Protection in buildings.* (Report TAB—01/3060), Lund, Sweden. Div. Energy and Building Design, Dept. Construction and architecture, Lund University.

Wall M. and Bülow-Hübe H. (2003) *Solar Protection in buildings. Part 2 2000-2002.* (Report EBD-R--03/1), Lund, Sweden. Div. Energy and Building Design, Dept. Construction and architecture, Lund University.

ZEMAX version February 3, 2005, ZEMAX Development Corporation, San Diego, California, USA

LUND UNIVERSITY

ISSN 1671-8136
ISBN 978-91-85147-22-9